COUPLED-INDUCTOR MAGNETICS IN POWER ELECTRONICS

Thesis by

Zhe Zhang

In Partial Fulfillment of the Requirements

for the Degree of

Doctor of Philosophy

California Institute of Technology

Pasadena, California

1987

(Submitted October 7, 1986)

Acknowledgements

I wish to express my deepest gratitude to my advisors, Professor S. Ćuk and Professor R. D. Middlebrook, for their encouragement and advice during the five years I have studied at Caltech.

I appreciate very much the financial support of the California Institute of Technology by the way of Graduate Teaching Assistantships. In addition, Graduate Research Assistantships supported by the International Business Machines, GTE, Emerson Electric, General Dynamics Corporations, and National Aeronautics and Space Administration Lewis Research Center are gratefully acknowledged.

Most importantly, I thank my wife Guo Zhan, son Zhang Pei, and my parents W. Y. Chang and C. S. Wang. Without their support and understanding my study at Caltech would never have been possible. In addition, I wish to thank Mr. Wang Senlin, my first teacher in electronics, and Mr. Xu Qinglu, my supervisor when I started my first job, for their training and support throughout the years.

In the years with the Power Electronics Group, I have learned from the Group much more than I have contributed. I thank all my fellow members of the Power Electronics Group for all their help and support.

Abstract

Leakages are inseparably associated with magnetic circuits and are always thought of in three different negative ways: either you have them and you don't want them (transformers), or you don't have them but want them (to limit transformer short circuit currents), or you have them and want them, but you don't have them in the right amount (coupled-inductor magnetic structures). The methods of how to introduce the leakages at appropriate places and in just the right amounts in coupled-inductor magnetic structures are presented here, in order to optimize the performance of switching dc-to-dc converters.

Contents

Chapter 1

INTRODUCTION

The switched mode power conversion concept emerged from the need of high power, high efficiency, compact and lightweight voltage regulators. In a typical linear regulator, the line voltage is converted to other voltages by the use of a transformer, then rectified into dc. The dc voltage is then regulated by the use of a transistor operating in linear mode (Fig 1.1a). In a linear regulator, the output voltage is regulated by controlling the voltage drop on the regulating transistor. The efficiency of this kind of circuit is usually less than 50%, mostly due to the voltage drop on the regulator transistor; also the size and weight of the regulator is largely due to the bulky 50/60 Hz transformer and the heat sink used to dissipate the heat generated by the power transistor. In a typical switched mode regulator, the line voltage is first rectified into a high dc voltage. This dc voltage is then converted to other voltages at the outputs by rapidly switching energy storage elements between the input and output. The switching frequency is usually above 20 kHz, and is usually done by transistors operating in switched mode. To isolate the outputs from the input, a transformer is often used in the circuit; it is also operating at the switching frequency (Fig 1.1b). The output voltage is regulated by changing the duty ratio of the square wave. In a switch mode regulator, the transistor switch is operating in switched mode; therefore, the power loss is minimal. The size and weight of the converter is reduced because the transistor heat sink can be much smaller; also, the size of the magnetic components (transformer, inductors) operating at 20 kHz is much

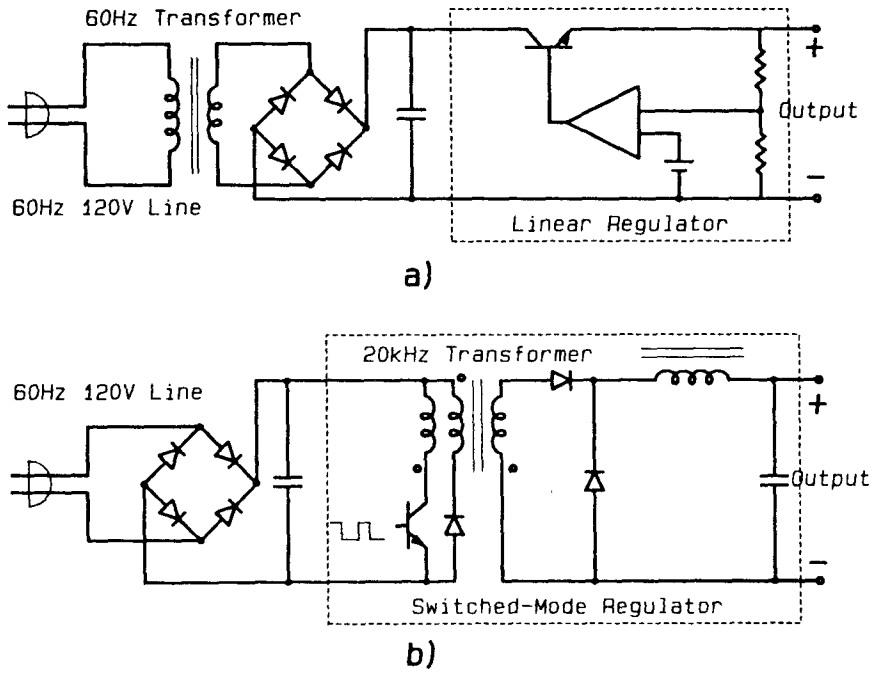

Figure 1.1: A typical off-line linear regulator (a), and a switched mode regulator (b).

smaller than that of their 50/60 Hz counterparts.

After many years of development, switched mode power conversion expanded from simple dc to dc converters (voltage regulators) to much more complicated dc to ac converters (inverters), ac to dc converters (controlled rectifiers), and ac to ac converters (cyclo converters). Due to the improvements in material, devices, technology, and converter circuit topology, the efficiency, size and weight, reliability, and cost of switched mode converters all improved dramatically. However, the magnetic components in a converter are still quite unfamiliar to most design engineers, and due to the rapid advance in other areas, it is becoming the bottle-neck of the converter design.

Even though magnetic devices operating at 20 kHz are much smaller and lighter than their line frequency counterparts, the size and weight of these components can take up to half the size and weight of the entire switching converter. Increasing the switching frequency to over 1 MHz, as proposed by many people, can theoretically further

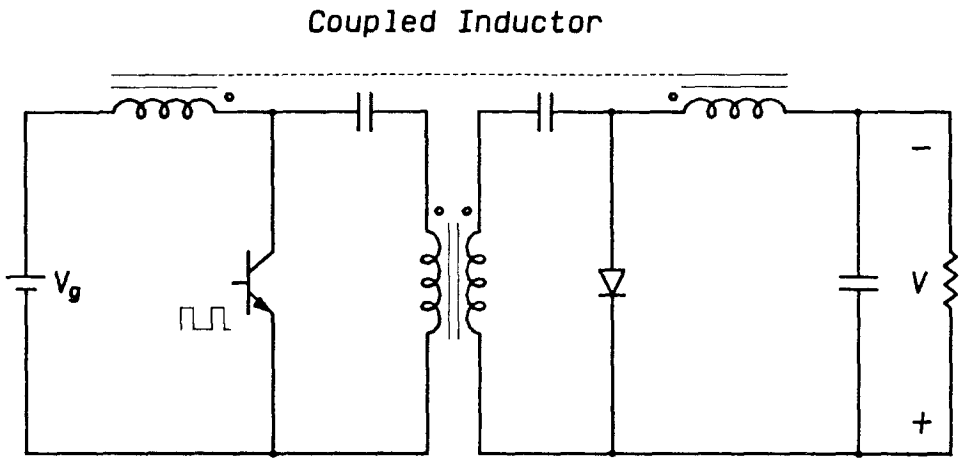

Figure 1.2: A coupled-inductor Ćuk converter.

decrease the size and weight of these components. However, due to the higher core loss at higher frequencies, the design has to be made using much lower flux density, which in turn reduces the effort to a point of diminishing returns. Another route to decrease the size and weight of the magnetic devices is to combine several magnetic components into one single structure, as was done in the three phase power transformer.

In the development of the Ćuk converter (Fig. 1.2), it was discovered that when the two inductors are coupled together, not only the size and weight of the inductors can be reduced, but also, under certain conditions, the ripple current in one of the inductors can be eliminated. Since then, many discussions had been made to explain this "zero ripple" phenomenon [1],[2]. However, due to the sensitivity of the zero ripple condition to the adjustments and also due to the lack of a complete design procedure, the coupled-inductor method never went into widespread use.

There are many ways to describe the "zero ripple" matching condition. Using

the appropriate models of the coupled-inductor, this presentation reveals a very simple and physically meaningful solution of this zero ripple condition.

The sensitivity of the zero ripple condition to the errors in the leakage, turns ratio, and other factors in the coupled-inductors can be reduced by *increasing* the leakage in the coupled-inductor structure. Contrary to the traditional transformer winding technique, which wants to minimize the leakage, the coupled-inductors require high, well controlled leakage. In some cases, the use of an additional leakage inductor is beneficial. However, a new structure using conventional EI or EE-cores described in this thesis eliminated the need of this external inductor, and the leakage of the windings can be easily calculated using a newly defined "leakage parameter" of the core. The values of this parameter for different cores are given in Appendix A.

The dc model of the new structure is also given in this presentation. By use of both the dc and ac (zero ripple) model, a closed form solution of the new coupled-inductor structure is derived for the first time. From this closed form solution, one can easily design the coupled-inductors.

The first eleven chapters of this thesis discuss the coupled-inductor structure. To insure that the reader is familiar with the subject, Chapter 2 contains a detailed review of the basics of magnetics, while Chapter 3 describes some of the advantages of coupling inductors in a switching converter.

In Chapters 4 to 6, the two winding coupled-inductors are discussed. In Chapter 4 the zero ripple condition of the two winding coupled-inductors is described in detail. Chapter 5 discusses the sensitivity issue of the coupled-inductors, points out that, to obtain low sensitivity, the coupled-inductors have to have high leakage. Chapter 6 shows a special case, in which there is a Ćuk converter with low leakage coupled-inductors, but a relatively leaky transformer. In this special case, not only the zero ripple condition no

longer exists, but even the characteristic of the basic Ćuk converter—continuous input and output currents, is changed.

Chapters 7 to 11 extend the basic coupled-inductor technique for more than two windings, to be used in multiple output converters. Chapter 7 describes a few practical winding structures, introduces the new structure using standard EI-cores. In Chapter 8 an important parameter, the *leakage parameter* is introduced. Using this parameter, we derive the closed form solution for the new structure. Then a detailed discussion of the design procedure is given. The next chapter gives a few alternative structures, including the most useful EE-core structure. In Chapter 10, the sensitivity of the new structure is analyzed. Finally, Chapter 11 gives a design example, in which a 150w, three output Ćuk converter is constructed using three different inductor structures. The result clearly shows the advantage of the new coupled-inductor structure.

The next four chapters discusses the cross-regulation problem in three types of multiple output converters, the flyback, the buck type, and the Ćuk converter. For some types of converters, the use of coupled-inductors could improve the cross regulation.

This thesis shows that the importance of the magnetic components in switch mode converters is no less than that of the electronic components. Because the unfamiliarity of most engineers with magnetic devices, the progress in this area is lagging behind other areas in power electronics, so the improvement in magnetic components can immediately benefit the development of the converter design. Even though the exact solution of the magnetic field problem in the magnetic devices is complicated, by thoroughly understanding the basics, one can derive simplified models to obtain results with very good accuracy.

Chapter 2

MAGNETIC CIRCUITS AND MODELS

To fully understand the advantages of a coupled-inductor or integrated magnetic structure and make a design for it, a thorough analysis of the structure is necessary. Unfortunately, magnetics is an area which most electrical engineers try to avoid, because it seems to be an area filled with those field equations better left for a physicist. However, if the magnetic structure is properly modeled, it can be fairly easy to understand and analyze.

This chapter reviews some basic models for analyzing a magnetic structure. Since there is not a single *best* model for all occasions, all these models will be used in the following chapters.

2.1 COUPLED-INDUCTOR EQUATIONS

2.1.1 Self Inductance and Mutual Inductance for Two Windings

In a single coil (Fig. 2.1a) the relation between the voltage and the flux in the coil is:

$$v = \frac{N d\phi}{dt} \tag{2.1}$$

Since the inductance of the coil is defined as:

$$L = \frac{N\phi}{i} \tag{2.2}$$

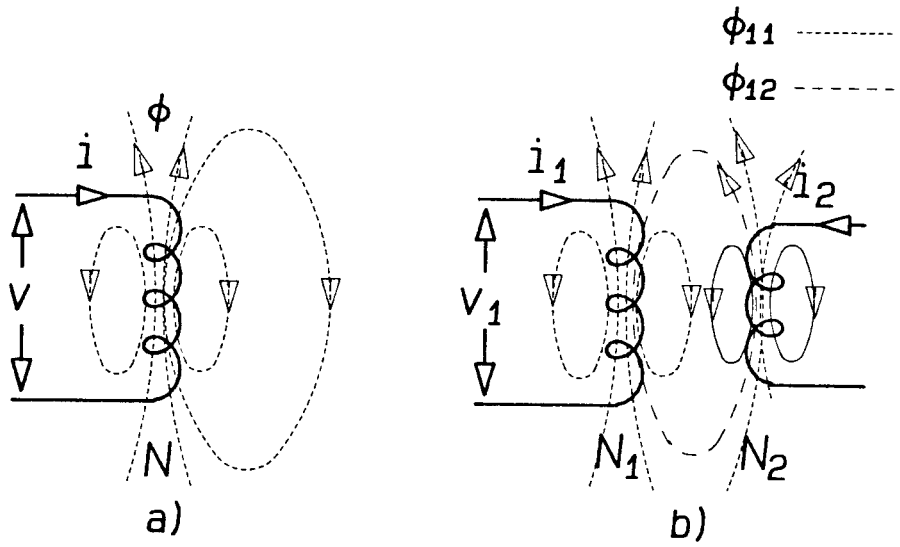

Figure 2.1: The flux, current, and voltage of a single inductor (a), and two inductors coupled (b).

we can write:

$$v = L\frac{di}{dt} \tag{2.3}$$

For two nearby coils (Fig. 2.1b), part of the flux ϕ_{22} generated by i_2 in the second winding is linked through the first winding. This part is called the *mutual flux* ϕ_{12}. (The rest is called *leakage flux* ϕ_{l2} of the second winding.) Therefore, the voltage on the first winding will depend on the rate of change of the *total* flux in that winding:

$$v_1 = N_1\frac{d\phi_{11}}{dt} + N_1\frac{d\phi_{12}}{dt} \tag{2.4}$$

or

$$v_1 = L_{11}\frac{di_1}{dt} + L_{12}\frac{di_2}{dt} \tag{2.5}$$

where

$$L_{11} = \frac{N_1\phi_{11}}{i_1}$$

is the *self-inductance* (measured inductance) of the first winding, and

$$L_{12} = \frac{N_1 \phi_{12}}{i_2}$$

is the *mutual inductance* between the two windings. Similarly:

$$v_2 = L_{21}\frac{di_1}{dt} + L_{22}\frac{di_2}{dt} \tag{2.6}$$

It can be proved that $L_{12} = L_{21}$, so we can write $L_M$for the mutual inductance.

2.1.2 Coupling Coefficients k, k_1 and k_2

When two inductors are coupled, the *coupling coefficient* k is usually used to measure the "tightness" of the coupling. The coupling coefficient is defined as [3]:

$$k \equiv \frac{L_M}{\sqrt{L_{11}L_{22}}} \tag{2.7}$$

The coupling coefficient can also be written as:

$$k \equiv \frac{L_M}{\sqrt{L_{11}L_{22}}} = \sqrt{\frac{L_{21}L_{12}}{L_{11}L_{22}}} = \sqrt{\frac{\phi_{21}\phi_{12}}{\phi_{11}\phi_{22}}} \tag{2.8}$$

For example, if the inductors are not coupled, the mutual inductance is zero; then $k = 0$; when the inductors are very tightly coupled, all the flux in one winding links through the other one, or, in other words, if there is no leakage flux, then $k = 1$.

This coupling coefficient is useful in determining the response of a resonant circuit, and in some other applications. However, it can not point out *where* the leakage lies; therefore, we call it "communication coupling coefficient." For example, the two coupled-inductors in Fig. 2.2 are drastically different. In the first structure, both windings have 20 percent leakage; that is, 80 percent of the flux generated by the current in one winding links through the other one. In contrast, in the second structure, since the second winding is inside the first one, only 64 percent of the flux generated by the current in the

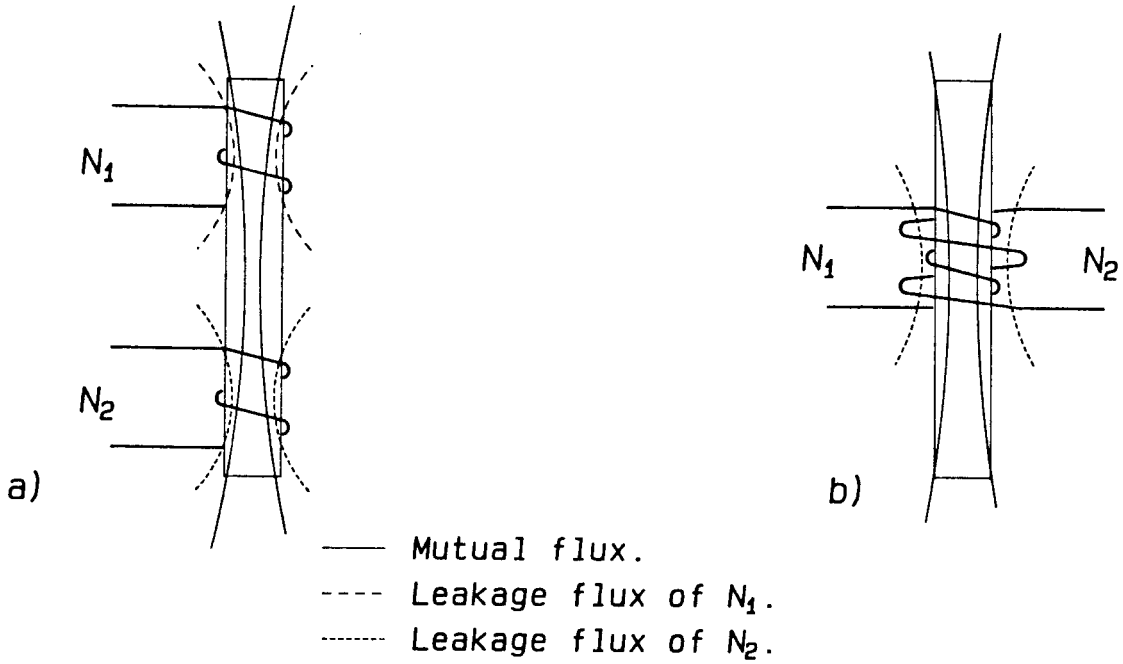

Figure 2.2: a) A coupled-inductor structure in which 80% of the flux generated by the current in either winding is coupled through the other winding. b) A coupled-inductor structure where all of the flux generated by the current in N_2 is coupled through N_1, but only 64% of the flux generated by the current in N_1 is coupled through N_2. Both coupled-inductors have the same coupling coefficient.

first winding links through the second one, but all the flux generated by the current in the second winding links through the first one. Using (2.8) both coupled-inductors gives the same coupling coefficient ($k = 0.8$).

In coupled-inductors used in switching converters, as discussed in Chapter 4, to analyze the ripple steering effect, it is very important to know where the leakages are. For example, obtaining zero ripple on the second winding only requires one to match the turns ratio with the ratio of the mutual flux to the total flux of the first winding; the leakage of the second winding has *no effect* on this matching condition. Therefore, instead of this "communication coupling coefficient," we introduce two coupling coefficients k_1, k_2 of the two windings [4].

In the coupled-inductors shown in Fig. 2.3a, assuming that the secondary

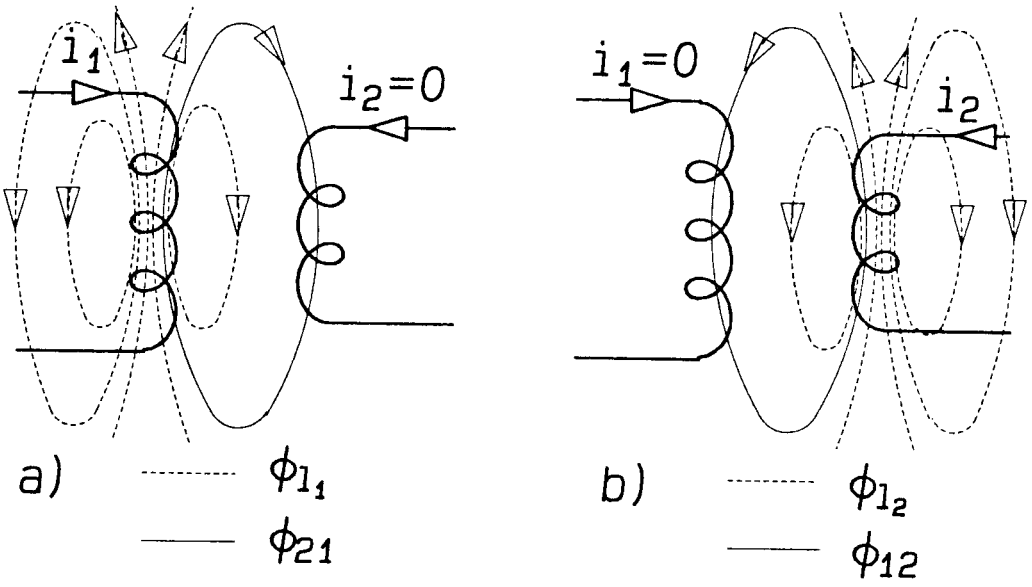

Figure 2.3: Fluxes in coupled-inductors when only one winding is driven.

current $i_2 = 0$, the total flux generated by winding one ϕ_{11} consists of two components:

1. ϕ_{21}—flux generated by primary winding that links through the secondary (mutual flux of the primary winding).

2. ϕ_{l_1}—flux generated by primary winding that does not link through the secondary (leakage flux of the primary winding).

The coupling coefficient of the primary k_1 is defined as the ratio between ϕ_{21} and the total flux ϕ_{11}.

$$k_1 \equiv \frac{\phi_{21}}{\phi_{11}} = \frac{\phi_{21}}{\phi_{21} + \phi_{l_1}} \tag{2.9}$$

Similarly, the coupling coefficient of the secondary k_2 (Fig. 2.3b) is:

$$k_2 \equiv \frac{\phi_{12}}{\phi_{22}} = \frac{\phi_{12}}{\phi_{12} + \phi_{l_2}} \tag{2.10}$$

Using (2.8), one can find that the relation between the "communication coupling coefficient" k and the two coupling coefficients k_1, k_2 is:

$$k \equiv \frac{L_M}{\sqrt{L_{11}L_{22}}} = \sqrt{\frac{\phi_{21}\phi_{12}}{\phi_{11}\phi_{22}}} = \sqrt{k_1 k_2} \tag{2.11}$$

As shown in this equation, k is just the average of k_1 and k_2. In the example of Fig. 2.2, for the first structure, $k = k_1 = k_2 = 0.8$, while in the second structure $k_1 = 0.64$, $k_2 = 1$ and $k = 0.8$.

2.1.3 Coupling Inductor Equations for More Windings

The coupling between three or more windings is more conveniently written in the matrix form:

$$\begin{bmatrix} v_1 \\ v_2 \\ \cdot \\ \cdot \\ v_n \end{bmatrix} = \begin{bmatrix} L_{11} & L_{12} & \cdot & \cdot & L_{1n} \\ L_{21} & L_{22} & \cdot & \cdot & L_{2n} \\ \cdot & \cdot & & & \cdot \\ \cdot & \cdot & & & \cdot \\ L_{n1} & L_{n2} & \cdot & \cdot & L_{nn} \end{bmatrix} \begin{bmatrix} \frac{di_1}{dt} \\ \frac{di_2}{dt} \\ \cdot \\ \cdot \\ \frac{di_n}{dt} \end{bmatrix} \tag{2.12}$$

It can also be proved that $L_{ij} = L_{ji}$; therefore the matrix is symmetric.

The coupled-inductor equations are covered in most circuit textbooks. Because of its mathematical form, it is very convenient to use in the dynamic analysis of a system. The values of the self-and mutual inductances can be obtained by the measurement of the device. However, the equations bear no direct relationship with the physical magnetic structure.

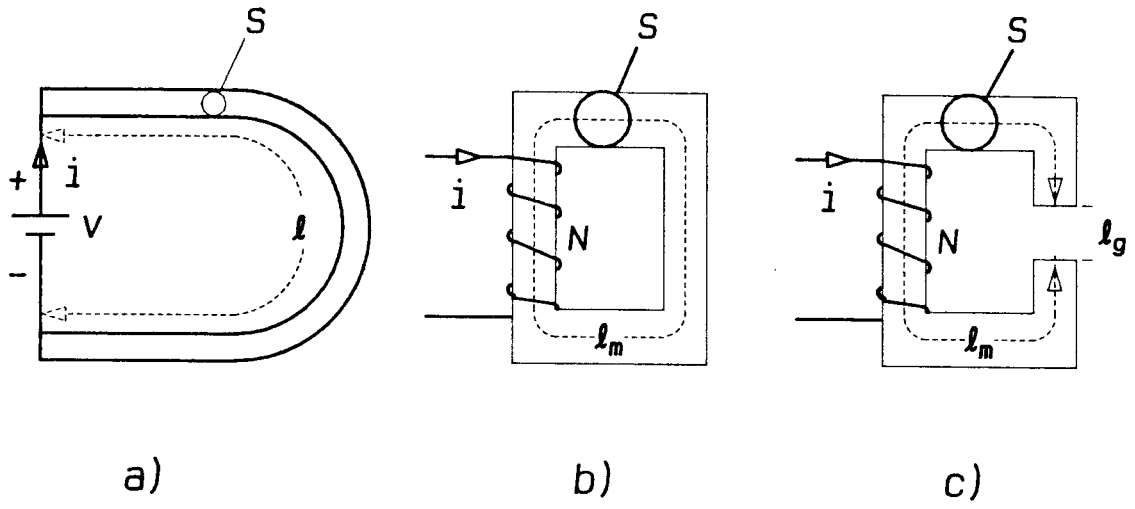

Figure 2.4: a) Electrical circuit. b) Magnetic circuit. c) Magnetic circuit with air-gap.

2.2 RELUCTANCE MODEL

2.2.1 The Reluctance Concept

The equations which describe an electric field and those which describe a magnetic field are strikingly similar:

$$I = \iint_S J\,dS \qquad \Phi = \iint B\,dS \tag{2.13}$$

$$emf = v = \int_l E\,dl \qquad mmf = Ni = \oint_l H\,dl \tag{2.14}$$

$$J = \sigma E \qquad B = \mu H \tag{2.15}$$

$$\oiint_S J\,dS = 0 \qquad \oiint_S B\,dS = 0 \tag{2.16}$$

The *electrical circuit* concept and the similarity between the electric and magnetic field equations lead to the concept of *magnetic circuit.*

In an electrical circuit (Fig. 2.4a), for a given voltage source v, knowing the length (l) and cross section S of the conductor (assuming S is uniform along l), one can

find the current in the conductor:

$$i = J\,S = \sigma\,E\,S = \sigma\frac{v}{l}S = \frac{\sigma\,S}{l}v \tag{2.17}$$

The field quantities can be bypassed and the current found by Ohm's law:

$$i = \frac{v}{R} \tag{2.18}$$

where $R \equiv \frac{l}{\sigma S}$ is the *resistance* of the conductor.

The same procedure can be used to find the flux in a magnetic circuit, assuming the uniform distribution of flux along the core cross section (Fig. 2.4b):

$$\Phi = B\,S = \mu\,H\,S = \mu\frac{N\,i}{l_m}S = \frac{N\,i}{\mathcal{R}} = N\,i\,\mathcal{P} \tag{2.19}$$

where $\mathcal{R} \equiv \frac{l_m}{\mu S}$ is the *reluctance* of the magnetic circuit, and $\mathcal{P} = \frac{1}{\mathcal{R}}$ is the permeance of the magnetic circuit.

Kirchhoff's laws in electrical circuits also hold true in magnetic circuits.

2.2.2 Inductance of an Inductor

The inductance of the inductor shown in Fig. 2.4b is:

$$L = \frac{N\phi}{i} = \frac{N}{i}\mu\,H\,S = N^2\frac{\mu S}{l_m} \tag{2.20}$$

Using the definition of reluctance and permeance, one can write:

$$L = \frac{N^2}{\mathcal{R}} = N^2\,\mathcal{P} \tag{2.21}$$

2.2.3 Air Gaps in Magnetic Circuits

As shown in Fig. 2.5a, the B-H characteristic of a ferromagnetic *material* is nonlinear and double-valued. For a given core *structure* as in Fig. 2.4b, ignoring the losses in the core material, scaling the B axis by the cross section S and scaling the H axis by

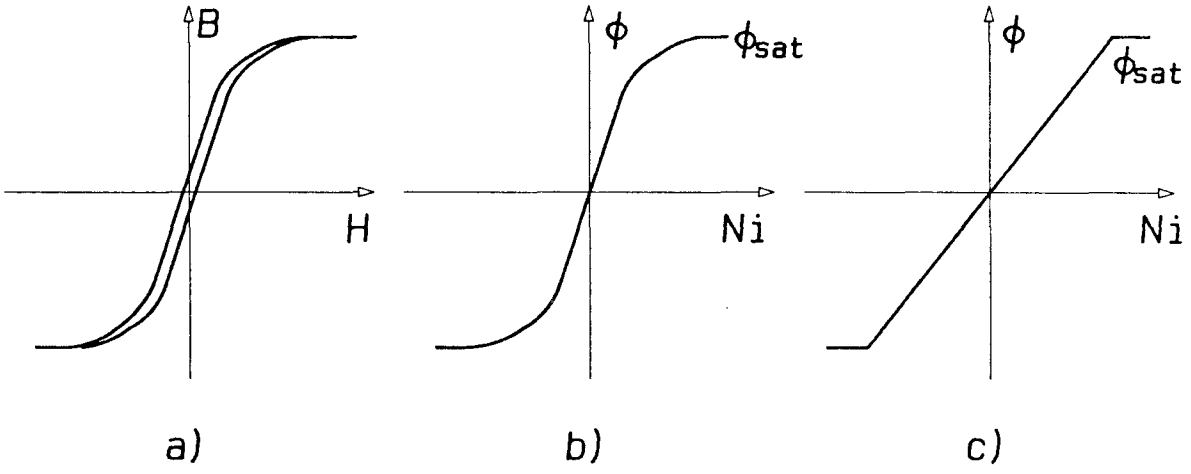

Figure 2.5: a) $B-H$ loop of ferromagnetic material. b)$\phi - Ni$ curve of ungapped core. c)$\phi - Ni$ curve of gapped core.

the mean path length l, give the ϕ vs. Ni curve shown in Fig. 2.5b; the slope of this curve is the permeance of the structure. Notice that: 1. There is a saturation point ϕ_{sat} after which $\mathcal{P}$ drops to a very low value. 2. The curve is nonlinear even when ϕ is well below ϕ_{sat}, which means that the permeance is not a constant.

If an air-gap is introduced in the structure (Fig. 2.4c), the total reluctance is now the sum of $\mathcal{R}_m$—the reluctance of the core and $\mathcal{R}_g$—the reluctance of the gap; therefore, the flux in the core and the permeance of the structure are:

$$\phi = \frac{Ni}{\mathcal{R}_g + \mathcal{R}_m} \qquad \mathcal{P} = \frac{1}{\mathcal{R}_g + \mathcal{R}_m} \tag{2.22}$$

where

$$\mathcal{R}_m = \frac{l_m}{\mu\, S} \qquad \mathcal{R}_g = \frac{l_g}{\mu_0\, S}$$

Now the inductor can handle a larger current without saturation, at the expense of lower inductance. Also because the reluctance of the air-gap is constant, the ϕ

vs. Ni curve becomes much more linear before the saturation point (Fig. 2.5c).

In most inductors designed to carry DC current, the required air-gap is big enough to make $\mathcal{R}_g \gg \mathcal{R}_m$, so that we can ignore the core reluctance and simply use the gap reluctance for the total reluctance:

$$\phi = BS \approx \frac{Ni}{\mathcal{R}_g} \qquad\qquad L \approx \frac{N^2}{\mathcal{R}_g} \tag{2.23}$$

The reluctance model is derived directly from the magnetic structure. In some applications, like finding the fluxes in the core, it is the only model to use. However, in an electrical circuit the conductivity σ of the conductor is usually more than 10^{15} times higher than that of the insulator, but the μ of a magnetic core is only 100 to 10^4 times higher than that of air. Therefore, the leakage flux of a magnetic structure sometimes cannot be ignored. Also, the leakage flux is distributed throughout the space, making the lumped reluctance model only a close approximation of the real structure.

2.3 CIRCUIT MODEL

The circuit model can be derived from ether the coupled-inductor equations or the reluctance model.

2.3.1 Deriving the Circuit Model From the Coupled-Inductor Equations

The coupled-inductor equations (2.5), (2.6) can be written as:

$$v_1 = L_{11}\frac{di_1}{dt} + L_M\frac{di_2}{dt} = (L_{11} - L_M)\frac{di_1}{dt} + L_M\frac{d}{dt}(i_1 + i_2) \tag{2.24}$$

$$v_2 = L_{22}\frac{di_2}{dt} + L_M\frac{di_1}{dt} = (L_{22} - L_M)\frac{di_2}{dt} + L_M\frac{d}{dt}(i_1 + i_2) \tag{2.25}$$

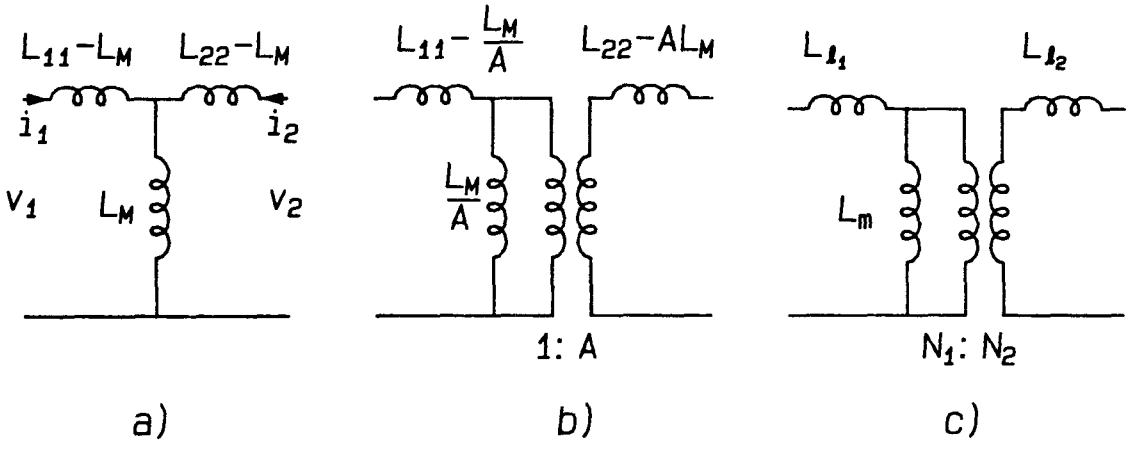

Figure 2.6: Circuit models for two winding coupled-inductors.

From these equations the circuit model can be drawn as Fig. 2.6a. However, the two equations can also be written as:

$$v_1 = L_{11}\frac{di_1}{dt} + L_M\frac{di_2}{dt} = (L_{11} - \frac{L_M}{A})\frac{di_1}{dt} + \frac{L_M}{A}\frac{d}{dt}(i_1 + A\,i_2) \tag{2.26}$$

$$v_2 = L_{22}\frac{di_2}{dt} + L_M\frac{di_1}{dt} = (L_{22} - A\,L_M)\frac{di_2}{dt} + A\,L_M\frac{d}{dt}(\frac{i_1}{A} + i_2) \tag{2.27}$$

and the circuit model is as Fig 2.6b, where A is an arbitrary number. This model is usually called the T-model.

It is more convenient to choose A to be the physical turns ratio N_2/N_1 so that the model will be closely related to the physical device (Fig. 2.6c). In this model L_m is called the magnetizing inductance. It is directly associated to the mutual flux path. L_{l_1} L_{l_2} are the leakage inductances of the primary and secondary windings and are directly associated with the corresponding leakage fluxes. We call this circuit model the "physical model" since each and every element is closely corresponded to the physical structure.

It can be shown that in the T-model for a three-winding structure (Fig. 2.7),

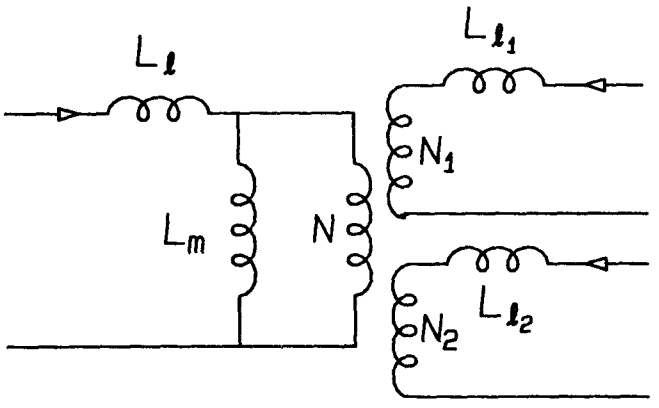

Figure 2.7: Circuit model for a three-winding structure.

the two turns ratios are uniquely determined, and a structure with four or more windings cannot generally be modeled as a T model.

2.3.2 Deriving the Circuit Model From the Reluctance Model

The circuit model can also be found from the magnetic structure through the reluctance model as discussed in the next section.

The circuit model is the easiest for the electrical engineer to understand, because it is in the same form as the rest of the circuit; that is, they are all in the form of an electrical circuit. This model is most convenient for the calculation of currents and voltages in a system.

2.4 DERIVING THE CIRCUIT MODEL FROM THE RELUCTANCE MODEL

2.4.1 Duality

In circuit theory, two networks are *dual* if the loop equations for one network are in the same form as the node equations for the other (they will be identical by just a change of the symbols). Only planar networks have duals [5]. Figure 2.8a shows a pair of dual circuits. Fig. 2.8b is the dual relationship of some circuit elements.

2.4.2 Using Duality to Derive the Circuit Model From the Reluctance Model

Since the equations that describe the magnetic circuit have the same form as those for the electrical circuit, the method used to find the dual of an electrical circuit can also be applied to find the dual of a magnetic circuit.

Figure 2.9 shows the structure and reluctance model of a coupled-inductor structure with leakage in both windings. The procedure of finding the electrical circuit model is as follows [6]:

1. A dot is put inside each loop of the original network N_1; an additional dot is put outside the network. These dots will become the nodes of the dual network N_2.

2. Place the dual of each element of N_1 across the original element, connecting the dots on both sides (Fig. 2.10a).

3. The direction of the new branches is obtained by rotating the direction of the original branch counter-clockwise until it coincides with the dual branch. Figure 2.10b shows the dual circuit.

4. The dual circuit can now be scaled by the appropriate number of turns (N_1) so that the permeances are multiplied by ${N_1}^2$ (Fig. 2.10c).

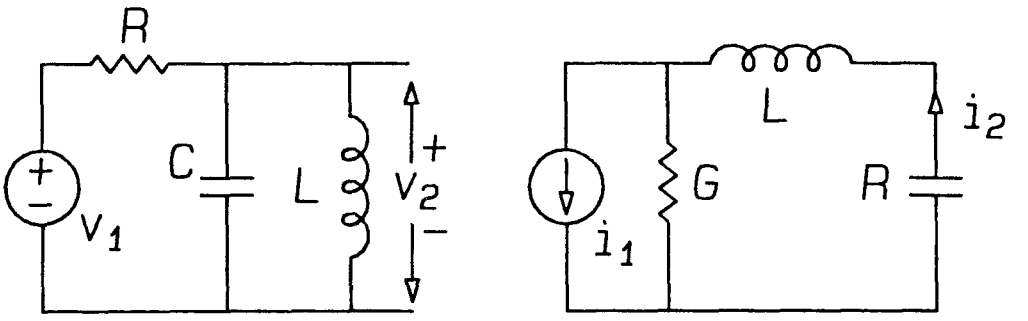

a)

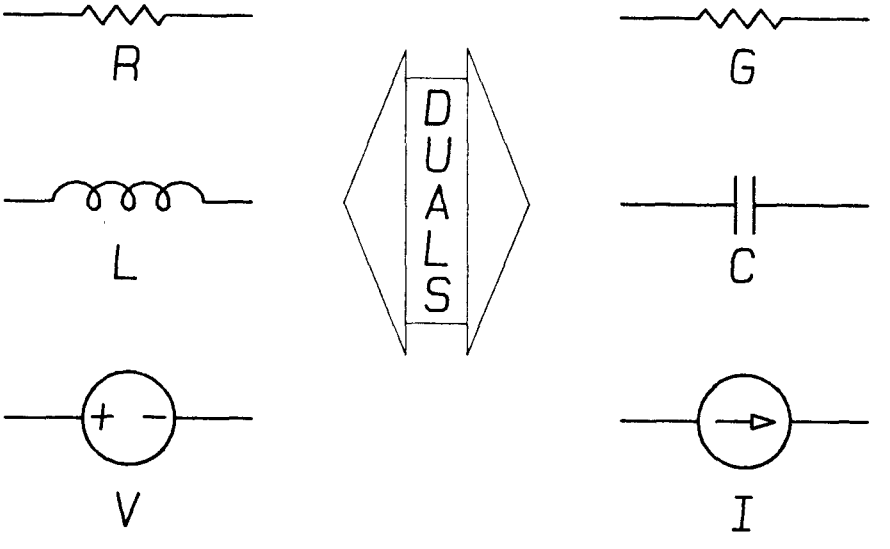

b)

Figure 2.8: (a) A pair of dual circuits. (b)Dual relationship of basic circuit elements.

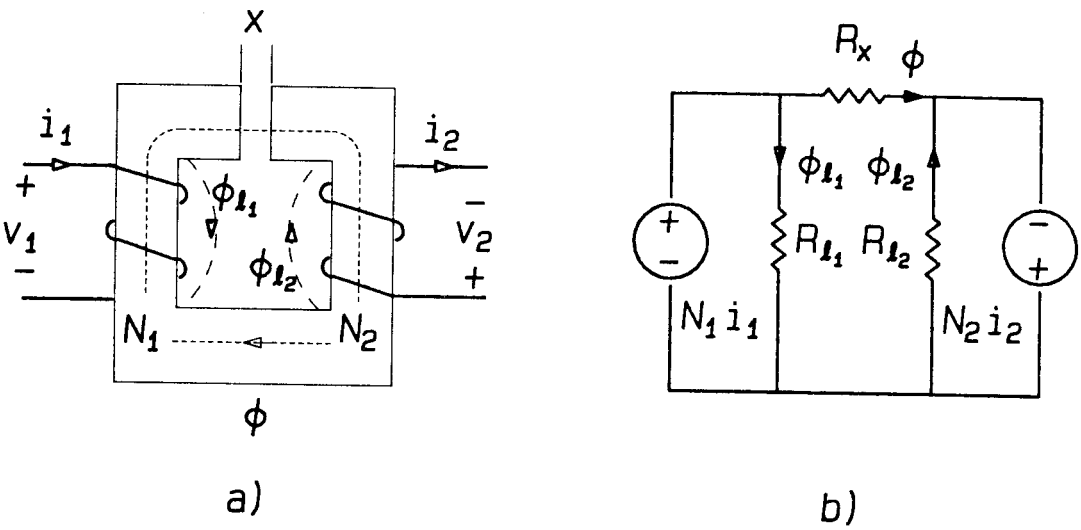

Figure 2.9: a) A coupled-inductor structure. b) The magnetic circuit.

5. Realizing that $v = N\frac{d\phi}{dt}$ and $L = N^2P$, one can redraw the dual circuit into the familiar circuit model (Fig. 2.10d).

6. Finally, as shown in Fig. 2.10e, we use an ideal transformer to match the input and output voltages and currents of the model with those of the original structure.

Note that in step 4, the dual circuit can be scaled by any number; however, choosing the appropriate physical turns ratio will result in a simpler form. Figure 2.11 shows the final results when the dual circuit is scaled by $N_2{}^2$ or scaled by 1 in step 4.

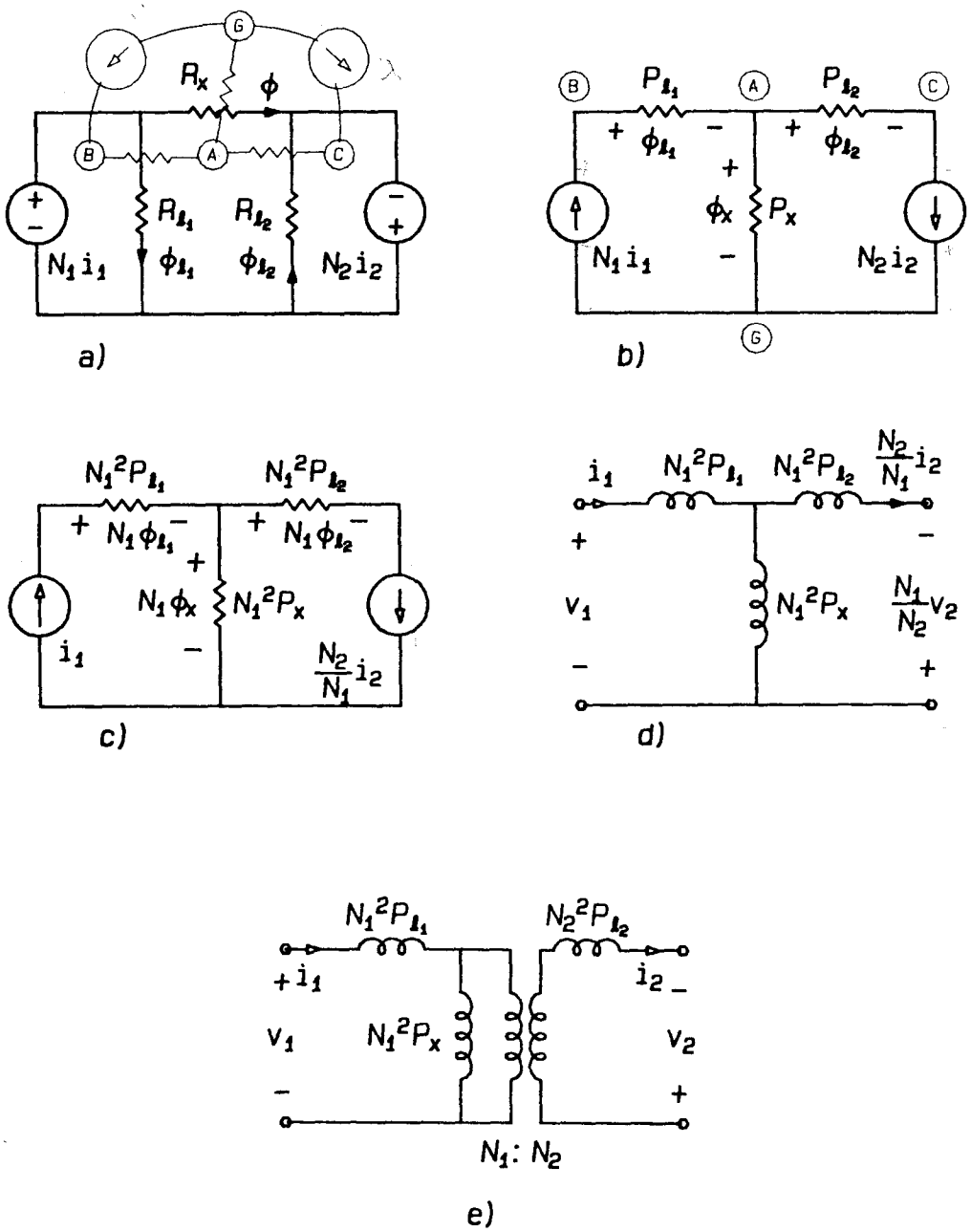

Figure 2.10: a) Finding the structure of the dual circuit. b) The dual circuit. c) Scaling the permeances by N^2. d) The circuit model. e) Scaling by an ideal transformer to match the input and output voltages and currents.

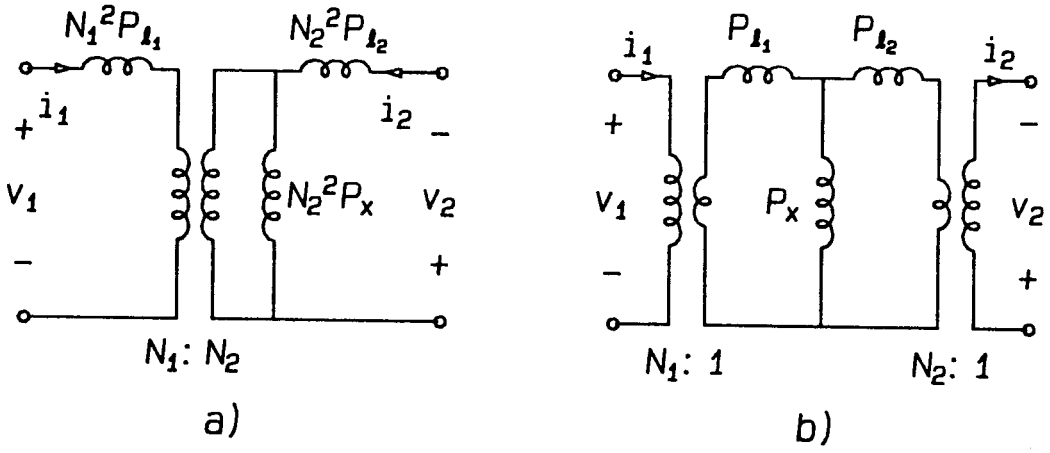

Figure 2.11: The circuit model when the dual circuit is scaled by N_2^2 (a), or 1 (b) in step 4.

Chapter 3

COUPLED-INDUCTORS AND INTEGRATED MAGNETIC CIRCUITS IN SWITCHING CONVERTERS

For a single phase 60Hz transformer, the volume and weight of the transformer grow more slowly than the handling power; that is, a 200w transformer is lighter than two 100w ones. The same can be said for transformers and inductors in a switching converter. When the voltage waveforms on different magnetic devices are the same, they can be integrated into a single structure (Fig. 3.1). The main advantage of this, besides weight and size reduction, is to obtain performance improvement.

Usually, the structure that consists of two or more inductors is called a *coupled-inductor* structure, and those that integrate the isolation transformer as well as the inductors are defined as *integrated magnetic* structure.

3.1 SIZE AND WEIGHT REDUCTION BY COUPLING TWO INDUCTORS INTO ONE STRUCTURE

3.1.1 Two Examples

Example 1

The structures of the two inductors shown in Fig. 3.2a are identical; the voltage

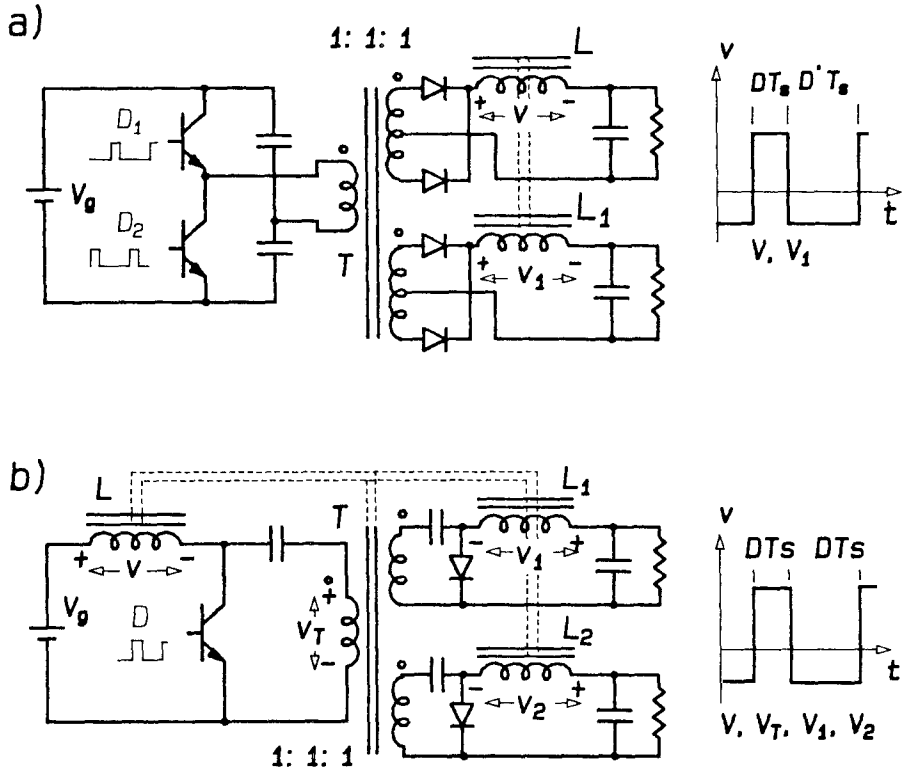

Figure 3.1: When the waveforms on the inductors and/or transformers are the same (a), they can be integrated into a single structure (b).

waveforms on the windings are also identical; therefore' the ac fluxes in both cores are also the same:

$$\phi = \frac{N i}{\mathcal{R}_m + \mathcal{R}_g} \tag{3.1}$$

where $\mathcal{R}_m$ is the reluctance of the core, and $\mathcal{R}_g$ is the reluctance of the air gap.

Note that the direction of the two fluxes can be made opposite in the center branch, which means that the total ac flux in that branch will then be *zero*, thus eliminating the need for this magnetic branch. Consequently, the two I pieces of the core can be removed (Fig. 3.2b), resulting in a smaller, lighter structure with less core loss, but maintaining the same energy storage capability and the same copper loss as before the removal. The removal of the I pieces leads directly to the removal of associated core

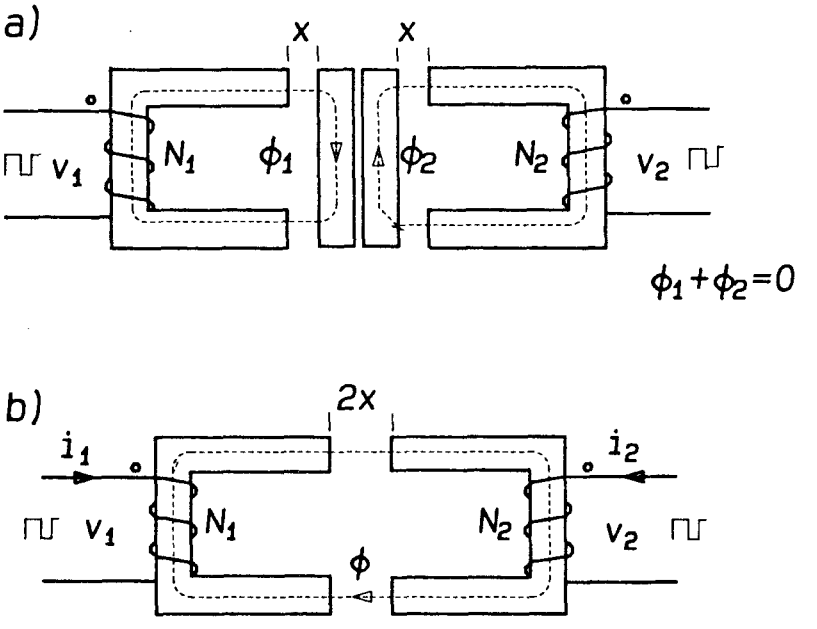

Figure 3.2: Saving core material and reducing core loss by coupling two inductors into one structure.

losses, thereby increasing the efficiency of the structure in addition to reducing the size and weight.

Example 2

Figure 3.3a shows two identical inductors in series. If the two cores are stacked together and the same number of turns is wound on this stacked core (Fig. 3.3b), the inductance and the energy storage capability (also core loss) will be the same as the two inductors in series; however, the total length of the copper wire is shorter, resulting in less copper weight and copper loss. Once again, both size and weight are reduced simultaneously with the increase of efficiency.

3.1.2 Magnetic Scaling Law

For a transformer, at a fixed operating frequency f_s, the maximum voltages V_1, V_2 on the primary or secondary winding that the core can support without saturation

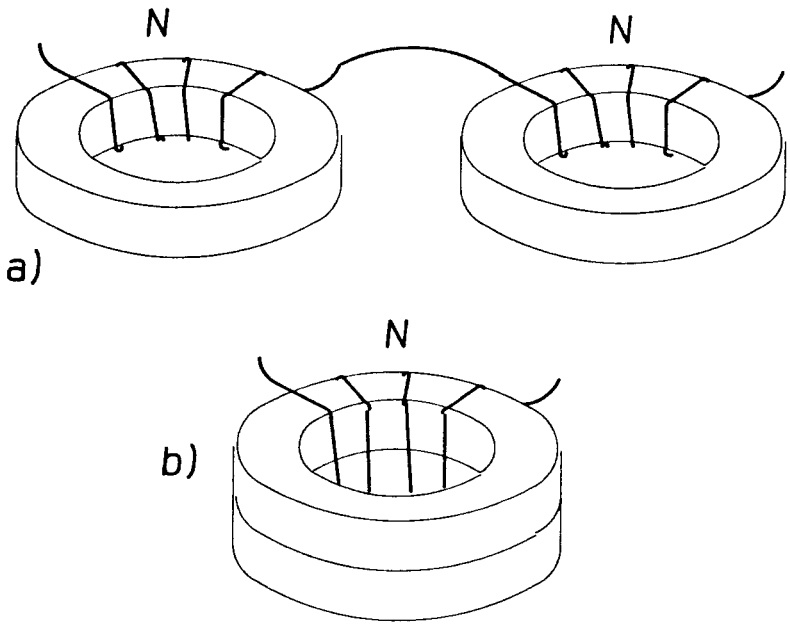

Figure 3.3: Saving copper wire and reducing copper loss by combining two inductors into one structure.

are:

$$V_1 = 4\,N_1\,B_{max}\,S\,f_s \tag{3.2}$$

$$V_2 = 4\,N_2\,B_{max}\,S\,f_s \tag{3.3}$$

where B_{max} is the maximum flux density in the core, S is the core cross section, and N_1, N_2 are the turns of each winding.

The window area W will be fully utilized when:

$$kW = \frac{1}{J}(N_1 I_1 + N_2 I_2) \tag{3.4}$$

where k is the empirical fill factor of the windings, and J is the current density in the windings.

Therefore, the power handling capability of the transformer is:

$$P = V\,I \propto kW\,S \propto l^4 \tag{3.5}$$

where l is the linear dimension of the core. However,

$$\text{volume, weight} \propto l^3 \propto P^{\frac{3}{4}} \tag{3.6}$$

If the relative copper loss $\frac{P_{Cu}}{P}$ is given instead of the current density J, the result will change a little:

$$\text{volume, weight} \propto l^3 \propto P^{\frac{3}{5}} \tag{3.7}$$

For inductors, the relations between the size (volume and weight) and the energy storage capability are the same as for transformers; that is: volume,weight $\propto (L\,I^2)^{\frac{3}{4}}$ for given current density, and volume, weight $\propto (L\,I^2)^{\frac{3}{5}}$ for given relative copper loss.

The above examples and equations show that the volume and weight of a transformer or inductor, as a function of linear dimension of the device, go up slower than the transformer power or the energy handling capability of an inductor. In other words, the transformer power density is higher when the total power being processed is larger, hence favoring a single, large power processing magnetic device over a number of smaller ones. Likewise, the energy storage density of an inductor is higher when the total energy storage is higher. This once again confirms the earlier observation that a number of inductors and transformers combined into a single magnetic structure will be more compact with higher energy storage density than separate inductors and transformers.

3.2 PERFORMANCE IMPROVEMENT

The fact that the waveforms on the inductors and transformer are the same in a Ćuk converter leads to the development of the coupled inductor version of the Ćuk converter and the integrated magnetics Ćuk converter, in which the inductors and the transformer are all coupled together in a single structure. In the experimental verification of the coupled-inductor Ćuk converter (Fig. 3.4), it was observed that if one changes

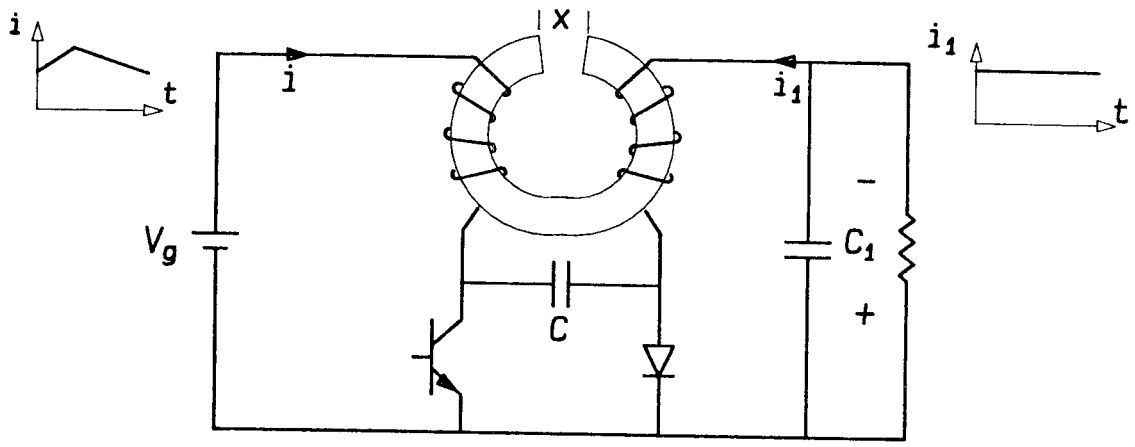

Figure 3.4: Changing the gap and number of turns of the coupled-inductors to obtain zero current ripple in one of the windings

the coupling and the turns ratio of the coupled-inductor, the switching ripple current in ether one of the windings can be adjusted to zero; In the Ćuk converter with the transformer coupled as well, both input and output current ripple can be adjusted to zero simultaneously.

In the following chapters, this *ripple reduction* or *ripple steering* effect will be discussed in detail, along with some of the second-order effects and the design considerations of some particular structures.

Chapter 4

ZERO RIPPLE CONDITIONS FOR TWO WINDING COUPLED-INDUCTORS

By properly adjusting the coupling of the inductors in the circuit of Fig. 3.1, one can even obtain zero current ripple in one of the windings. This zero ripple condition is, to the first order, a property of the coupled-inductor magnetic structure, appropriately driven by the identical voltage waveforms. Therefore, in order to zero in at the current ripple steering phenomena alone, free from the second-order effects, the switching converter itself may be eliminated, since its only role was to create identical voltage waveforms driving the two windings. Fig 4.1 then shows the coupled-inductor magnetic structure driven by two identical square-wave like voltage sources, as they were in the original switching converter circuit. Note that, unlike the two winding transformer magnetic structure, in which only one, the input or primary side is driven by the voltage source, here, in the coupled-inductor structure, both windings are driven simultaneously. Hence, in a controlled laboratory experiment configured to verify the analytical predictions of this section, the two windings should actually be driven from the common oscillator source (square wave or sine wave), as it was already been done in the past [7].

The ripple current steering phenomenon of the coupled-inductor structure and its most important practical result—zero ripple current feature—are analyzed in this section under the most idealized conditions in order to arrive at good physical grasp of the

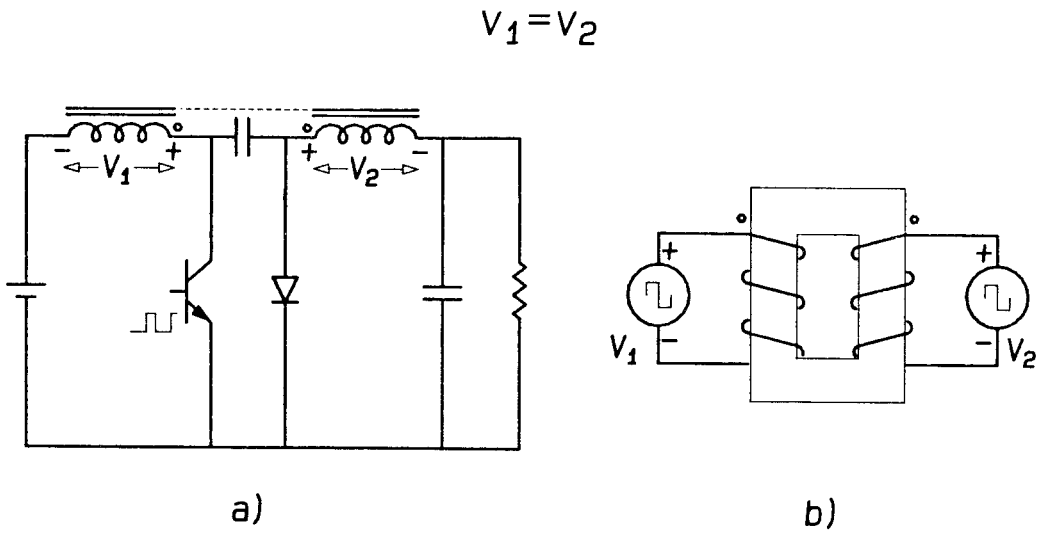

Figure 4.1: Coupled-inductors driven by a Ćuk converter (a), or two identical voltage sources (b).

problem as well as at some very basic and simple analytical zero ripple conditions. The analysis brought out by this section is very general and applicable to all switching converters in which the coupled-inductor technique may be practiced to advantage. The nonidealities brought by the switching converter and the resulting first-and second-order effects influencing the idealized zero ripple current condition are then tackled in Chapter 5.

The importance of properly understanding both qualitatively as well as quantitatively the results of this chapter cannot be underestimated, since they naturally lead toward proper generalization of the coupled-inductor configuration toward very useful and practical multi air-gap, multiple magnetic branch structures in later chapters.

The observed ripple current steering phenomenon showed in Fig. 3.4 of Chapter 3 is *independent* of the dc operating point of the switching converter (dc current in the windings) and it is only an ac phenomenon. Hence, in actual switching converters,

even under no load condition (zero dc current in both windings), the same ripple currents will be observed. Therefore, the analysis of this chapter will focus on the understanding of this ripple current steering phenomenon alone and will assume all dc currents to be zero. With respect to Fig. 4.1, voltage sources as well as corresponding winding currents are ac only, with no superimposed dc part. The effect of the dc currents present in the windings of actual dc-to-dc switching converters, in addition to the ac (ripple) currents, will be analyzed separately in later chapters.

Three distinct models of the coupled-inductor configuration are developed in this section. The equivalent circuit model derived from the coupled-inductor equations is followed by the "physical" equivalent circuit model, linking the leakage inductances to their physical leakage flux paths, and finally, the reluctance circuit model is presented. Zero ripple current condition is developed in the framework of each of the three models, and their comparative merits and drawbacks are pointed out.

4.1 SEPARATION OF DC AND AC CURRENTS

All inductors used in switching converters are carrying dc currents. As discussed in Section 2.2.3, an air gap is then required to prevent the core from saturating, The presence of the air-gap makes the flux vs. ampere-turn (ϕ vs. Ni)characteristic even more linear than it is otherwise (Fig. 2.5). In this case, following the principle of superposition on linear circuits, we can separate the ac and dc components of the currents in the windings and the fluxes in the core, and study them separately (Fig. 4.2). Only the ac components will be considered in the next few chapters. The dc conditions for the multiple winding structure obtained separately in Chapter 8 will then be combined with these ac conditions to develop a full model.

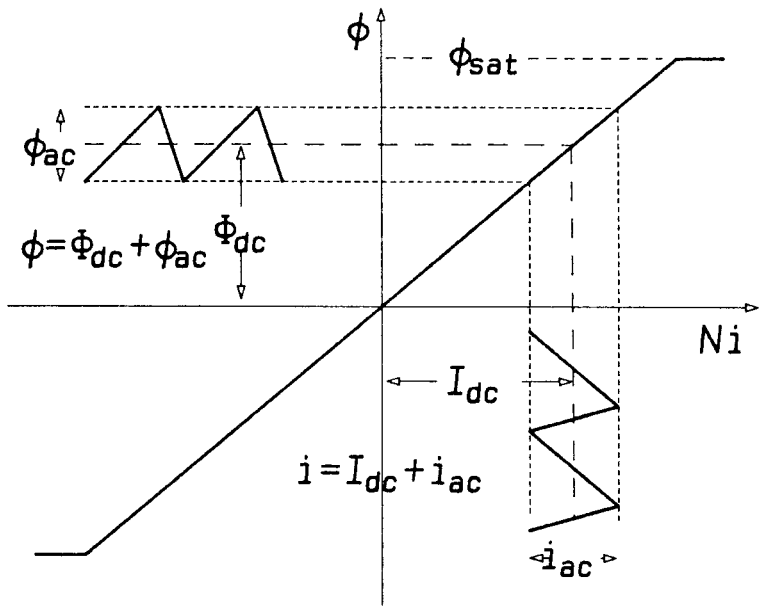

Figure 4.2: Separating ac and dc components.

4.2 USING COUPLED-INDUCTOR EQUATIONS TO FIND THE ZERO RIPPLE CONDITION

The general coupled-inductor equations are:

$$\begin{aligned} v_1 &= L_{11}\frac{di_1}{dt} + L_{12}\frac{di_2}{dt} \\ v_2 &= L_{21}\frac{di_1}{dt} + L_{22}\frac{di_2}{dt} \end{aligned} \tag{4.1}$$

where $L_{12} = L_{21} = L_M$ is the mutual inductance between the windings quantifying the effect of the change of current in one winding upon the induced voltage in the other. For the special case of the circuit in Fig. 4.1, with identical voltage waveforms, we have:

$$v_1 = v_2 \tag{4.2}$$

If the output current ripple is adjusted to zero, the additional constraint is:

$$\frac{di_2}{dt} = 0 \tag{4.3}$$

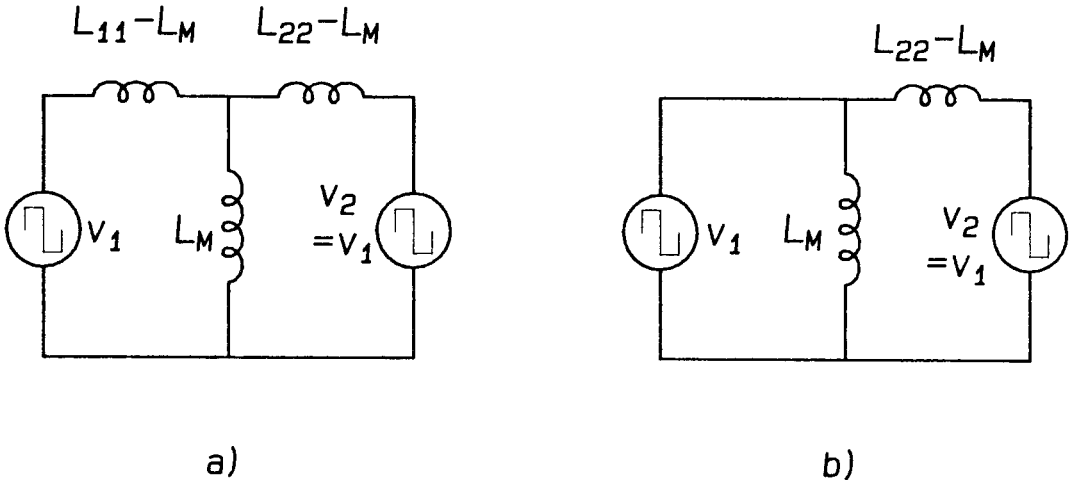

Figure 4.3: a) The three inductance model from coupled-inductor equations. b) Model for zero output ripple.

leading to a zero ripple condition from (4.1) as:

$$L_{11} = L_M \qquad\qquad L_{22} \neq L_M \tag{4.4}$$

The T-shaped three inductance equivalent circuit model of the general coupled-inductor equations of Fig. 4.1 is shown as Fig 4.3a. Under zero ripple conditions (4.4), this model simplifies to a two inductance model of Fig 4.3b.

If one conditionally calls the two inductances in series with the the input and output of the model in Fig 4.3a as "leakage" inductances, it will appear that the zero output ripple current is obtained when the input leakage is reduced to zero. Note that although this result (4.4) is correct quantitatively, it may lead to some qualitatively wrong and misleading interpretations as will be seen in later parts of this section.

4.2.1 Writing the Zero Ripple Condition Using the Coupling Coefficient k

Substituting the zero ripple condition (4.4) into the definition of the coupling coefficient k (2.9) gives:

$$k \equiv \frac{L_M}{\sqrt{L_{11}\,L_{22}}} = \frac{L_{11}}{\sqrt{L_{11}\,L_{22}}} = \sqrt{\frac{L_{11}}{L_{22}}} \equiv n \tag{4.5}$$

The zero ripple condition can now be written in a compact form as:

$$k = n \tag{4.6}$$

where n is called an effective turns ratio, because it is very close, although not equal to the actual turns ratio N_1/N_2, as seen from the following approximations:

$$n \equiv \sqrt{\frac{L_{11}}{L_{22}}} = \sqrt{\frac{N_1^2(L_{l_1} + L_M)}{N_2^2(L_{l_2} + L_M)}} \approx \frac{N_1}{N_2} \tag{4.7}$$

valid when the leakages L_{l_1} and L_{l_2} are small compared to the mutual inductance L_M.

It is interesting to point out that the expression (4.6) for zero ripple condition was derived at the very beginning of the coupled-inductor development [2]. It was originally called "the matching condition" and has been considered all along the simplest, most compact and most revealing interpretation of the zero ripple phenomenon. However, this last attribute must now be taken away. Although the matching condition (4.6) is perfectly correct quantitatively (after all, it has been confirmed experimentally in earlier work as in [1]), it is actually very much misleading on a qualitative basis. From the definition of the coupling coefficient (2.7) and the effective turns ratio n, it seems that both sides of the matching condition (4.6) involve the mutual inductance L_{12} as well as the primary and secondary leakage inductances L_{l_1} and L_{l_2}. However, as will be seen next when the "physical" circuit model of the coupled-inductors is used, this qualitative picture is not quite correct.

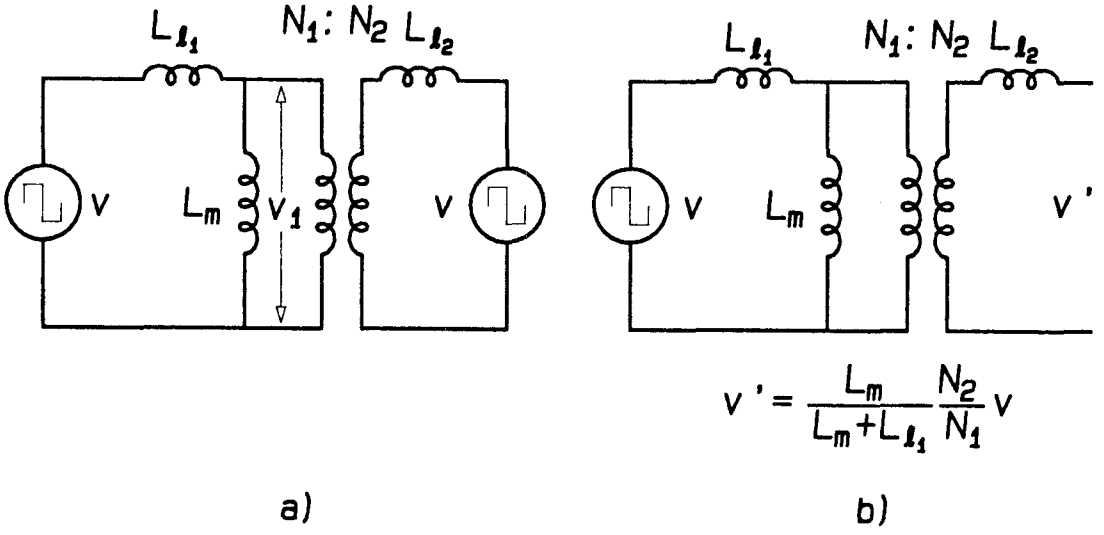

Figure 4.4: a) Circuit model of a coupled-inductor structure. b) If $v' = v_2$, there will be no ripple in N_2 when v_2 is reconnected.

4.3 USING THE CIRCUIT MODEL TO FIND THE ZERO RIPPLE CONDITION

Another circuit model of the two-winding coupled-inductor structure is shown in Fig. 4.4a. In this model the actual number of turns in the primary N_1 and secondary N_2 windings is an integer part of the model representing a ideal transformer with the turns ratio N_2/N_1. Often this coupled-inductor model is referred to also as a "physical" model, since the corresponding leakage inductances L_{l1} of the primary and L_{l_2} of the secondary windings do correlate directly to the actual leakage fluxes of the windings.

The existence of the zero ripple current at the secondary side can now be easily understood. Assume, for the moment, only the primary side is driven by a rectangular or square-wave like ac waveform, and the secondary winding is disconnected from the voltage source as in Fig. 4.4b. The primary leakage inductance L_{l_1} and the magnetiz-

ing inductance L_m form an effective inductive divider, so that the voltage v_1 on the magnetizing inductance retains the same waveform but is reduced in magnitude to:

$$v_1 = \frac{L_m}{L_{l_1} + L_m} v \tag{4.8}$$

However, if the turns ratio N_2/N_1 is just right to step up the magnitude v' of this waveform on the secondary side, to its original value v, zero ripple current is obtained. Namely, if now the external drive is reapplied to the secondary winding, the net voltage on the secondary leakage inductance L_{l_2} is zero throughout the switching period. The secondary leakage inductance L_{l_2} can be arbitrary, but as long as it is finite and not zero (physically it can not be zero), from $L_{l_2}\, di_2/dt = 0$, it follows that di_2/dt must be zero; hence, zero ripple current. Of course, the ripple current at the output side does not "vanish," as if it may appear, but has been merely shifted to the input winding which now carries all the ripple current. One can express these conditions in equation form:

$$v' = \frac{N_2}{N_1} v_1 = \frac{N_2}{N_1} \frac{L_m}{L_{l_1} + L_m} v \tag{4.9}$$

which for $v' = v$, gives the zero ripple condition:

$$\frac{N_1}{N_2} = \frac{L_m}{L_{l_1} + L_m} \tag{4.10}$$

Let us now compare this result with the previous matching condition (4.6). This result should not be understood only as another very simple quantitative relationship, it is also very important to understand this result qualitatively. The important point here is that the zero ripple current condition on the secondary side is *independent* of the leakage inductance L_{l_2} on the secondary side. The inductive divider ratio has to be matched to the *actual* turns ratio N_1/N_2 and not to some effective turns ratio n. It is now also easy to understand qualitatively why the output, or secondary ripple current, can be adjusted to zero by adjusting the air-gap. Note that the variation of the air-gap

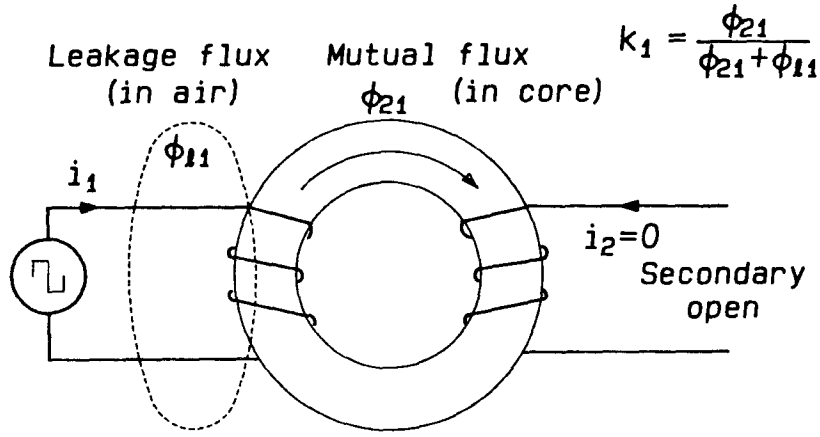

Figure 4.5: Definition of k_1.

will effectively change the mutual flux and magnetizing inductance L_m, but will leave the leakage flux and leakage inductance L_{l_1} essentially unchanged. Therefore, the inductive ratio as defined in (4.10) may be changed over the wide range from zero to approximately 1. When the air-gap is adjusted so that the inductive divider ratio matches the winding turns ratio N_1/N_2, zero ripple current in the secondary side is obtained. Note also that for zero ripple criteria (4.10) only the ratio of turns is important and not their actual absolute values. Of course, the increase of the number of turns will lead to an increase of the input inductance, and therefore will result in a reduced ripple current on the input or primary side.

4.3.1 Writing the Zero Ripple Condition Using Coupling Coefficients k_1, k_2

As pointed out in Chapter 2, instead of using the customary coupling coefficient k, for the magnetic structures such as transformers and coupled-inductors, where leakages play a major role in the performance, we find it much more appropriate to utilize the

coupling coefficients k_1 and k_2 defined separate for each winding.

Recall from section 2.1.2, the coupling coefficient k_1 is defined when the secondary current i_2 is zero ($i_2 = 0$) (see Fig. 4.5), which is the same as the zero ripple condition on the secondary side. Hence, the new matching condition is:

$$k_1 \equiv \frac{\phi_{21}}{\phi_{11}} = \frac{\phi_{21}}{\phi_{21} + \phi_{l_1}} \tag{4.11}$$

It only remains to express these ratios of fluxes in terms of turns ratios as follows. Since for the zero ripple condition, $i_2 = 0$, the voltages on the windings can be found from Faraday's Law:

$$\begin{aligned} v_1 &= N_1 \frac{d\phi_{11}}{dt} \\ v_2 &= N_2 \frac{d\phi_{21}}{dt} \end{aligned} \tag{4.12}$$

For the identical drive voltages on the two windings ($v_1 = v_2$), integrating (4.12), we get:

$$\begin{aligned} \phi_{11} &= \frac{\phi_0}{N_1} \\ \phi_{21} &= \frac{\phi_0}{N_2} \end{aligned} \tag{4.13}$$

where $\phi_0 = \int v\, dt$ is common for both equations. Note that here we are interested only in the ac properties (ripple currents); hence, the integration constants corresponding to the dc flux Φ_{dc} is neglected.

Substitution of (4.13) in (4.11) results in a new matching condition as:

$$k_1 = \frac{N_1}{N_2} \tag{4.14}$$

Note a very simple form of this new matching condition in which for zero ripple condition on the secondary side, only the coupling coefficient of the primary side plays a significant role. The secondary side enters the equation only through the actual number of turns N_2. It is interesting now to compare this matching condition against the one derived previously in (4.6).

4.3.2 Comparison of the Matching Conditions

The matching condition (4.6) was derived early in the coupled-inductor method development [1][2]. For quite a long time, it was considered as the most compact and most revealing form to express the zero ripple condition. In fact, for a while it was thought that there was no better way to express it. However, with the development of the new zero ripple condition (4.14), it turns out that the old matching condition (4.6), although *quantitatively correct*, is also *qualitatively misleading*, as can be seen from comparison of their analytical expressions:

$$\begin{aligned} &\text{old:} \quad k = n \quad \Rightarrow \quad \frac{L_{21}}{\sqrt{L_{11}L_{22}}} = \sqrt{\frac{L_{11}}{L_{22}}} \\ &\text{new:} \quad k_1 = \frac{N_1}{N_2} \quad \Rightarrow \quad \frac{N_1}{N_2}\frac{L_{21}}{L_{11}} = \frac{N_1}{N_2} \end{aligned} \tag{4.15}$$

where various coupling coefficients and effective turns ratio n are expressed in turns of the inductances. For example, since $k = \sqrt{k_1 k_2}$, from the old matching condition it seems that coupling coefficients of both primary winding k_1 and secondary winding k_2 are important which is *not true*, since only the primary winding coupling coefficient k_1 is needed. In fact, even such a cumbersome language construction as "the effective turns ratio" was needed to describe the right-hand side of the old matching condition. It got its name "effective" since it is not equal to the actual turns ratio, although for small leakages it is in very close approximation. Consequently, the old matching condition implies that all parameters of both primary and secondary sides are needed for correct qualification, whereas the new matching condition involves the primary side alone, with the only secondary parameter needed is the actual number of turns N_2. Although the two expressions lead to different qualitative interpretations, they are quantitatively identical. That is, when both sides of the new matching condition are multiplied by the same factor

shown below in the brackets, the old matching condition can be obtained:

$$\left(\frac{N_2}{N_1}\sqrt{\frac{L_{11}}{L_{22}}}\right) k_1 = \frac{N_1}{N_2}\left(\frac{N_2}{N_1}\sqrt{\frac{L_{11}}{L_{22}}}\right) \tag{4.16}$$

This new matching condition will be adapted for all future coupled-inductor analysis, since not only does it correctly express zero ripple condition quantitatively, but its qualitative interpretation leads to a satisfying physical understanding.

4.4 USING THE RELUCTANCE MODEL TO FIND THE ZERO RIPPLE CONDITION

Although the circuit model is very useful, the nature of the leakage flux distribution, which is the key to understanding the coupled-inductor structures, is even better understood after the reluctance model is introduced. The reluctance model introduces the direct physical correlation with various flux paths and points us toward better ways of synthesizing the new coupled-inductor magnetics structures, as will be demonstrated in later chapters.

The coupled-inductor structure and its reluctance models are shown in Fig. 4.6. In the models of Fig. 4.6b and c, $\mathcal{R}_m$ is the reluctance of the main magnetic coupling flux path, which is essentially the reluctance of the air gaps, since the reluctance of the magnetic material may be neglected. The reluctances $\mathcal{R}_{l_1}$ and $\mathcal{R}_{l_2}$ model the leakage flux paths of the two windings. As before, this reluctance model can be separated into an ac model and a dc model, with only the ac model analyzed here. When the current ripple in the secondary winding N_2 is adjusted to zero, then $i_2 = 0$, and the ac model can be simplified to that of Fig. 4.6c. From this simplified model a loop equation and a node equation may be written as:

$$\begin{aligned} &\text{loop equation} && \mathcal{R}_m\phi_m = \mathcal{R}_{l_1}\phi_{l_1} \\ &\text{node equation} && \phi = \phi_m + \phi_{l_1} \end{aligned} \tag{4.17}$$

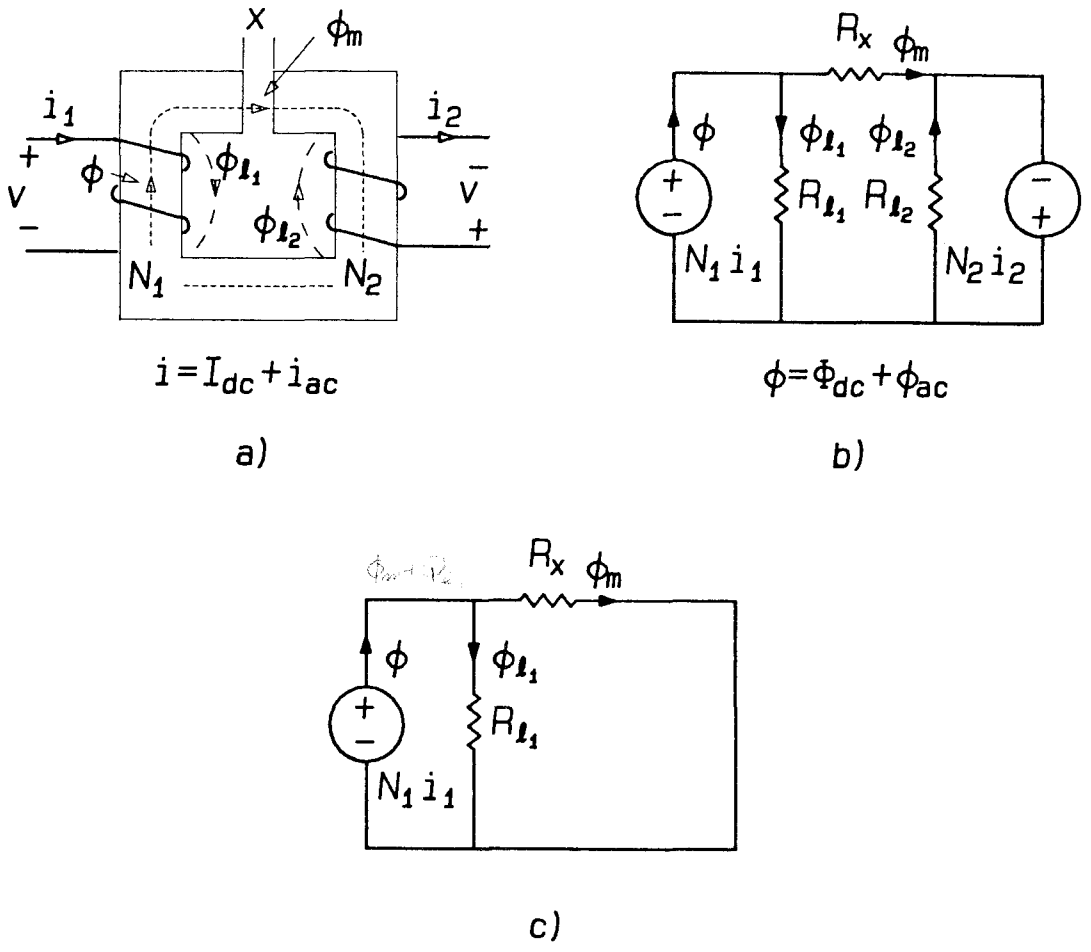

Figure 4.6: a) A coupled-inductor structure. b) The reluctance model of the coupled-inductor structure. c) The ac model for zero current ripple in the secondary winding.

Also, from Faraday's law:

$$\begin{aligned} N_1 \phi &= \int v\, dt = \phi_0 \\ N_2 \phi_m &= \int v\, dt = \phi_0 \end{aligned} \tag{4.18}$$

The solution of these equations gives the zero ripple condition as:

$$\frac{\mathcal{R}_{l_1}}{\mathcal{R}_m} = \frac{N_2}{N_1} - 1 \tag{4.19}$$

Note again that in agreement with the previous results, the leakage reluctance of the secondary does not affect the zero ripple condition. This is, of course, apparent from the model of Fig. 4.6c, in which the reluctance $\mathcal{R}_{l_2}$ is eliminated by shorting out the voltage source $N_2 i_2$, when $i_2 = 0$.

4.5 AGREEMENT OF THE THREE METHODS

In this section the analytical expressions for zero ripple condition originating from different models are shown to be equivalent.

4.5.1 Reluctance Model vs. Circuit Model

The zero ripple condition for the reluctance model (4.19) can be written as:

$$\frac{N_1}{N_2} = \frac{\mathcal{R}_m}{\mathcal{R}_{l_1} + \mathcal{R}_m} \tag{4.20}$$

In the circuit model the magnetizing and primary leakage inductances are:

$$L_m = \frac{{N_1}^2}{\mathcal{R}_m} \qquad\qquad L_{l_1} = \frac{{N_1}^2}{\mathcal{R}_l} \tag{4.21}$$

substitute into (4.20) gives:

$$\frac{N_1}{N_2} = \frac{L_m}{L_m + L_{l_1}} \tag{4.22}$$

which is the zero ripple condition for the circuit model.

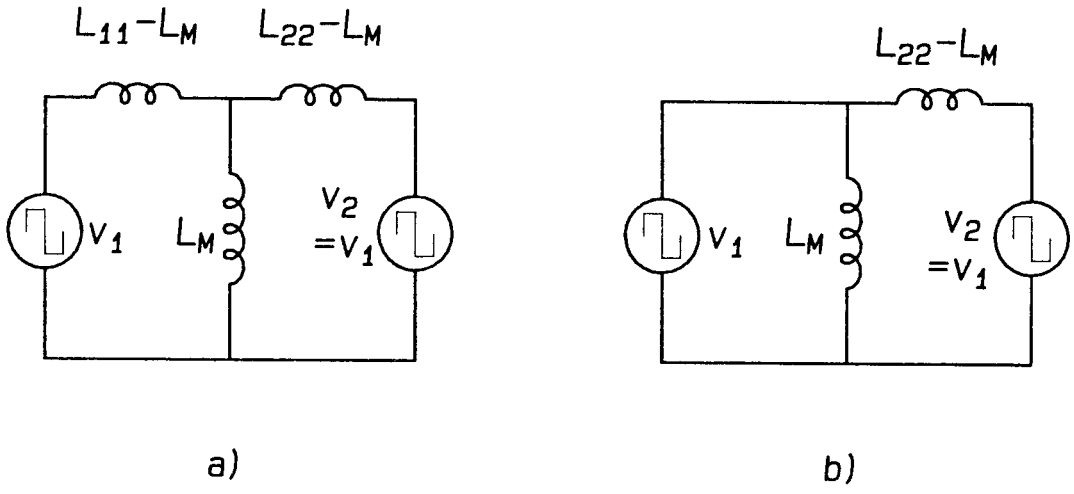

Figure 4.7: a) Another form of the circuit model. b) Simplified model for zero output ripple.

4.5.2 Circuit Model vs. Coupled-Inductor Equations

Using (2.24), (2.25), we can also draw the circuit model shown in Fig 4.4a as Fig 4.7a, where:

$$\begin{aligned} L_{11} - L_M &= L_{l_1} + \left(1 - \frac{N_2}{N_1}\right) L_m \\ L_{22} - L_M &= L_{l_2} + \left(\frac{N_2}{N_1}\right)\left(\frac{N_2}{N_1} - 1\right) L_m \\ L_M &= \frac{N_2}{N_1 L_m} \end{aligned} \tag{4.23}$$

The zero ripple condition for the circuit model (4.10) can be written as:

$$\frac{N_2}{N_1} = 1 + \frac{L_{l_1}}{L_m} \tag{4.24}$$

Under the zero ripple condition, the inductance on the left in Fig. 4.7a ($L_{11} - M$) will become zero and the circuit can be simplified as Fig. 4.7b. From this circuit we have the

zero ripple condition as:

$$L_{11} = M \qquad\qquad L_{22} \neq M \tag{4.25}$$

which is the zero ripple condition for the coupled-inductor equations.

4.6 HARDWARE IMPLICATION OF THE LEAKAGE INDUCTANCE

The zero ripple condition shows that the leakage inductance of the input winding (the winding which is carrying the ripple) must be well controlled; also, as will be shown in the next chapter, to obtain low residual ripple and low sensitivity, at least one winding must have relatively high leakage. Therefore, the techniques used for transformer winding, which, with the objective to obtain the lowest leakage, can no longer be used for the coupled-inductors. Instead, the opposite objective of *high leakage inductance* is desired. There are, however, several ways to obtain a well-controlled, relatively high leakage inductance.

4.6.1 Using External Leakage Inductor

The most straightforward and obvious method to achieve high leakage inductance is to wind low leakage, tightly coupled-inductors, and then use a separated inductor in series with the input winding as the leakage inductance as illustrated in Fig. 4.8. One advantage of this method is that the addition of an external inductor allows an easy way to control exactly the right amount of the primary leakage inductance needed to achieve zero ripple condition as quantified earlier in this chapter. This would have been much more difficult to achieve with the intrinsic, built-in leakage inductance of the primary inductance itself, which is rather elusive and hard to determine in just the right amount needed for zero ripple. On the other hand, this method seems to defeat the original

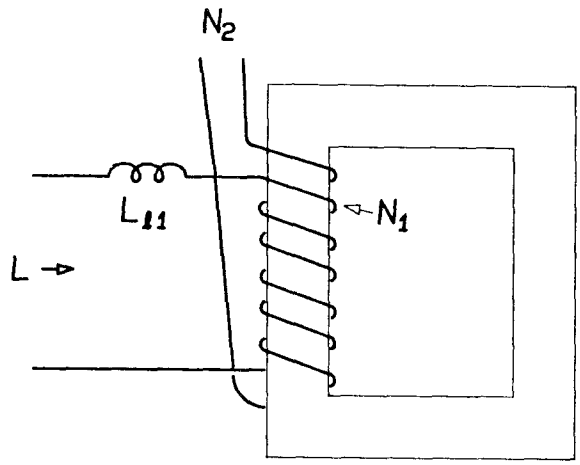

Figure 4.8: Leakage inductance is provided by an external inductor added to the primary of the tightly coupled-inductor structure

objective of coupling the inductors, that is, the reduction of the number of magnetic components and their overall size and weight. Although this method makes it relatively easy to design for zero ripple, it involves another magnetic element which is directly contradictory to our basic objectives of magnetic integration. Hence, the more elegant alternatives should be pursued further first.

4.6.2 Using a Leakage Magnetic Path in the Magnetic Structure

Instead of building a separate inductor complete with an additional magnetic core and winding, a simpler alternative for us is to build an additional magnetic branch for the leakage flux path into the already existing coupled-inductor structure as illustrated in Fig. 4.9a. In this way, the need for an additional winding is eliminated, and yet the advantages of a direct and easy control for zero ripple current adjustment are still retained. If we assume that there are no other leakages in this structure, the reluctance

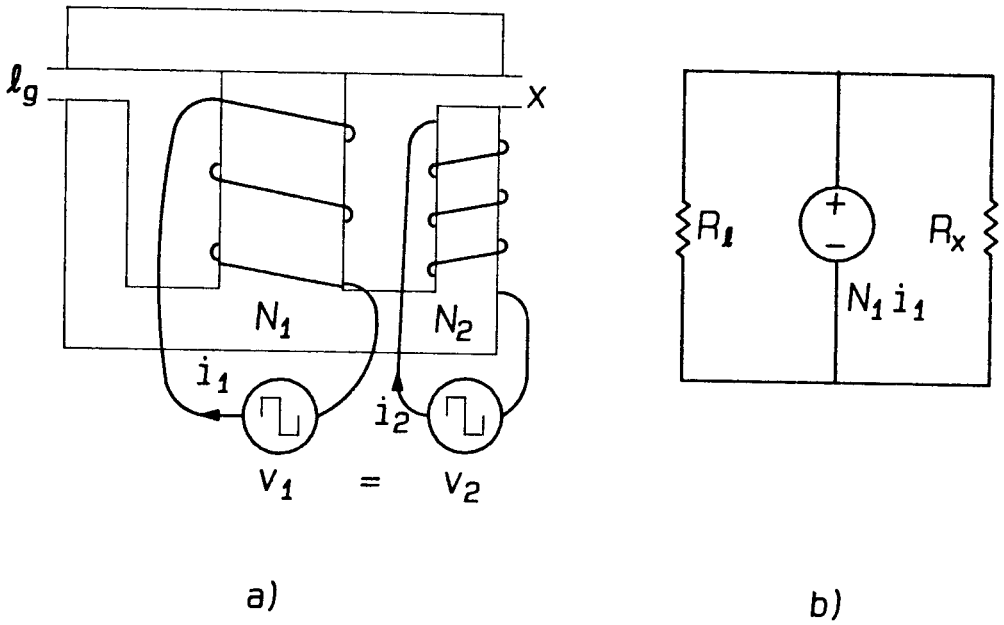

Figure 4.9: A high leakage coupled-inductor structure (a), and the reluctance model for zero ripple in N_2 (b).

model for zero output current ripple is as in Fig. 4.9b. If the cross sections S of the outer legs are the same, then:

$$\mathcal{R}_x = \frac{x}{\mu_0 S} \qquad \mathcal{R}_l = \frac{l_g}{\mu_0 S} \tag{4.26}$$

where l_g is the air-gap of the leakage flux path. The zero ripple condition shown in (4.19) after simplification, can now be rewritten as:

$$\frac{x}{l_g} = \frac{N_2}{N_1} - 1 \tag{4.27}$$

For the special case where the two gaps are the same ($x = l_g$), the zero ripple condition is obtained when:

$$N_2 = 2\,N_1 \tag{4.28}$$

Note that the addition of another magnetic branch did not require any special magnetic core structure. As seen in Fig. 4.9, the standard EI-core is suitable for this application, although it is used in a somewhat unconventional way: the outer legs are gaped instead of the center leg, as in usual single inductor case.

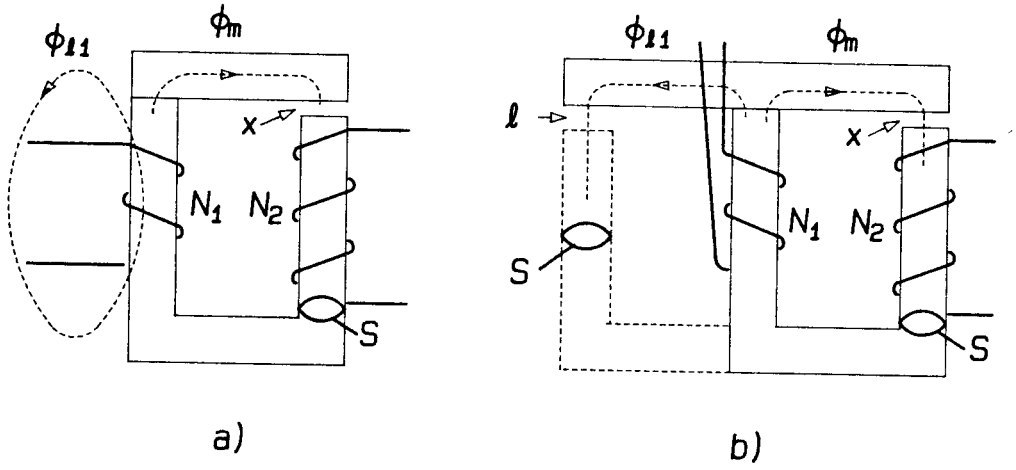

Figure 4.10: Leakage flux ϕ_l of the winding (a),and its equivalent flux in an imaginary core with cross section S, and air-gap l .

After the success of this approach, one is encouraged to ask:

Could the ripple be well controlled even without the addition of an extra magnetic branch? In other words, can one easily control the ripple current by using the original structure with only two windings and one physical magnetic flux path?

The answer to this question is affirmative, as demonstrated in this section qualitatively and fully supported quantitatively in later chapters and the appendix.

4.6.3 Using the Leakages of the Windings Only

Let us now eliminate even the extra "leakage" magnetic branch of Fig. 4.9a and reduce the magnetic core to just a standard UI-core, with two windings placed on opposite legs as shown in Fig. 4.10a. An air-gap is also introduced in the leg carrying the

winding N_2. The winding N_1 will still have a substantial leakage flux ϕ_{l_1} associated with it. In this case, this leakage flux is not nicely contained in the magnetic branch as it was in the previous case, but it is scattered through the surrounding air space. Nevertheless, one *can measure* the leakage inductance L_l associated with it and calculate an effective leakage reluctance $\mathcal{R}_l$ from

$$\mathcal{R}_l = \frac{N_1^2}{L_l} \tag{4.29}$$

It is now not difficult to imagine an equivalent EI-core, in which the *same leakage flux* ϕ_{l_1} is now contained in a well defined extra magnetic branch (shown in dashed lines in Fig. 4.10b) with a cross section S and an air-gap l.

From the geometry of this equivalent leakage flux path and the fact that the air-gap reluctance dominates its total reluctance, we have:

$$l \equiv \mathcal{R}_l \mu_0 S \tag{4.30}$$

where l is now introduced here for the first time and given a name "leakage parameter."

Note that despite relatively wide changes of the actual physical air-gap of the UI-core of Fig. 4.10a, the corresponding leakage flux ϕ_0 remains essentially the same, since its flux pattern in the air is hardly disturbed by the air-gap change. This will in turn, from (4.29) and (4.30), result in a relatively constant $\mathcal{R}_l$ and eventually constant leakage parameter l. Consequently, this leakage parameter l can be utilized somewhat like a thumb-print to characterize the particular core of given geometry with respect to its leakage flux properties.

When this leakage parameter is well characterized and evaluated for a number of cores of different shapes and geometries as documented in Appendix A, it could be used in a design with just the right amount of leakage inductance needed for zero ripple performance built in. The beauty of it, of course, is that this time the leakage comes free, since neither extra winding nor extra cores are needed. It seems that the extra effort

needed to fully understand and characterize this leakage parameter will be worthwhile, since the big payoff in ultimate design simplicity and performance could be achieved, as demonstrated in later chapters.

Chapter 5

SENSITIVITY AND RESIDUAL RIPPLE

It may now seem rather surprising that, despite the apparent and demonstrated advantages (possible order of magnitude improvement in ripple currents and reduced size and weight), the coupled-inductor method was largely ignored and very rarely implemented in the past. The following are the key reasons.

1. Perceived Sensitivity of the Design

Although a very convincing laboratory demonstration with a variable air-gap [1] unquestionably proved the existence of zero-ripple current condition, it also backfired, since many who saw the demonstration at the conference exhibits envisioned that a very fine "tuning" of the air-gap was needed to achieve this condition. Hence, the question of the sensitivity of the ripple current to the change of the air-gap and turns ratio was raised.

2. Possibility of Having Ripple Currents Even Larger than with the Equivalent Separate Inductors

When the turns ratio N_2/N_1 in Fig. 4.4 in the last chapter is increased past the point when zero ripple is obtained, the output ripple current reverses polarity and a "negative" ripple current is obtained as observed in Fig. 5.1c. Thus, not only the most desirable zero-ripple case (Fig. 5.1a) or still somewhat improved balanced ripple current case (Fig. 5.1b) can be obtained, but even this highly undesirable negative ripple current may be practically possible. Note that in that case the input current ripple has to be even

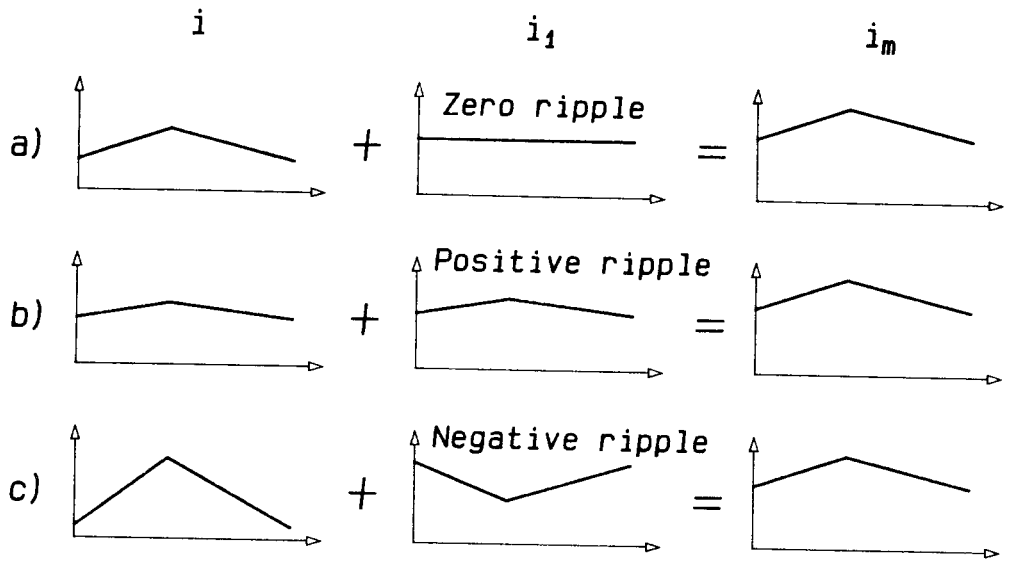

Figure 5.1: Three salient ripple current cases: a) Zero ripple on the output. b) Balanced ripple current. c) "Negative" ripple current on the output.

larger than before the coupling in order to compensate for the "negative" ripple current in the output. In fact, as seen in Fig. 5.1, in all three cases the magnitude of the the magnetizing current i_m is identical, despite the changes of the turns ratio. This further reinforces our qualitative understanding of the ripple-shifting feature, which maintains the sum of the two ripple currents as a constant independent of the turns ratio change.

Consequently, the coupled-inductor structure may, under certain circumstances, result in even much larger ripple currents on both windings (Fig. 5.1c) than what they would be if the same windings were uncoupled and made into separated inductors. This is true especially when a high sensitivity, relatively complex multiple winding structure with a single common air-gap is utilized, as was the case in almost all coupled-inductor applications in the past.

3. Complex Winding Arrangement

In most applications in the past, the coupled-inductor winding configuration directly imitated that of the transformer, often resulting in a configuration even more elaborate and complicated than the transformer itself. As a result, the cost of winding the combined structure often exceeded that of the separate inductors. In addition, this winding configuration also gave high sensitivity of the ripple current to small changes in the winding configurations.

However, once the source of these problems was correctly understood, the coupled-inductor magnetic core configuration and winding technique can be selected which completely eliminates all of the above problems simultaneously.

The importance of the sensitivity issue cannot be over-emphasized. It is easy to design a coupled-inductor converter (or almost anything) and make one or two prototypes. However, to be able to go into mass production, the design has to be relatively insensitive to unavoidable tolerances in the manufacturing process. In this chapter, the sensitivity of the coupled-inductor will be studied, together with the method of estimating and reducing the residual ripple and sensitivity. The conclusion is: The conventional method of winding a transformer—trying to get the leakages as low as possible—is *not* the way to wind coupled-inductors for reducing switching ripple.

5.1 MODELS FOR SENSITIVITY AND RESIDUAL RIPPLE CALCULATION AND THE IMPORTANCE OF HIGH LEAKAGE

The zero ripple current condition derived in Chapter 4 is:

$$\frac{N_1}{N_2} = k_1 = \frac{L_m}{L_{l_1} + L_m} \tag{5.1}$$

where k_1 is the coupling coefficient of the primary winding.

This zero ripple condition is derived under the assumption of identical drive

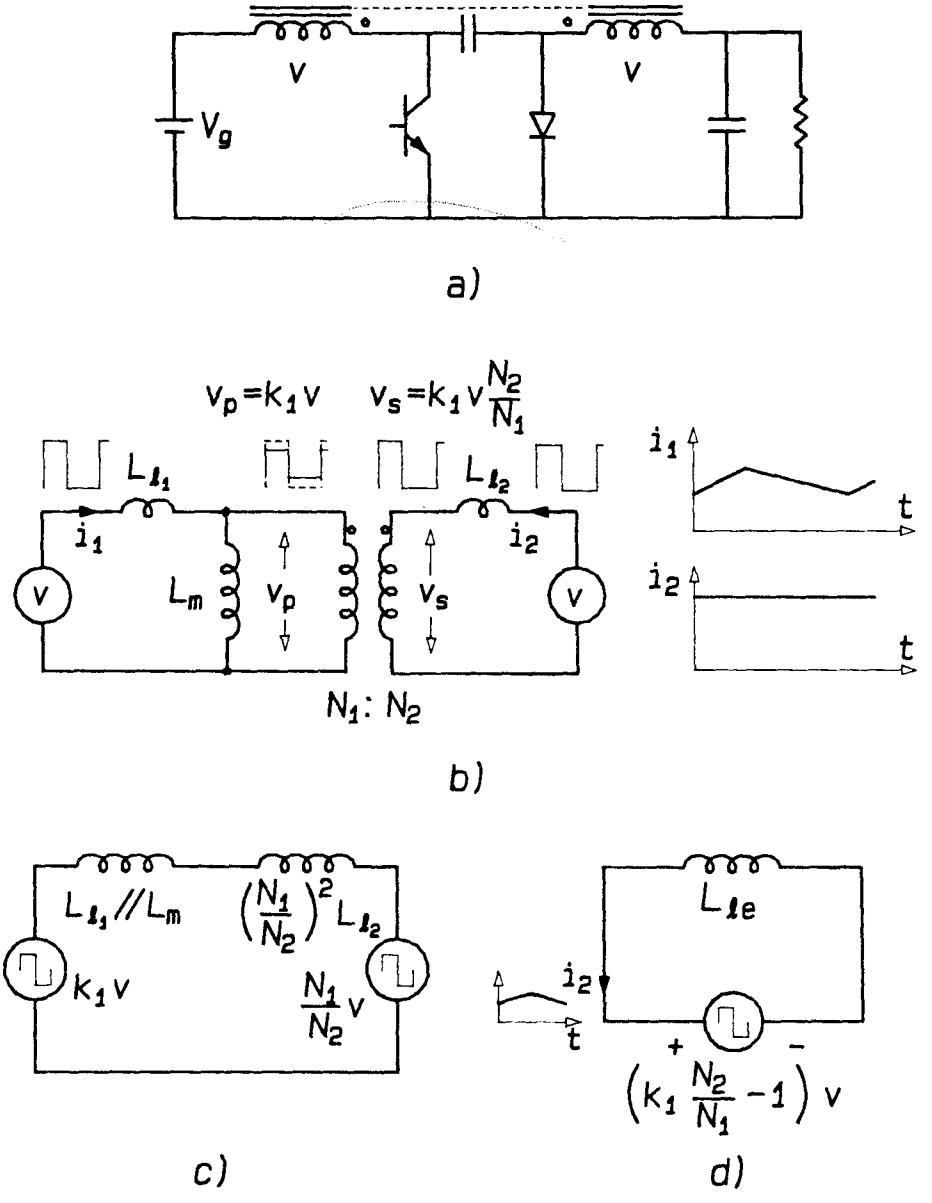

Figure 5.2: a) A coupled-inductor Ćuk converter. b) The circuit model of the two winding coupled-inductors to obtain zero ripple in N_2. c) The equivalent circuit of the coupled-inductors. d) The model used for sensitivity and residual ripple calculation.

voltage waveforms. However, in the real switching converter of Fig. 5.2a, the finite energy transferring capacitance, the losses in the converter and the inductor windings themselves, would result in a slight difference in the drive voltage waveforms across the two windings. Consequently the resulting differential voltage will lead to a small residual ripple current. More importantly, due to the discrete nature of the turns ratio N_2/N_1 adjustment, and the errors in the air-gap thickness, the zero ripple condition itself cannot be perfectly met. How can this residual ripple current and also the sensitivity of the ripple current to the errors in the air-gap and turns ratio be reduced? The answer to this becomes obvious when the coupled-inductor model of Fig. 5.2b is simplified to the one shown in Fig. 5.2c and d. Note that the mismatch in the equivalent voltages in Fig. 5.2c (either due to the matching condition mismatch or due to the difference between the two initial driving voltage waveforms) will appear directly across an equivalent inductance (Fig. 5.2d), which is a series connection of the appropriately reflected input and output leakage inductances. This equivalent leakage inductance is calculated to be:

$$\begin{aligned} L_{l_e} &= \left(\frac{N_2}{N_1}\right)^2 (L_m \parallel L_{l_1}) + L_{l_2} = \left(\frac{L_{l_1} + L_m}{L_m}\right)^2 (L_m \parallel L_{l_1}) + L_{l_2} \\ &= \frac{L_m + L_{l_1}}{L_m} L_{l_1} + L_{l_2} \end{aligned} \tag{5.2}$$

However, even in high leakage coupled-inductors, the leakage inductances are usually still small compared to the magnetizing inductance L_m ($< 30\%$), the equivalent leakage inductance can be written as:

$$L_{l_e} \approx L_{l_1} + L_{l_2} \tag{5.3}$$

Practically, one does not need to and usually cannot calculate the residual ripple and sensitivity exactly, since most factors involved are of the second order. In estimating the residual ripple and sensitivity, we usually consider an accuracy within 50% acceptable. In this case, considering the secondary leakage to be in the same ballpark as the primary

leakage, we can even write:

$$L_{l_e} \approx 2\, L_{l_1} \tag{5.4}$$

The sensitivity and residual ripple of the coupled-inductor structure can be directly calculated from the above model. It is obvious that to obtain small current ripple, one would favor the magnetic configurations in which at least one of the input or output leakage inductances is large.

Therefore, contrary to the transformer configurations where, ideally, all leakage inductances should be minimized, the coupled-inductor structures to obtain zero ripple current should be chosen such that the leakage inductances are relatively large.

The coupled-inductor configurations utilized in the past were directly emulating the transformer winding and core configurations, with the exception of the single large air-gap. Thus, it should come as no surprise that both the residual ripple and the sensitivity of the ripple current to air-gap and turns ratio changes were very high, since the inherent low leakages of the tightly coupled-inductor structures led to a small equivalent series inductance in the model of Fig. 5.2d.

The following sections in this chapter will discuss the mismatch or error voltages due to variations in the coupled-inductors themselves and in the converter circuit. The resulting ripple can then be calculated from the model shown in Fig. 5.2d.

5.2 FIRST-ORDER ERRORS AND SENSITIVITY

In Chapter 4, using the reluctance model, we found the zero ripple condition to be:

$$\frac{N_1}{N_2} = \frac{\mathcal{R}_m}{\mathcal{R}_{l_1} + \mathcal{R}_m} \tag{5.5}$$

This zero ripple condition gives zero ripple on the winding N_2, and depends on the turns ratio and the ratio of the reluctances in the structure. However, the number

of turns in a winding can only be integer numbers; this will upset the turns ratio N_2/N_1, therefore changing the left-hand side of (5.5). Also, an error in the air-gap size x will change the magnetizing reluctance $\mathcal{R}_m$, thus changing the right-hand side of the equation. In both cases, the zero ripple condition is upset, and the winding N_2 will no longer have zero ripple current in it. These errors are called *first order* errors as they directly upset the zero ripple condition. At the same time, the turns ratio and the air-gap are the two factors most subject to changes in the production. Therefore, what is considered the sensitivity of the structure is actually the sensitivity of the ripple current to these changes.

5.2.1 Error Voltage Due to Turns Ratio Errors

In a inductor winding, the smallest change in the number of turns is one single turn. Therefore, the ultimate objective is to find out the ripple current change when the secondary winding is changed by a single turn.

The error voltage in Fig. 5.2d is:

$$v_{error} = \left(k_1 \frac{N_2}{N_1} - 1\right) v \tag{5.6}$$

where

$$k_1 = \frac{L_m}{L_{l_1} + L_m}$$

If the zero ripple condition is met, we will have:

$$\frac{L_m}{L_{l_1} + L_m} = \frac{N_1}{N_2} \tag{5.7}$$

and the error voltage will be zero; thus, the current ripple is zero ($i_2 = 0$). However, if the number of turns in the secondary N_2 is changed by ΔN_2, and the inductance ratio has not been adjusted to accommodate this change, the error voltage will now be:

$$v_{e_1} = \left(k_1 \frac{N_2 + \Delta N_2}{N_1} - 1\right) v = \left(\frac{N_1}{N_2} \frac{N_2 + \Delta N_2}{N_1} - 1\right) v$$

$$= \frac{\Delta N_2}{N_2} v \tag{5.8}$$

The ripple current i_2 can then be calculated by applying this error voltage across the effective leakage inductance:

$$i_2 = \frac{1}{L_{l_e}} \int v_{e_1} dt = \frac{\Delta N_2}{N_2} \frac{1}{L_{l_e}} \int v \, dt \tag{5.9}$$

We can simplify this expression by referring the output ripple to the primary current ripple i_1. The primary ripple current i_1 is:

$$i_1 = \frac{1}{L_m + L_{l_1}} \int v dt = \frac{1}{L} \int v dt \tag{5.10}$$

Using the approximation of L_{l_e} (5.4), we can write the output ripple current (5.9) as:

$$i_2 = \frac{\Delta N_2}{N_2} \frac{L_m + L_{l_1}}{L_{l_e}} i_1 \approx \frac{\Delta N_2}{N_2} \frac{L}{2\,L_{l_1}} i_1 \tag{5.11}$$

Considering that for typical high leakage coupled-inductors, $L_{l_1} \approx 20\%\, L$, for estimating the sensitivity, one can rewrite (5.11) as:

$$i_2 = 2 \frac{\Delta N_2}{N_2} i_1 \tag{5.12}$$

For a single turn change in N_2:

$$i_2/\text{Turn} = \frac{2\, i_1}{N_2} \tag{5.13}$$

Note that the ripple current is inversely proportional to the effective leakage inductance. Hence, coupled-inductors with higher leakages will give lower ripple current under a given turns ratio error and thus, lower sensitivity.

Example

Assume in the circuit shown in Fig. 5.2a that the input voltage $V_g = 15V$, duty ratio $D = 0.5$, switching frequency $f_s = 50kHz$. The primary winding of the coupled-inductors has $N_1 = 24$ turns, secondary winding has $N_2 = 30$ turns. Both primary and

secondary leakage inductances $L_{l_{1,2}}$ are $30\mu H$; and the magnetizing inductance L_m is $120\mu H$.

The drive voltage on the coupled-inductor windings is a square wave, the amplitude is the same as the input voltage:

$$v = V_g = 15V$$

The peak-to-peak input current ripple is:

$$i_1 = \frac{v}{L}\Delta t = \frac{v}{L_m + L_{l_1}}\frac{D}{f_s} = 1A$$

When the output winding N_2 is changed by one single turn, by (5.8, the change of the output ripple current is:

$$v_{e_1} = \frac{\Delta N_2}{N_2} v = 0.5V$$

This waveform of this error voltage is also a square wave. The sensitivity of the output current ripple can be found by applying the error voltage v_{e_1} onto the effective leakage inductance L_{l_e}:

$$i_2/\text{Turn} \approx \frac{v_{e_1}}{L_{l_e}}\Delta t = 80mA$$

Or we may use (5.13) to directly estimate the sensitivity:

$$i_2/\text{Turn} \approx \frac{2}{N_2} i_1 = 67mA$$

From the above results it is clear that, since adding or removing a single turn from the output winding N_2 will change the output ripple current by $\sim 70mA$, if the output ripple is originally less than half that amount, adjusting the number of turns on the coupled-inductors *will not* further reduce the output ripple. Further reducing the output current ripple will require fine-tuning the air-gap or redesigning the coupled-inductors to increase the leakage inductance, and/or increase the number of turns on the windings to reduce the sensitivity.

5.2.2 Error Voltage Due to Air-Gap Errors

The magnetizing inductance of the coupled-inductors is inversely proportional to the air-gap size, while the leakage inductance is relatively insensitive to the air-gap [8]. Therefore, a change in the air-gap Δx will change the primary coupling coefficient k_1, thus upsetting the zero ripple condition. The magnetizing inductance after the gap change is:

$$L'_m = L_m \frac{x}{x+\Delta x} = \frac{L_m}{1+\frac{\Delta x}{x}}$$

And the error voltage can be written as:

$$v_{e_2} = \left(\frac{L'_m}{L_{l_1}+L'_m}\frac{N_2}{N_1} - 1\right) v = \left(\frac{1}{1+\frac{\Delta x}{x}\frac{L_{l_1}}{L_m+L_{l_1}}}\frac{L_m}{L_{l_1}+L_m}\frac{N_2}{N_1} - 1\right) v \tag{5.14}$$

Because the turns ratio has not been changed to match the inductance change:

$$\frac{L_m}{L_{l_1}+L_m} = \frac{N_1}{N_2}$$

and when δ is small:

$$\frac{1}{1+\delta} \approx 1-\delta$$

Thus, if the air-gap change is small (5.14) can be written as:

$$v_{e_2} = \frac{\Delta x}{x}\frac{L_{l_1}}{L_m+L_{l_1}} v \tag{5.15}$$

The resulting ripple current can also be found by applying this error voltage across the effective leakage inductance.

$$i_2 = \frac{1}{L_{l_e}}\int v_{e_2} dt = \frac{\Delta x}{x}\frac{L_{l_1}}{L_m+L_{l_1}}\frac{1}{L_{l_e}}\int v dt \tag{5.16}$$

By use of (5.10) and (5.4), (5.16) can be written as:

$$i_2 \approx \frac{\Delta x}{x}\frac{i_1}{2} \tag{5.17}$$

It is interesting to notice that (5.15) suggests that the increase of the primary leakage inductance L_{l_1} will increase the error voltage under a given percentage of air-gap change, thus increasing the sensitivity of the ripple current to the air-gap change, which seems opposite to our earlier suggestion that the coupled-inductors should have relatively high leakage. However, this is not the case, since the effective leakage inductance also increases with the leakage inductances; actually, as shown in (5.17), the ripple current sensitivity will remain relatively unchanged regardless of the value of the leakage inductances. Considering the sensitivity of the ripple current to other factors (sensitivity to turns ratio, and second order effects), one will still favor coupled-inductors with relatively high leakages.

5.3 SECOND-ORDER EFFECTS

In Chapter 4 the zero ripple condition was derived under the assumption the drive voltage waveforms on both windings of the coupled-inductors are ideal and identical. However, due to the nonidealities in the waveforms on the coupled-inductors in the actual converter circuit, the two waveforms might not be exactly the same. Therefore, there will be a mismatch voltage across the effective leakage inductance in Fig. 5.2d. Because this mismatch voltage comes from the second-order parasitics in the coupled-inductors and the converter circuit, it is named "second-order " error. Unlike the first-order effects discussed in the last section, the ripple current generated by the second-order errors are generally not triangular and cannot be reduced by re-adjusting the coupled-inductors. Therefore, the ripple current generated by the second-order effects are named *residual ripple*.

5.3.1 Error Voltage Due to Inductor Copper Losses

Error Voltage Due to Inductor Copper Losses—Sinusoidal Drive Voltages

For the first look at this problem, it is assumed that the drive voltages are sinusoidal, because, it is much easier to analyze and obtain a good qualitative picture; in addition, the rectangular drive voltages, as in the converter, are composed of sinusoidal waveforms. Therefore, getting an understanding of the effects with a sine wave will serve as a good guide to the analysis with a rectangular waveform.

The circuit model of the coupled-inductors, with the copper losses in the windings and driven by two identical sinusoidal voltage sources, is shown in Fig. 5.3a. The goal is to adjust the turns ratio $n_t = \frac{N_2}{N_1}$ to obtain minimum ac current i_2 in the secondary winding. This circuit model can also be drawn as Fig. 5.3b, or as the Thevenin equivalent circuit as Fig. 5.3c. Note that in Fig. 5.3c, since the resistances of the windings R_1 and R_2 are small compared with the impedances of the leakage inductances L_{l_1} and L_{l_2}, the R_L network can be reduced to the effective leakage inductance as shown in Fig. 5.2d. Figure 5.3d shows the relation between the various voltages in the circuit.

In Fig. 5.3d, the voltage $v_{e_3} = v_1 - v_b$ is the error voltage across the R-L network, which determines the ac current i_2 in the secondary winding N_2. By adjusting the air-gap of the magnetic structure, one can change the magnetizing inductance L_m, thus changing the amplitude of v_b to adjust the error voltage to a minimum. However, since there is a phase difference between v_1 and v_b, the error voltage cannot be reduced to zero.

As shown in Fig. 5.3d, the *minimum error voltage* is obtained when v_{e_3} is perpendicular to v_b. This implies:

$$n_t = \frac{v_a}{v_b} \tag{5.18}$$

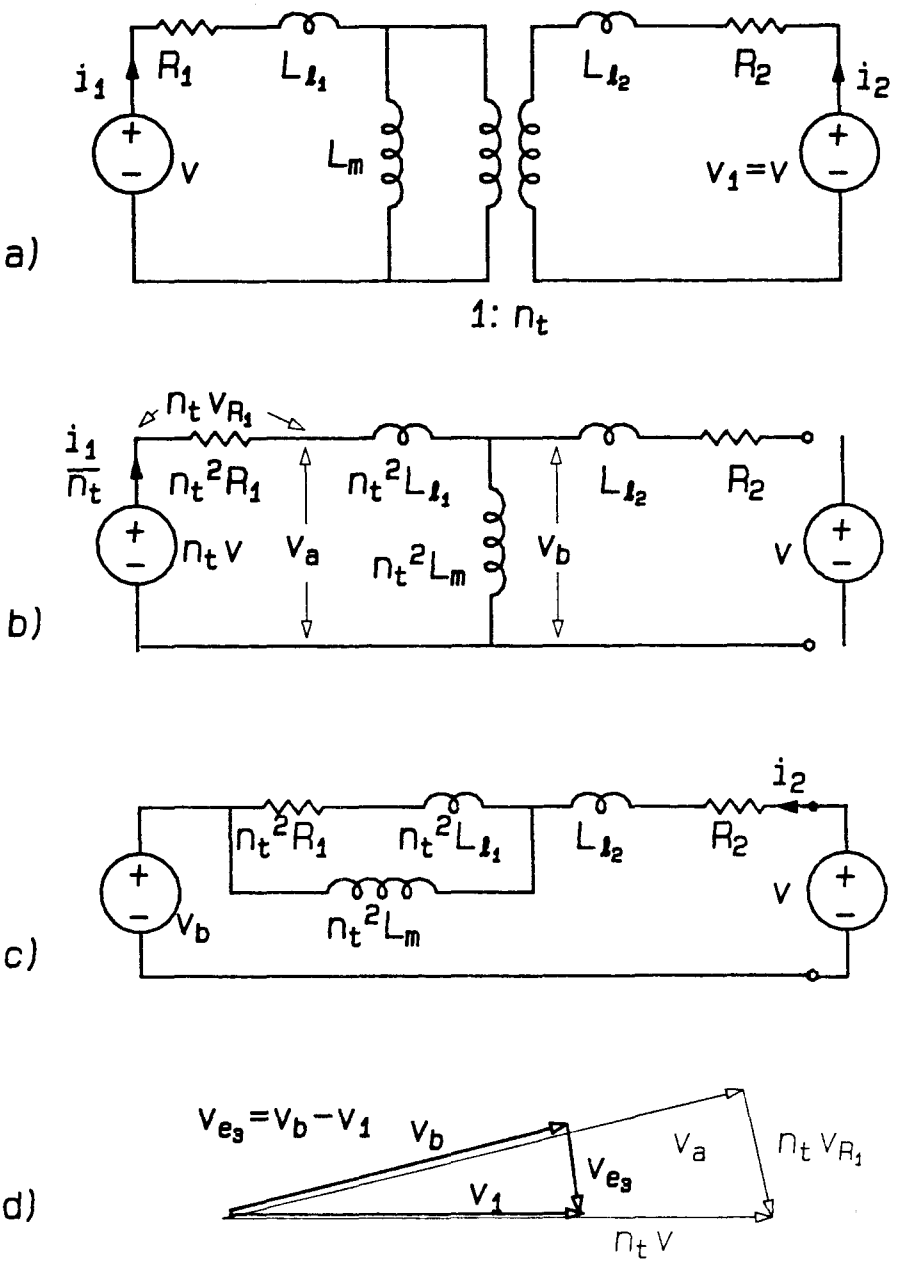

Figure 5.3: Circuit model (a) and equivalent circuits (b,c) of coupled-inductors with copper loss. d) Voltage relations in the equivalent circuits when the drive voltage is sinusoidal.

or

$$\frac{1}{n_t} = \frac{N_1}{N_2} = \frac{L_m}{L_m + L_{l_1}} \tag{5.19}$$

which is the zero ripple condition for the ideal condition. The minimum ripple voltage is:

$$v_{e_3} = \frac{R_1}{2\pi\omega L} v \tag{5.20}$$

where L is the input inductance of the coupled-inductors:

$$L = L_m + L_{l_1}$$

The ripple current i_2 is thus:

$$i_2 = \frac{v_{e_3}}{Z} \approx \frac{v}{2\pi\omega(L_{l_1} + L_{l_2})} \frac{R_1}{2\pi\omega L} \tag{5.21}$$

Again, (5.21) clearly shows that coupled-inductors with high leakage will result in lower residual ripple. It is interesting to notice that the secondary winding resistance does not affect the error voltage.

Error Voltage Due to Inductor Copper Loss—Rectangular Drive Voltages

In a real converter, the switching waveforms are rectangular. In this case, the situation can be simulated by two identical rectangular voltage sources driving the two sides of the coupled-inductors, or by just changing the two drive voltages in Fig. 5.3 to rectangular waveforms. If the copper loss is small, the minimum ripple condition will be, as in the sine wave drive case, the same as the zero ripple condition for lossless coupled-inductors (5.1):

$$\frac{N_1}{N_2} = \frac{L_m}{L_m + L_{l_1}} \tag{5.22}$$

The voltage waveforms v, v_1, v_a and v_b for the various points in Fig. 5.3 are now as shown in Fig. 5.4a,b. The waveform of the error voltage v_{e_3} is the difference between

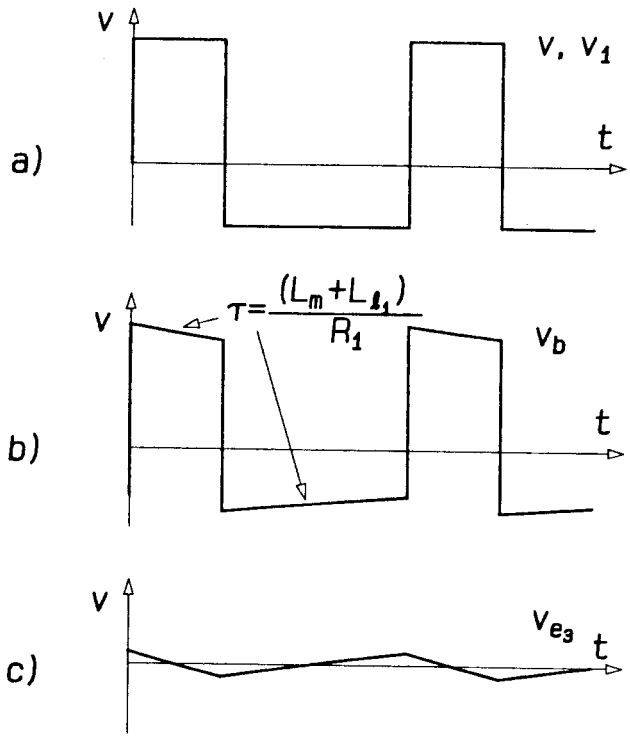

Figure 5.4: Waveforms for coupled-inductors with copper losses.

v_1 and v_b and is as shown in Fig. 5.4c. Note that both the top and bottom of v_a, v_b or the error voltage v_{e_3} should be exponential curves, but when the copper loss is small, or the switching period T_s is much less than the time constant $\frac{L_{l_1}+L_m}{R_1}$, they can be approximated as straight lines; thus the peak to peak error voltage is simply:

$$v_{e_3} = i_1 R_1 = v_1 \frac{D}{f_s} \frac{R_1}{L} \tag{5.23}$$

where D is the duty ratio of the drive waveform, F_s is the frequency of the drive voltage, and $L = L_m + L_{l_1}$ is the input inductance of the coupled-inductor:

5.3.2 Error Voltage Due to Energy Transfer Capacitor

In a Ćuk converter (Fig. 5.5a), the charging and discharging current of the energy transfer capacitor will generate a voltage ripple on the capacitor, making the voltage waveforms on the two windings of the coupled-inductors slightly different (Fig. 5.5b). The error voltage v_{e_4} is the difference between the two drive voltages, or in this case the

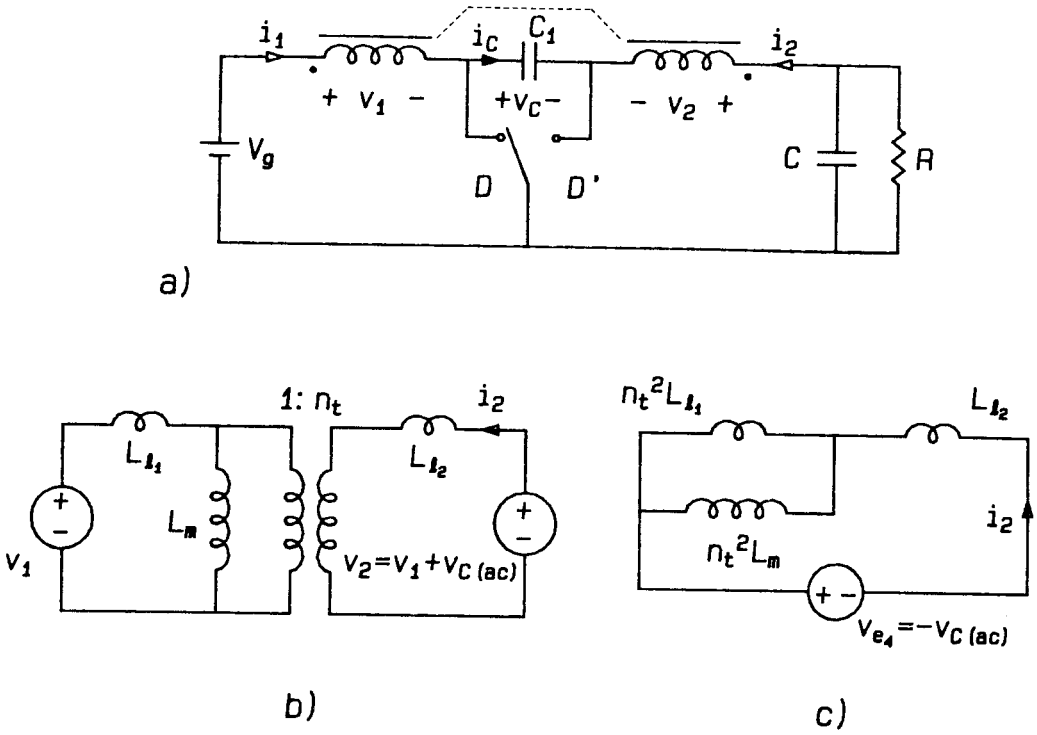

Figure 5.5: a) Ćuk converter. b) The circuit model for the coupled-inductors. c) The error voltage v_{e_4} is the ac component of v_C.

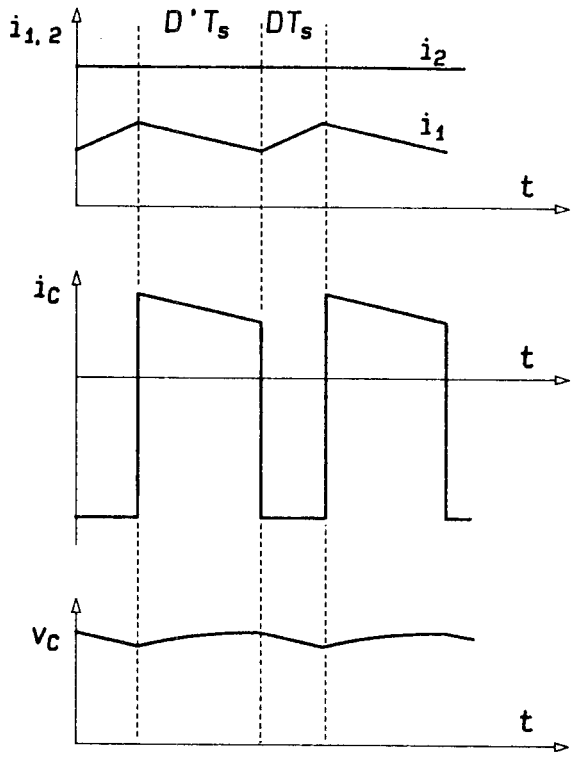

Figure 5.6: Current and voltage waveforms for Fig. 5.5.

ac voltage on the capacitor. Thus, the error voltage is also applied across the effective leakage inductance shown in Fig. 5.2d.

If the voltage ripple on C is small, the current waveforms in the inductors will not be affected (to the first order) by this voltage ripple. Figure 5.6a shows the waveforms of the inductor currents. The capacitor current (Fig. 5.6b) is the output current $-i_2$ in the period DT_s when the transistor is on, and the input current $-i_2$ in DT_s when the diode is on. The capacitor voltage waveform or the error voltage v_{e_4} (Fig. 5.6c) is obtained by integrating the current waveform:

$$v_{e_4} = \frac{1}{C}\int i_C dt \tag{5.24}$$

As in all the cases before, the residual ripple i_2 is obtained by applying the error voltage v_{e_4} across the effective leakage inductance L_{l_e}; hence, as before, increasing the leakages will decrease the residual ripple.

The ESR of the energy transfer capacitor has a similar effect. The waveform of this error voltage (v_{e_5}) is the same as the capacitor current (Fig. 5.6b) instead of the integral of it. The rectangular part of this waveform can be cancelled out by adjusting the turns ratio of the coupled-inductors, but since the amplitude of this error voltage is proportional to the capacitor current which is load-dependent, the cancellation can be made only at one particular operating point.

5.3.3 Error Voltage Due to Inductor Core Loss

The core loss of the inductor can be modeled as a resistor across the the magnetizing inductance. If the leakage flux paths are also in magnetic material, they should also be modeled as resistors in parallel with the leakage inductances [9]. The effects of these resistors are similar to those of the copper loss previously discussed. However, the loss of the magnetic material changes with the frequency and the flux excitation of the core; hence, the resistors are also nonlinear. Therefore, the calculations are quite complicated. Fortunately, in the coupled-inductors used in switching converters, due to the large dc current in the windings, the flux in the core is mainly dc. Therefore, the ac flux swing and core loss are generally very small. Compared with the others, the core loss can be ignored.

5.4 ESTIMATING THE RESIDUAL RIPPLE AND SENSITIVITY

All the above error voltages are across the same effective leakage inductance; therefore, the total ripple current on the secondary can now be calculated by simply integrating the total error voltage:

$$i_{ripple} = \frac{1}{L_{l_e}} \int (v_{e_1} + v_{e_2} + v_{e_3} + v_{e_4}) dt \tag{5.25}$$

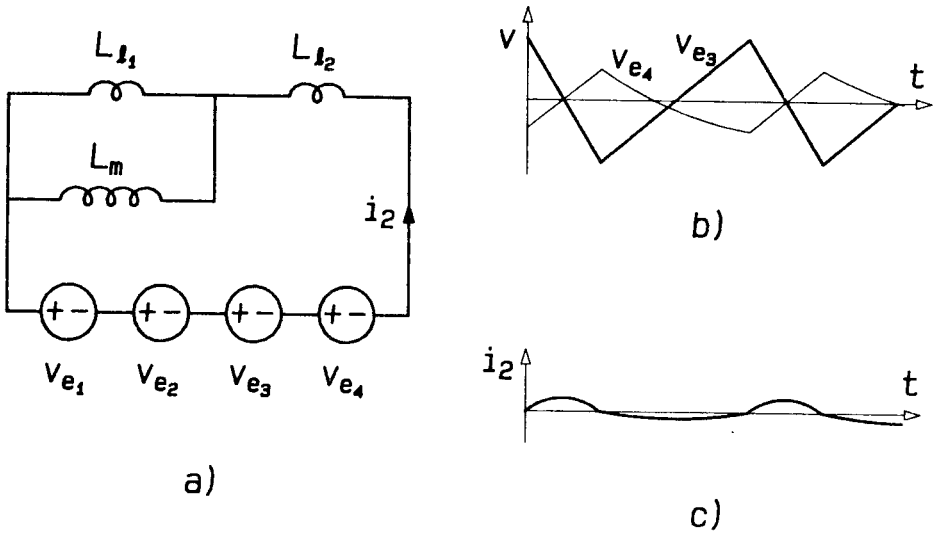

Figure 5.7: a) All the error voltages are across the effective leakage inductance. b) v_{e_3} and v_{e_4} partially cancel each other. c) The current waveform of the residual ripple.

Note that:

1. The error voltages v_{e_3} (from the copper loss) and v_{e_4} (from the energy transfer capacitor) (Fig. 5.9b) will partially cancel out each other; however, since v_{e_4} is load-dependent and v_{e_3} is not, it is very hard to take advantage of this in a practical converter design.

2. The waveforms of the error voltages v_{e_3} and v_{e_4} are triangular; therefore, the residual ripple current ripple will have a waveform that is the integral of the triangular waveform. This waveform looks more or less like a sine wave (Fig. 5.7c). The amplitude of this ripple current *cannot* be reduced by adjusting the turns ratio of the coupled-inductors. The error voltages v_{e_1} and v_{e_2} are generated by the mismatch of the zero ripple condition, their waveforms are rectangular, and the corresponding ripple current waveform is then triangular. The amplitude of the triangular ripple current *can* be changed by adjusting

the coupled-inductors.

3. The solution to reducing residual ripple and sensitivity is to increase the effective leakage inductance L_e seen by the error voltage, or, in other words, to design a coupled-inductor with *as high leakage inductance as possible.* However, in order to satisfy the zero ripple condition (5.1), one has to increase the number of turns N_2 on the secondary winding to compensate for the high primary leakage and large attenuation ratio. Therefore, while leakage inductance will be very large, so will the copper losses and a very inefficient design will result. Hence, in view of both the sensitivity and low residual ripple, as well as low copper losses, the high leakage inductance is still desired but limited only to certain optimum value. This optimum value will be determined in later chapters on multiple air-gap coupled-inductor structures. Here, it is sufficient to note that this optimum primary leakage inductance is still quite high and on the order of 20% of the total input inductance. This is still much higher than that of a low-leakage transformer, which has about 0.5% leakage relative to its magnetizing or input inductance.

5.5 AN EXAMPLE

To illustrate the effect of the leakage inductances on both residual ripple and sensitivity, an experimental switching converter was built. Figure 5.8 shows the coupled-inductor Ćuk converter built with two different coupled-inductors. The switching frequency f_s is 50khz, with duty ratio $D = 0.5$. The inductors in (a) are tightly coupled with low leakage, while inductors in (b) are simulating a high-leakage inductance case, and built with an external leakage inductor. The ac flux swing in the ferrite cores is only about 0.03Tesla, so the core losses can be ignored. The ESR of the energy transfer capacitor is very low.

The peak-to-peak error voltages can be calculated as follows:

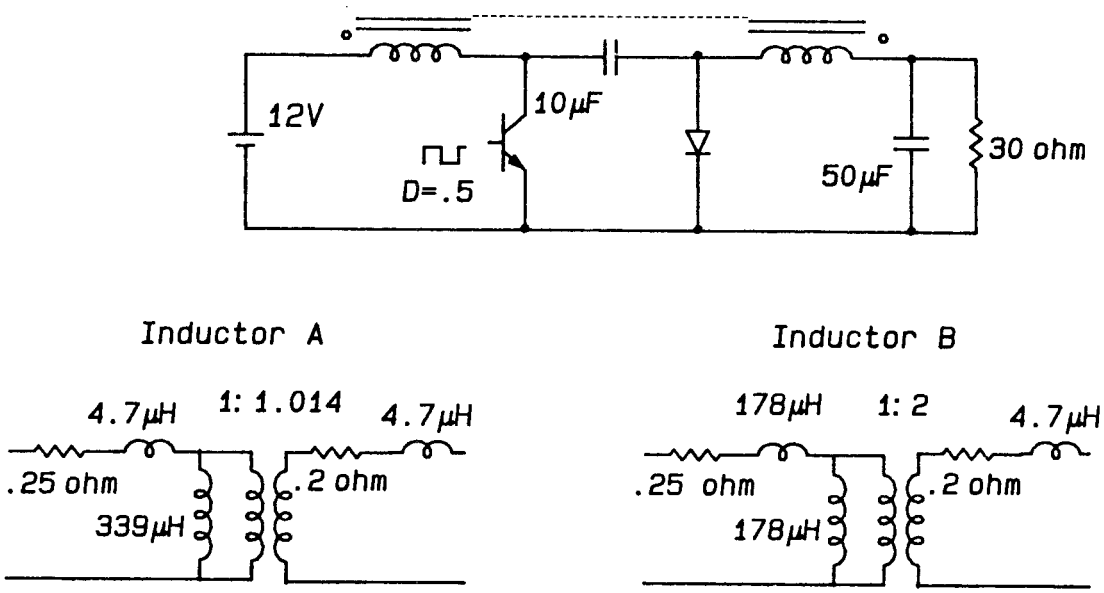

Figure 5.8: Ćuk converter using two different coupled-inductors.

$$v_{e_3} = R_1 i_1 = 75mV \tag{5.26}$$

$$v_{e_4} = \frac{1}{C}\int i_C dt = 360mV \tag{5.27}$$

Both waveforms are (basically) triangular and tend to cancel each other, so the total error voltage is $285mV$.

The effective inductance is $9.6\mu H$ for the first inductor and $360\mu H$ for the second. The peak-to-peak residual ripple currents for the two inductors are calculated to be:

$$i_{ripplea} \approx 70mA \qquad\qquad i_{rippleb} \approx 2mA$$

while the measured values are $50mA$ and $1.6mA$.

If the coupled-inductor secondary turns N_2 are increased by 1.67%, then the peak-to-peak error voltage becomes:

$$v_{e_1} = 200mV$$

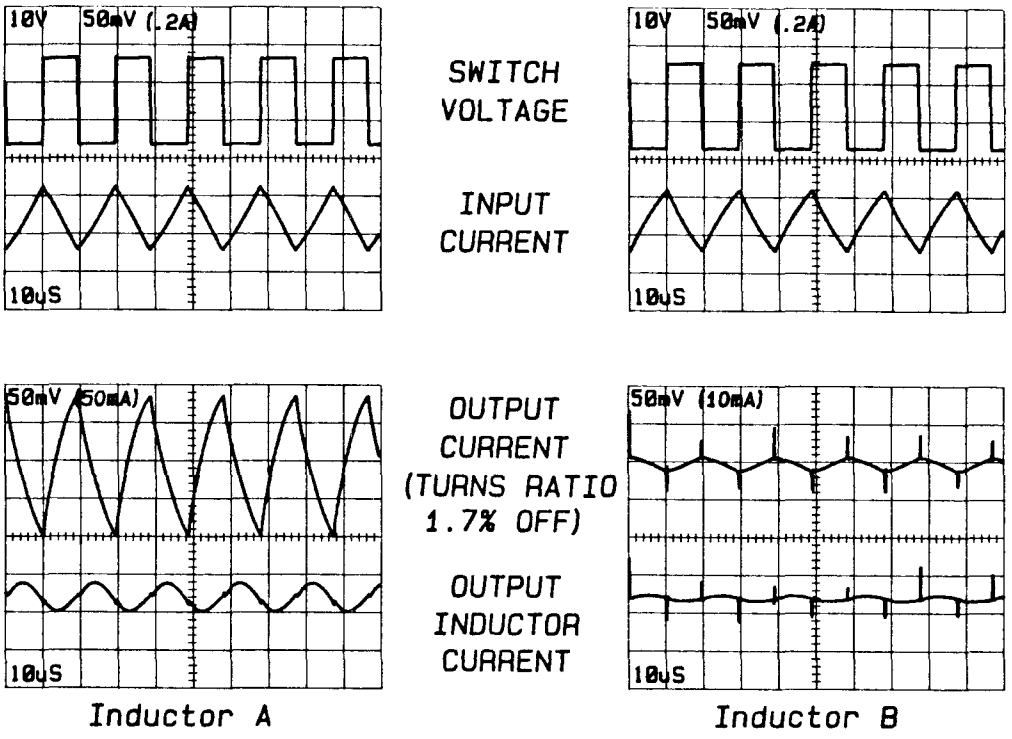

Figure 5.9: The output ripple current is much smaller for the high leakage coupled-inductors.

The waveform for this error voltage is rectangular. The ripple currents for the two inductors are then:

$$i_{ripplea} \approx 210mA \qquad i_{rippleb} \approx 5.5mA$$

The measured values are $180mA$ and $4mA$ for the two inductors.

Figure 5.9 shows the measured waveforms for the circuit. Note that the current ripple for the loosely coupled-inductor is more than 30 times smaller than that of the tightly coupled-inductors.

Chapter 6

EFFECT OF THE ISOLATION TRANSFORMER LEAKAGES IN A COUPLED-INDUCTOR ĆUK CONVERTER

In the last chapter, the sensitivity and residual ripple of the coupled-inductors was discussed. The conclusion is—the coupled-inductors should be relatively loosely coupled, to reduce the sensitivity of the current ripple to changes in the turns ratio, and to reduce the residual ripple. In a coupled-inductor Ćuk converter with isolation transformer (Fig. 6.1a), the isolation transformer should have no effect on the converter operation, other than to isolate the output from the input. However, in some cases the measured current waveforms will be somewhat like that in Fig. 6.1c. In addition to the familiar triangular switching current ripple and possible sine wave like residual ripple, there are some spikes or even steps on the waveforms. One can clearly see the steps in the $5V$ output current waveform of the $150W$ converter discussed in Chapter 11 (the top waveform of the center scope picture in Fig. 11.7).It has also been noticed that if the output capacitor is removed, the spikes will disappear.

The question now is: How could the isolation transformer affect the ripple current waveforms, and how can one reduce these spikes and steps to an acceptable level? The answers are fairly simple: The spikes and steps in the current ripple waveforms are due to the leakage of the isolation transformer, and to reduce the spikes, besides reduc-

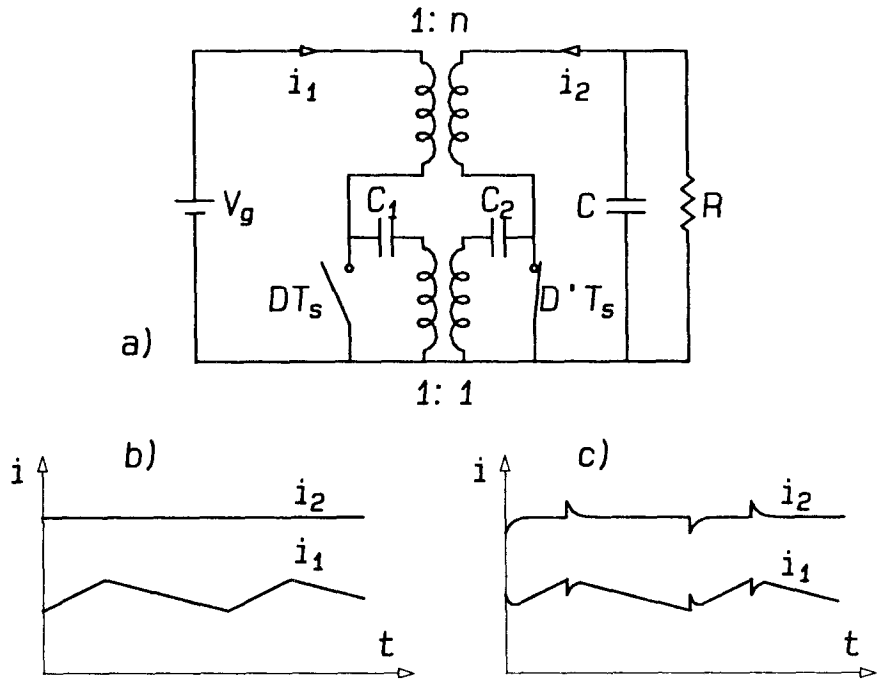

Figure 6.1: a) Coupled-inductor Ćuk converter. b) Normal input and output current waveforms. c) Current waveforms when transformer leakage inductance is high.

ing the transformer leakage inductance, one has to make the coupled-inductors *loosely coupled*, or, in other words, to design coupled-inductors with relatively *high leakage*. In this chapter, the details of the effects of the transformer leakage will be studied.

The circuit of the Ćuk converter with the leakages of both the coupled-inductors and transformer is shown in Fig. 6.2a. Without loss of generality, the isolation transformer turns ratio is assumed to be 1 : 1, to simplify the circuit. The transformer leakage inductance is L_{l_T}. The magnetizing inductance of the transformer is usually many times higher than any other inductance in the circuit; therefore, the magnetizing current and the magnetizing inductance itself are ignored in this analysis. In Section 2.3.1, it has

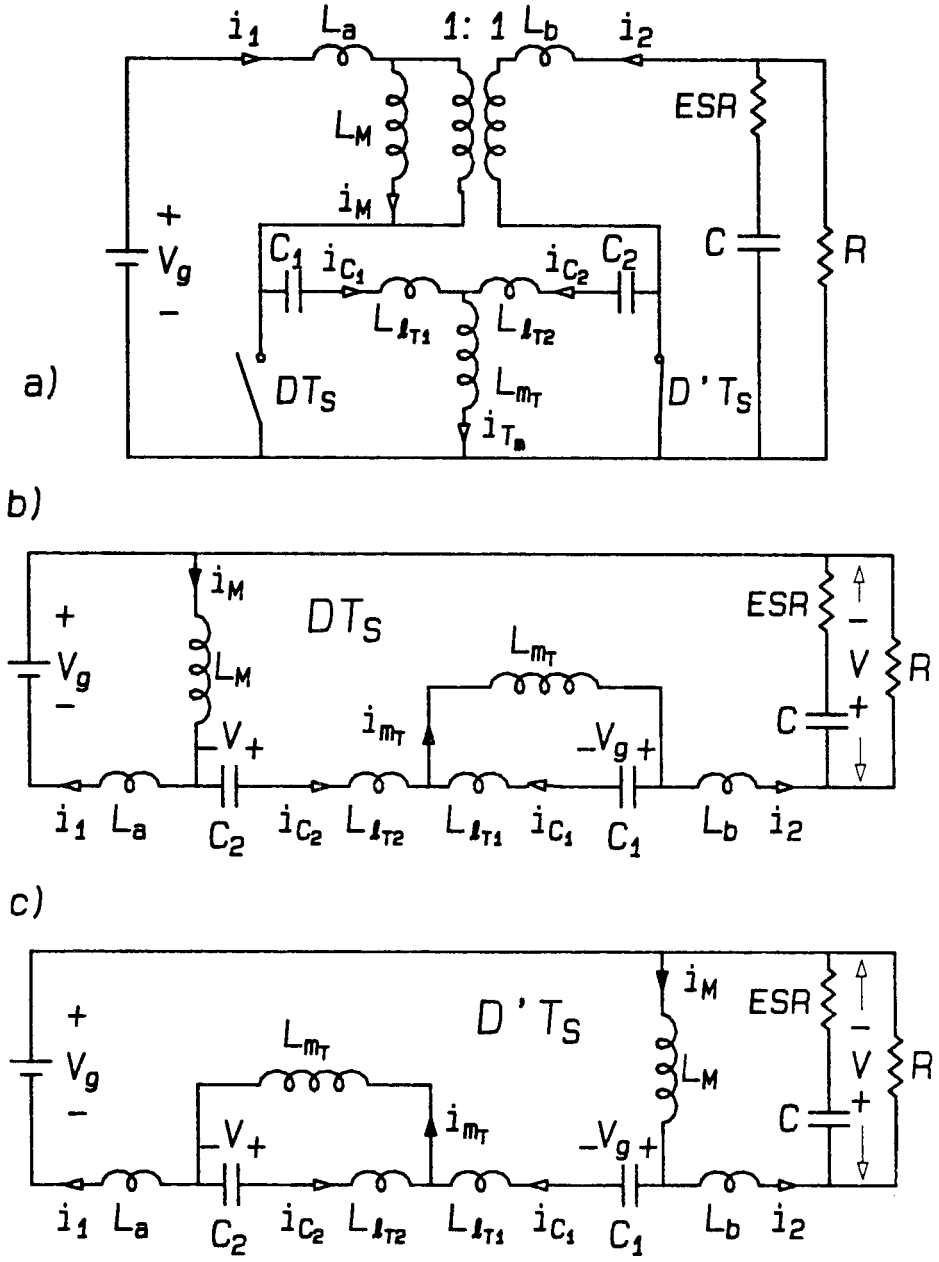

Figure 6.2: a) Coupled-inductor Ćuk converter with both coupled-inductors and transformer leakages. b,c) Equivalent circuit for DT_S and $D'T_S$.

been shown that, in the circuit model of the coupled-inductors, the voltage transfer ratio of the ideal transformer A can be arbitrarily chosen. Usually, as in all the other chapters of this thesis, A is chosen to be the physical turns ratio of the coupled-inductors; thus this "physical model" will closely represent the physical structure of the coupled-inductors. However, in the discussion of this chapter, to simplify the circuit, A is chosen to be 1, reducing the circuit model to the T model. Generally, in the T model, the two "leakage" inductances $L_{11} - L_M$ and $L_{22} - L_M$ could be positive, zero or negative values. For the discussion in this chapter, it is assumed that the coupled-inductors are adjusted for zero ripple current on the output side. In this case, as shown in Section 4.2, $L_{11} - L_M = 0$ and $L_{22} - L_M > 0$. To prevent confusion with the leakage inductances L_{l_1} and L_{l_2} in the "physical model," we use the notation L_a and L_b to represent the "leakage" inductances $L_{11} - L_M$ and $L_{22} - L_M$. Figure 6.2b, c shows the equivalent circuits for the two time periods, DT_S and $D'T_S$.

To avoid analyzing unnecessary complicated circuit models, but also to avoid making too many simplifications as to affect the final results, we will study some simplified circuit models first to get an understanding of the circuit operation, then important parasitics will be added in one at a time to better simulate the actual circuit.

The following cases will be studied:

1. No leakages in either the transformer or the coupled-inductors.

2. Leakages in the coupled-inductors only.

3. Leakages in the transformer only.

4. Leakages in both the transformer and coupled-inductors.

It is assumed that all the capacitors are large, so that the capacitor voltages are constants throughout the switching cycle.

6.1 NO LEAKAGES IN EITHER THE TRANSFORMER OR COUPLED-INDUCTORS

The simplest case for the coupled-inductor Ćuk converter is the one without any leakages (Fig. 6.3a). Fig. 6.3b,c shows the equivalent circuits for duration DT_S and $D'T_S$. For the time period DT_S, the voltage on the inductor is the source voltage V_g; for $D'T_S$ the inductor voltage is the output voltage $-V$. The volt-second balance on the inductor gives the output voltage of the converter:

$$\frac{V}{V_g} = \frac{D}{D'} \tag{6.1}$$

The inductor current ripple (Fig. 6.3d) will be divided between i_1 and i_2 according to the source and load impedances, that is, according to the source internal resistance R_g, and the effective series resistor (ESR) of the output capacitor C.

6.2 LEAKAGES IN THE COUPLED-INDUCTORS ONLY

The next case is a coupled-inductor Ćuk converter with leakage in the coupled-inductors only (Fig. 6.4a). Fig. 6.4b,c shows the equivalent circuits for duration DT_S and $D'T_S$. This is the same as the non-isolated version of the coupled-inductor Ćuk converter, as an ideal transformer should have no other effect on the circuit than isolation between the output and input.

In this circuit, due to the zero impedance of the source and the large capacitance of the energy transfer capacitor C_1, the ac component of the voltage v_a is zero. Due to the large capacitance of the output capacitor C, the ac component of the output voltage v is also zero. Therefore, the voltage v_{L_b} across L_b is a constant. The output current i_2 in L_b is then:

$$i_2 = \frac{1}{L_b}\int v_{L_b}\,dt = \frac{v_{L_b}\,t}{L_b} + constant \tag{6.2}$$

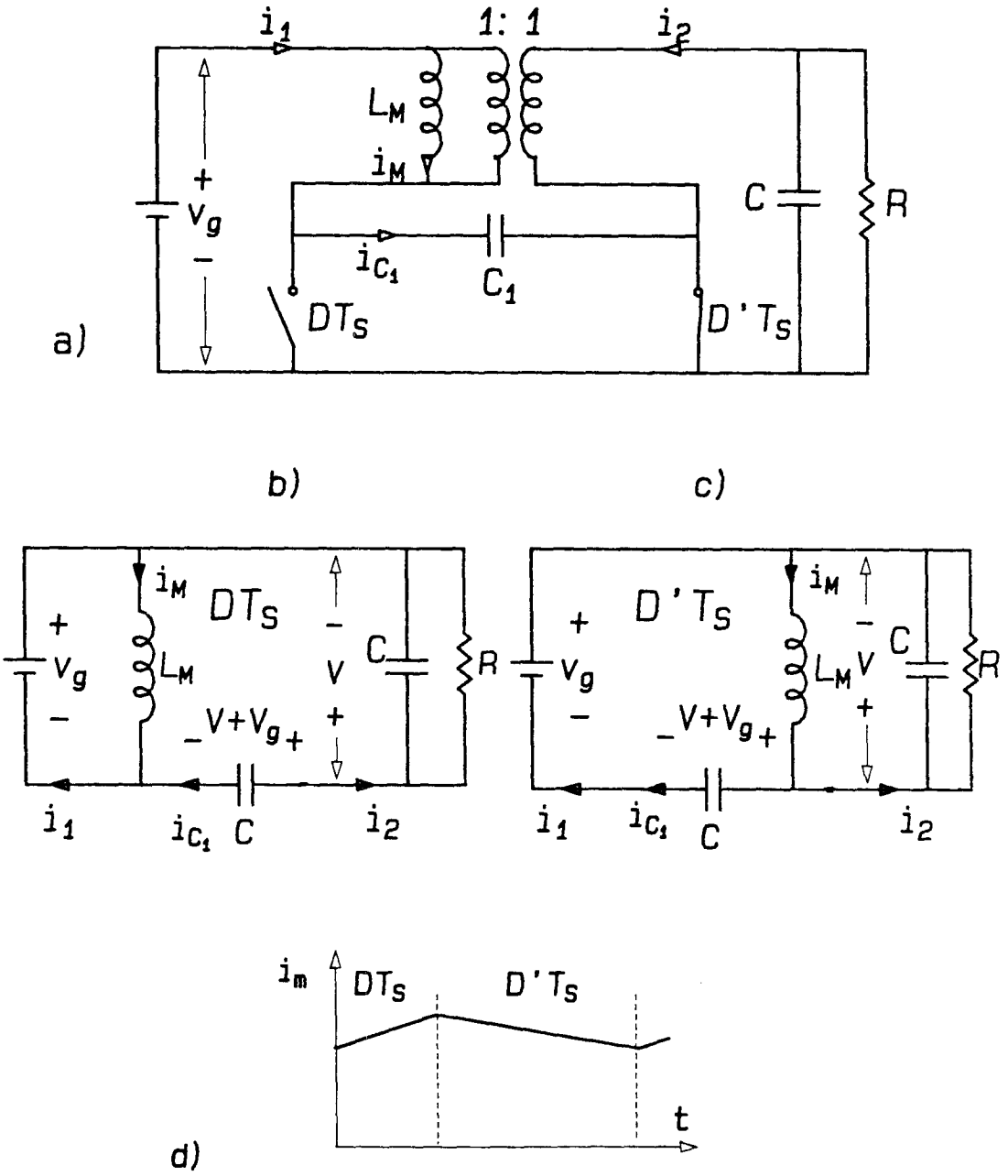

Figure 6.8: a) Coupled-inductor Ćuk converter with no leakage in the coupled-inductors or transformer. b,c) Equivalent circuits for periods DT_S and $D'T_S$. d) Inductor current waveform.

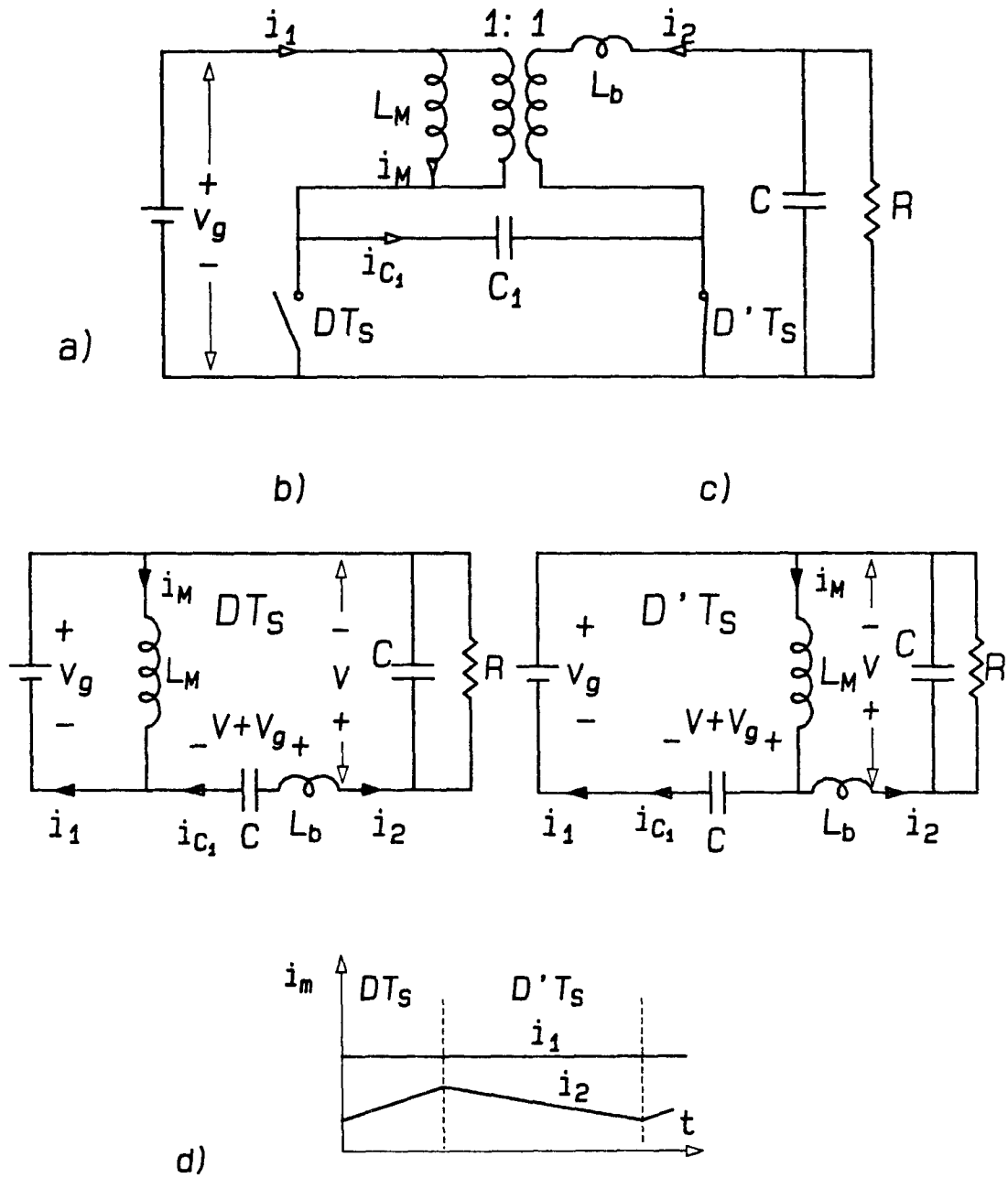

Figure 6.4: a) Coupled-inductor Ćuk converter with leakage in the coupled-inductors only. b,c) Equivalent circuits for periods DT_S and $D'T_S$. d) Input and output current waveforms.

The output current i_2 and the inductance L_b both are finite; therefore, v_{L_b} has to be zero, and the output current i_2 will be a constant (zero output ripple). All the inductor current ripple will be steered into i_1, (Fig. 6.3d). Note again, that in this case the two inductances L_a and L_b in the T model used in this chapter *should not* be confused with the two leakage inductances L_{l_1} and L_{l_2} in the "physical" circuit model.

6.3 LEAKAGES IN THE TRANSFORMER ONLY

6.3.1 Leakage in Transformer Only; Output Capacitor ESR is Zero

Figure 6.5a-c shows the coupled-inductor Ćuk converter with transformer leakage inductance.

The capacitors in the circuit are assumed to be large so that their voltages are constants; therefore, the voltage across the inductance L_{l_T} is also a constant, and it must be zero; otherwise, the current i_{C_1} through the inductor will increase to infinity. Since the voltage across L_{l_T} is zero throughout the switching cycle, the inductor current i_{C_1} is also a constant. However, since this current is also the charging current for the capacitor C_1, the average value should be zero (or the capacitor voltage will be charged up to infinity); therefore :

$$i_{C_1} \equiv 0 \tag{6.3}$$

or in other words, *the energy transfer capacitor is not passing through any current!* The voltage gain and input/output current waveforms (Fig. 6.5d) are just like those of a flyback converter.

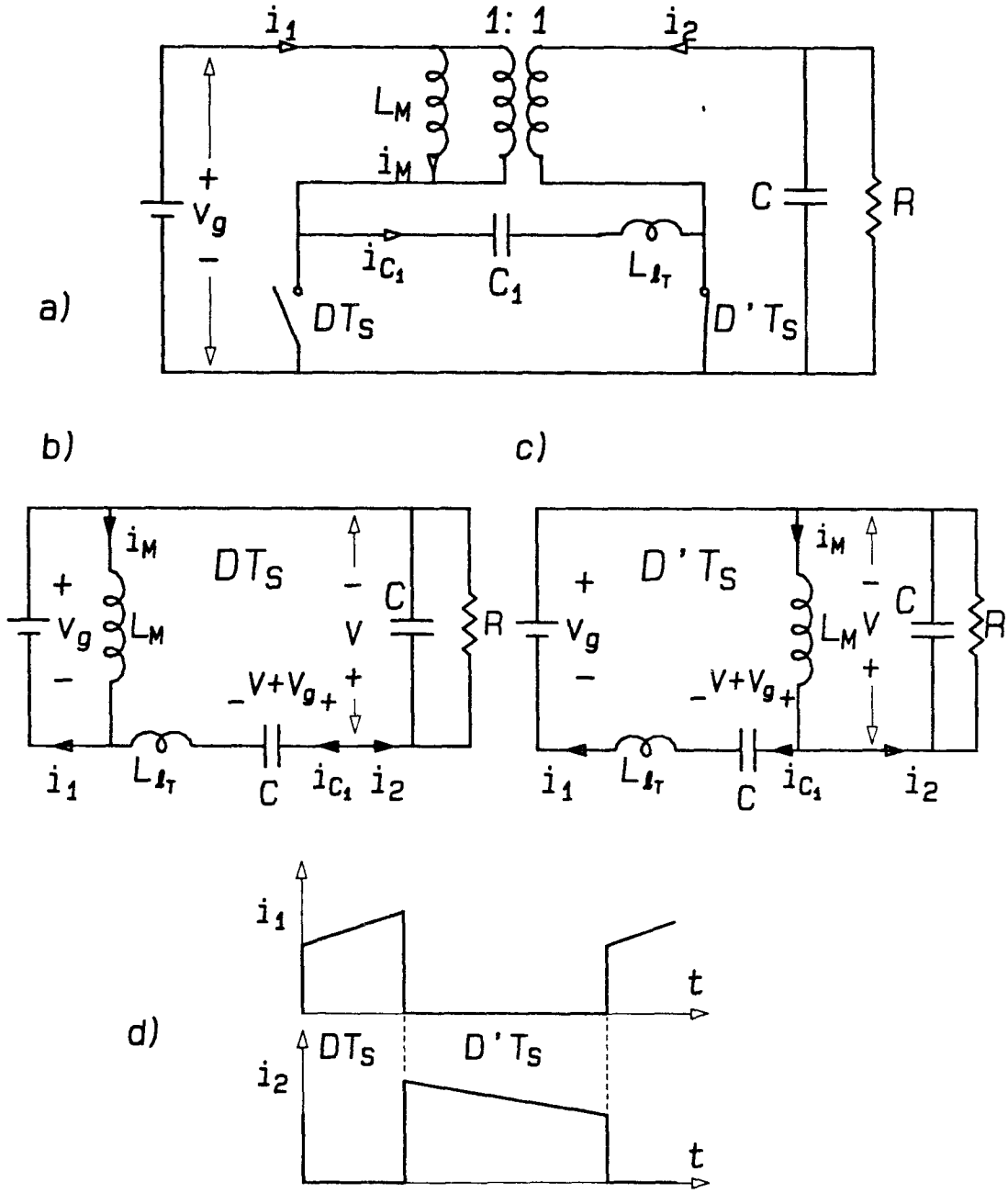

Figure 6.5: a) Ćuk converter with transformer leakage inductance. b,c) Equivalent circuits for DT_S and $D'T_S$. d) Input and output current waveforms.

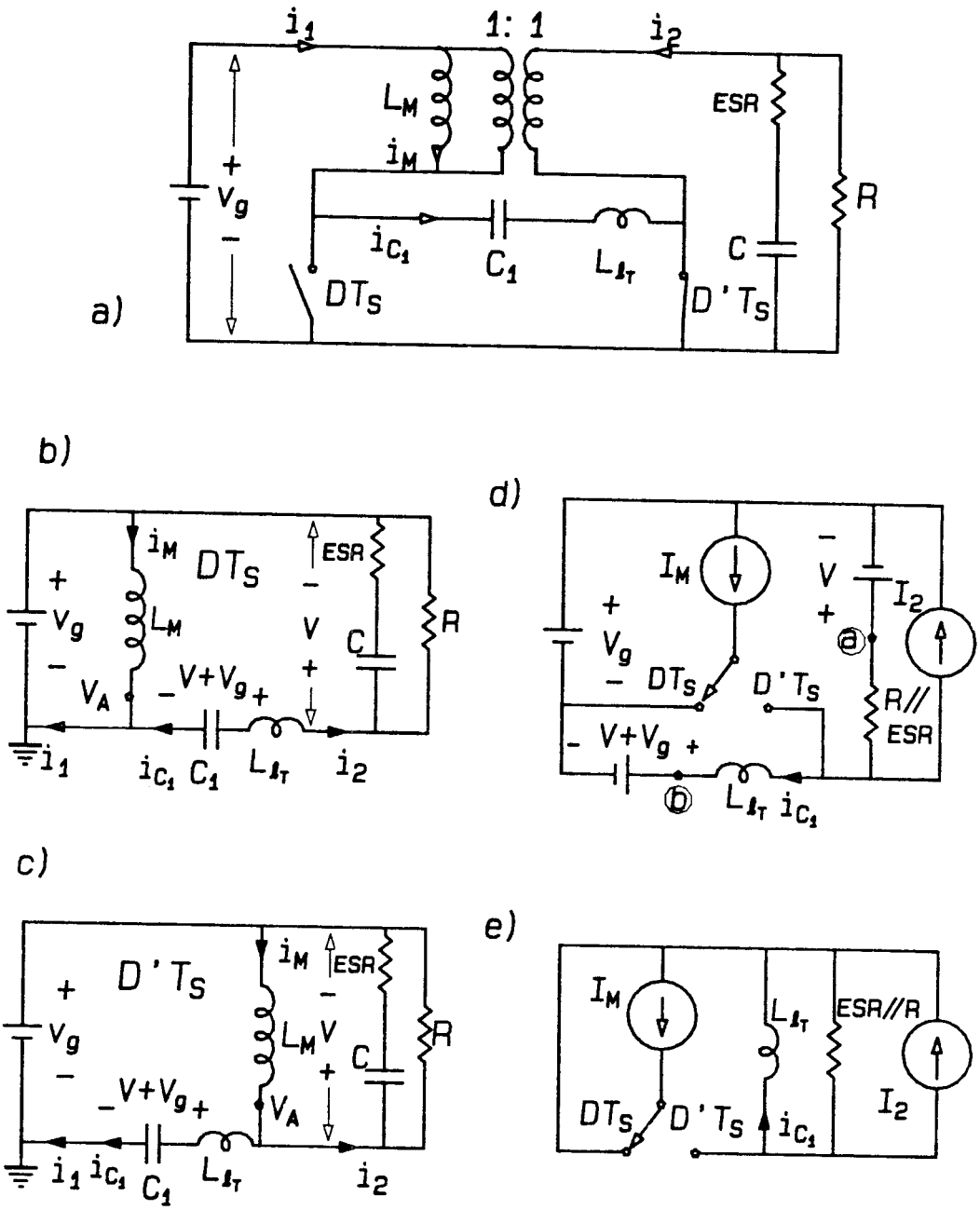

Figure 6.6: a) Coupled-inductor Ćuk converter with transformer leakage inductances and ESR of the output capacitor. b,c) Equivalent circuits for DT_S and $D'T_S$. d,e) Simplifying the equivalent circuits.

6.3.2 Leakage in Transformer Only; Output Capacitor ESR is Not Zero

The circuit for this case is shown in figure 6.6a. Under the assumption that L_M is large so that the inductor current ripple is negligible, the equivalent circuits for the two time periods DT_S and $D'T_S$ (Fig. 6.6b,c) can be combined and redrawn as Fig. 6.6d. In this circuit model, I_M is the inductor current, which is the sum of the average input and output currents I_1 and I_2. The load resistor R is much larger than the ESR of the output capacitor, so one can assume that all the ripple of the output current i_2 goes into the capacitor, and the current in the load resistor is just the dc component I_2. Note that in Fig. 6.6d, since the voltage difference between point a and point b is always zero, for finding the voltage and current of the transformer leakage inductance L_{l_T}, the circuit can be further simplified as Fig. 6.6e.

Also assume that the $R - L$ time constant determined by $\frac{L_{l_T}}{ESR \| R}$ is much smaller then either DT_S or $D'T_S$ so that the circuit is always in steady state when the switch changes position.

For convenience, assume that the converter switches from D to D' at t_0 and switches back to D at t_1.

At t_0^- (Fig. 6.6e), the circuit is already in the first steady state. The current in the transformer leakage inductance i_{C_1} (which is the same as the energy transfer capacitor charging current) is the opposite of the output current:

$$i_{C_1(t_0^-)} = -I_2 \tag{6.4}$$

At t_0^+, the switch changes to position D'; however, the current in the inductor L_{l_T} cannot change instantaneously:

$$i_{C_1(t_0^+)} = -I_2 \tag{6.5}$$

When the switch is at position D', the steady- state value of the current in the inductance

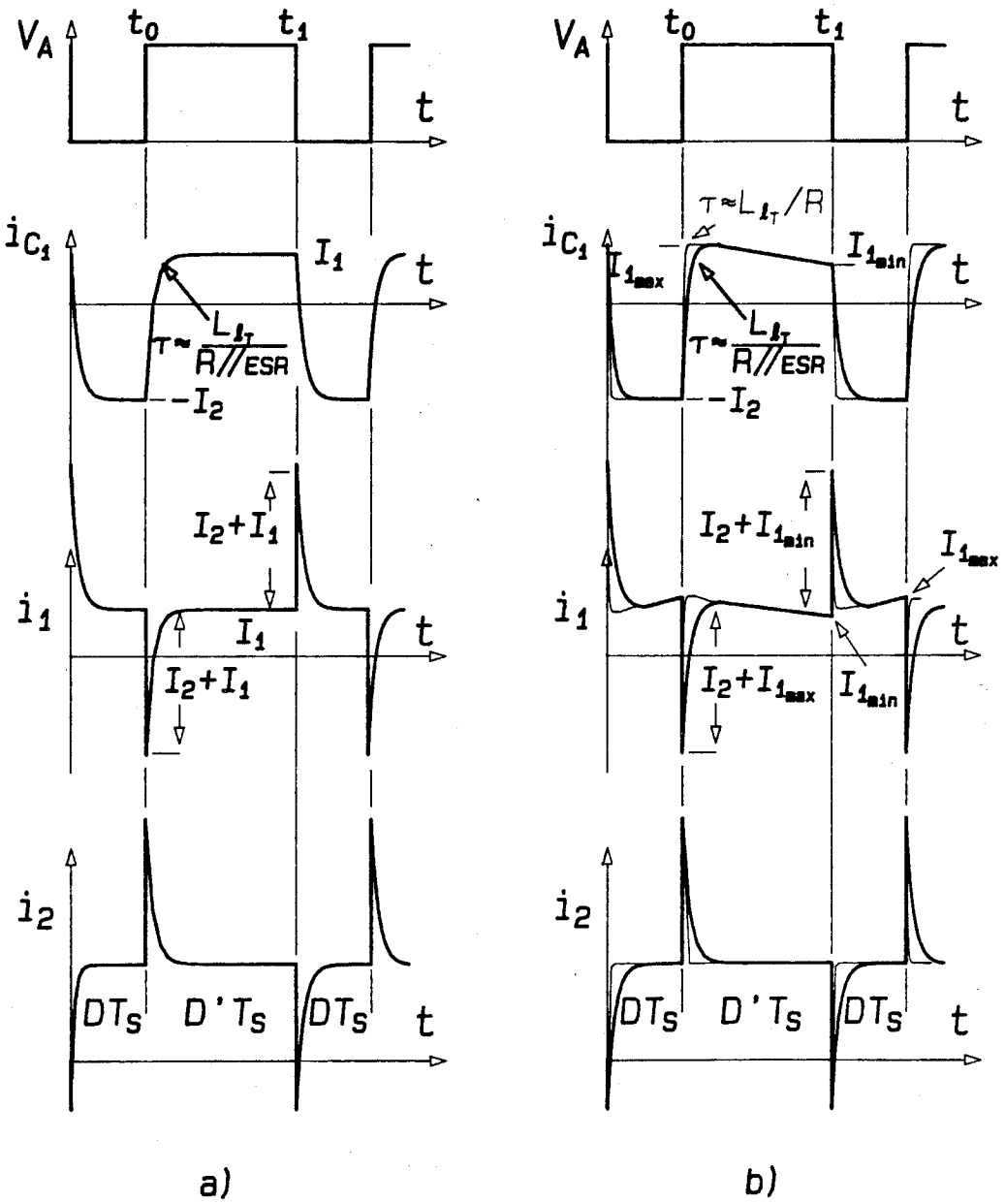

Figure 6.7: The waveforms of the converter without (a) and with (b) the inductor current ripple.

L_{l_T} is $I_M - I_2 = I_1$. The inductor current will increase exponentially from the initial value $(-I_2)$ to this second steady-state value:

$$i_{C_1} = (I_1 + I_2)(1 - e^{-\frac{t-t_0}{\tau}}) - I_2 \tag{6.6}$$

where τ is the $R - L$ time constant:

$$\tau = \frac{L_{l_T}}{ESR \parallel R}$$

Since it is already assumed that $t_1 - t_0 \gg \tau$, so at $t_1{}^-$, just before the switch switches back to D, the current i_{C_1} is already at the second steady state:

$$i_{C_1(t_1-)} = I_1 \tag{6.7}$$

At $t_1{}^+$, the switch is back to the position D, but the current i_{C_1} remains the same:

$$i_{C_1(t_1+)} = I_1 \tag{6.8}$$

and it will decrease back to the steady state value $-I_2$ exponentially:

$$i_{C_1} = (I_1 + I_2)e^{-\frac{t-t_1}{\tau}} - I_2 \tag{6.9}$$

The input and output currents i_1 and i_2 can be found from the current relationships in Fig. 6.6b,c:

For DT_S :	For $D'T_S$:
$i_1 = i_{C_1} + I_M$	$i_1 = i_{C_1}$
$i_2 = -i_{C_1}$	$i_2 = -i_{C_1} + I_M$

(6.10)

The waveforms for an entire switching cycle is shown in Fig. 6.7a. If the ripple current in the inductor L_M is not negligible, the inductor current ripple will be added to the waveforms (Fig. 6.7b.)

Note that the decay time constant for the inductor current is $\frac{L_{l_T}}{ESR \| R}$; if the output capacitor is removed, the decay time will be much shorter, and the spikes in the input and output waveforms will likely be covered by the rise and fall times of the switch.

6.4 LEAKAGES IN BOTH TRANSFORMER AND COUPLED-INDUCTORS

In a properly designed coupled-inductor Ćuk converter, the coupled-inductors will have relative high leakage. The transformer leakage should be as low as possible, to reduce the voltage spikes on the transistor and diode switches. However, due to physical limitation, the transformer leakage inductances cannot be reduced to zero. This small transformer leakage will still generate some spikes on the input and output current waveforms. Under the assumption that both the transformer and coupled-inductors turns ratio are 1 : 1, the circuit for this case is shown in Fig. 6.8. In this circuit the leakage inductances will generate voltage spikes on the switches; these spikes are clamped to V_+ and V_- by two diodes. The coupled-inductors are designed to have zero current ripple on the output side, so $L_a = 0$ and $L_b > 0$. The equivalent circuits for periods DT_S and $D'T_S$ are shown in Fig. 6.8b,c. As in the last case, the inductor L_M is assumed to be large, so that the inductor current I_M, which is the sum of the average input and output currents I_1 and I_2, is constant. The ESR of the output capacitor is much smaller than the load resistor R; therefore, the output capacitor takes all the ripple current in i_2, and the current through the load R is the dc component I_2. The two circuits for DT_S and $D'T_S$ can now be combined as Fig. 6.8d. Note that in Fig. 6.8d, the voltage difference

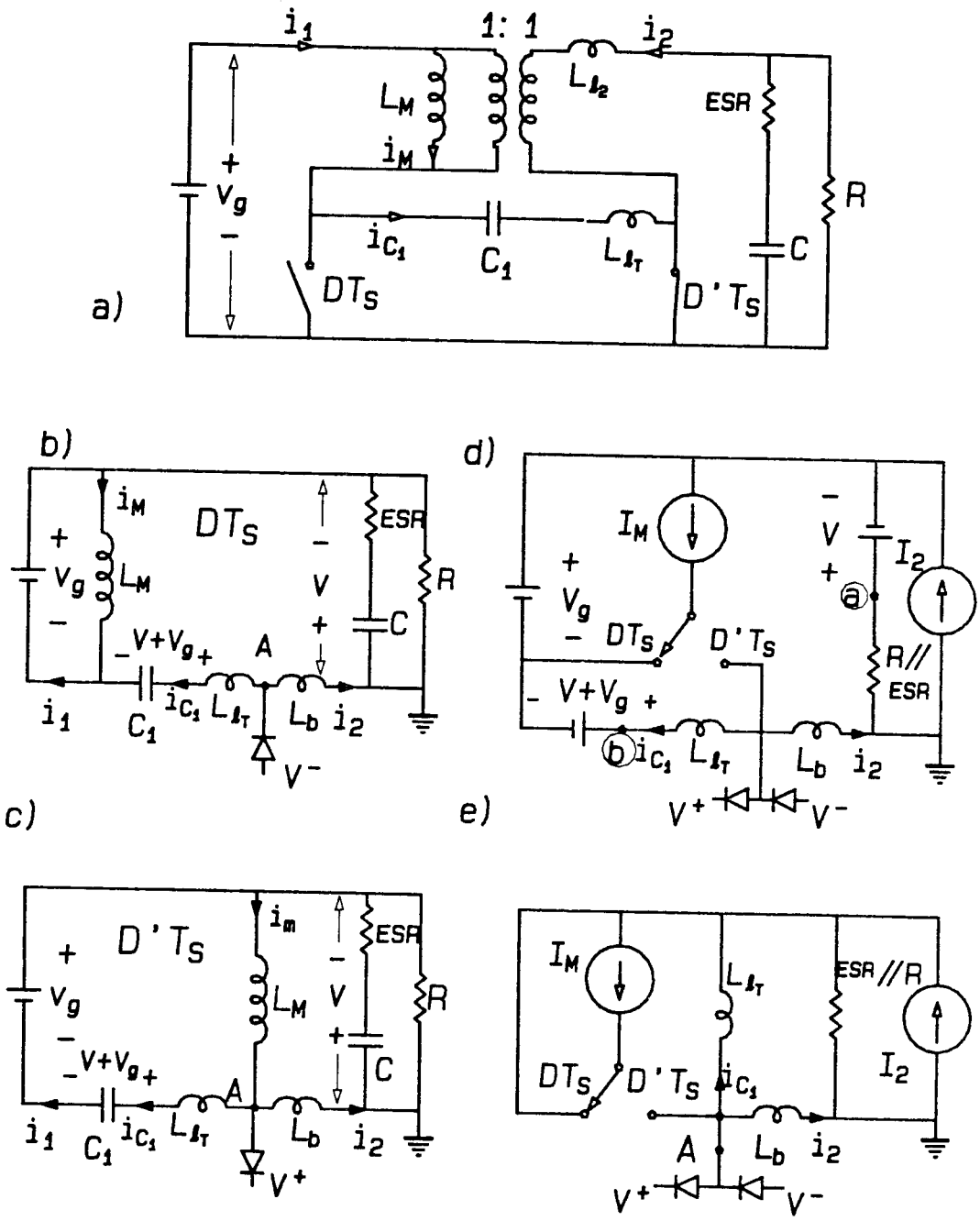

Figure 6.8: a) Coupled-inductor Ćuk converter with leakages in the transformer and coupled-inductors. b,c) Equivalent circuits for DT_S and $D'T_S$. d,e) Simplified equivalent circuits.

between point a and point b is zero; the circuit can be further simplified as Fig. 6.8e to find the voltages and currents of the two inductors L_{l_T} and L_b.

It is also assumed that the time constant determined by:

$$\tau = \frac{L_{l_T} + L_{l_2}}{ESR \parallel R} \approx \frac{L_{l_T} + L_{l_2}}{ESR} \tag{6.11}$$

is much smaller than either DT_S or $D'T_S$, so that the circuit is in steady state whenever the switch changes position.

For convenience, assume that the converter switches from D to D' at t_0 and switches back to D at t_1.

At t_0^- (Fig. 6.8e, 6.9a), the currents in the two inductors L_b, L_{l_T} are in their first steady state:

$$\begin{aligned} i_{C_1(t_0^-)} &= -I_2 \\ i_{2(t_0^-)} &= I_2 \end{aligned} \tag{6.12}$$

At t_0^+, the switch changes to position D', and the current from the current source I_M is injected into point A in Fig. 6.8e. However, the currents in the two inductors cannot change instantaneously, so there will be a positive voltage spike at point A. This voltage spike is clamped by a diode to V^+. This V^+ will be across both L_{l_T} and L_{l_2} (since the voltage drop on the ESR is small), so both inductor currents will increase with the slopes $\frac{V^+}{L_T}$ and $\frac{V^+}{L_b}$, until $t_0 + t_{V+}$, when the sum of the two inductor currents is the same as I_M (Fig. 6.9a).

The width of the spike and the two inductor currents at the end of the spike can be calculated from the waveforms in Fig. 6.9a:

$$t_{V+} = \left(1 + \frac{I_1}{I_2}\right) \frac{L_{l_T} \parallel L_{l_2}}{V^+}$$

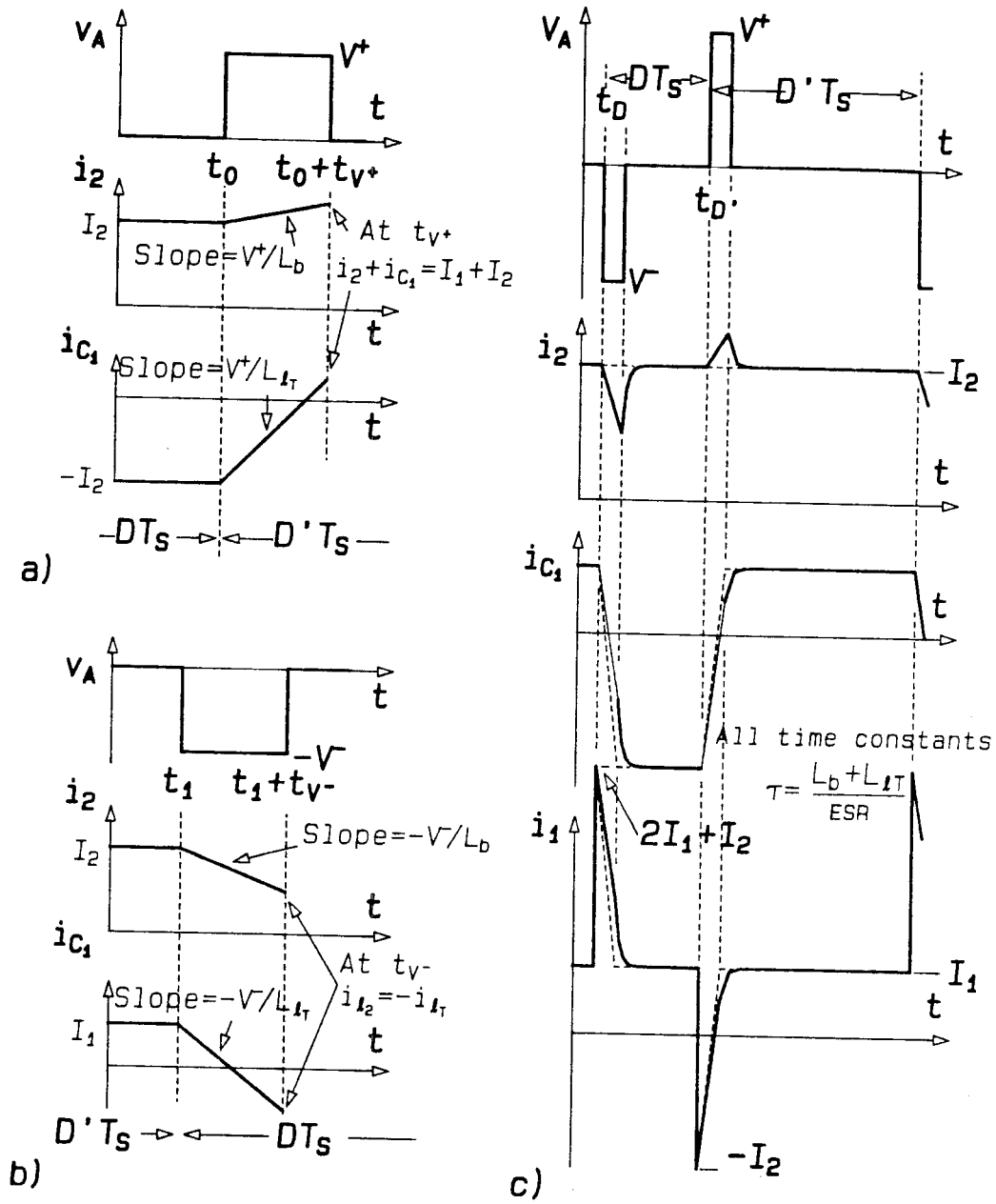

Figure 6.9: a,b) Waveforms during transients. c) Waveforms for a switching cycle (Dash lines are for $L_b \gg L_{l_T}$).

$$i_{2(t=t_0+t_{V+})} = I_2 + (I_2 + I_1)\frac{L_{l_T}}{L_{l_T} + L_b}$$
$$i_{C_1\ (t=t_0+t_{V+})} = -I_2 + (I_2 + I_1)\frac{L_b}{L_{l_T} + L_b} \tag{6.13}$$

After the voltage spike the two inductor currents will decay exponentially to their second steady-state value:

$$i_2 = I_2 \qquad\qquad i_{C_1} = I_1 \tag{6.14}$$

with the time constant

$$\tau = \frac{L_{l_T} + L_{l_2}}{ESR \parallel R} \approx \frac{L_{l_T} + L_{l_2}}{ESR} \tag{6.15}$$

Under the earlier assumption that $t_1 - t_0 \gg \tau$, so that at $t_1{}^-$ just before the switch changes back to D (Fig. 6.9b), the inductor currents are already at their second steady-state values (6.14). At $t_1{}^+$, the switch is back to position D', the current I_M is removed from point A, and there will be a negative voltage spike at point A. Since this voltage spike is clamped to V^-, both inductor currents will decay with the slopes $\frac{V^-}{L_T}$ and $\frac{V^-}{L_b}$, until $t_1 + t_{V-}$, when the two inductor currents become the same (Fig. 6.9b).

The width of this spike and the two inductor currents at the end of the spike are calculated from Fig. 6.9b:

$$t_{V-} = \frac{I_1 + I_2}{V^-\left(\frac{I_1}{L_{l_T}} + \frac{I_2}{L_b}\right)}$$
$$i_{2(t=t_1+t_{V-})} = -i_{C_1(t=t_1+t_{V-})} = I_1 I_2 \frac{L_b - L_{l_T}}{I_1 L_b + I_2 L_{l_T}} \tag{6.16}$$

After this voltage spike the two inductor currents will decay exponentially to their steady-state value $i_2 = I_2$ and $i_{C_1} = -I_2$ with the same time constant τ (6.15).

From Fig. 6.8b,c, for the period DT_S, the input current i_1 is the sum of I_1, I_2 and i_{C_1}; while it is i_{C_1} for $D'T_S$.

Note that in (6.13), if $L_b \gg L_{l_T}$, the values of the two currents at the end of the spike $t_0 + t_V{}^+$ will be about the same as the second steady-state values given in (6.14).

For the output current i_2, the steady-state value for both DT_S and $D'T_S$ is the same, so there will be no spike in the output current. The same holds true for the transient from D' to D (6.16).

Figure 6.9c shows the waveforms of I_C, i_1 and i_2 for the entire switching cycle. The dashed lines in the waveforms are for $L_b \gg L_{l_T}$. Note the absence of the current spikes in i_2. If the inductor L_M is not assumed to be infinity, the current ripple in i_M will be superimposed onto the waveforms similar to Fig. 6.7. It can also be shown that the gain of the converter is basically the same as the basic Ćuk converter (6.1).

The above study shows that in the case of a coupled-inductor converter, the isolation transformer should be designed to obtain very low leakage. This will not only reduce the voltage spikes on the switching transistor and diode, but also will reduce the current spikes in the input and output current waveforms. However, the coupled-inductors, for all the reasons given in the last two chapters, should be designed with relatively *high leakage*!

Chapter 7

MULTIPLE WINDING STRUCTURES

Most multiple output converters need a separate inductor for each output to filter the switching ripple. Therefore, if we couple all of these inductors into a single structure, more savings in the size, weight, and cost of the magnetics can be obtained.

7.1 CONVENTIONAL MULTIPLE WINDING COUPLED-INDUCTOR STRUCTURE

The conventional approach for coupling the inductors in multiple output switching converters, such as the Ćuk converter in Fig. 7.1a, is to combine input and all output windings on a common bobbin in a magnetic circuit with a single air-gap (Fig. 7.1b). In this transformer look-alike structure, the primary and secondary windings are typically wound in layers from bottom to top, following the typical tightly coupled transformer winding arrangement. This arrangement is actually the *worst* possible implementation of the coupled-inductor method, with many practical drawbacks, such as:

a) The amount of coupling needed between the input winding and the output windings, in order to satisfy zero ripple condition, is hard to calculate; therefore, the design usually has to be made by trial and error.

b) Because of the tight coupling (low leakages) between the inductor windings, the sensitivity to slight changes of the winding configurations (number of turns, etc.) in the windings is very high; the residual ripple currents on the output windings are also

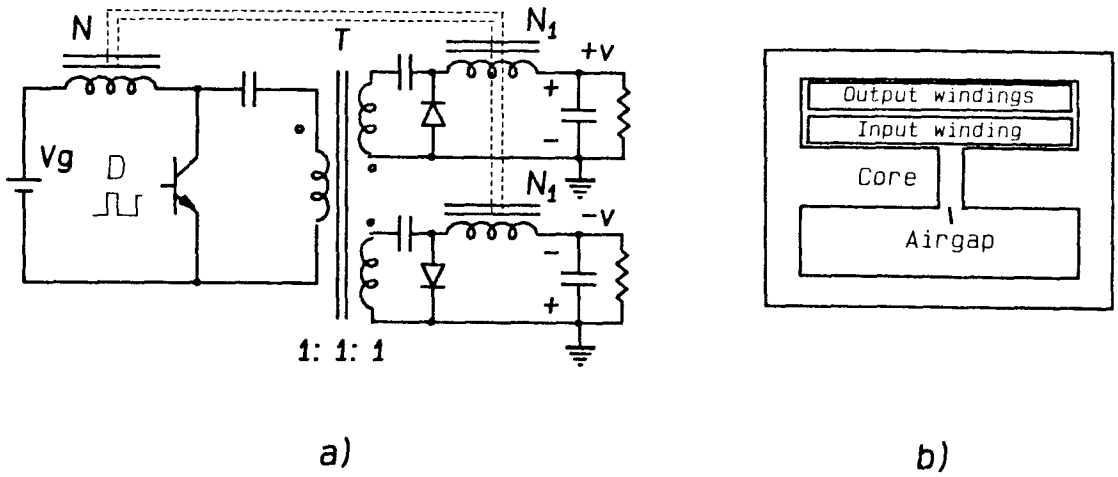

Figure 7.1: a) A two-output coupled-inductor Ćuk converter. b) The conventional winding arrangement.

quite large. In a practical design, it might even be necessary to use additional external "leakage" inductors on each secondary to control the sensitivity and residual ripple.

c) The insulation between the windings must withstand the high voltage between the input and output of the converter, thereby decreasing the effective window area of the core and increasing the cost of the structure.

d) The coupled-inductor used in a switching converter is carrying mainly dc current; the ac flux in the core is small, so is the core loss. However, the windings must carry all the dc current; therefore, the copper loss and the heat build-up problems in the windings are often a limiting factor in an inductor design. Unfortunately, this winding arrangement makes the problem even worse because of the high build-up of the windings.

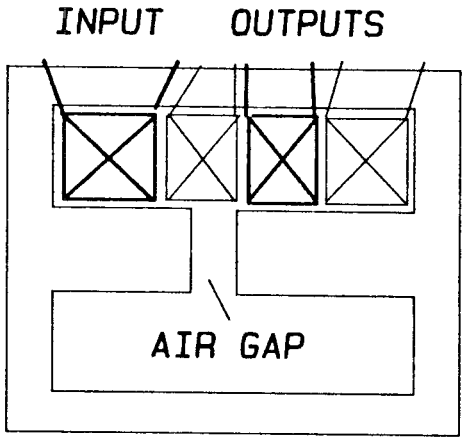

Figure 7.2: The improved winding arrangement.

7.2 IMPROVED MULTIPLE WINDING COUPLED-INDUCTOR STRUCTURE

Another winding arrangement for the same coupled-inductor is shown in Fig. 7.2. In this structure, the windings are wound side by side, with the input winding at one end. It has been shown that, if the width of the window is larger than the height (as shown in Fig 7.2), this structure will have much higher leakage between the windings than the structure shown in Fig. 7.1b [10] and therefore, much lower sensitivity to air-gap and turns ratio errors, and much smaller residual ripple. However, the difficulty in analyzing and designing the structure, the insulation problem, and the heat build-up problem still remain.

7.3 MULTIPLE AIR-GAP STRUCTURE

Most of the problems associated with the conventional transformer-like winding arrangement can be solved by using a special multiple air-gap structure. Figure 7.3

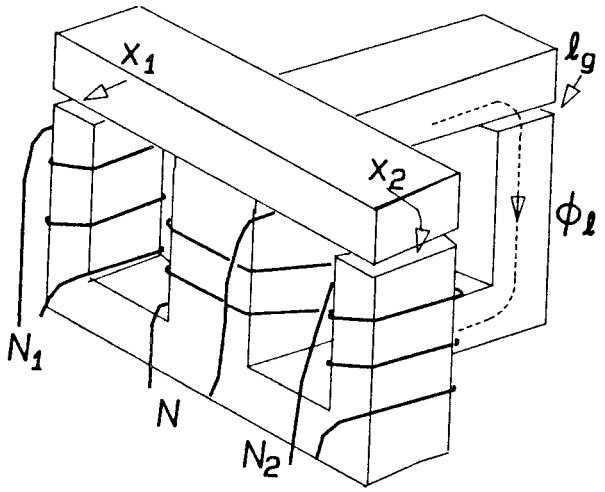

Figure 7.8: Multiple air-gap structure for a three winding coupled-inductor.

shows an example of this structure for a two-output Ćuk converter. It is easy to see that this structure is just a generalization of the magnetics structure shown in Fig. 4.8. The input winding is placed on the center leg of the core with cross section S; the two output windings are on two outer branches with cross section $S/2$, whereas the leakage flux is built through an additional "leakage" branch with the same cross section as the center leg, and with an air-gap l_g. Unlike the two other structures, the zero ripple condition for this structure can be easily found.

In the following analysis, it is assumed that the drive voltages on all three windings are identical; that is, the turns ratio of the isolation transformer in Fig 7.1a is $1:1:1$.

The reluctance equivalent circuit model of the magnetic circuit in Fig. 7.3 is shown in Fig. 7.4a. In this model, the leakages of the outer leg windings are represented by the reluctances $\mathcal{R}_{l_1}$ and $\mathcal{R}_{l_2}$; it is assumed that there is no other leakage for the input

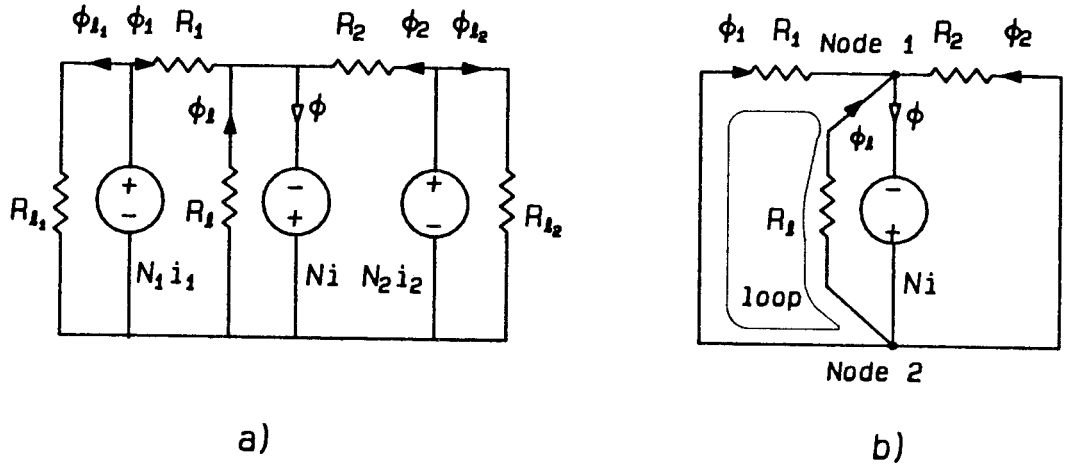

Figure 7.4: a)Complete reluctance model of the structure shown in Fig. 7.3. b) Ac reluctance model for the zero ripple condition.

winding N besides the leakage in the "leakage leg," therefore, the reluctances $\mathcal{R}_1$, $\mathcal{R}_2$ and $\mathcal{R}_l$ represent the reluctances of the three air-gaps, which are considered to dominate the total reluctance of the outer legs. The three air-gap reluctances are then defined by:

$$\mathcal{R}_1 = \frac{x_1}{\mu_0 S/2} = \frac{2\,x_1}{\mu_0 S} \tag{7.1}$$

$$\mathcal{R}_2 = \frac{x_2}{\mu_0 S/2} = \frac{2\,x_2}{\mu_0 S} \tag{7.2}$$

$$\mathcal{R}_l = \frac{l_g}{\mu_0 S} \tag{7.3}$$

Note that the factor 2 comes out as a result of the two outer legs with the windings having half the cross section of the center leg S, which is assumed throughout this analysis.

This model can be further significantly simplified under the assumption of zero ripple currents ($i_1 = 0, \quad i_2 = 0$), which effectively short out the two generators in the model and also eliminate the leakages of the outer leg windings $\mathcal{R}_{l_1}$ and $\mathcal{R}_{l_2}$ from the model. Consequently, it becomes obvious why only the leakage of the winding into

which the ripple current is steered is important. This winding is usually the center leg winding, because the symmetry of the core results in much simpler analytical expressions and models for the structure. From Fig. 7.4a, the model in Fig. 7.4b is obtained for zero ripple current conditions.

The circuit in Fig. 7.4b can be solved by setting one loop equation and one node equation for the fluxes, such that

$$\mathcal{R}_1\phi_1 = \mathcal{R}_2\phi_2 = \mathcal{R}_l\phi_l = Ni \qquad \text{loop equation} \tag{7.4}$$

$$\phi = \phi_1 + \phi_2 + \phi_l \qquad \text{node equation} \tag{7.5}$$

In addition to these two equations, we can set up three equations based on Faraday's law. that is, even though the current ripples in outer windings are zero, the current ripple in the center leg winding still produces ac fluxes, ϕ_1 and ϕ_2, which through Faraday's law are inducing voltage v to counter-balance externally applied voltage v in the outer windings N_1 and N_2. Consequently, for each of the magnetic branches and for each winding we can write:

$$v = N\frac{d\phi}{dt} \qquad v_1 = N_1\frac{d\phi_1}{dt} \qquad v_2 = N_2\frac{d\phi_2}{dt} \tag{7.6}$$

where all the three voltages on the windings are identical ($v = v_1 = v_2$). Since at present we are only considering ac fluxes:

$$\phi = \frac{1}{N}\phi_0 \qquad \phi_1 = \frac{1}{N_1}\phi_0 \qquad \phi_2 = \frac{1}{N_2}\phi_0 \tag{7.7}$$

where $\phi_0 = \int v\,dt$ is the same common factor, which will eventually be eliminated from the relationships.

After simplification,

$$\begin{aligned} \frac{\mathcal{R}_1}{\mathcal{R}_l} &= N_1\left(\frac{1}{N} - \frac{1}{N_1} - \frac{1}{N_2}\right) \\ \frac{\mathcal{R}_2}{\mathcal{R}_l} &= N_2\left(\frac{1}{N} - \frac{1}{N_1} - \frac{1}{N_2}\right) \end{aligned} \tag{7.8}$$

Note that the solution for $\mathcal{R}_2/\mathcal{R}_l$ was obtained from the remaining loop equation for the magnetic circuit model of Fig. 7.4b.

These zero ripple conditions can be further simplified by the substitution of the reluctance definitions ((7.1)-(7.3)) into (7.8):

$$\begin{aligned} \frac{x_1}{l_g} &= \frac{N_1}{2}\left(\frac{1}{N} - \frac{1}{N_1} - \frac{1}{N_2}\right) \\ \frac{x_2}{l_g} &= \frac{N_2}{2}\left(\frac{1}{N} - \frac{1}{N_1} - \frac{1}{N_2}\right) \end{aligned} \tag{7.9}$$

This result is similar to the zero ripple condition for the coupled inductor shown in Fig. 4.8 but will result in the *simultaneous* zero current ripple in both windings.

As assumed earlier, the two outputs are restricted to be of equal magnitude but could have opposite polarity. However, in case of the different output voltages, all outputs can be reflected through the transformer turns ratio to an effective 1:1:1 isolation transformer and result in essentially the same circuit as in Fig. 7.1a. After the design of the magnetics circuit in Fig. 7.3 is completed, the windings can be scaled back to the original voltages required on the output.

Additional (more than two) output inductors can be handled by attaching corresponding additional magnetic branches to the circuit of Fig. 7.3b, as was proposed before [11]. However, these magnetic structures, although most ideal from the standpoint of the simultaneous achievement of zero-ripple currents in all output windings, are highly impractical. Even the extra "leakage" branch of the magnetic circuit in Fig. 7.3 makes the structure three dimensional and quite awkward to manufacture and handle. Therefore, from the practical standpoint there is a great incentive to stay within the realm of standard two-dimensional core configurations, such as the EI or EE series of magnetic cores, and yet to preserve, as much as possible, the simplicity of the zero ripple condition.

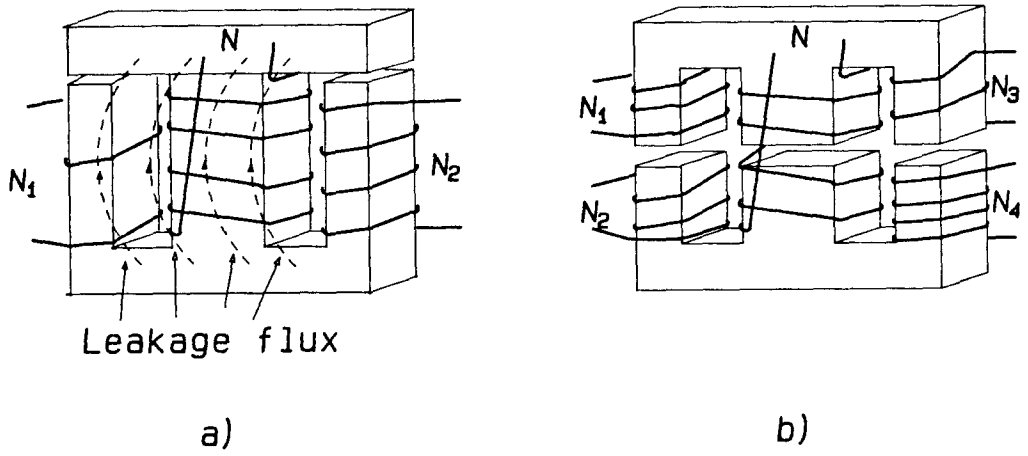

Figure 7.5: a) EI-core multiple air-gap structure for a three-winding coupled-inductor. b) EE-core structure for a five-winding coupled-inductor.

7.4 MULTIPLE AIR-GAP STRUCTURE USING STANDARD EE AND EI CORES

All of the problems associated with the three structures in the preceding sections are essentially eliminated by the use of the conventional EI and EE cores (with the cross section of the center leg twice that of the outer legs) in an unconventional manner. Instead of the "three dimensional" core configuration of Fig. 7.3, a simple EE or EI core configuration with the "three-phase" winding arrangement of Fig. 7.5a is used for the coupled inductor in the two output switching converter of Fig. 7.1a. Note that the separate magnetic branch to define the leakage flux of the center branch is now eliminated,

and one relies on the ever present leakage flux in the air as illustrated in Fig. 7.5a by the flux lines. The measurements show that the leakage inductance associated with this flux path may be quite large, typically reaching up to one-fourth of the total inductance of the center winding. The leakages of the outer branches are also high, resulting in low residual ripple and low sensitivity. Fortunately, for a given core, the leakage reluctance of this flux path varies very little with the size of the air-gap and the winding configuration, so it can be used as a design parameter.

In order to accommodate more than two outputs, the additional output windings may be put on the outer legs side by side, as illustrated in Fig. 7.5b. In this way the leakages of all the windings are maximized, leading to the lowest sensitivity and smallest residual ripple current possible. The only drawback of this configuration is that the division of the ripple currents among the windings on the same magnetic branch is difficult to calculate and a somewhat empirical approach has to be used.

In addition to the ac ripple condition, the dc conditions are important as well. The air-gaps have to be large enough to prevent saturation of any branches due to the dc current and dc fluxes. The ac condition (zero ripple condition) and the dc condition (preventing the saturation of the core) along with the design equations of this new coupled-inductor structure will be discussed in the next chapter.

Chapter 8

DESIGN-ORIENTED COUPLED-INDUCTOR ANALYSIS

As mentioned in the last chapter, the multiple air-gap coupled-inductor structure using standard EE and EI-cores eliminated almost all of the problems associated with the earlier designs, including low residual ripple, low sensitivity to turns and air-gap errors, low cost, and low temperature rise. However, to analyze the structure, first one has to characterize the reluctance of the center winding leakage flux path. Fortunately, for any given core, this reluctance is fairly constant regardless of the size of the air-gaps, the winding configuration and the number of turns. With the definition of the leakage parameter, the analysis of the structure and the derivation of the design equations become straightforward: first the equations for zero ripple condition will be found, followed by dc conditions, and the input inductance. The resulting complete set of equations is then solved for the general case and then simplified for a case of particular importance—equal air-gaps in both outer legs. In the next chapter, this result will then be easily modified into a most desired practical implementation involving a uniform air-gap in an EI-core or an EE-core (equal gap on all three magnetic branches—center as well as outer legs).

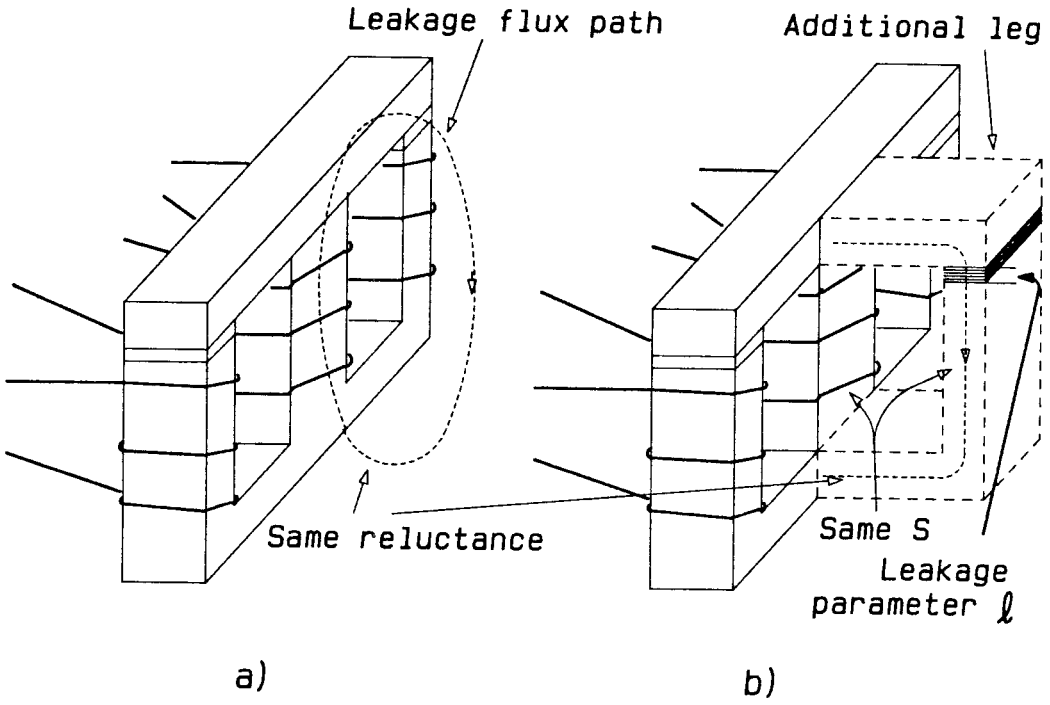

Figure 8.1: Defining the leakage parameter l.

8.1 INTRODUCTION OF A NEW LEAKAGE PARAMETER *l*

The leakage parameter l was defined earlier in Chapter 4 for the UI-core configuration. Now the leakage parameter l is generalized as in Fig 8.1 for EI and EE-cores. Let us now assume that all the leakage flux of the center winding is confined by an imaginary leg with the same cross section (S) as the center leg, as shown by the dotted lines in Fig 8.1b. The required air-gap l to make the reluctance of this "leakage leg" equal to the reluctance of the leakage flux path in the original structure (Fig 8.1a) is called the leakage parameter. As shown in Appendix A, the reluctance (or permeance) of the center leg leakage flux path in an EI or EE core is relatively independent of either the air-gap size or the number of turns in the windings. The measurement of the leakage inductance L_l for different air-gaps and number of turns results in a relatively constant

leakage reluctance $\mathcal{R}_l$ according to

$$\mathcal{R}_l = \frac{N^2}{L_l} \tag{8.1}$$

Then for a given core with a cross section S of the center leg and μ_0-permeability of free space ($\mu_0 = 4\pi \times 10^{-7} H/m$), the corresponding "leakage parameter" l can be calculated from

$$l = \mu_0 S \, \mathcal{R}_l \tag{8.2}$$

Therefore, for any given core (say EI-50), both $\mathcal{R}_l$ and l will be known quantities, and will be used in the analysis in the next two chapters as known parameters. The leakage parameter l is further characterized in Appendix A for some most commonly used EE and EI cores. Therefore, this parameter l becomes like a fingerprint for a particular core with respect to its coupled-inductor implementation. Its characterization and introduction make the whole design procedure for zero ripple much simpler and leads to a very practical design-oriented analysis.

8.2 THE ANALYSIS OF THE THREE WINDING GAPED EI-CORE COUPLED-INDUCTORS

The following analysis is broken into three parts. Ac conditions which offer zero current ripples in two windings are found first. Then, the dc currents in the windings are included and an additional constraint is imposed, so that none of the magnetic branches is saturated in their presence. Finally, the remaining ripple current in the center winding is specified through an inductance L of the center branch.

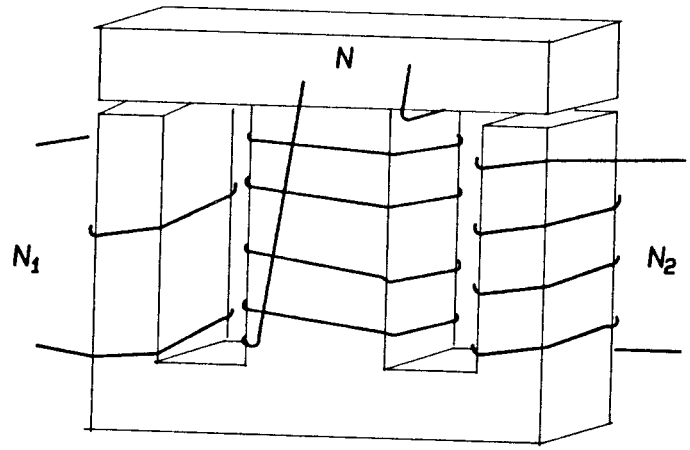

Figure 8.2: A coupled-inductor using an EI-core.

8.2.1 Determination of Zero-Current Ripple Conditions

Problem Definition:

Given the leakage parameter l of the core of Fig 8.2, determine the two air-gaps x_1 and x_2 and the turns ratio N_1/N and N_2/N, so that zero current ripple is obtained simultaneously in both outer leg windings.

Note that the same basic assumption holds as before; that is, all of the windings are subjected to the same identical voltage waveforms v.

The reluctance model of the magnetic circuit in Fig 8.2 is shown in Fig 8.3a. The only difference between this reluctance model and the one in Fig 7.3 is that in this case the center winding leakage flux is going through the air, instead of through a separate magnetic branch; therefore, the leakage reluctance $\mathcal{R}_l$ is calculated from the leakage parameter l instead of the real gap l_g in the extra leg. Similar to Fig 7.3 and

Fig 7.4, this model can be further simplified under the assumption of zero ripple currents in the outer windings ($i_1 = 0$, $i_2 = 0$), which shorts out two generators in the model and also eliminates the leakages of the outer leg windings from the model. As in Section 7.4, only the leakage of the center winding, into which the ripple current is steered, is important. From Fig 8.3a, the model in Fig 8.3b is obtained for zero ripple current conditions.

In the model of Fig 8.3b, the reluctances $\mathcal{R}_l$,$\mathcal{R}_{l_1}$ and $\mathcal{R}_1$ are the reluctances of the leakage paths of the three windings, while $\mathcal{R}_1$ and $\mathcal{R}_2$ represent the air-gap reluctances, which are considered to dominate the total reluctance of the outer legs. The later two reluctances are then defined by:

$$\mathcal{R}_1 = \frac{x_1}{\mu_0 S/2} = \frac{2x_1}{\mu_0 S} \tag{8.3}$$

$$\mathcal{R}_2 = \frac{x_2}{\mu_0 S/2} = \frac{2x_2}{\mu_0 S} \tag{8.4}$$

Note that the cross section of the outer legs is again assumed to be $S/2$, where S is the cross section of the center leg.

The zero ripple condition of this structure can be solved by exactly the same method as in Section 7.3, e. g. through the reluctance model shown in Fig. 8.3b. However, in this chapter the circuit model (Fig. 8.3c) will be used to solve the zero ripple condition.

The circuit model shown in Fig. 8.3c is derived from the reluctance model using *duality* (Section 2.4). In this model, on the primary side

$$L_l = \frac{N^2}{\mathcal{R}_l} \qquad L_{m_1} = \frac{N^2}{\mathcal{R}_1} \qquad L_{m_2} = \frac{N^2}{\mathcal{R}_2} \tag{8.5}$$

on the secondary side,

$$L_{l_1} = \frac{N^2}{\mathcal{R}_{l_1}} \qquad L_{l_2} = \frac{N^2}{\mathcal{R}_{l_2}} \tag{8.6}$$

In Fig. 8.3c, to obtain zero ripple in both secondary windings N_1, N_2 simultaneously , the voltages v_1, v_2 both have to be the same as the applied voltage v. For the

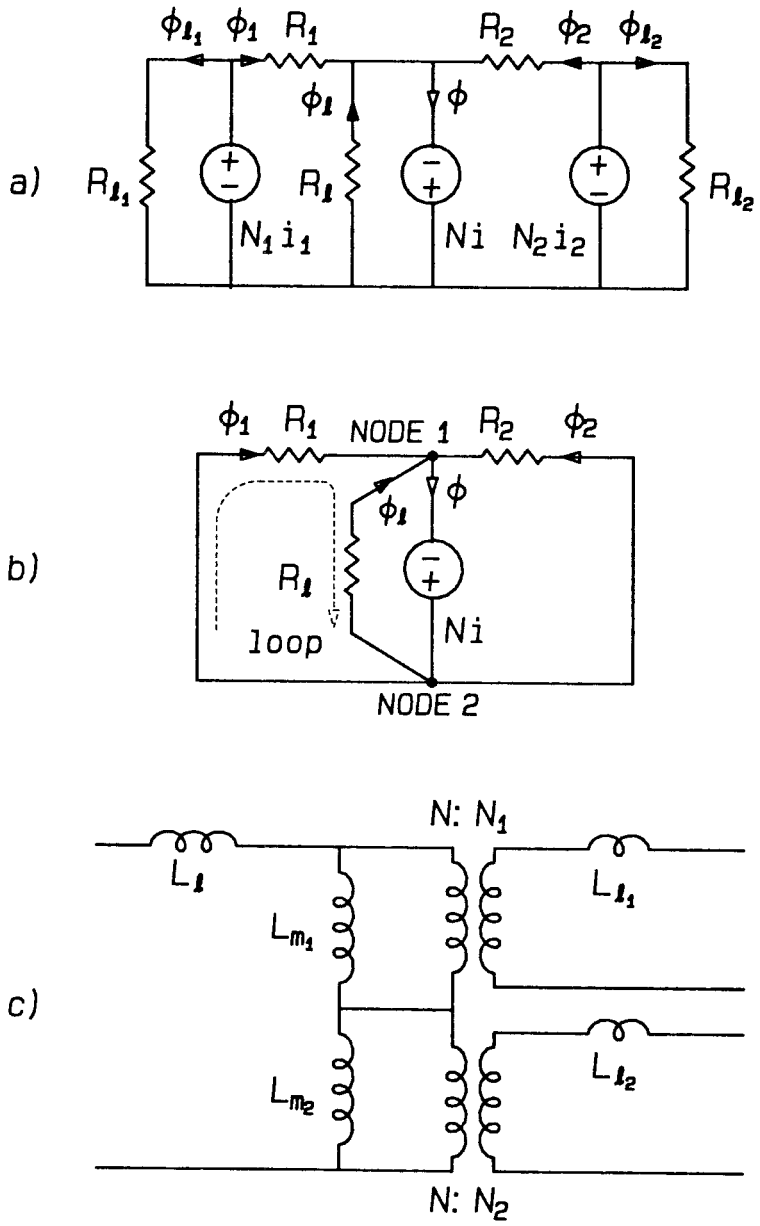

Figure 8.3: a)The reluctance model for the EI-core structure shown in Fig 8.2. b) The reluctance model for zero current ripple in the outer windings. c) The circuit model for the structure.

moment, assume that the two voltage sources v are disconnected from the two secondaries N_1, N_2, then:

$$v_1 = \frac{L_{m_1}}{L_l + L_{m_1} + L_{m_2}} \frac{N_1}{N} v \tag{8.7}$$

$$v_2 = \frac{L_{m_2}}{L_l + L_{m_1} + L_{m_2}} \frac{N_2}{N} v \tag{8.8}$$

if $v_1 = v$ and $v_2 = v$; then, when the two voltage sources are reconnected, the voltages across both secondary leakage inductances will be zero, and the secondary current ripples will also be zero.

$$\frac{L_{m_1}}{L_l + L_{m_1} + L_{m_2}} = \frac{N}{N_1} \tag{8.9}$$

$$\frac{L_{m_2}}{L_l + L_{m_1} + L_{m_2}} = \frac{N}{N_2} \tag{8.10}$$

By use of the relation between the three inductances and their corresponding reluctances (8.5), (8.9), (8.10) can be written as:

$$\frac{\frac{1}{\mathcal{R}_1}}{\frac{1}{\mathcal{R}_l} + \frac{1}{\mathcal{R}_1} + \frac{1}{\mathcal{R}_2}} = \frac{N}{N_1} \tag{8.11}$$

$$\frac{\frac{1}{\mathcal{R}_2}}{\frac{1}{\mathcal{R}_l} + \frac{1}{\mathcal{R}_1} + \frac{1}{\mathcal{R}_2}} = \frac{N}{N_2} \tag{8.12}$$

Comparing the two equations gives:

$$\frac{N_1}{\mathcal{R}_1} = \frac{N_2}{\mathcal{R}_2} \tag{8.13}$$

Rearranging (8.11), (8.12), with (8.13) gives:

$$\begin{aligned} \frac{\mathcal{R}_1}{\mathcal{R}_l} &= N_1 \left(\frac{1}{N} - \frac{1}{N_1} - \frac{1}{N_2} \right) \\ \frac{\mathcal{R}_2}{\mathcal{R}_l} &= N_2 \left(\frac{1}{N} - \frac{1}{N_1} - \frac{1}{N_2} \right) \end{aligned} \tag{8.14}$$

These zero ripple conditions can be further simplified by the use of the reluctance definitions as in (8.2), (8.3), and (8.4) and substituting into (8.14) to result

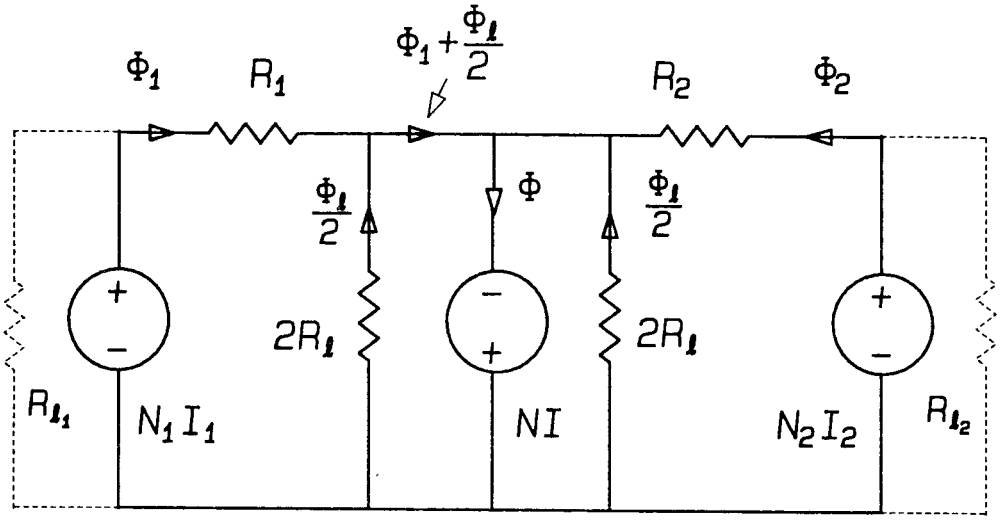

Figure 8.4: The reluctance model for dc condition.

in:

$$\begin{aligned} \frac{x_1}{l} &= \frac{N_1}{2}\left(\frac{1}{N} - \frac{1}{N_1} - \frac{1}{N_2}\right) \\ \frac{x_2}{l} &= \frac{N_2}{2}\left(\frac{1}{N} - \frac{1}{N_1} - \frac{1}{N_2}\right) \end{aligned} \tag{8.15}$$

Note that the actual air-gaps needed for zero ripple performance are determined only by the *ratio* of the turns (not their absolute value) and the leakage parameter l; also, the secondary leakages have no effect on zero ripple condition (they will, however, affect the sensitivity of the design).

In addition to ac ripple condition, the air-gaps have to be large enough to prevent saturation of any branches due to the dc current and dc fluxes.

8.2.2 Dc Saturation Conditions

The reluctance model modeling the dc current and dc flux conditions is shown in Fig 8.4. In addition to satisfying ac zero ripple conditions, the air-gaps have to be large

enough to prevent saturation of any of the magnetic branches. Because the air-gaps are concentrated in the outer legs (no air-gap in the center leg), this condition will be met, when the fluxes in both of the two loops are below saturation limit Φ_{sat}. Note also, to be precise, one has to include the leakage flux of the center leg, such that the worst case for avoiding saturation (peak flux density) is $\Phi_1 + \frac{\Phi_l}{2}$ or $\Phi_2 + \frac{\Phi_l}{2}$ (whichever is greater) and is occurring at the center leg to outer leg connection. Although this leakage flux Φ_l is normally quite small when compared to the main flux (Φ_1 or Φ_2), typically one-fifth of it, and although its omission may cause a relatively small error, its inclusion turns out to be very important since it leads to a very simple and elegant result in closed form (also makes the results more accurate). The leakage flux of the outer legs (shown in dashed lines in Fig. 8.4) should also be included, and the maximum flux density should be found by comparing $\Phi_1 + \frac{\Phi_l}{2}$, $\Phi_1 + \Phi_{l_1}$, $\Phi_2 + \frac{\Phi_l}{2}$ and $\Phi_2 + \Phi_{l_2}$. However, since the outer winding leakage reluctances $\mathcal{R}_{l_1}$ and $\mathcal{R}_{l_2}$ are about ten times larger than $\mathcal{R}_l$ (see Appendix A), Φ_{l_1} and Φ_{l_2} are almost always smaller than $\Phi_l/2$ (and much smaller than Φ_1 and Φ_2 anyway), so the effect of the outer leg leakages can be safely ignored.

From the model in Fig 8.4 we have the following conditions (inequality constraints), modeling the avoidance of dc saturation:

$$\frac{B_m S}{2} \geq \frac{N_1 I_1 + N I}{\mathcal{R}_1} + \frac{N I}{2\mathcal{R}_l} \tag{8.16}$$

$$\frac{B_m S}{2} \geq \frac{N_2 I_2 + N I}{\mathcal{R}_2} + \frac{N I}{2\mathcal{R}_l} \tag{8.17}$$

Note that in the model of Fig 8.4 the total leakage reluctance $\mathcal{R}_l$ is split into the parallel connection of two leakage reluctances of value $2\mathcal{R}_l$, thus leading to the symmetrical model and (8.16) and (8.17). Note also that, since the outer leg cross section is half that of the center leg, $S/2$ is used in the above equations.

Again, by taking into account the reluctance definitions (8.2), (8.3), and (8.4)

we get:

$$\frac{B_m}{\mu_0} \geq N\,I\left(\frac{1}{x_1}+\frac{1}{l}\right)+N_1 I_1\frac{1}{x_1} \tag{8.18}$$

$$\frac{B_m}{\mu_0} \geq N\,I\left(\frac{1}{x_2}+\frac{1}{l}\right)+N_1 I_1\frac{1}{x_2} \tag{8.19}$$

8.2.3 Derivation of Inductance L

The ripple currents that are steered from the outer windings into the center winding will result in some finite ripple current Δi in that winding. The original design requirement to have a particular ripple Δi may be translated into a requirement for a total self-inductance of this winding. This inductance will consist of the inductance due to the main mutual flux path as well as the inductance due to the leakage flux path. Therefore,

$$L = N^2\left(\frac{1}{\mathcal{R}_1}+\frac{1}{\mathcal{R}_2}+\frac{1}{\mathcal{R}_l}\right) \tag{8.20}$$

Again, by use of the reluctance definitions (8.2), (8.3), and (8.4) we have:

$$L = \mu_0 S\,N^2\left(\frac{1}{2x_1}+\frac{1}{2x_2}+\frac{1}{l}\right) \tag{8.21}$$

8.3 THE DESIGN EQUATIONS FOR THE THREE WINDING COUPLED-INDUCTORS

The pertinent equations can now be summarized as follows.

$$\frac{x_1}{l} = \frac{N_1}{2}\left(\frac{1}{N}-\frac{1}{N_1}-\frac{1}{N_2}\right) \tag{8.22}$$

$$\frac{x_2}{l} = \frac{N_2}{2}\left(\frac{1}{N}-\frac{1}{N_1}-\frac{1}{N_2}\right) \tag{8.23}$$

$$\frac{B_m}{\mu_0} \geq N\,I\left(\frac{1}{x_1}+\frac{1}{l}\right)+N_1 I_1\frac{1}{x_1} \tag{8.24}$$

$$\frac{B_m}{\mu_0} \geq N\,I\left(\frac{1}{x_2}+\frac{1}{l}\right)+N_2 I_2\frac{1}{x_2} \tag{8.25}$$

$$L = \mu_0 S\,N^2\left(\frac{1}{2x_1}+\frac{1}{2x_2}+\frac{1}{l}\right) \tag{8.26}$$

Now, from these five equations we need to solve for five unknowns: N, N_1, N_2, x_1 and x_2, given the known parameters L, I, I_1, I_2, l, and constants B_m and μ_0. However, before attempting to solve it, we need to derive some important relationships, so that the simple closed form solutions can be obtained.

8.3.1 Derivation of Important Analytical Relations

Although Equations (8.22) through (8.26) seem quite complex, some simple relations can be derived, which will make the closed form solution possible.

From (8.13) we get directly:

$$\frac{N_1}{x_1} = \frac{N_2}{x_2} \tag{8.27}$$

From (8.26) we get:

$$\frac{L}{N} = N\left(\frac{1}{\mathcal{R}_1} + \frac{1}{\mathcal{R}_2} + \frac{1}{\mathcal{R}_l}\right) \tag{8.28}$$

Expressing $\frac{1}{\mathcal{R}_2}$ and $\frac{1}{\mathcal{R}_l}$ in terms of $\frac{1}{\mathcal{R}_1}$ by use of (8.13) and (8.14) and substitution in (8.28) results in:

$$\frac{L}{N} = \frac{N_1}{\mathcal{R}_1} \tag{8.29}$$

or equivalently,

$$\frac{L}{N} = \frac{\mu_0 S}{2}\frac{N_1}{x_1} = \frac{\mu_0 S}{2}\frac{N_2}{x_2} \tag{8.30}$$

With the help of these relations, we can now find the solution of Equations (8.22) through (8.26) for both the general case and the special case with the most practical interest, that is, equal air-gap on both sides.

8.3.2 Toward Analytical Solution in a closed Form

Is designing a single winding inductor, to fully utilize the flux capability of the core, the inductor is normally designed to have its flux density reaching the maximum

allowed flux density B_m of the core. Therefore, it seems natural that the optimum design for coupled-inductors would also be obtained when the flux density, in outer core legs as well as in the center leg, is allowed to reach the peak flux density B_m simultaneously. This effectively corresponds to transforming the two inequality dc conditions (8.24), (8.25) into equalities. However, we are in for a big surprise. By making such as assumption *a priori*, under certain conditions we may obtain a very inefficient design as the following analysis will reveal.

Under equal peak flux density B_m in both magnetic loops, the dc conditions turn into following equalities:

$$\frac{B_m}{\mu_0} = N\,I\left(\frac{1}{x_1}+\frac{1}{l}\right)+N_1 I_1\frac{1}{x_1} \tag{8.31}$$

$$\frac{B_m}{\mu_0} = N\,I\left(\frac{1}{x_2}+\frac{1}{l}\right)+N_2 I_2\frac{1}{x_2} \tag{8.32}$$

Now, we are looking for an explicit solution of Equations (8.22) (8.23) (8.26) (8.31) (8.32) for N, x_1, x_2, and N_1, N_2, knowing B_m, μ_0, S, l, I_1, I_2, and I.

Adding (8.31) and (8.32) together and dividing by two gives:

$$\frac{B_m}{\mu_0} = N\,I\left(\frac{1}{2\,x_1}+\frac{1}{2\,x_2}+\frac{1}{l}\right)+\frac{I_1}{2}\frac{N_1}{x_1}+\frac{I_2}{2}\frac{N_2}{x_2} \tag{8.33}$$

Solving (8.26) for $\frac{1}{2\,x_1}+\frac{1}{2\,x_2}+\frac{1}{l}$, also solving (8.30) for $\frac{N_1}{x_1}$ and $\frac{N_2}{x_2}$, then substituting into (8.33), gives:

$$B_m = \frac{L}{S\,N}(I+I_1+I_2) \tag{8.34}$$

after rearranging

$$N = \frac{L(I+I_1+I_2)}{B_m S} \tag{8.35}$$

Solving (8.30) for $\frac{N_1}{x_1}$ and substituting into(8.31) gives:

$$x_1 = \frac{N\,I}{\frac{B_m}{\mu_0}-\frac{N\,I}{l}-\frac{2L}{N}\frac{I_1}{\mu_0 S}} \tag{8.36}$$

This equation can be further simplified by solving (8.35) for B_m and substituting into the equation, giving:

$$x_1 = \frac{L_l}{L(1-\alpha) - L_l} l \tag{8.37}$$

where α is called a relative current imbalance parameter defined as:

$$\alpha = \frac{I_1 - I_2}{I}$$

and L_l is:

$$L_l = \frac{N^2 \mu_0 S}{l}$$

the equation for x_2 can be solved similarly:

$$x_2 = \frac{L_l}{L(1+\alpha) - L_l} l \tag{8.38}$$

Finally, solving equation (8.30) for N_1, N_2 and substituting into (8.37), (8.38) give the equations for N_1, N_2:

$$N_1 = 2N \frac{L}{L(1-\alpha) - L_l} \tag{8.39}$$

$$N_2 = 2N \frac{L_l}{L(1+\alpha) - L_l} \tag{8.40}$$

Therefore, the design equations can be summarized as follows:

CLOSED FORM SOLUTION:

$$N = \frac{L(I + I_1 + I_2)}{B_m S} \tag{8.41}$$

$$L_l = \frac{N^2 \mu_0 S}{l} \tag{8.42}$$

$$x_1 = l \frac{L_l}{L(1-\alpha) - L_l} \tag{8.43}$$

$$x_1 = l \frac{L_l}{L(1+\alpha) - L_l} \tag{8.44}$$

$$N_1 = 2N \frac{L}{L(1-\alpha) - L_l} \tag{8.45}$$

$$N_2 = 2\,N\,\frac{L_l}{L\,(1+\alpha) - L_l} \tag{8.46}$$

where

$$\alpha = \frac{I_1 - I_2}{I} \tag{8.47}$$

The calculation of the required turns N, N_1, N_2 and the air-gap x_1, x_2 follows in the same sequence as in the design equations. For the given choice of the core and its cross section S, from (8.41) one calculates first the center leg turns N. With this now known, the leakage inductance L_l is calculated next from (8.42). Now, both N and L_l are known and can be used to calculate N_1 and N_2 from (8.43) and (8.44). Note also that the current imbalance parameter used in these equations can easily be calculated from the definition (8.47) and three known dc currents I_1, I_2, and I. Finally, the air-gaps x_1 and x_2 are calculated from (8.45) and (8.46), since leakage parameter l is a known quantity for a given core with a given cross section S.

We have finally succeeded in arriving at an analytical solution in a *closed form* as represented by Equations (8.41) through (8.47). However, as indicated earlier, these results may in some cases break down and result in a solution that is far from optimum. Take, for example, a very practical case, in which the two outer leg windings carry highly unbalanced currents. For example, take $I_1 = 5\,I_2$, and center leg dc current $I = I_1 + I_2$. These lead to imbalance parameter $\alpha = 2/3$. In addition, assume that $L_l/L = 0.25$, a very reasonable assumption in itself. The closed form solution leads to:

$$N_1 = 24\,N \tag{8.48}$$

$$N_2 = \frac{24}{17}\,N \tag{8.49}$$

$$\frac{x_1}{l} = 3 \tag{8.50}$$

$$\frac{x_2}{l} = \frac{3}{17} \tag{8.51}$$

Note how the closed form solution (8.48) resulted in the worst possible case, an extremely large number of turns (24 times that of the center winding) needed for the winding carrying by far the largest current I_1. The fact that the other outer leg winding has a much smaller number of turns (slightly higher than the number of turns in the center winding N) with much smaller current is of very little consolation. Although the losses of N_2 will be very small, the losses in the high current winding N_1 will be overwhelming, making the design very inefficient and in fact completely impractical.

One might now ask the questions: *What went wrong? How could this have happened? Is there any hope to make acceptable low-loss design in case of unbalanced currents?*

Here is a qualitative explanation why this result should have been expected.

For a design with different currents in the two outer leg windings, the design equations (8.50), (8.51) will result in a design with a larger air-gap in the leg with the high current winding than in the other leg. The ac flux generated by the center leg winding is distributed between the two legs according to the permeance of each leg. Therefore, the leg with the high current winding (large gap) will receive less ac flux (the two outer leg windings that have zero current ripple in them, generate no ac flux). The high current leg winding, with less ac flux, will then require more turns to generate the voltage to counterbalance the externally applied voltage v and needs a smaller wire size. More turns, smaller wire size, plus larger current, results in a much higher copper loss in the high current winding.

Although this qualitative reasoning seems to support the earlier quantitative results, the quantitative results (8.48) to (8.51) obtained from (8.43) to (8.46) are, in fact, much worse than this qualitative analysis indicates. There is a very simple explanation for that. The very first assumption that was made at beginning of this closed form solution

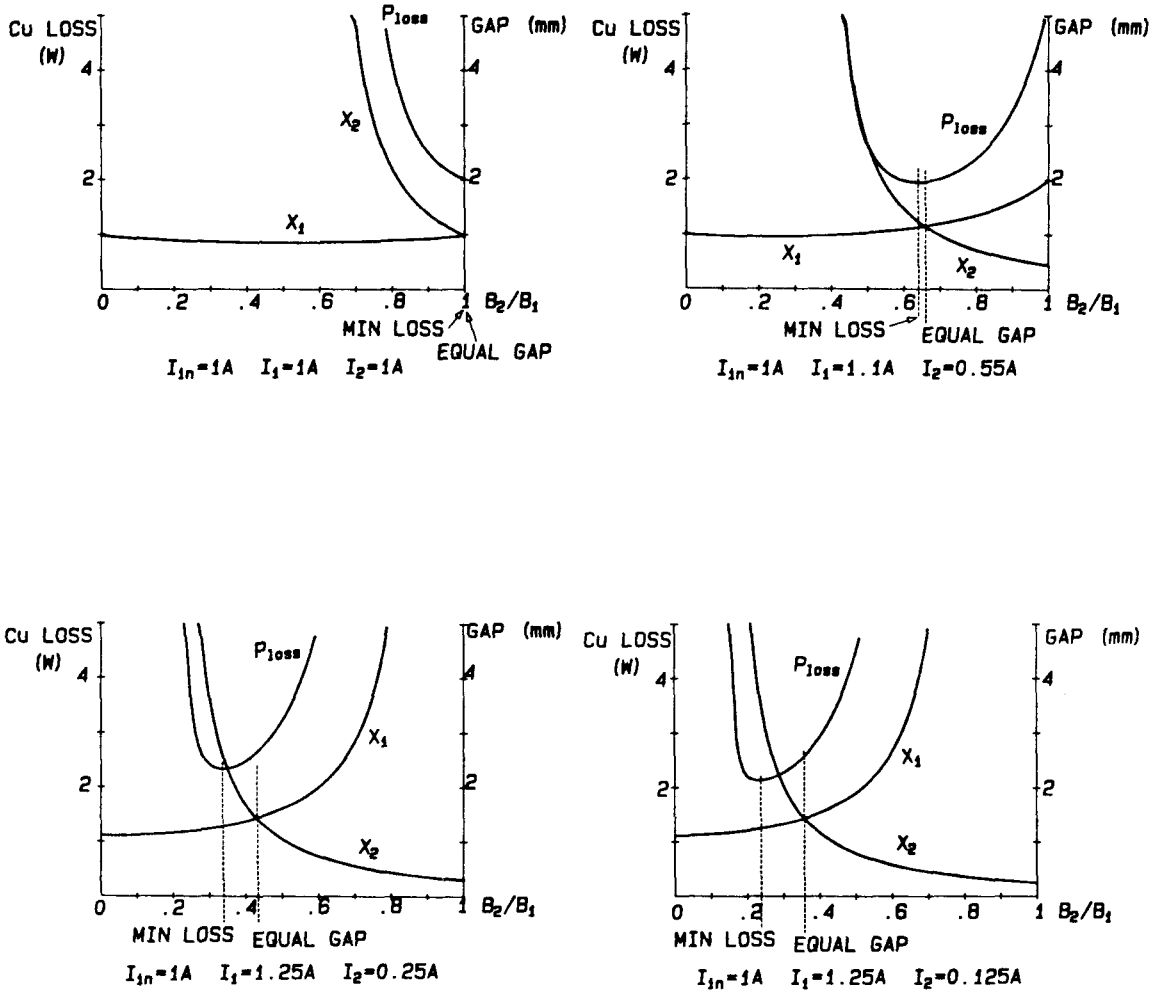

EI-50 Core, B_1=.35Tesla, L_{in}=2mH

Figure 8.5: Examples for different designs show that equal air-gap gives almost minimum copper loss.

derivation, maximum flux density B_m in both outer legs, is the cause of all our problems. Suppose now that only the high current side is reaching the peak flux density, that is, $B_1 = B_m$, while the leg with the low current winding is allowed to have flux density less than the maximum flux density B_m, or $B_2 < B_m$, by increasing its air-gap. The total copper loss for the coupled-inductors will be reduced, since more ac flux generated by the center winding will now be directed into the high current leg, thereby requiring fewer turns on the high current winding. To find the optimum flux density in the low current leg, one may vary the relative ratio B_2/B_1 of the fluxes in two legs and compute the resultant copper losses and air gaps. The result of these computer simulation for balanced as well as several unbalanced current cases is shown in Fig. 8.5. Note how these computer generated plots verify the previous finding of extremely high losses when B_2 approaches B_m, when the currents in the outer legs are grossly unbalanced.

The correct approach to derive the analytical results having high efficiency and low copper loss in mind, would be to assume that only *one* of the dc saturation inequality constraints is reduced to equality, and that is the one for the leg with the high current winding. Unfortunately, for this case, we cannot obtain the solution in a closed form but are directed instead toward computer simulations.

Is there any use for the already derived closed form solution we found to be so inefficient? The answer is affirmative for a special case of balanced or equal currents in outer legs. The current imbalance parameter α becomes zero in this case, and the closed form solution simplifies to the following design equations:

DESIGN EQUATIONS FOR BALANCED CURRENTS $i_1 = i_2$:

$$N = \frac{L(I + 2I_1)}{B_m S} \tag{8.52}$$

$$L_l = \frac{N^2 \mu_0 S}{l} \tag{8.53}$$

$$x = x_1 = x_2 = l \frac{L_l}{L - L_l} \tag{8.54}$$

$$N_1 = N_2 = 2\,N\,\frac{L}{L - L_l} \tag{8.55}$$

Note that this closed form solution obtained for the special case $I_1 = I_2$ is also acceptable from the standpoint of copper losses and efficiency. This is not surprising, since $I_1 = I_2$ implies equal gaps $x_1 = x_2$, and then the two dc saturation equations are identical; hence, original assumption that the flux density in both legs should reach the maximum flux density of the core is correct. This result is also verified in Fig. 8.5a, in which the simulation shows that the minimum loss occurs when *the two air-gaps are equal* and peak flux densities B_m in *both legs simultaneously.*

It is interesting to note that the equal air-gaps will result in *almost* minimum total copper losses even when the outer leg currents are *highly unbalanced.* This certainly serves as a very good motivation to investigate the equal air-gap case and find if the closed form solution can be found even for unbalanced currents in outer legs. As another motivation, the equal air-gaps in outer legs can, with minimum modifications be transformed into a configuration with a single uniform spacer, as illustrated later in Fig. 9.1 of Chapter 9. A very elegant and practical solution would then be obtained, since the uniform paper spacer eliminates a rather messy and costly gaping of the outer legs.

8.4 CLOSED FORM SOLUTION FOR EQUAL GAPS

The zero ripple conditions and dc saturation equations can be considerably simplified, when equal air-gaps in the outer legs are assumed. Equal air-gaps $x_1 = x_2$ lead from (8.27) to equal turns on the outer legs:

$$x = x_1 = x_2 \implies N_1 = N_2 \tag{8.56}$$

The zero ripple condition (Equation (8.22, (8.23)) under the equal gap as-

sumption (8.56) becomes:

$$\frac{x}{l} = \frac{N_1}{2\,N} - 1 \tag{8.57}$$

The peak flux density, which is dependent on the dc currents in all three windings and governed by Equations (8.24) and (8.25), under the assumption (8.56) become:

$$\frac{B_m}{\mu_0} \geq N\,I\left(\frac{1}{x}+\frac{1}{l}\right) + N_1 I_1 \frac{1}{x} \tag{8.58}$$

$$\frac{B_m}{\mu_0} \geq N\,I\left(\frac{1}{x}+\frac{1}{l}\right) + N_1 I_2 \frac{1}{x} \tag{8.59}$$

Note that, if $I_1 \geq I_2$, only Equation (8.58) is critical and (8.59) is *automatically satisfied.* In other words, only the leg carrying higher current I_1 will be optimally designed to carry maximum peak flux density B_m, while the other leg will actually be operating at a lower flux density.

Note that this is in complete agreement with previous discussions and the computerized simulation results (Fig. 8.5), which for low copper losses required that only the leg with the high current winding operates at the peak flux density.

Together with the definition for the the primary inductance L, the complete set of equations which needed to be solved is:

$$\frac{x}{l} = \frac{N_1}{2\,N} - 1 \tag{8.60}$$

$$\frac{B_m}{\mu_0} = N\,I\left(\frac{1}{x}+\frac{1}{l}\right) + N_1 I_1 \frac{1}{x} \tag{8.61}$$

$$L = \mu_0 S\,N^2\left(\frac{1}{x}+\frac{1}{l}\right) \tag{8.62}$$

Now, we are looking for an explicit solution of Equations (8.60) to (8.62) for N, x and N_1 knowing B_m, μ_0, S, l, I_1 and I. Fortunately, this time there is a closed form solution even for the unbalanced case $I_1 \geq I_2$. The derivation follows the same steps as in Section 8.2 and gives:

DESIGN EQUATIONS FOR EQUAL GAPS:

$$N = \frac{L(I + 2I_1)}{B_m S} \tag{8.63}$$

$$L_l = \frac{N^2 \mu_0 S}{l} \tag{8.64}$$

$$x = l \frac{L_l}{L - L_l} \tag{8.65}$$

$$N_1 = 2N \frac{L}{L - L_l} \tag{8.66}$$

The calculations then proceed in the same order as the above equations. Namely, for the given absolute remaining ripple current Δi in the center winding, one calculates the required inductance L and from (8.52) the center winding turns N. The leakage inductance L_l is then evaluated from (8.53) and substituted in (8.54) to give the required air-gap x (assuming leakage parameter l for the core is known). Finally, the number of turns on the two outer legs are calculated from (8.55).

Note that the design equations for equal air-gaps are identical in form to those obtained earlier for balanced currents ((8.52)–(8.55)), except that this time they are valid even for the imbalanced currents, that is, for $I_1 \geq I_2$. The same problem of high copper losses still exists, though it is better than using unequal air-gaps ((8.41)–(8.47)).

8.5 "BLOW-UP" PROBLEM IN THE COUPLED-INDUCTOR DESIGN

Closer examination of the design equations (8.63) to (8.66) reveals that even an unexpected "blow-up" problem exists. As seen from (8.65) and (8.66), when required inductance L approaches the built in leakage inductance L_l, the denominator approaches zero, and infinitely large gaps x_1, x_2 are required together with infinite number of turns N_1 and N_2. Clearly, this will lead to an extremely inefficient design, in fact, to an "infinitely" inefficient design. The fact that this is possible can be seen from the first two

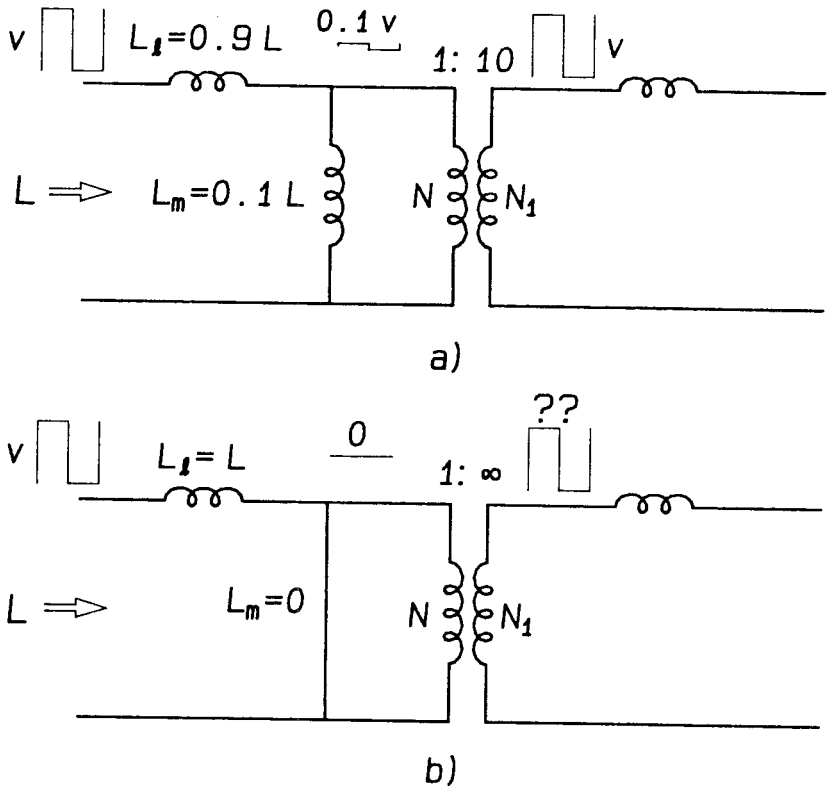

Figure 8.6: Equivalent circuit models illustrating the "blow-up" problem. a) Case when leakage inductance L_l is 90% of the primary inductance L. b) Degenerate case when $L_l = L$.

Equations, (8.63) and (8.64). While the required inductance L grows linearly proportional to the increase of the number of turns N on the center winding, the leakage inductance L_l, being an air-core phenomena, grows with the square of the number of turns on the center winding. Consequently, at some high enough number of turns on the center winding, which we call *critical turns* N_c, the two inductances become equal; thus, the "blow-up" occurs.

This phenomenon can also be understood quantitatively from the equivalent circuit models in Fig. 8.6. Note that the total required inductance L is composed of the sum of the primary leakage inductance L_l and the magnetizing inductance L_m, as

seen in Fig. 8.6a. When leakage inductance L_l approaches L (say $L_l = 0.9\,L$), the magnetizing inductance L_m (inductance due to the magnetic core flux) becomes very small ($L_m = 0.1\,L$), leading to a large attenuation (here, a factor of 10) of the input drive waveform. Consequently, large turns ratio step-up of 1:10 or $N_1 = 10\,N$ is needed to compensate for that, to result in zero ripple current in the secondary. The large number of turns N_1 required result in large total amper-turns; hence, large air-gaps are required as well to prevent core saturation. In the extreme case when $L_l = L$, the the picture is degenerated to the point where the magnetizing inductance is zero; hence, an infinite number of turns are needed to bring the drive voltage back to the initial magnitude (Fig.8.6b).

Another way to interpret these circuit models is from the standpoint of high dc current requirements, instead of requirement of high inductance L, which led to the large number of turns. High dc currents require large air-gaps, hence small magnetizing inductance. But the leakage inductance L_l is relative independent of air-gap sizes, so it remains large. Then the turns ratio N_1/N again needs to be large to bring the secondary voltage up to the original value.

From the above discussions, it seems that a design requiring large currents and large inductance will almost always face this "blow-up" problem. Even if it can be avoided, the design will still be relatively inefficient. Fortunately, one free parameter, the core cross section S can be chosen appropriately to avoid this problem. Namely, if we have already chosen a core with a small cross section S, but require a relatively large inductance L, then the design will indeed need a large number of turns, and clearly be in the highly inefficient area. However, if a core with a large cross section S is chosen, a relatively small number of turns will give the required inductance L, and both the potential "blow-up" and inefficient problems are avoided. Of course, the penalty for this

is the usual one: the higher the efficiency, the larger the required core size.

The natural question now is: How can one pick the core size which will give a good balance between efficiency and size? The design equations (8.63) to (8.66), as they are written, do not seem to answer the question, since they are based on a preselected core cross section S and then calculate the number of turns N, N_1 from that cross section. Although a number of trial and errors with different cross section S could be made, and a small, efficient design chosen from the results, a more direct design procedure can be established as follows.

First, the design equations (8.65), (8.66) are modified as:

$$\frac{N_1}{2\,N} = \frac{1}{1 - L_l/L} \tag{8.67}$$

$$\frac{x}{l} = \frac{L_l/L}{1 - L_l/L} \tag{8.68}$$

Both equations depend on the ratio L_l/L. From the first two design equations (8.63) and (8.64), this ratio can be written as:

$$\frac{L_l}{L} = \frac{\mu_0 I_e N}{B_m l} \tag{8.69}$$

where I_e is defined as effective dc current:

$$I_e \equiv I + 2\,I_1 \tag{8.70}$$

The dimensionless inductive ratio L_l/L can further be expressed in turns of the turns ratio:

$$\frac{L_l}{L} = \frac{N}{N_c} \tag{8.71}$$

$$N_c \equiv \frac{B_m l}{\mu_0 I_e} \tag{8.72}$$

where N_c is defined as the critical number of turns on the center leg for which the "blow-up" will occur. If $N = N_c$, then the leakage inductance L_l will be the same as the

required primary inductance L, and both the secondary turns N_1 and the air-gap x will be infinite. The farther away from this "blow-up" point, the more efficient but the larger the design will be. The question of how far away from this point the design should be can now be even quantitatively answered. Substituting (8.71) into (8.67) and (8.68) gives:

$$\frac{N_1}{2N} = \frac{1}{1 - N/N_c} \tag{8.73}$$

$$\frac{x}{l} = \frac{N/N_c}{1 - N/N_c} \tag{8.74}$$

These two dimensionless curves are plotted in Fig. 8.7 as a function of N/N_c. These curves can now be used for quantitative assessment as to how to choose the number of turns N, and then indirectly from (8.63) to choose the required core cross section S.

It is once again important to distinguish clearly the two extreme cases. When N approaches the critical turns N_c, a highly inefficient design requiring a large number of turns N_1 on the secondaries is obtained. If N is much smaller than N_c (say 10% or below), smaller number of turns N_1 lead to an efficient design. However, a large core size is required. In addition, a relatively low leakage inductance L_l will make the zero current ripple adjustment quite sensitive. The best trade-off is, of course, somewhere in between these extremes. As seen from the curves on Fig. 8.7, the "blow-up" problem becomes significant at the point where the linear portion of the curves at low values of N/N_c (less than 0.15) changes into a highly nonlinear part at higher values of N/N_c (say above $0.3 \sim 0.4$). Hence, the best trade-off of the moderate size and the simultaneous high efficiency is obtained when N is chosen to be around 20% of the critical turns N_c.

The following design procedure can now be established:

Step 1. Estimate the critical number of turns N_{c_0}:

$$N_{c_0} = \frac{B_m l_0}{\mu_0 I_e} \tag{8.75}$$

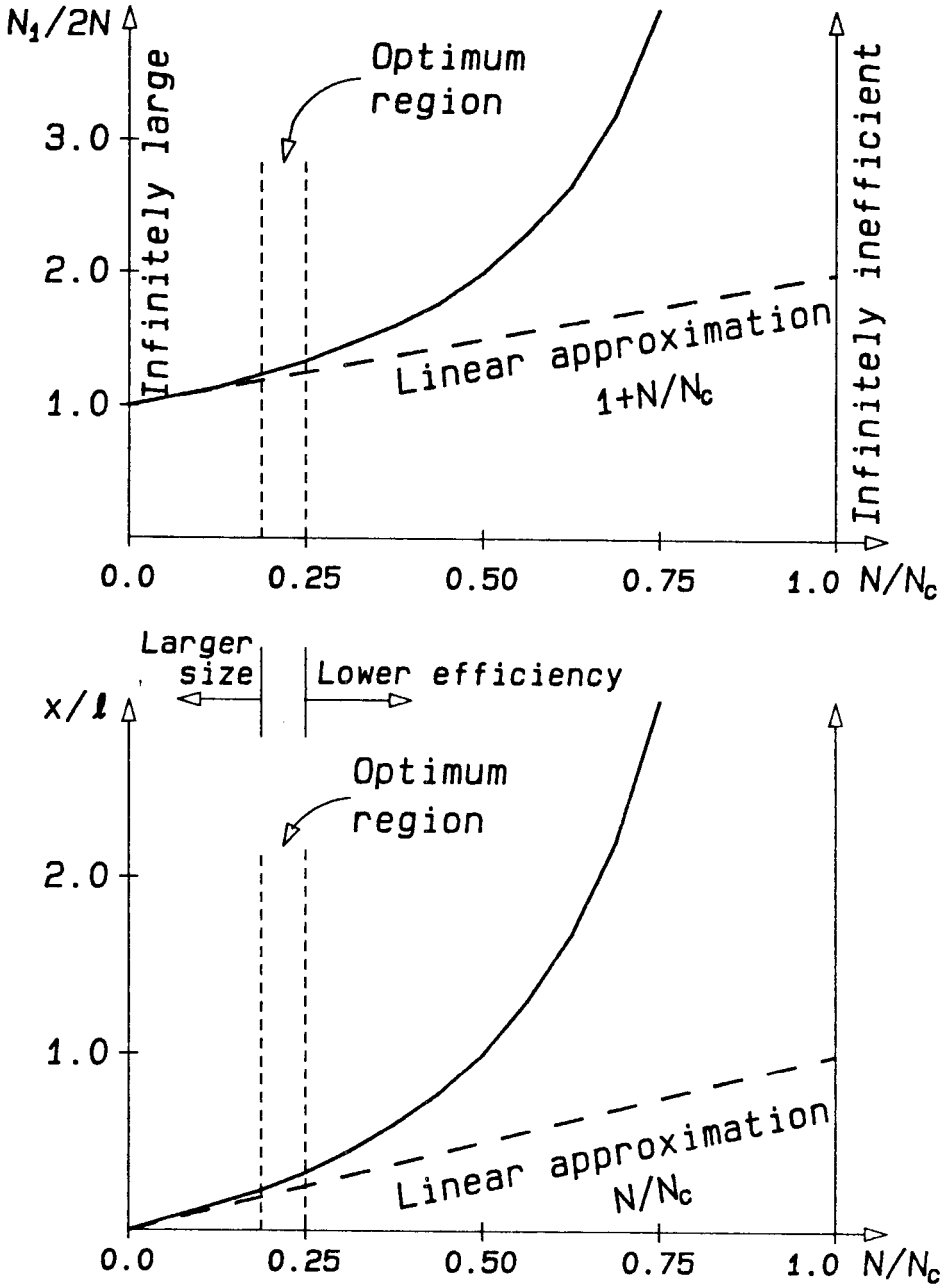

Figure 8.7: Design curves to quantitatively assess the "blow-up" problem.

The leakage parameter l_0 used for estimation can be chosen as $2mm$ for gapped cores and small cores using spacers, $4mm$ for large cores using spacers.

Step 2. Choose a nominal center leg turns N_0:

$$N_0 = 0.2N_{c_0} \tag{8.76}$$

Step 3. Evaluate the core cross section needed:

$$S_0 = \frac{L\,I_e}{B_m N_0} \tag{8.77}$$

and choose a core with the closest cross section S.

Step 4. Use the chosen core cross section S and leakage parameter l to recalculate the critical number of turns and the number of turns for the center winding:

$$N_c = \frac{B_m l}{\mu_0 I_e} \tag{8.78}$$

$$N = \frac{L\,I_e}{B_m S} \tag{8.79}$$

Step 5. Calculate the number of turns on the outer legs:

$$N_1 = \frac{2\,N}{1 - N/N_c} \tag{8.80}$$

Step 6. Find the required air-gap x:

$$x = \frac{N/N_c}{1 - N/N_c}\,l \tag{8.81}$$

Since both L_l and L are defined with respect to the same cross section S, it is not surprising that their relative ratio L_l/L is independent of S. Consequently, the critical number of turns N_c as defined by (8.72) also does not depend on S. In fact, the critical turns N_c are dependent only on one design variable, the effective dc current I_e, since all other parameters are design constants, such as B_m, l and μ_0. If the effective dc current I_e is substantially increased, the critical turns N_c will decrease, and require a

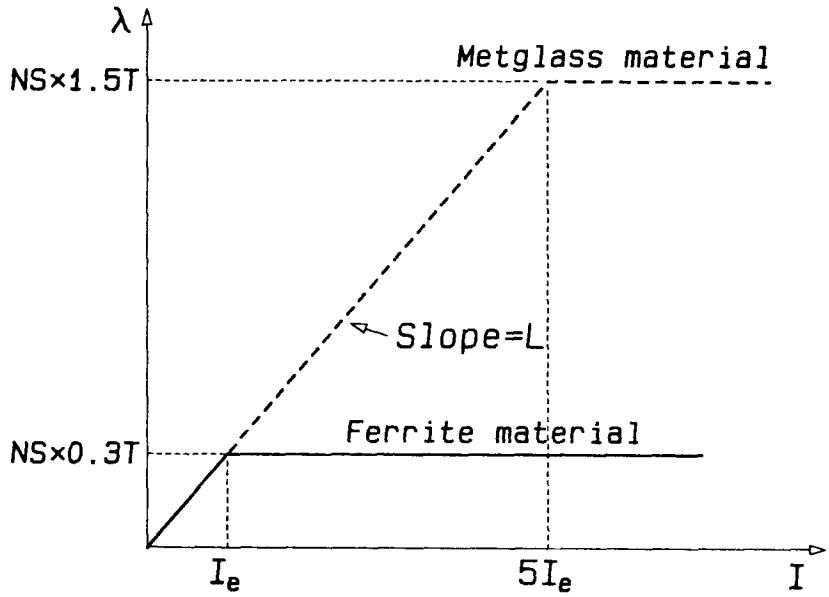

Figure 8.8: Core material with higher maximum flux density B_m permits higher effective dc current I_e before saturation.

proportionally reduced N for an efficient design. Therefore, from the definition of N_c, the limitation of the design at very high currents becomes apparent, for example, for typical numbers, such as $B_m = 0.3T$ for ferrite material, $l = 2mm$, $\mu_0 = 4\pi \times 10^{-7} H/m$ and $I_e = 10A$.

$$I_e = 10\text{A} \Longrightarrow N_c = 48\text{Turns} \tag{8.82}$$

If N is chosen to be 20% of N_c, then $N \approx 10$ Turns. If the effective current I_e is increased to 50A, only two turns on the center winding will be allowed for an efficient design.

However, the situation may not be as bad as it may seem, since another parameter, the flux density B_m can be increased if we change the core material. For example, if a core material with a high maximum flux density, such as "metglass" with $B_m = 1.5$T, the same core size, air-gaps, and number of turns, will allow five times greater effective

current before the core saturation. This is represented in Fig. 8.8, where the same slope of flux linkages λ vs. dc current I_e indicates the same inductance L, and the same number of turns N, but the effective dc current can be increased proportionally to the maximum flux density of the core material.

Let us now illustrate the above design procedure using a practical design example.

8.6 DESIGN EXAMPLE

The coupled-inductors are designed to be used in a two output Ćuk converter operating at $500kHz$. The input voltage is $30V$, output voltages are $\pm 18V$. The two output currents are rated at $1.2A$ each. All the ripple current is steered to the input; the peak-to-peak input ripple current is $1.6A$. The flux density of the core is chosen to be 0.3Tesla.

For a Ćuk converter, the voltage transfer ratio is given by:

$$\frac{V}{V_g} = \frac{D}{D'} \tag{8.83}$$

For $V_g = 30V$, $V = 18V$, the required duty ratio is:

$$D = \frac{V}{V_g + V} = 0.375 \tag{8.84}$$

Considering the losses in the circuit, set the duty ratio $D = 0.4$. For switching frequency $f_s = 500kHz$, duty ratio $D = 0.4$, and input voltage $V_g = 30V$, peak-to-peak ripple current $\Delta i = 1.6A$, the input inductance is calculated to be:

$$L = \frac{V}{\Delta i}\Delta t = \frac{V}{\Delta i}\frac{D}{f_s} = 15\mu H \tag{8.85}$$

The average input current is:

$$I_a = (I_1 + I_2)\frac{D}{D'} = 1.6A \tag{8.86}$$

The peak input current I is the average input current plus the peak ripple current:

$$I = I_a + \frac{\Delta i}{2} = 2.4A \tag{8.87}$$

The effective current is:

$$I_e = I + 2\,I_1 = 4.8A \tag{8.88}$$

The coupled-inductors are designed using (8.75) to (8.81):

Step 1. Using $l_0 = 2mm$ for the leakage parameter, the trial critical number of turns N_{c_0} is:

$$N_{c_0} = \frac{B_m l_0}{\mu_0 I_e} = 100\,\text{Turns} \tag{8.89}$$

Step 2. The nominal number of turns on the center leg N_0 is:

$$N_0 = 0.2 N_{c_0} = 20\,\text{Turns} \tag{8.90}$$

Step 3. The required core cross section is:

$$S_0 = \frac{L\,I_e}{B_m N_0} = 0.12cm^2 \tag{8.91}$$

An EE-16 core is chosen. The cross section of the core is $0.2cm^2$; the leakage parameter is $1.35mm$.

Step 4. The critical number of turns and the number of turns for the center winding are recalculated to be:

$$N_c = \frac{B_m l}{\mu_0 I_e} = 67\,\text{Turns} \tag{8.92}$$

$$N = \frac{L\,I_e}{B_m S} = 12\,\text{Turns} \tag{8.93}$$

The ratio of N/N_c is 0.179.

Step 5. The number of turns on the outer legs are:

$$N_1 = \frac{2\,N}{1 - N/N_c} = 29\,\text{Turns} \tag{8.94}$$

Step 6. The air-gap x is:

$$x = \frac{N/N_c}{1 - N/N_c} l = 0.295mm \tag{8.95}$$

Because an EE-core is used, the spacer should be half the calculated value (see Chapter 9).

The design can be summarized as follows:

The input inductance L for the coupled-inductors is $15\mu H$. The core is EE-16 core with a $0.15mm$ spacer. The number of turns for each winding is: 12 Turns for the input winding on the center leg, 29 Turns for each output winding on the outer legs. The ratio of N/N_c is only 0.179, so a smaller core could be used if size is important.

Chapter 9

OTHER EI AND EE-CORE STRUCTURES FOR COUPLED-INDUCTORS

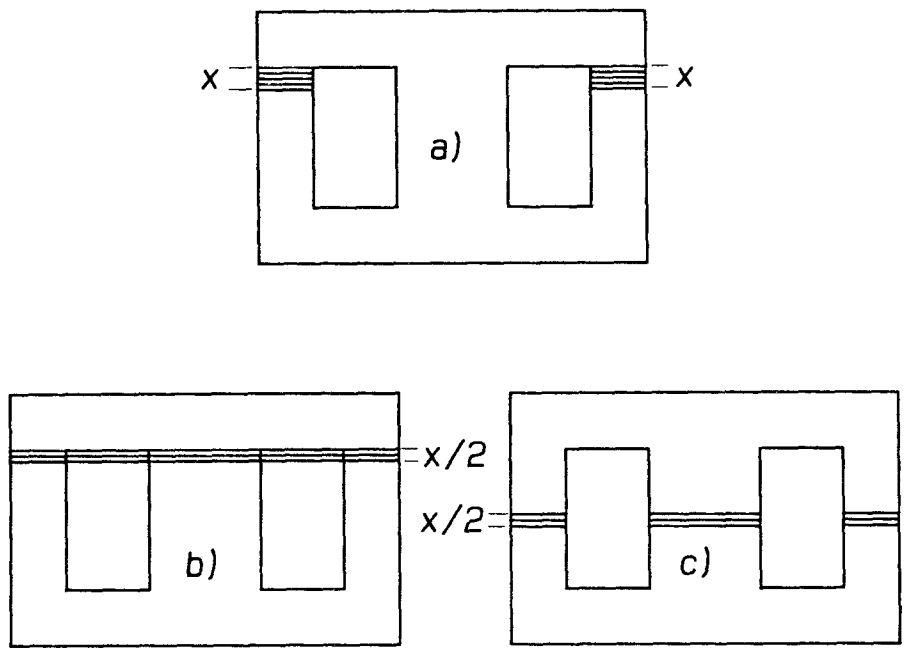

Figure 9.1: Converting the two equal concentrated gaps (a) into a single uniform spacer gap with half the thickness in an EI-core (b) or three equal gaps in an EE-core.

The EI-core coupled-inductor structure, with an air-gap in each outer leg, as described in the last chapter, has many advantages compared with earlier designs. The air-gap grinding, however, is extremely messy in the prototype optimization and quite expensive in large scale production. The equal gap design, also discussed in the last

chapter, leads to the new design using a uniform spacer for the air-gap; that is, instead of using two separated air-gaps on the two outer legs, a common spacer of half the thickness is placed between the unground E-piece and I-piece of the core (Fig. 9.1b). This configuration leaves the core intact and therefore eliminates the core grinding process. Another new configuration that uses an EE-core with equal air-gaps in all three legs (Fig. 9.1c) not only eliminates the core grinding, but also brings up another advantage: the ease of designing multiple-winding (more than three windings) coupled-inductors, because of the symmetry of the structure.

9.1 THE EI-CORE COUPLED-INDUCTOR STRUCTURE USING A COMMON SPACER

9.1.1 The Reluctance Model and the Circuit Model

The structure discussed in the last chapter, has gaps on the outer legs (gapped core structure) as shown in Fig. 9.2a; all the leakage flux paths of the primary winding can be lumped into one single leakage reluctance R_l (Fig 9.2b). Therefore, there is only one leakage inductance in the circuit model (Fig 9.2c).

The reluctance model of the the EI-core structure using a common spacer (spacer core) is shown in Fig. 9.3b, and the corresponding circuit model is shown in Fig. 9.3c. Note that now in the reluctance model there are two leakage reluctances $\mathcal{R}_{l_a}$ and $\mathcal{R}_{l_b}$ across the primary winding. The first one, $\mathcal{R}_{l_a}$, corresponds to the leakage flux path directly around the primary winding (ϕ_{l_a} in Fig. 9.3a); the second one, $\mathcal{R}_{l_b}$, corresponds to the leakage flux path from the I piece to the bottom of the E piece (ϕ_{l_b} in Fig. 9.3a). The two primary leakage reluctances, lead to the two leakage inductances L_{l_a}, L_{l_b} in the primary of the circuit model Fig. 9.3c. This model, while seeming to be quite accurate, makes the circuit very hard to analyze. The two leakage reluctances are

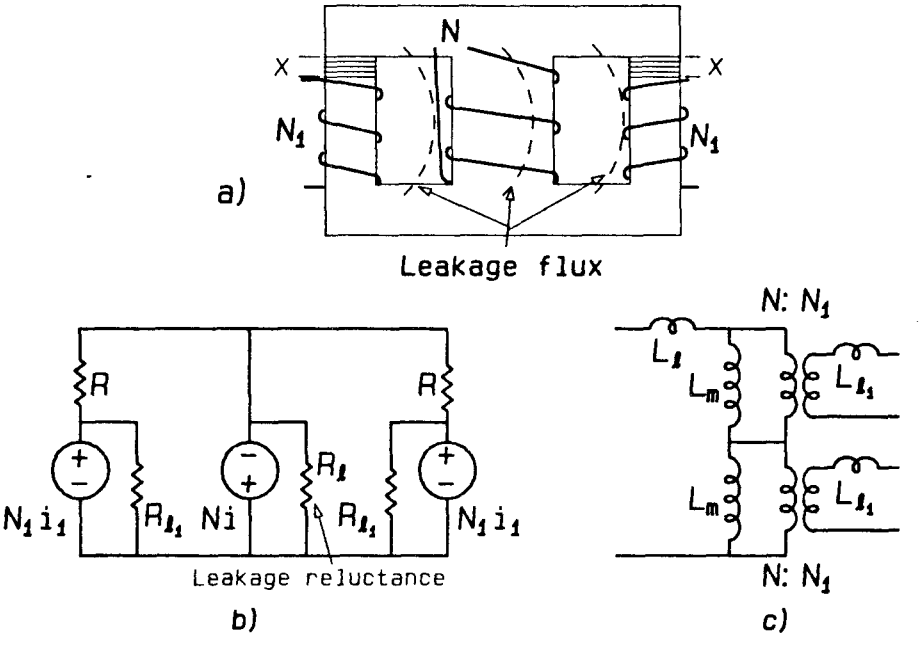

Figure 9.2: In the EI-core structure with two gaps on the outer legs (a), all the primary leakage flux paths can be lumped into one single leakage reluctance in the reluctance model (b). The circuit model (c) has only one leakage inductance in the input side.

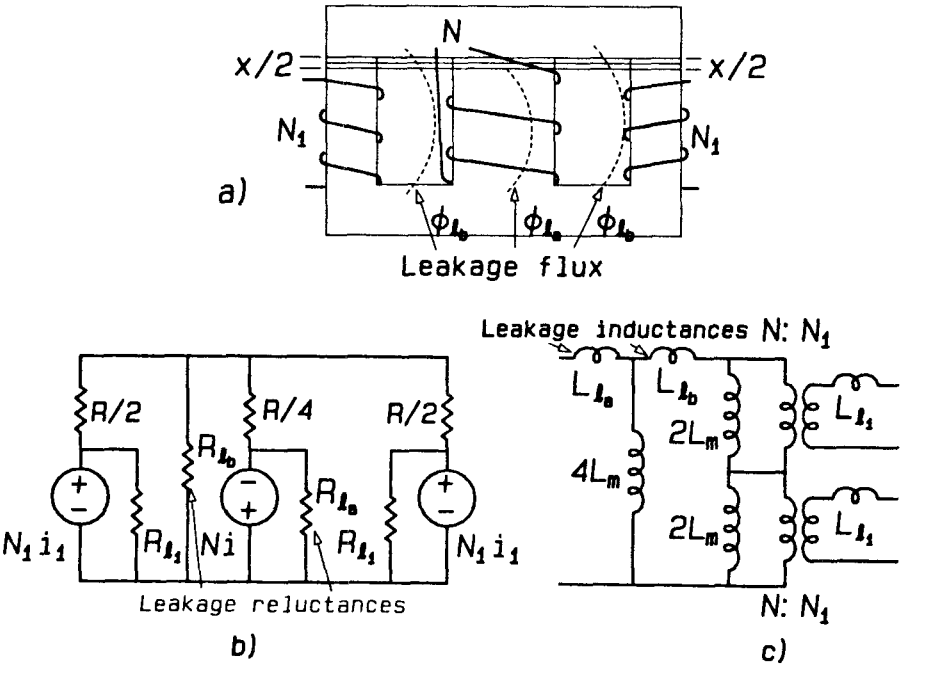

Figure 9.3: The EI-core structure using common spacer (a), the reluctance model (b), and the circuit model (c).

also very hard to measure using conventional methods. A simplified model is needed to represent the spacer core structure.

If either one of the two leakage reluctances is much larger than the other, it can be omitted (Fig. 9.4)a,b, and the resulting simplified models will be much easier to handle.

The two simplified models can easily be converted from one to the other by the use of $\Delta - Y$ conversion in circuit theory; therefore, both models are identical when measured from the ports, and either one can be used for deriving the design equations, without affecting the zero ripple condition. However, since the flux distribution in the cores is different for the two models, finding the simplified reluctance and circuit models which closely represent the actual physical structure could reduce the errors in the dc flux density calculation and might make the final results more accurate.

Since both simplified models are equivalent when measured from the ports, the conventional measuring method gives no hint for selecting the best model. However, because of the geometrical similarity of the spacer core structure to the gaped core structure, the flux distribution of the two cores should be similar; therefore, the value of the primary and secondary leakage reluctances $\mathcal{R}_l$, $\mathcal{R}_{l_1}$ for the "correct" model should be close to $\mathcal{R}_l$ and $\mathcal{R}_{l_1}$ for the gaped core model.

Figure 9.4c shows the circuit model of the gaped core structure. Compare with the two possible simplified models given in Fig. 9.4a,b; it is obvious that model 2 is the better simplification for the model of the spacer core, because the primary and secondary leakage inductances and reluctances are much closer to the gaped core model than model 1.

Unfortunately, as usual, better often means impossible. In this case, the "better" model makes the closed form solution very difficult, if not impossible, to obtain. The

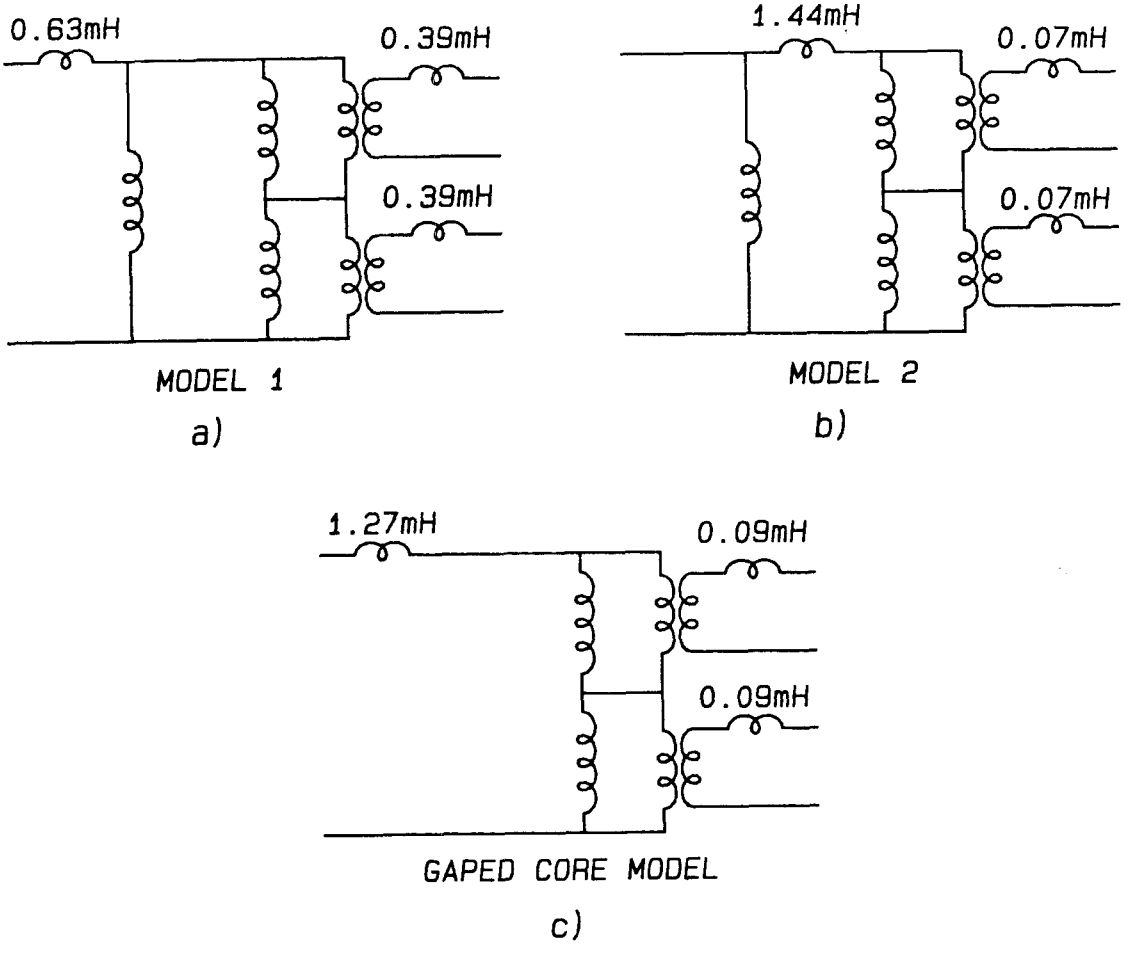

Figure 9.4: a,b) An example of two possible simplified models of the spacer core structure. The values for both models are from the data of an EI-50 core with 100 *turns on each leg. Measured from the ports, the two models are identical. c) The model for the gaped EI-core structure. The values are for an EI-core with a gap on each outer leg, and* 100 *turns for each winding.*

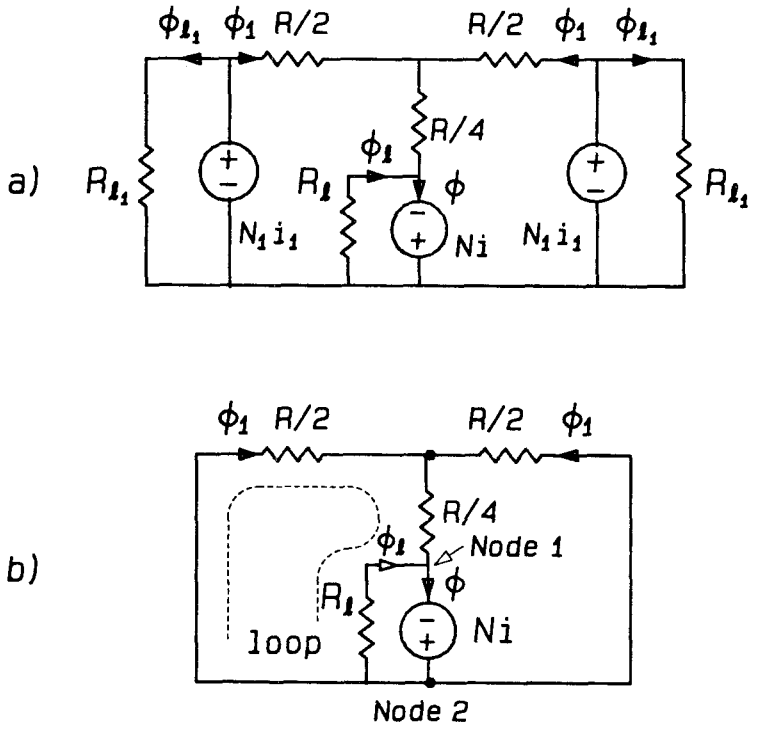

Figure 9.5: a) The complete reluctance model for the EI-core using spacer gaps. b) The ac model for the zero ripple condition.

results, because of the complex forms, have little practical use and will not be presented here. We just have to go back to model 1 and derive a practical closed form solution. The errors in dc flux density, by using the "wrong" model, will not affect the zero ripple condition at all; also, these errors have been calculated to be less than 10%, thus will not likely to affect the core saturation.

9.1.2 The Analysis of the Spacer Core Structure

The complete reluctance model used for the analysis is shown in Fig. 9.5a. To make the results compatible with those for the gaped core, the spacer thickness is set to be $x/2$. However, the air-gap reluctance $\mathcal{R}$ is still defined for an air-gap x with cross section $S/2$, as in the last chapter:

$$\mathcal{R} = \frac{x}{\mu_0 S/2} = \frac{2x}{\mu_0 S} \tag{9.1}$$

Therefore, the reluctances for the outer legs are $\mathcal{R}/2$, and the reluctance for the center leg, which have twice the cross section of the outer legs, is $\mathcal{R}/4$. The leakage parameter is defined as in Chapter 8:

$$l = \mu_0 S \mathcal{R}_l \tag{9.2}$$

Since the magnetic structure is symmetrical, the ac flux in both outer legs will be identical; thus, the number of turns N_1 required on each outer leg to obtain zero ripple current will be the same. The analysis of the spacer core structure is very similar to the analysis of the gaped core structure done in the last chapter. The ac or zero ripple condition is found first, then the dc condition to insure that the core will not saturate, and finally, the inductance of the center winding. After all these relations are found, the equations are solved to find the unknowns: number of turns in the center winding N, the number of turns of the outer windings N_1, and the thickness of the spacer $x/2$.

Ac (Zero Ripple) Condition

If zero current ripple on the two outer legs is assumed, the two voltage sources $N_1 I_1$ in the reluctance model shown in Fig. 9.5a will be effectively shorted, and the model will be simplified as Fig. 9.5b. From this model a loop equation and node equation can be set:

$$\mathcal{R}\phi_1 = \mathcal{R}_l\phi_l = Ni \qquad \text{loop equation} \tag{9.3}$$

$$\phi = 2\phi_1 + \phi_l \qquad \text{node equation} \tag{9.4}$$

Even though the current ripples in outer windings are zero, the current ripple in the center leg winding still generates ac flux ϕ, part of which is linked through the outer windings N_1, inducing voltages v_1 in the windings to counter-balance the externally applied voltage v. Therefore, based on Faraday's law, for each of the magnetic branches

and for each winding:

$$v = N\frac{d\phi}{dt} \qquad v_1 = N_1\frac{d\phi_1}{dt} \tag{9.5}$$

where $v = v_1$. Since for zero ripple condition we are considering only ac fluxes, the two equations can be integrated as:

$$\phi = \frac{1}{N}\phi_0 \qquad \phi_1 = \frac{1}{N_1}\phi_0 \tag{9.6}$$

where $\phi_0 = \int v\,dt$.

Solving the equations for $\mathcal{R}/\mathcal{R}_l$ gives

$$\frac{\mathcal{R}}{\mathcal{R}_l} = \frac{N_1}{N} - 2 \tag{9.7}$$

or by using the reluctance definition (9.1), (9.2), written as:

$$\frac{x}{l} = \frac{N_1}{2\,N} - 1 \tag{9.8}$$

where

$$L_l = \frac{N^2\mu_0 S}{l}$$

Dc Condition

The reluctance model for the dc conditions is shown in Fig. 9.6. The leakage reluctances of the outer windings, being much larger than the reluctances of the gaps, are neglected in the calculations. To prevent core saturation, the maximum flux density anywhere in the core must be less than or equal to the maximum flux density B_{max}:

$$\frac{B_m S}{2} \geq \frac{1}{\mathcal{R}}[N\,I + N_1(1.5\,I_1 - 0.5\,I_2)] + \frac{N\,I}{2\mathcal{R}_l} \tag{9.9}$$

$$\frac{B_m S}{2} \geq \frac{1}{\mathcal{R}}[N\,I + N_1(1.5\,I_2 - 0.5\,I_1)] + \frac{N\,I}{2\mathcal{R}_l} \tag{9.10}$$

If it is assumed that $I_1 \geq I_2$, only (9.9) is critical, and (9.10) will be automatically satisfied. That is, the leg with the high current winding will be designed to operate at

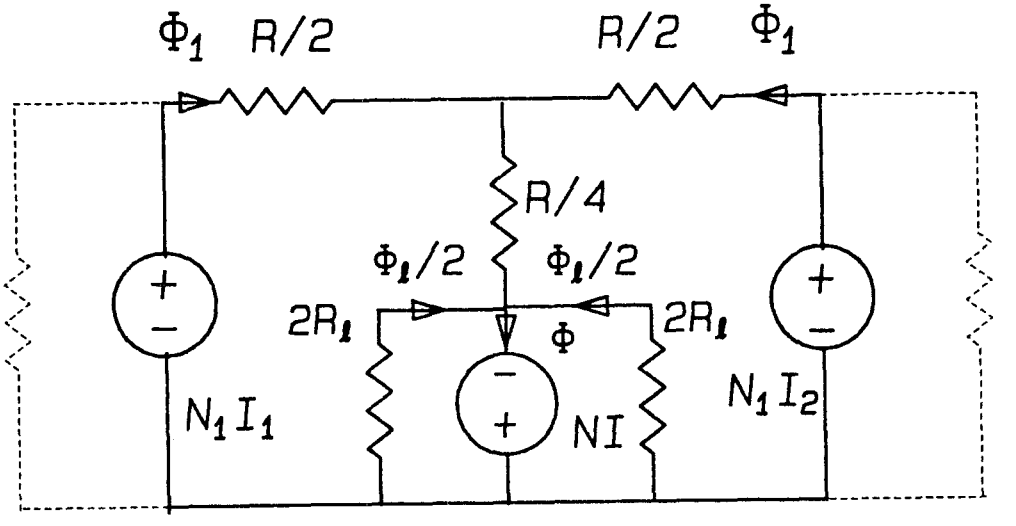

Figure 9.6: The reluctance model for dc condition.

full flux density, and the flux density in the other leg will allowed to be lower. Again, using the reluctance definition, we can rewrite this equation as:

$$\frac{B_m}{\mu_0} = N\,I\left(\frac{1}{x}+\frac{1}{l}\right) + N_1(1.5\,I_1 - 0.5\,I_2)\frac{1}{x} \tag{9.11}$$

Note that from the above equation, the worst case for saturation would be when $I_2 = 0$, or a no load condition on one of the outer windings. The other leg would then have the highest dc flux, exceeding that obtained for the concentrated gaps in the last chapter. This is the price one has to pay for the simplicity of the uniform gap implementation. However, for Ćuk converters, usually the input winding is on the center leg. In this case, when there is no load on one output, the input current I will decrease and partially compensate this effect.

The Inductance L

The input inductance of the coupled-inductors can be derived from the model in Fig. 9.5b:

$$L = \mu_0 S N^2 \left(\frac{1}{x} + \frac{1}{l}\right) \tag{9.12}$$

9.1.3 The Design Equations for the Spacer Core Structure

The set of equations needed to be solved to obtain the design equations can be summarized as:

$$\frac{x}{l} = \frac{N_1}{2N} - 1 \tag{9.13}$$

$$\frac{B_m}{\mu_0} = N I \left(\frac{1}{x} + \frac{1}{l}\right) + N_1(1.5\, I_1 - 0.5\, I_2)\frac{1}{x} \tag{9.14}$$

$$L = \mu_0 S N^2 \left(\frac{1}{x} + \frac{1}{l}\right) \tag{9.15}$$

Note that the only difference from the equations for equal air-gaps (8.60) to (8.62), is in (9.14) where the current associated with N_1 is $(1.5\, I_1 - 0.5\, I_2)$, while in (8.61) it is I_1. Therefore, the design equations for the spacer gap EI-core structure can be obtained by the substitution of $(1.5\, I_1 - 0.5\, I_2)$ for I_1 in the design equations for the equal air-gap structure (8.63) to (8.66).

DESIGN EQUATIONS FOR EI-CORE USING SPACER GAP:

$$N = \frac{L(I + 3\, I_1 - I_2)}{B_m S} \tag{9.16}$$

$$L_l = \frac{N^2 \mu_0 S}{l} \tag{9.17}$$

$$x = l\, \frac{L_l}{L - L_l} \tag{9.18}$$

$$N_1 = 2\, N\, \frac{L}{L - L_l} \tag{9.19}$$

The design procedure outlined at the end of Section 8.4 ((8.75) to (8.81) can then be used for the design of spacer gap coupled-inductors. Note now the effective current I_e is $(3\,I_1 - I_2)$, where I_1 is the larger of the two outer leg currents.

9.2 THE COUPLED-INDUCTOR STRUCTURE USING EE-CORES

The EE-core structure, like the EI-core structure using a single, uniform spacer, does not need the core to be ground. Although the uniform air-gap is a bit more complicated, requiring three identical spacers in the three legs, the other advantages far outweigh it: the air-gaps are shielded by the windings; therefore, the stray magnetic flux is bounded within the windings, unlike the EI-core structure where the stray flux is spilled everywhere. The inherent symmetry of the core geometry makes the design of a multiple output (more than two outputs) converter much easier, as will be discussed later in this chapter.

9.2.1 The Reluctance Model and the Circuit Model

The reluctance model and circuit model of the EE-core coupled-inductor structure (Fig 9.7b,c) are exactly the same as the models for the spacer EI-core, so the analysis, design equations and the design procedures are all the same as for the EI-core spacer gap structure.

9.2.2 The Use of EE-Core Structures in Coupled-Inductors With More than Three Windings

In a structure with four windings, there will be two windings on one of the outer legs. As described in Chapter 5, and later in Chapter 10, to obtain low residual ripple and sensitivity, one has to make the leakage inductances rather high. Short of

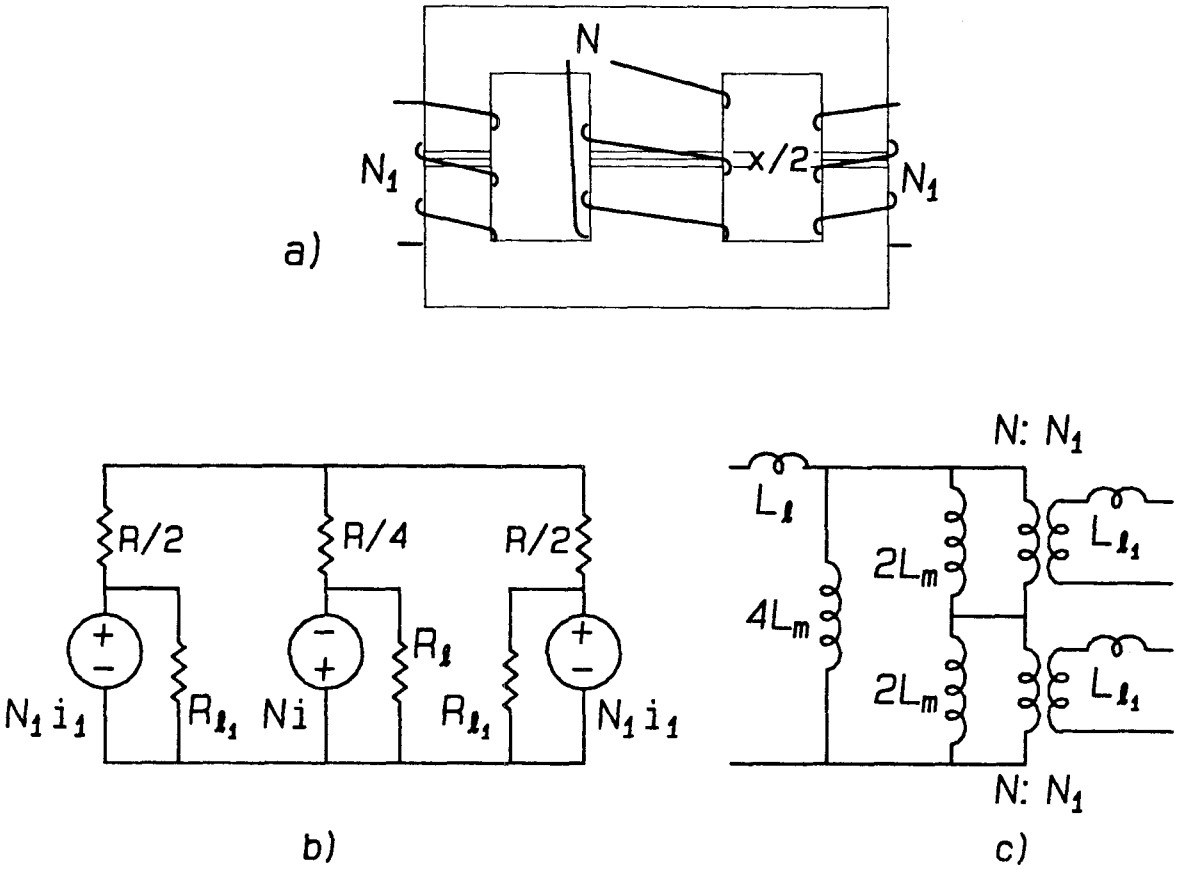

Figure 9.7: a)The EE-core structure. b) The reluctance model. c) The circuit model.

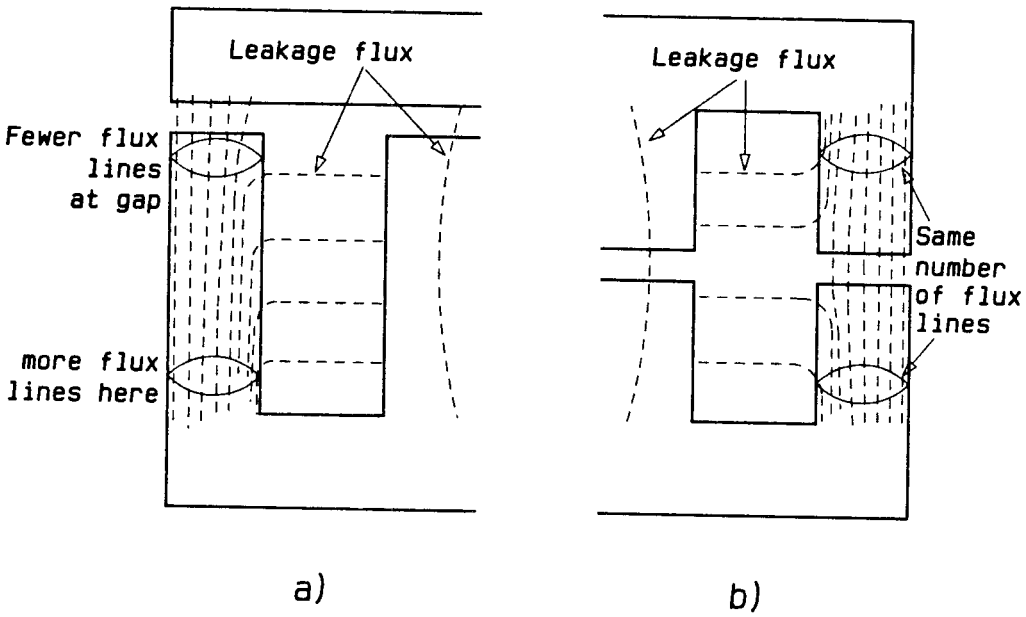

Figure 9.8: a) The outer windings in an EI-core structure has less flux at the gap side of the core. b) In an EE-core structure the outer leg flux is symmetrical around the air-gap.

using an extra leg for the fourth winding, the best way is to put the two windings side by side on one outer leg of the core.

In the reluctance model, the center leg leakage flux is modeled as a single reluctance. However, the real flux distribution is more like that shown in Fig. 9.8; that is, some of the ac leakage flux in the center leg also spills through part of the outer leg windings. In an EI-core structure (Fig. 9.8a), this means that the ac flux in the outer legs decreases toward the gap. If two windings are put side by side on this outer leg in order to obtain high leakage inductance between the windings, the winding next to the air-gap will have less ac flux linked through, thus needing more turns to generate the required voltage. To calculate the flux along any point on the core involves a much more complicated distributed model, which makes it impossible to obtain a closed form

solution. Therefore, the design of this kind of structure is still mainly by trial and error. However, in an EE-core structure (Fig. 9.8b), the flux distribution in ether of the outer legs is symmetrical around the air-gap, so both side-by-side windings will produce the same voltage as a single full width winding (providing the side-by-side windings have the same number of turns and each take half the width of the window). The design of this EE-core coupled-inductor structure is then the same as the design for a three-winding structure. Therefore, the use of an EE-core structure can make the design of coupled-inductors with four, five or even six (if the ripple is steered into two windings) windings the same as the design of a three-winding structure.

Chapter 10

SENSITIVITY AND RESIDUAL RIPPLE OF THE NEW STRUCTURES

In Chapter 5, the sensitivity and residual ripple of a two-winding structure were discussed. In that discussion, it was shown that when the drive voltage on the two inductor windings are identical, the zero ripple condition is:

$$\frac{N_1}{N_2} = \frac{L_m}{L_m + L_{l_1}} \tag{10.1}$$

However, due to the nonidealities of the coupled-inductors and the converter circuit, the drive voltages on the two windings will not be exactly identical. Because the number of turns in the windings can be only integer numbers, the actual number of turns will, in most cases, differ from the calculated number by up to half a turn. In the manufacturing procedure, the setting of the air-gap also cannot be exact. Therefore, there will be a source of voltage mismatches, which generate a triangular ripple current in the secondary windings, which should have no ripple at all. The amount of ripple current generated by a such an error is called the *sensitivity* of the design. Also, due to the voltage drop on the inductor winding resistances and the voltage drop on the energy transfer capacitor in a Ćuk converter, there will be another source of voltage mismatches. After the triangular switching ripple current is steered to one winding, these voltage mismatches (which are usually considered as second-order effects) will show up in the current waveforms in the "zero ripple winding." The waveform of this ripple current is generally not triangular

and is called *residual ripple*. The solution to reduce both residual ripple and sensitivity is to design coupled-inductors with relatively high leakage inductances.

All the sources of error (mismatch) voltages discussed in Chapter 5 still exist in the multiple winding structures, However, because the models are different, the calculations of the residual ripple and sensitivity are different. Even worse, due to the cross coupling between the different windings, the ripple current can propagate from one winding to another, making the adjustment difficult without some understanding of the problem.

In this chapter the sensitivity and residual ripple will be discussed on the three-winding coupled-inductors using the new EI and EE-core structure. The "ripple propagation" will not be discussed. In other words, if there is an error in the first output winding, the ripple current for that winding will be calculated, but the resulting ripple on the second output will not. This is because, even though the resulting ripple on the second winding can be calculated, the calculation is so messy that it will have little use in guiding the designer to obtain better results. Since the design using EI-cores with unequal air-gaps does not give the best result as discussed in Chapter 8, it will be assumed that the two air-gaps are identical.

In the testing of a converter using coupled-inductors, it is much easier to fine-tune the number of turns in the coupled-inductor output windings one by one, by disconnecting the other windings from the circuit. In this case, the ripple currents in the untested windings will always be zero, eliminating the ripple propagation. This method is called the *test mode* and will also be discussed.

As in Chapter 5, the circuit model for calculating the ripple current is discussed first, following a discussion of the sensitivity of the ripple current to the turns ratio and air-gap errors. Finally, there is a brief discussion of the second-order errors—the

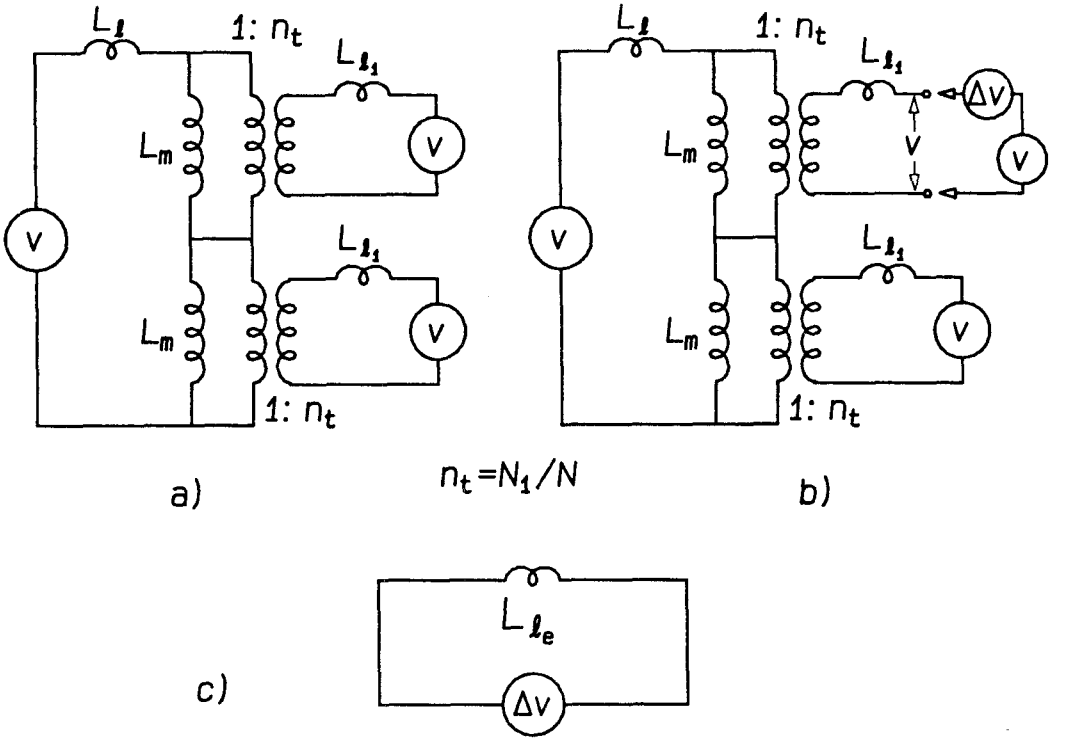

Figure 10.1: a) The circuit model for the new EI and EE-core structures. b) The circuit model for calculating the ripple current in the first output winding. c) The equivalent circuit for b).

mismatch voltage due to the nonidealities in the coupled-inductors and converter circuit.

In a real design, calculating the exact sensitivity of the structure is not necessary nor possible, because most of the factors involved are second-order effects in the circuit. Therefore, in all the calculations in this chapter, approximations are used when justified to simplify the equations.

10.1 THE CIRCUIT MODEL FOR THE SENSITIVITY AND RESIDUAL RIPPLE CALCULATION

10.1.1 The Operating Mode

The circuit models for the EI and EE-core structures are shown in Fig. 10.1a. From Chapter 8, the zero ripple condition is:

$$\frac{1}{n_t} = \frac{N_1}{N_2} = \frac{L_m}{L_m + L_l} \tag{10.2}$$

For calculating the ripple current when there is an error voltage v_{error} on the first output winding N_1, the circuit can be drawn as Fig. 10.1b. This circuit can be simplified as Fig. 10.1c using Thevenin's theorem. The effective leakage inductance in this circuit is:

$$L_{l_e} = \left[\left(L_l + L_m \parallel \frac{L_{l_1}}{n_t^2}\right) \parallel L_m\right] n_t^2 + L_{l_1} \tag{10.3}$$

For the optimum design of the coupled-inductors (Chapter 8), the turns ratio $n_t \approx 2.5$, therefore, $L_l \approx 0.5\, L_m$. Also from the data given in Appendix A, for all the cores tested, scaled for the same number of turns, the secondary leakage inductance is less than the primary leakage (so $L_{l_1} n_t^2 = (0 \sim 1) L_l$). Therefore, the effective leakage inductance can be written as:

$$L_{l_e} \approx \{[L_l + 2\, L_l \parallel (0 \sim 1) L_l] \parallel 2\, L_l + (0 \sim 1) L_l\}\, n_t^2 \approx 8\, L_l \tag{10.4}$$

The ripple current can be found by applying the error voltage Δv across this effective leakage inductance.

10.1.2 The Test Mode

In the test mode, when adjusting one secondary winding to obtain zero ripple, the other secondary winding is disconnected from the circuit. This makes the converter effectively a single output converter, and relatively easy to adjust. In this mode, the

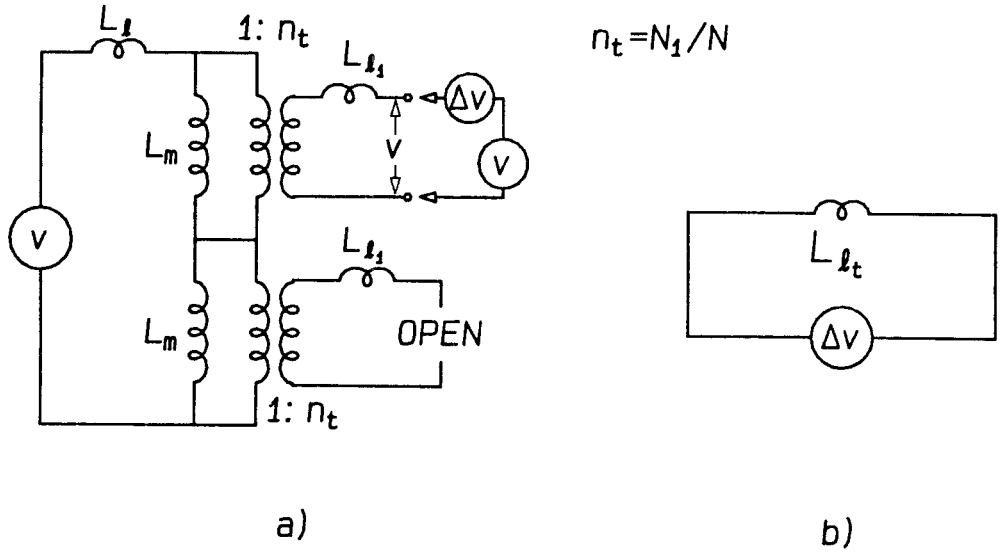

Figure 10.2: a) The circuit model for calculating the ripple current in the first output winding when the converter is in the test mode. b) The equivalent circuit for a).

sensitivity of the ripple current to the turns ratio and air-gap of the coupled-inductors can serve as a useful guide for the adjustment. For example, in the test mode, the output tested has 0.5A positive ripple current, and the sensitivity in this mode is 100mA/turn. One just have to add 5 turns to that winding to obtain zero ripple.

The circuit model for the test mode is shown in Fig. 10.2a. Note that the second output winding is now open. By Thevenin's theorem, this model is simplified as Fig. 10.2b. The effective leakage inductance is:

$$L_{l_t} = [(L_l + L_m) \parallel L_m]\, n_t^2 + L_{l_1} \tag{10.5}$$

Or by use of the same approximation as in the last section:

$$L_{l_t} \approx 2L \tag{10.6}$$

where L in the primary inductance of the coupled-inductors ($L = l_l + 2\,L_m$). Note that in the test mode, the effective leakage inductance is much higher than in the normal operating condition. This makes the sensitivity in the test mode much lower.

10.2 FIRST-ORDER ERRORS

The first-order errors are defined the same as in Chapter 5, namely, the errors in the turns ratio and the air-gap size. These errors directly upset the zero ripple condition and can be corrected by readjusting the coupled-inductors. The sensitivity of the coupled-inductors actually is the sensitivity of the ripple current to these errors.

10.2.1 Ripple Current Due to Drive Voltage Errors

If the number of turns in the first secondary winding N_1 has an error ΔN_1, the turns ratio of that output will become $(N_1 + \Delta N_1)/N$ (Fig. 10.3). This is equivalent to having an error $v_{e_1} = v\,\Delta N_1/N_1$ in the drive voltage for that winding. The ripple current is found by applying this error voltage on the effective leakage inductance.

For normal operation this ripple current i_1 is:

$$i_1 = \frac{1}{L_{l_e}} \int v_{e_1} dt = \frac{\Delta N_1}{N_1} \frac{1}{L_{l_e}} \int v dt \tag{10.7}$$

We can simplify this expression by referring the output ripple to the primary ripple current i:

$$i = \frac{1}{2\,L_m + L_l} \int v dt = \frac{1}{L} \int v dt \tag{10.8}$$

Using the approximation of L_{l_e} (10.4), we can write the output ripple current (10.7) as:

$$i_1 = \frac{\Delta N_1}{N_1} \frac{L}{L_{l_e}} i \approx \frac{\Delta N_1}{N_1} \frac{L}{8\,L_l} i \tag{10.9}$$

Note that the ripple current is inversely proportional to the effective leakage inductance. Hence, coupled-inductors with higher leakages will give lower ripple current under a given

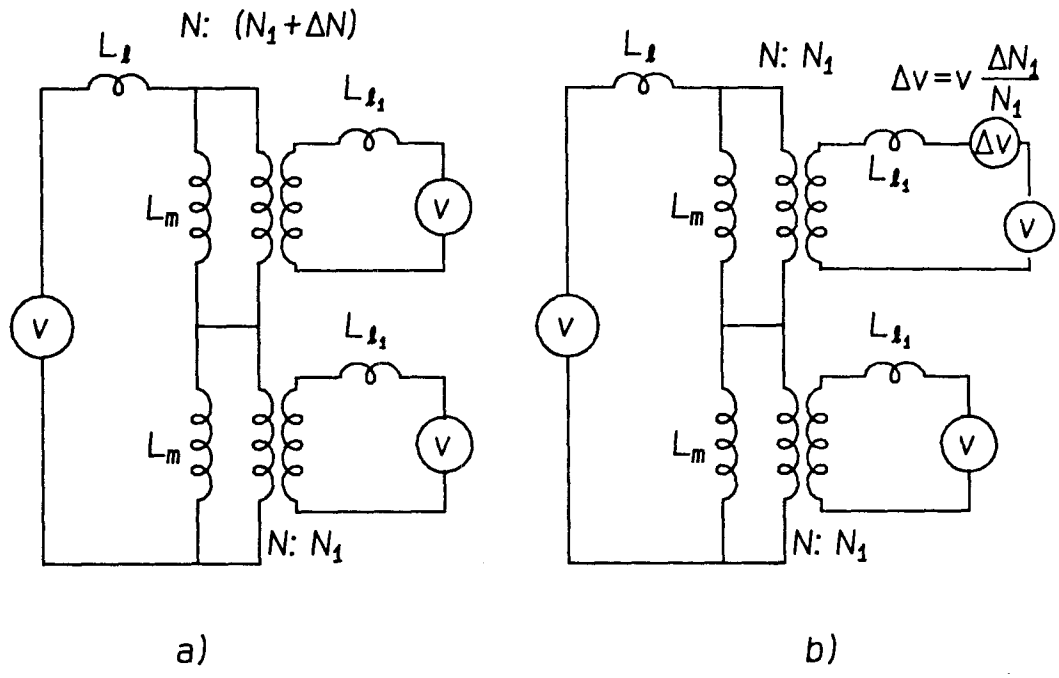

Figure 10.3: a) The circuit model for calculating the ripple current due to the turns ratio error. b) The equivalent circuit.

turns ratio error and thus lower sensitivity.

The same can be calculated for the test mode by substituting the effective leakage inductance L_{l_t} for the test mode:

$$i_1 = \frac{\Delta N_1}{N_1}\frac{L}{L_{l_t}} i \approx \frac{\Delta N_1}{N_1}\frac{L}{2L} i = \frac{1}{2}\frac{\Delta N_1}{N_1} i \tag{10.10}$$

10.2.2 Ripple Current Due to Air-Gap Errors

In the circuit model (Fig. 10.4a), the two magnetizing inductances of the coupled-inductors are inversely proportional to the air-gap size, while the leakage in-

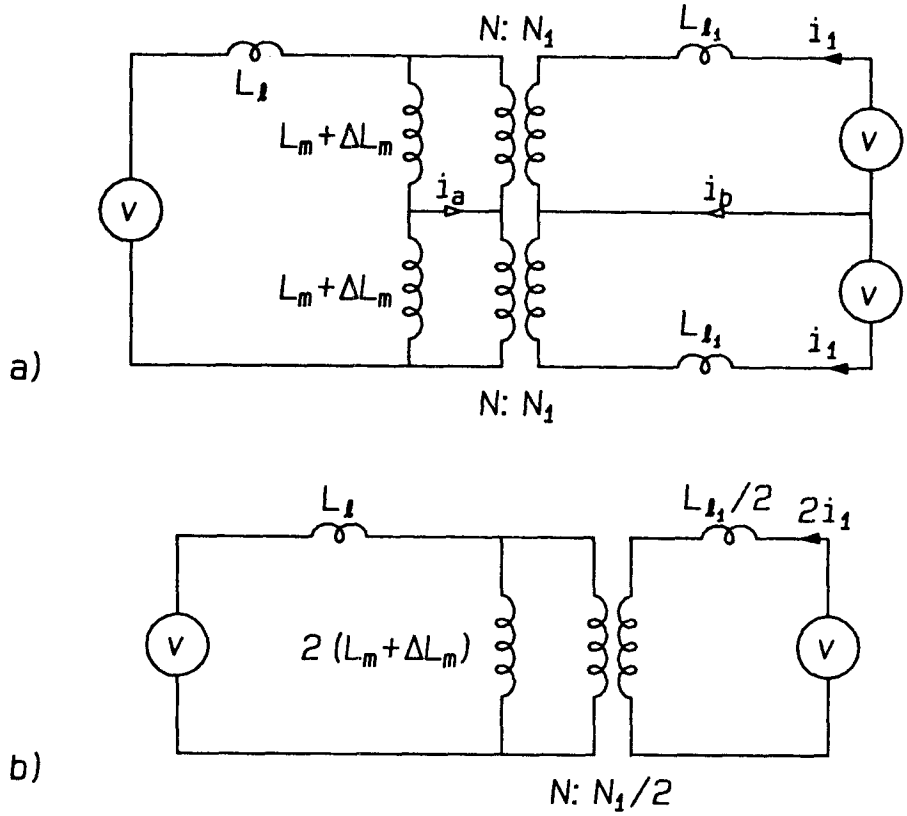

Figure 10.4: a) The circuit model for calculating the ripple current in due to the air-gap error. Note that the currents i_a and i_b are zero. b) The simplified circuit.

ductance is relatively insensitive to the air-gap. Therefore, if the air-gap increases by $\Delta x/x$, the two magnetizing inductances will decrease by the same factor, upsetting the zero ripple condition. Since both inductances are always the same, the current i_a and i_b in Fig. 10.4a will be zero, and the circuit can be simplified as Fig. 10.4b. This circuit is the same as the one used to discuss the air-gap error in Chapter 5.2.2 (Fig. 5.2b), only with different values. Therefore, results for that section can be modified for Fig. 10.4b. From (5.16), using the values given in Fig. 10.4b, we can find the output ripple current due to air-gap errors:

$$i_1 = \frac{1}{2}\frac{\Delta x}{x}\frac{L_l}{2L_m + L_l}\frac{1}{L_{eff}}\int v\,dt \tag{10.11}$$

where the effective inductance is the inductance looking in from the secondary side:

$$L_{eff} = \left(\frac{n_t}{2}\right)^2 (2L_m \parallel L_l) + \frac{L_{l_1}}{2} = \frac{L_l + 2L_m}{2L_m} L_l + \frac{L_{l_1}}{2} \approx L_l + \frac{L_{l_1}}{2} \tag{10.12}$$

Writing the ripple current in terms of the primary ripple current i (10.8) gives:

$$i_1 \approx \frac{\Delta x}{2x} \frac{L_l}{L_l + L_{l_1}/2} i \tag{10.13}$$

From the data given in Appendix A, for EI-cores with two air-gaps on the outer legs $L_{l_1} \approx n_t^2 L_l/10 \approx 0.6\, L_l$, thus:

$$i_1 \approx \frac{\Delta x}{x} \frac{i}{3} \tag{10.14}$$

For EI or EE-cores using spacer gaps $L_{l_1} \approx 0.6\, n_t^2 L_l \approx 4\, L_l$, so:

$$i_1 \approx \frac{\Delta x}{x} \frac{i}{6} \tag{10.15}$$

From the above equations, EI-core structures using separated gaps will have higher sensitivity than the cores using spacers. This is another reason for favoring the spacer core structures.

Due to the fringing flux of the air-gap, the magnetizing inductance L_x changes more slowly than the change of the air-gap. This will make the measured sensitivity and residual ripple higher than the calculated value.

10.3 SECOND-ORDER EFFECTS AND RESIDUAL RIPPLE

Due to the nonidealities in the coupled-inductors and the converter circuit, the drive voltages on the three inductor windings will not be exactly the same. Therefore, there will be additional error voltages. As discussed in Chapter 5, because of the nature of the nonidealities, the waveforms of these error voltages are generally not the same as the switching voltage waveform, and thus cannot be reduced by readjusting the coupled-inductors. The error voltages from these second-order effects can be calculated using the methods given in Section 5.3. The resulting residual ripple is calculated by applying the error voltage across the effective leakage inductance (10.4).

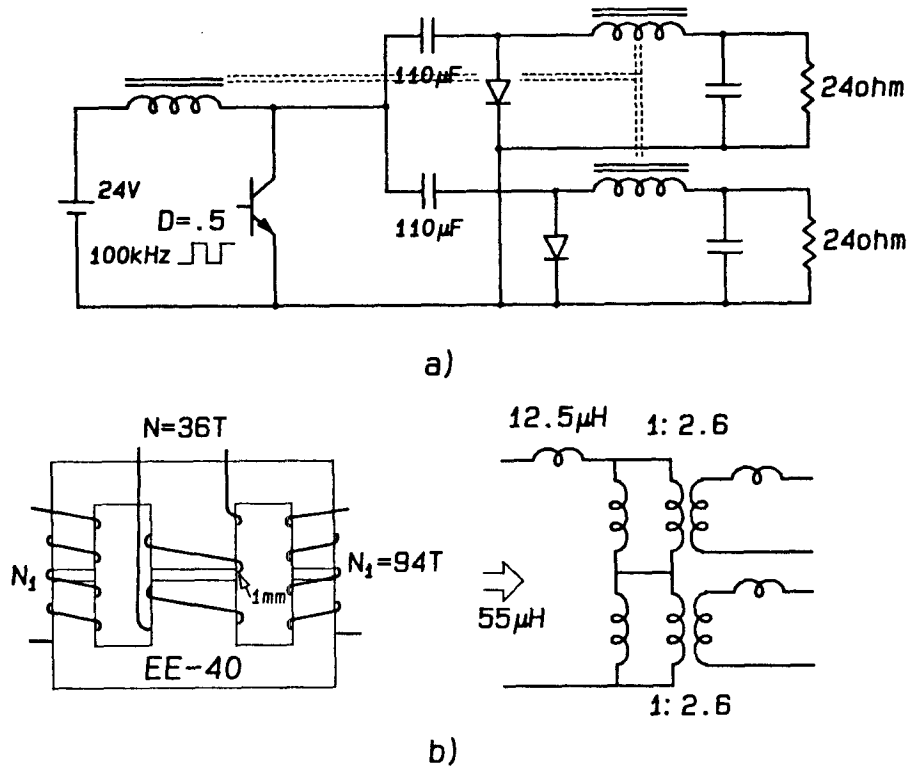

Figure 10.5: a) Two-output Ćuk converter. b) The coupled-inductors.

10.4 EXAMPLE

A two-output Ćuk converter (Fig. 10.5a) is built to verify the residual ripple and sensitivity calculations. The structure and the circuit model of the coupled-inductors are shown in Fig 10.5b. The converter input voltage is $24V$, and the duty ratio is $D = 0.5$.

10.4.1 Sensitivity

To test the sensitivity of the structure, first the spacer thickness is increased from $1.0mm$ to $1.18mm$. The ripple currents are calculated from (10.15):

$$i_1 = \frac{\Delta x}{x}\frac{i}{5} = \frac{0.18}{1.0}\frac{2.2A}{6} = 66mA$$

The output ripple current measured from the circuit is about 35mA. This discrepancy from the calculated values is because, due to the fringing effect around the air-

gaps, while the spacer thickness increases 18%, the magnetizing inductance only decreases about 10%.

The next test is to increase N_1 from 94 turns to 100 turns, when keeping the spacer thickness at 1mm. From (??),the output ripple current is:

$$i_1 \approx \frac{\Delta N_1}{N_1} \frac{L}{8\,L_l} i = 65mA$$

The measured ripple current for output 1 is 55mA, slightly smaller than calculated. However, the measured ripple for output 2 is now 35mA, which is due to the "ripple propagation" discussed at the beginning of this chapter.

10.4.2 Residual Ripple

The input current waveform is shown in Fig. ??a; the input ripple current is $2.2A$ peak-to-peak. This current ripple generates a $0.44V$ peak-to-peak voltage drop on the $0.2\,ohm$ primary winding copper resistance (Fig. ??b).

The charging current waveform of the energy transfer capacitors is shown in Fig ??c, while the voltage waveform of the capacitors is as Fig. ??d. The peak-to-peak error voltage is $0.045V$. As discussed in Chapter 5 these two voltage will tend to cancel out each other; therefore, the total error voltage is $0.4V$.

From (??) the effective leakage inductance is $100\mu H$; thus, the output ripple current should be:

$$i_1 \approx 5mA$$

The residual ripple is measured to be $8mA$ for both outputs.

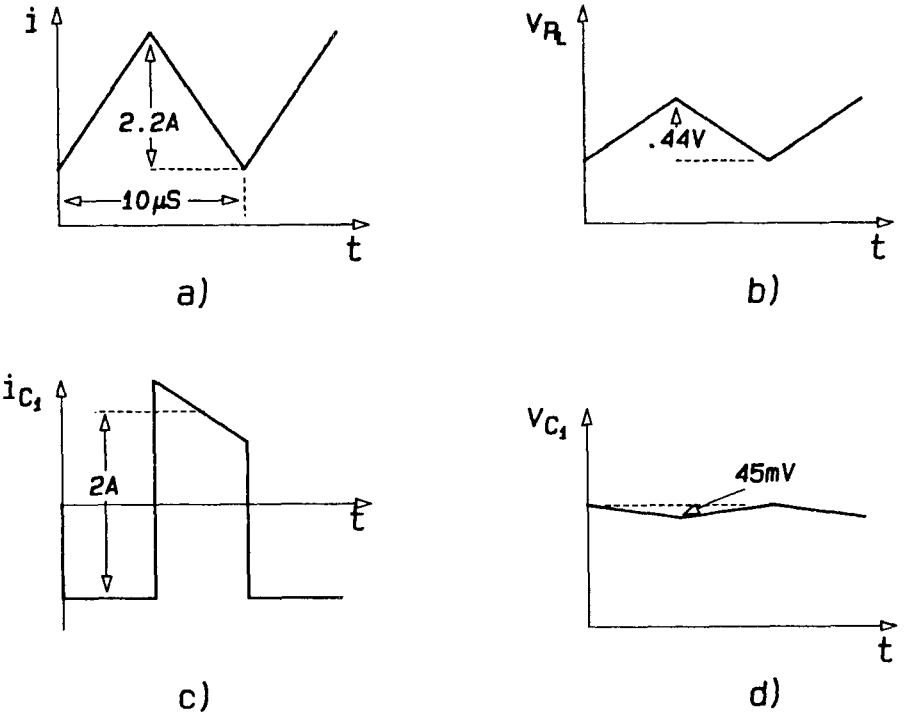

Figure 10.6: a) The input current waveform. b) The voltage drop on the primary copper resistance. c) The energy transfer capacitor current waveform. d) The ripple voltage on the capacitor.

Chapter 11

DESIGN CONSIDERATIONS AND DESIGN EXAMPLE

11.1 DESIGN CONSIDERATIONS

Using the design equations given in the last two chapters, one can already make the design of a coupled-inductors. However, there are some practical problems one should consider before making the coupled-inductor design. Some of the more common design considerations are discussed in this section.

11.1.1 Coupled-Inductors for Different Output Voltages

As assumed in all the earlier calculations, the drive voltage of all three windings are the same; therefore, the dc outputs are restricted to being of equal magnitude, but they could have opposite polarity. In the case of different output voltages, all outputs can be reflected through the transformer turns ratio to obtain an effective 1:1:1 isolation transformer, this reflection results in exactly the same model as discussed before. After the design of the magnetics circuit is completed, the windings can be scaled back to the original voltages and currents required on the output.

11.1.2 The Selection of the Input Inductance

In a coupled-inductor Ćuk converter, unless there are special specifications limiting the input ripple, all the ripple is usually steered to the input. Especially in off-line switchers, where the filtering capacitor of the line rectifier also serves as the hold-up capacitor for the system, the rectifier filtering capacitor is large enough so that any amount of input current ripple of the converter will be filtered out and will not be fed back into the ac line. In this case, if the input ripple current is allowed to be larger, the primary inductance of the coupled-inductors can be smaller, then the number of turns and the copper loss of the coupled-inductors can also be smaller. However, if the input ripple current is increased, the input peak current will also go up, increasing the rms current in the primary winding, in turn increasing the copper losses of the coupled-inductors. An optimum primary ripple current can be found to minimize the losses of the coupled-inductors. On the other hand, if the losses of the coupled-inductors remains the same, this optimum ripple current will result in the smallest size of the coupled-inductors. In normal coupled-inductors designed for zero ripple current in the outputs, because of the dc currents in the outputs, even when the input ripple current is large, the total ac flux swing is still much smaller compared with the dc flux. This means that, in most cases, the core loss is small, and the copper loss is still the dominating loss in the coupled-inductors. Therefore, the problem can now be defined as:

For a given core size, find the primary current ripple to give minimum copper loss in the coupled-inductors.

To get some insight into the problem, the simplest case—a single inductor will be studied first; then the results will be extended to the multiple winding coupled-inductor structure.

The design procedure of a simple inductor is as follows:

The maximum flux in the core is:

$$\Phi_{max} = B_m S = \frac{N I_p}{\mathcal{R}_g} \tag{11.1}$$

where I_p is the peak current in the winding, and $\mathcal{R}_g$ is the reluctance of the magnetic path; for gapped cores $\mathcal{R}_g$ is essentially the air-gap reluctance.

The inductance of the inductor is given as:

$$L = \frac{N^2}{\mathcal{R}_g} \tag{11.2}$$

Solving the two equations give the number of turns and the gap reluctance:

$$N = \frac{L I_p}{B_m S} \qquad \mathcal{R}_g = \frac{N I_p}{B_m S} \tag{11.3}$$

For a given core size and maximum flux density, from equation (11.3) we can write:

$$N \propto L I_p \tag{11.4}$$

The copper loss in the inductor is:

$$P_{cu} = R I_{rms}^2 = \rho \frac{N^2 t I_{rms}^2}{k W} \propto L^2 I_p^2 I_{rms}^2 \tag{11.5}$$

where t is the mean length per turn of the winding, W is the window area for the winding, and k is the fill factor of the winding.

Fig. 11.1 shows the inductor current waveform when the converter is operating in continuous conduction mode (CCM), noting that the slope of the current is proportional to $1/L$, and the duty ratio and average current are constants for a given output voltage, we can write:

$$L \propto \frac{1}{\Delta i} \tag{11.6}$$

where Δi is the peak-to-peak ripple current.

The inductor's rms current can be found from the current waveform in Fig 11.1:

$$I_{rms}^2 = I_a^2 + \frac{1}{12}\Delta i^2 \tag{11.7}$$

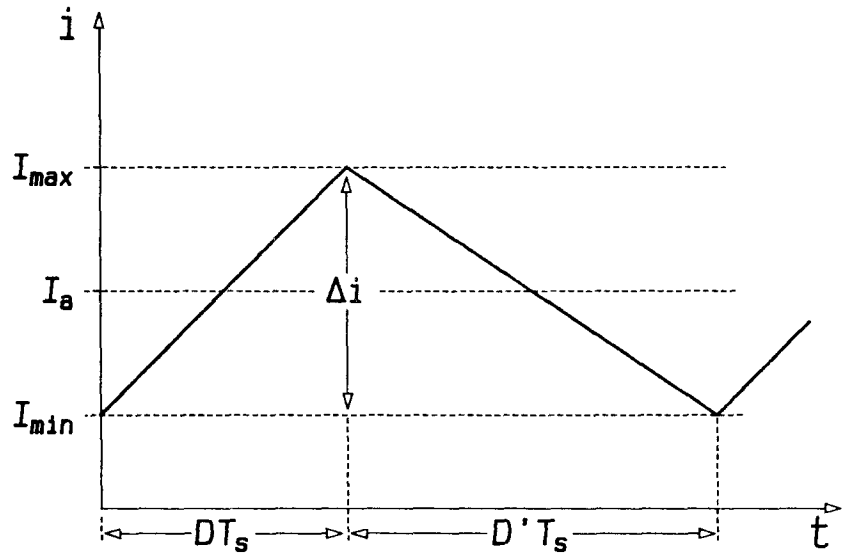

Figure 11.1: The current waveform of an inductor in a switching converter in continuous conduction mode.

where I_a is the average inductor current. The inductor peak current is:

$$I_p = I_a + \frac{1}{2}\Delta i \tag{11.8}$$

Then the copper loss is proportional to:

$$P_{cu} \propto \left(\frac{I_a^2}{\Delta i^2} + \frac{1}{12}\right)\left(1 + \frac{1}{2}\frac{\Delta i}{I_a}\right)^2 \tag{11.9}$$

From equation (11.5), the minimum copper loss is found to be when the ripple current is:

$$\Delta i \approx 2.9 I_a \tag{11.10}$$

When the converter is in discontinuous conduction mode (DCM), the current waveform is as shown in Fig 11.2. To obtain constant output voltage, the ratio $D/(D+D_2)$ remains the same regardless of the idling period D_3; note that now the peak current is equal to the peak-to-peak ripple current ($I_p = \Delta i$).

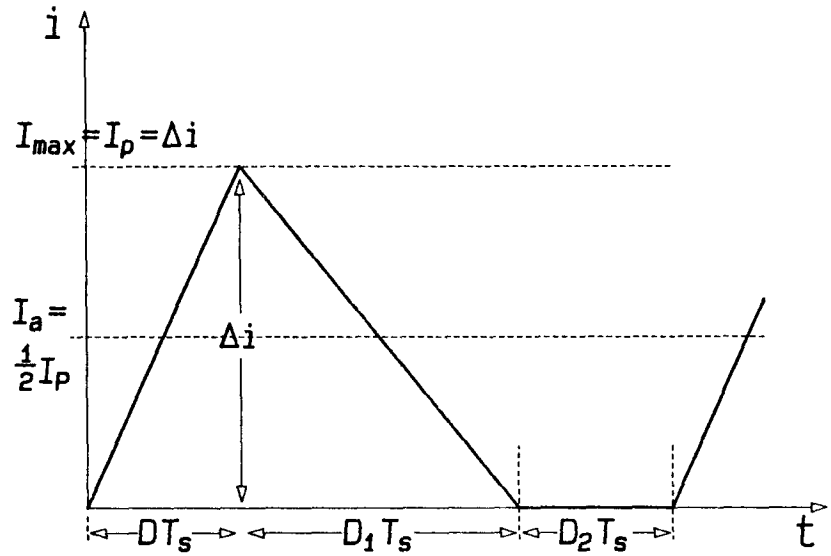

Figure 11.2: The current waveform of an inductor in a switching converter in discontinuous conduction mode.

The rms current in the inductor can be found from the current waveform in Fig 11.2:

$$I_{rms}^2 = \frac{D + D_2}{D + D_2 + D_3} \frac{\Delta i^2}{3} \tag{11.11}$$

However, the average current is:

$$I_a = \frac{D + D_2}{D + D_2 + D_3} \frac{\Delta i}{2} \tag{11.12}$$

To maintain a constant average input current (constant input power), one must have:

$$\frac{D + D_2}{D + D_2 + D_3} = \frac{2\, I_a}{\Delta i} \tag{11.13}$$

The rms current can now be written as:

$$I_{rms}^2 = \frac{2}{3} I_a \Delta i \tag{11.14}$$

If the peak current is allowed to increase by a factor of two, for the same average current I_a, the period $(D\,T_s + D_2 T_s)$ will be cut in half, and the slope of the current increases by

a factor of four. Therefore:

$$L \propto \frac{1}{\Delta i^2} \tag{11.15}$$

From (11.5), the copper loss is:

$$P_{cu} \propto L^2 I_p^2 I_{rms}^2 \propto \frac{1}{\Delta i^4} \Delta i^3 = \frac{1}{\Delta i} \tag{11.16}$$

so for the DCM, the higher the current ripple (the lower the inductance), the lower the copper loss.

The core loss of the inductor, however, will increase when the current ripple (and flux swing) increases in both the CCM and the DCM mode.

For coupled-inductors using gapped EI-core, the primary turns are:

$$N = \frac{L(I_p + I_1 + I_2)}{B_m S} \propto L(I_p + I_1 + I_2) \tag{11.17}$$

Compare with (11.3) for the single-winding inductor; the only difference is that the current used to determine the number of turns in the primary winding is the effective current $I_e = I_p + I_1 + I_2$. The total copper loss in the CCM mode will be:

$$\begin{aligned} P_{cu} = R\, I_{rms}^2 + R_1 I_1^2 + R_2 I_2^2 &= \frac{\rho}{k}\left(\frac{t N^2 I_{rms}^2}{W} + \frac{t_1 N_1^2 I_1^2}{W_1} + \frac{t_1 N_2^2 I_2^2}{W_1}\right) \\ &\propto \frac{1}{B_m S} L^2 (I_p + I_1 + I_2)^2 I_{rms}^2 + \frac{t_1 W}{t W_1}(N_1^2 I_1^2 + N_2^2 I_2^2) \end{aligned} \tag{11.18}$$

where t and t_1 are the mean length per turn of the primary and secondary windings; W and W_1 are window areas allocated to the primary and secondary windings.

Comparing this equation to (11.5) of a single inductor, in the first term, the peak current is $I_p + I_1 + I_2$ instead of I_p; therefore, the first term goes up more slowly when the primary ripple current Δi (and the peak current I_p) increases. Also, because the number of turns of the secondaries N_1, N_2 always decrease with L, the second term will always go down when Δi increases. The total effect is that either the total copper loss will continue to go down with the decrease of the primary inductance, or the minimum

copper loss will happen when the ripple current is much higher than the optimum point of the single winding inductor ($\Delta i > 2.9I_a$), The design equations for the spacer EI-core and the EE-core give similar results.

For the DCM mode, a similar calculation shows that, like the single winding inductor, the copper loss of the coupled-inductors always decreases with the input inductance L.

The core loss of the coupled-inductors also increases when the current ripple increases. However, because the secondary currents are dc, and the number of turns of the secondaries are more than twice of that of the primary, the dc flux generated by the secondary windings is always a larger portion of the total flux. Therefore, the relative flux swing will always be much smaller than the relative current ripple in the primary, and the core loss of the coupled-inductors will be smaller than that of a single winding inductor with the same current ripple. Unless the switching frequency is very high, there is usually no need to be concerned about the core loss in the coupled-inductors.

However, even when the primary current ripple (peak-to-peak) is around three times the average primary current, the current stress (and loss) on the switching elements will already be quite high, so one probably will never want to design a converter with a ripple current much higher than that. For practical design purposes it can be said that the higher the input ripple, the lower the losses in the coupled-inductors (or the smaller the inductor size); the main limiting factor for increasing the ripple current is the stress on the switches in the converter.

11.1.3 The "Worst Case" Design for Spacer EI and EE-Core Structures

From the design equation (??), the flux in the outer legs in the spacer EI-core or EE-core coupled-inductors can be written as (assuming $I_1 > I_2$):

$$\Phi = B_m S/2 = \frac{L\,(I_p + 3\,I_1 - I_2)}{2\,N} = \frac{L\,(I_a + \Delta i/2 + 3\,I_1 - I_2)}{2\,N} \tag{11.19}$$

where I_p is the primary peak current, I_a is the primary average current, and Δi is the primary peak-to-peak ripple current.

Note that from this equation, the worst case for saturation would be when $I_2 = 0$, or the no-load condition for one of the outputs. The other leg would then have the highest dc flux, which exceeds that obtained for the concentrated gaps discussed in Chapter 8. This is the worst case condition for the inductor design and should be used for the converter design. However, in a Ćuk converter, when there is no load on one output, the input peak current I_p will decrease and partially compensate for this effect.

For a Ćuk converter, the relation between the input and output currents is:

$$I_a = \frac{D}{D'}(I_1 + I_2) \tag{11.20}$$

substituting into (11.19) gives:

$$\Phi = \frac{L\left[\Delta i/2 + \left(3 + \frac{D}{D'}\right) I_1 + \left(\frac{D}{D'} - 1\right) I_2\right]}{2\,N} \tag{11.21}$$

From this equation, one can easily see that when the duty ratio $D < 0.5$, the flux will increase as I_2 decreases, and the worse case will be when $I_2 = 0$; when $D > 0.5$, the flux will increase with I_2, the worse case is when $I_2 = I_{2\,max}$; and when the duty ratio is exactly 0.5, the change of I_2 will not affect the maximum flux.

This is an unusual example in which maximum current in the windings will not result in the maximum flux density in the core.

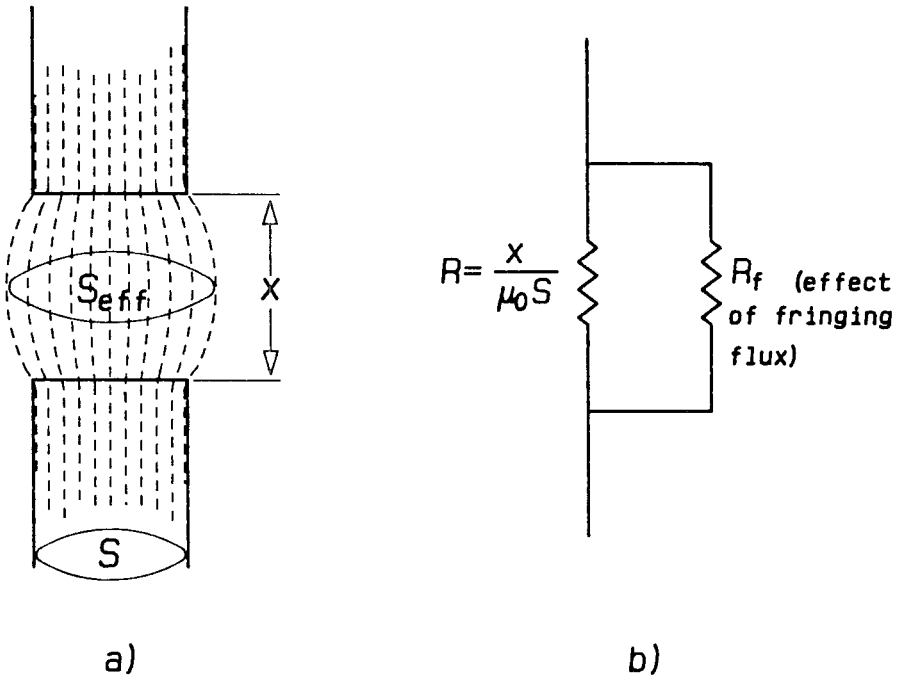

Figure 11.8: a) The fringing flux across an air-gap. b) The reluctance model of the air-gap.

11.1.4 Correction for the Fringing Flux

In any magnetic structure with air-gaps (Fig. 11.3a), the magnetic flux at the gap will spill outwards, making the reluctance of the gap smaller than calculated. Therefore, the inductance of the inductor will be larger than that from the calculation, this error can be up to 50% in a design with a large gap. With this fringing effect in mind, the physical air-gap (x_g) used in the coupled-inductors structures should be larger than the calculated gap x found from the design equations given in the last two chapters. Several experimental equations have been introduced to correct this fringing effect [6], [12]. Unfortunately, those corrections are just complicated enough to make the deriving of closed form design equations impossible. However, the measurement on the EI and EE-core structures in Appendix A shows that, for a given core and structure, the difference between the measured and calculated permeance of the gap is almost a constant despite the large variation of the air-gap, or in other words, the fringing effect is like having a

fixed reluctance across the uncorrected reluctance of the gap (Fig 11.3b):

$$\mathcal{R} = \mathcal{R}_g \parallel \mathcal{R}_f = \frac{\mathcal{R}_g \mathcal{R}_f}{\mathcal{R}_g + \mathcal{R}_f} \tag{11.22}$$

where $\mathcal{R}$ is the corrected reluctance of the air-gap, or the reluctance calculated from the design equations; $\mathcal{R}_f$ is the reluctance of the fringing flux path; and $\mathcal{R}_g$ is the uncorrected reluctance, or the reluctance of the air-gap calculated using the simple equation:

$$\mathcal{R}_g = \frac{x_g}{\mu_0 S} \tag{11.23}$$

where x_g is the size of the air-gap.

Using this method, we can make the correction *after* the calculated gap x is found from the design equations. The physical air-gap x_g is then calculated from:

$$x_g = \mathcal{R}_g \mu_0 S = \frac{\mathcal{R}_f \mathcal{R}}{\mathcal{R}_f - \mathcal{R}} \mu_0 S = \frac{l_f x}{l_f - x} \tag{11.24}$$

where l_f is called the fringing flux parameter, which is the effective gap of the fringing flux path reluctance $\mathcal{R}_f$:

$$l_f = \mathcal{R}_f \mu_0 S \tag{11.25}$$

the value of l_f for selected EE and EI-cores can be found in Appendix A.

11.1.5 The Window Area for the Input Winding

The total copper loss of coupled-inductors using the new structures also depends on how the window area is divided between the primary and secondary windings. If much of the window area is taken by the primary winding, the copper loss in the primary will be small, but the window area left for the secondaries will be small, and the secondary copper losses will be high. On the other hand, if the window area given to the primary is very small, the copper loss in the secondaries will be small, while the primary copper loss will be high.

Since the number of turns in the secondary windings are about three times that in the the primary winding, the copper loss in the primary is relatively small compared with the secondary copper loss. Therefore, most of the window area should be allocated to the secondaries. The easiest way to allocate the window area is according to the ampere-turns of the windings. For example, an EI-core coupled-inductor structure has 100 turns for the primary and 240 turns for each secondary. The primary current is $1.2A$; the two secondary currents are $1.5A$ each. Therefore, the primary ampere-turns are 120 A-T, while the secondary ampere-turns are 360 A-T. In this case 25% of the window area should be given to the primary, and the remaining 75% is for the secondary.

11.2 150W OFF-LINE SWITCHER EXAMPLE

The off-line switcher shown in Fig. 11.4 is an 150w, triple output power supply based on the isolated coupled-inductor Ćuk converter. The outputs are 5V @10A, 12V @ 4A and -12V @ 4A. The switching frequency is 23kHz with a normal duty ratio of 0.30. The simplified schematic of the power stage is shown in Fig. 11.4b.

11.2.1 Design Requirements and Considerations

The converter is designed to operate off the 115/230V 50/60Hz ac line voltage. The dc voltage, after rectifying, is about 270V. Since the hold-up time requirement requires a large capacitor ($250\mu F$) at the input of the converter, any input current ripple will be easily filtered out and will not be fed back to the line. Therefore, in the design, all the ripple is steered to the input, and to keep the size of the inductor down, without putting too much stress on the transistor switches, the input ripple is chosen to be about 1.7A peak-to-peak. Considering the efficiency of the converter, the average input current is about 0.6A. From the input ripple requirement, the input inductance of the

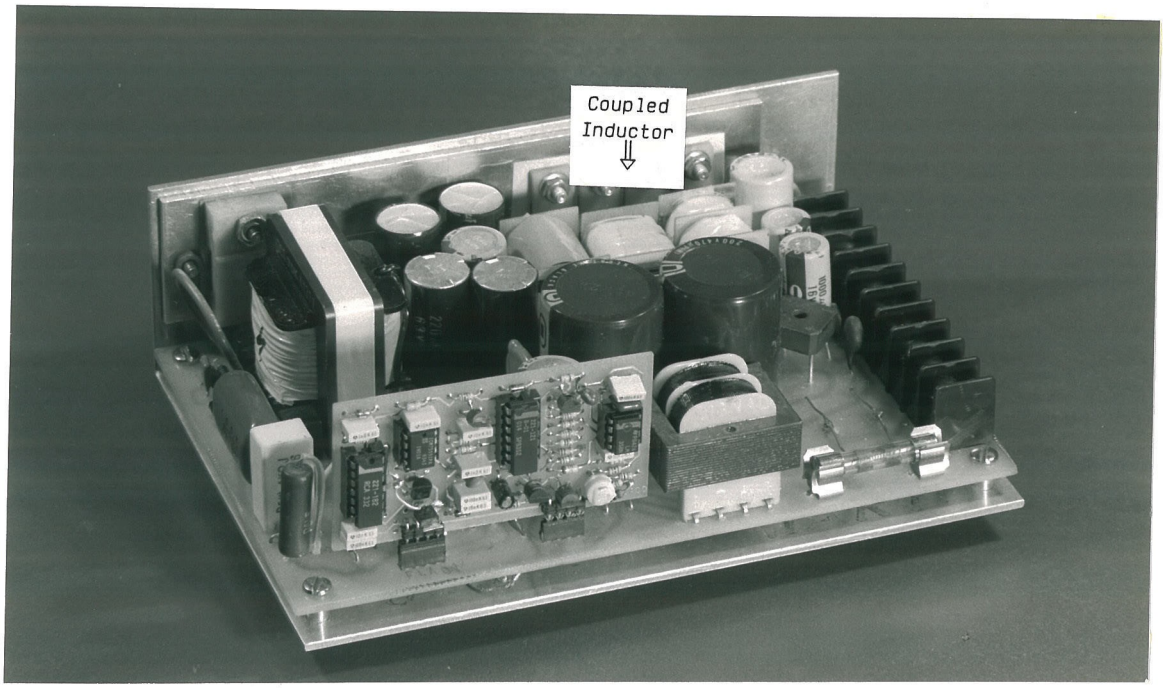

a)

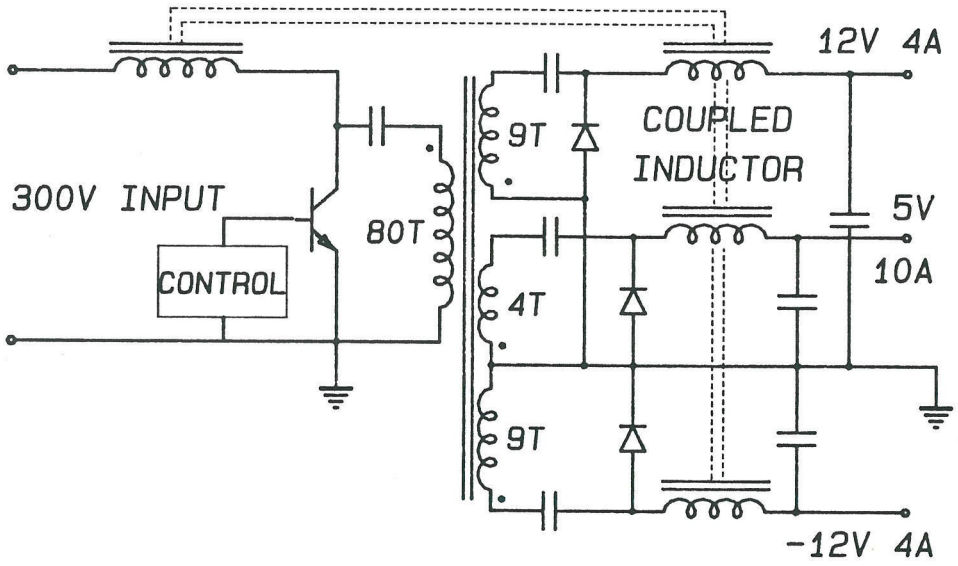

b)

Figure 11.4: a)150w three-output Cuk converter. b) The schematic of the power stage.

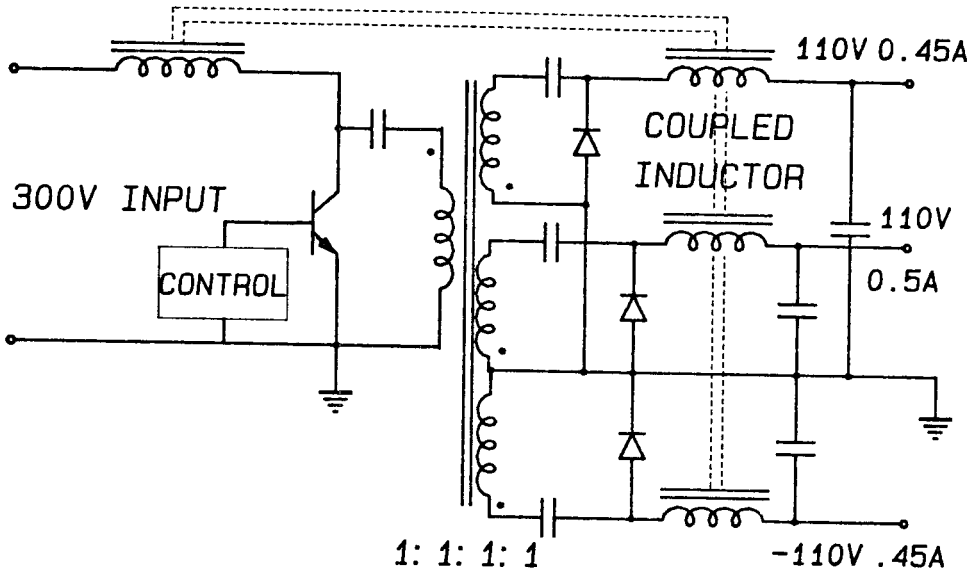

Figure 11.5: Converter circuit after scaling to obtain 1:1:1:1 transformer turns ratio.

coupled-inductors should be 2.0mH.

11.2.2 Design of the Coupled-Inductors

The first step is to reflect all the outputs through the transformer turns ratio (80:4:9:9) to obtain an effective 1:1:1:1 isolation transformer (Fig. 11.5). After this scaling the winding voltages and currents are:

Input: 1.45A peak (1.25A when +5V output is open)

Output 1 (+5V 10A before scaling): 110V @ 0.5A

Output 2 (+12V 4A before scaling): 110V @ 0.45A

Output 3 (-12V 4A before scaling): 110V @ 0.45A

Because a total of four windings are required and output 2, output 3 are symmetrical, an EE-core is chosen, with the input winding on the center leg of the core, output 1 on one outer leg, and output 2, output 3 wound side by side on the other outer leg. The maximum flux density is chosen to be 0.35Tesla. In the design equations, the current of output 1 is I_2, while I_1 is the sum of the currents of output 2 and output 3. The converter is a Ćuk converter operating at a duty ratio less than 0.5; therefore, the worst case is when $I_2 = 0$, with a corresponding input peak current $I = 1.25A$.

The effective current is:

$$I_e = I + 3\,I_1 - I_2 = 1.26 + 2.7 - 0 = 3.95A \tag{11.26}$$

The coupled-inductors are designed using the design procedure given in Section 8.5.

Step 1. Using $l_0 = 4mm$ for the leakage parameter, the trial critical number of turns N_{c_0} is:

$$N_{c_0} = \frac{B_m l_0}{\mu_0 I_e} = 282\text{Turns} \tag{11.27}$$

Step 2. The nominal number of turns on the center leg N_0 is:

$$N_0 = 0.2 N_{c_0} = 57\text{Turns} \tag{11.28}$$

Step 3. The required core cross section is:

$$S_0 = \frac{L\,I_e}{B_m N_0} = 3.9cm^2 \tag{11.29}$$

However, a core with a $4cm^2$ cross section is too large; therefore, we will sacrifice the efficiency for a more compact size. The core chosen is an EE-50 core. The cross section S of the core is $2.25cm^2$; leakage parameter l is $4.6mm$.

Step 4. The critical number of turns and the number of turns for the center winding are recalculated to be:

$$N_c = \frac{B_m l}{\mu_0 I_e} = 324\text{Turns} \tag{11.30}$$

$$N = \frac{L\, I_e}{B_m S} = 100\text{Turns} \tag{11.31}$$

The ratio of N/N_c is 0.31.

Step 5. The number of turns on the outer legs are:

$$N_1 = \frac{2\, N}{1 - N/N_c} = 290\text{Turns} \tag{11.32}$$

Step 6. The air-gap x is:

$$x = \frac{N/N_c}{1 - N/N_c}\, l = 2.07mm \tag{11.33}$$

Because an EE-core is used, the spacer should be half the calculated value (see Chapter 9).

The next step is to scale the windings back to the original voltages and to select the wire sizes according to the currents and the window area. The effect of the fringing flux for EE-cores is negligible. Note that because an uniform spacer is used for the air-gap, the thickness of the spacer should be half that of the calculated air-gap x. The initial design is now completed:

Primary: 100 Turns #24 AWG

5V 10A: 14.5 Turns 4x#18 AWG

12V 4A: 32.6 Turns #18 AWG

Spacer: 1.04mm

The copper loss of the coupled-inductors is calculated to be about 3W.

The final design, after the adjustment to obtain the lowest current ripple in all the output windings, is shown in Fig. 11.6. Note that the number of turns for all the windings agrees almost exactly with the calculations.

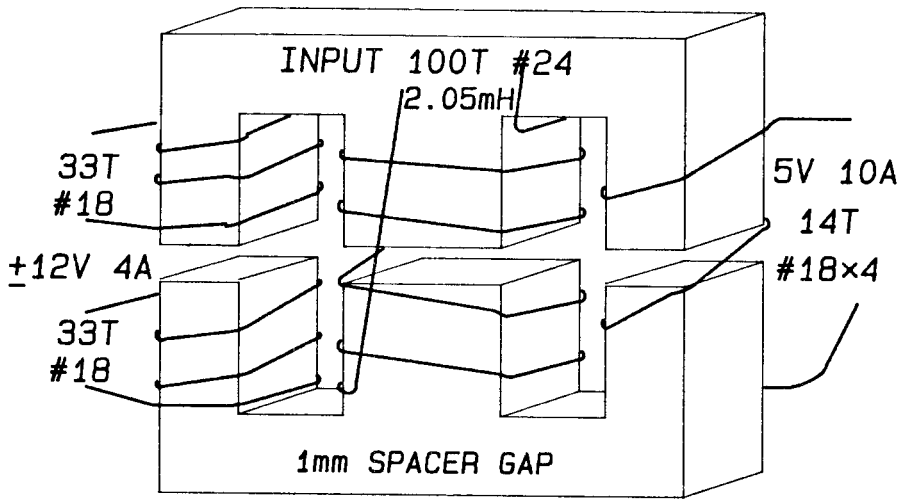

Figure 11.6: The design of the coupled-inductors.

11.2.3 Comparison With Other Magnetic Structures

To compare the performance of the new design with some more conventional designs, two other inductor structures were built. One is a tightly coupled coupled-inductor structure using the traditional transformer winding configuration and a single air-gap on a PQ 40/40 core. Since the coupling between the windings is quite tight, additional "leakage" inductors must be added in the secondary circuits to reduce the current caused by the slight difference in the isolation transformer output voltages. The other design tries to simulate the coupled-inductors with four separate inductors. The input inductor is wound on an EI-22 core, the 5V 10A inductor uses an EI-60 core and the 12V 4A inductors are wound on EI-50 cores.

Figure 11.7a shows the size and weight of the three structures, while Fig. 11.7b shows the current waveforms of each winding when the inductor is used in the 150W

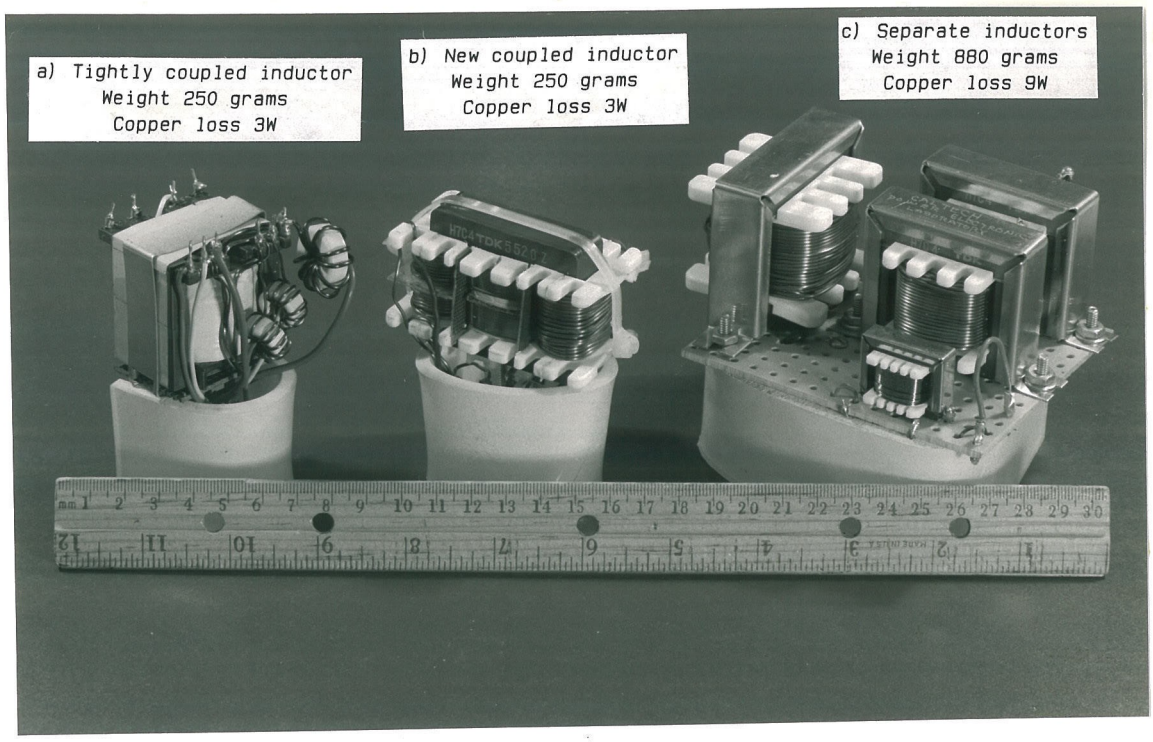

a)

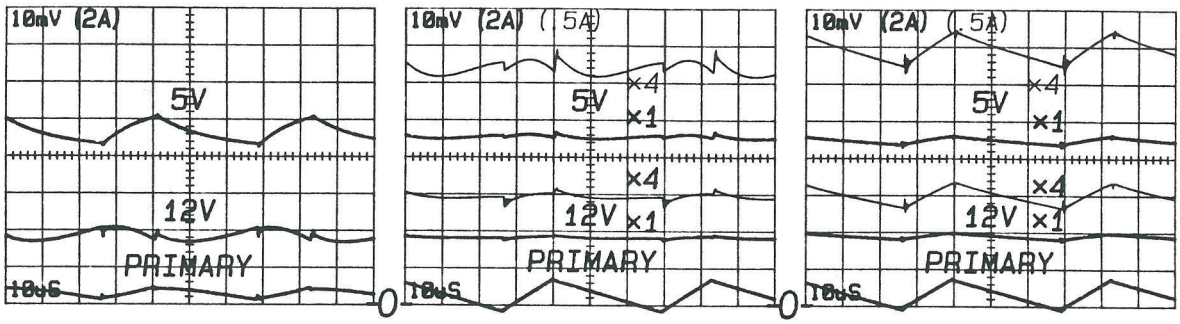

b)

Figure 11.7: a) Three different coupled-inductor structures used in the 150W converter. Note the external leakage inductors used in the tightly coupled design. b) The current waveforms for the three different structures.

converter shown in Fig. 11.4. Note that the weight and power loss of the new design are about one fourth and one third of those of the separate inductors; however, the ripple currents are still lower than the separate inductors. The weight and loss of the tightly coupled-inductors are about the same as the new design, but the output ripple current of the new design is only about 15% of that of the tight coupled design.

Chapter 12

CROSS-REGULATION PROBLEM IN SWITCHING CONVERTERS

In a switch mode regulator, output voltage is usually controlled by the duty ratio of the switching transistor. Therefore, in a multiple output switching converter (Fig. 12.1), only one output can be regulated. The other output voltages may then vary according to the load currents. This is called the cross-regulation of the converter. Although there are different methods to regulate more than one output at the same time [13], the complication of the circuits makes it impractical for most applications. In an ideal switching converter (no parasitics) operating in continuous conduction mode, the output voltages depend only on the duty ratio of the switch and is independent of the load current. In this case, even though only one output is regulated, the other outputs will not change from their normal voltages even when the load currents are changed. However, when the converter is operating in the discontinuous conduction mode, the output voltages will depend not only on the duty ratio, but also on the load currents. In this case, regulating one output will make that output voltage constant regardless of the load currents, but the other output voltages may still change when the load current is changing.

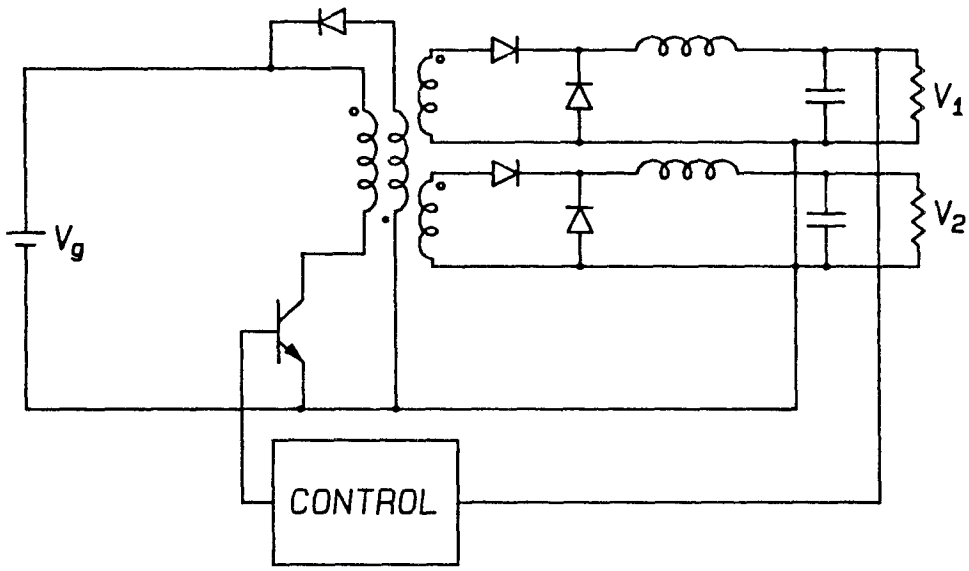

Figure 12.1: In a multiple output switching converter, usually only one output is regulated.

12.1 THE DISCONTINUOUS CONDUCTION MODE (DCM) OF SWITCHING CONVERTERS

Figure 12.2a shows a simple buck converter. As shown in the inductor waveforms (Fig. 12.2b), in the period DT_S, the switching transistor is turned on; thus, the voltage across the inductor is $V_g - V$, and the inductor current ramps up; in the period $D'T_S$, the transistor is turned off, the inductor current flows through the diode, the inductor voltage is now $-V$, and the inductor current ramps down. Since the inductor current is finite, the average inductor voltage must be zero. Therefore, in the inductor voltage waveform, the positive area is equal to the negative area, or $(V_g - V)DT_S = V\,D'T_S$. This is called the *volt-second balance*, Using this equation, one can calculate the output voltage:

$$\frac{V}{V_g} = D \tag{12.1}$$

Note that the output voltage is independent of the load current.

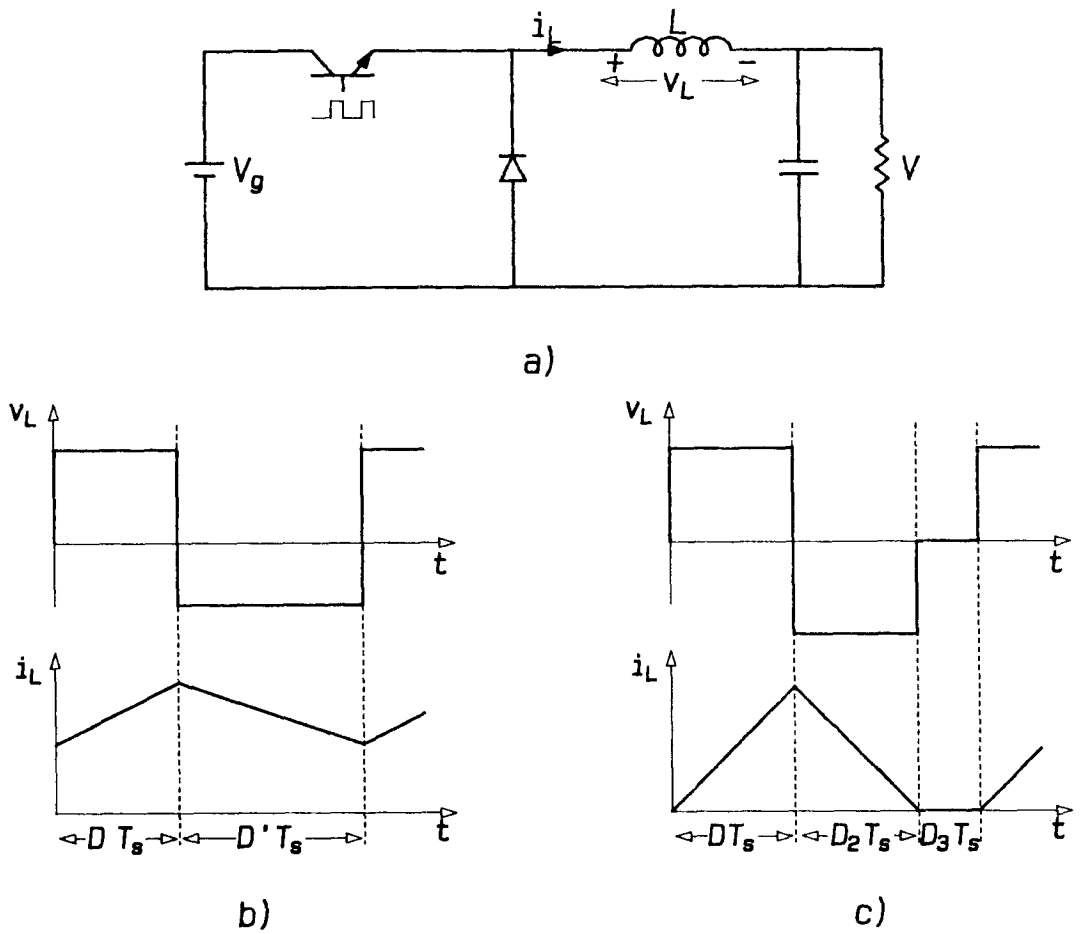

Figure 12.2: a) A buck converter. b) The inductor voltage and current waveforms under various load currents. c) The inductor voltage and current waveforms in DCM mode.

If the load current is reduced, the average inductor current is also reduced, but the slopes of the current will be the same as before (Fig. 12.2b). When the load current is reduced to a certain value, the minimum inductor current will be zero. If the load current is further reduced, the minimum inductor current should dip below zero. However, unlike an ideal switch, the diode will turn off as soon as the inductor current reaches zero, and the inductor current will remain at zero until the beginning of the next switching cycle. In this third period, the inductor current is constant (zero), therefore, the voltage across the inductor is also zero (Fig. 12.2c). This operation mode of the

converter is called *discontinuous conduction mode* or DCM. In this mode, there are three periods in a switching cycle: DT_S, when the transistor is on and the diode is off; D_2T_S, when the transistor is off but the diode is on; and D_3T_S, when both the transistor and the diode are off. By use of the volt-second balance, and the 100% efficiency property of the ideal converter, the output voltage is calculated as:

$$\frac{V}{V_g} = \frac{2}{1+\sqrt{1+4K/D_1^2}} \tag{12.2}$$

where

$$K \equiv \frac{2Lf_s}{R}$$

Note that now the output voltage is also dependent of the load; if the load current is reduced to zero (the load resistance increases to infinity), the output voltage V will increase to V_g, and the duty ratio control of the output voltage will be lost.

The DCM mode exists in all converter topologies, unless bidirectional switches (switching devices that can conduct current in both directions) are used in the circuit.

12.2 CROSS-REGULATION IN MULTIPLE OUTPUT CONVERTERS

In discontinuous conduction mode, the output voltage is load-dependent. We would expect the cross-regulation problem to be most serious when the converter is operating in DCM.

The cross-regulation characteristics of different converter topologies differ widely. For example, the typical cross-regulation characteristic for a two output flyback converter operating at a fixed duty ratio is shown in Fig. 12.3a. As seen from the curves, when one of the the output currents is decreased, the output voltages will first increase slightly; then, after that output current is decreased to a certain point, the converter will get into discontinuous mode (DCM), and both output voltages will increase

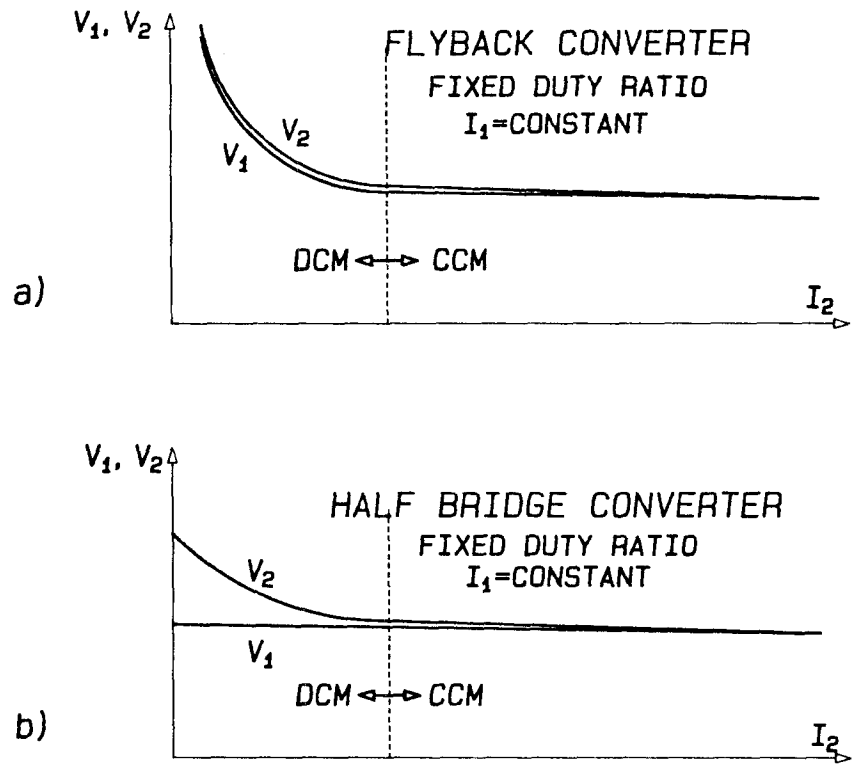

Figure 12.3: a) In a flyback converter, the tracking between the outputs is good. b) For a half bridge converter, each output goes into DCM independently; the tracking is poor.

rapidly. When the total load current decreases toward zero, the output voltage goes up toward infinity. However, despite this voltage increase, the *ratio* of the two outputs will always be about the same; in other words, the *tracking* between the outputs is close. In this case, regulating one output will also bring the other output close to the rated voltage. Fig. 12.3b shows the cross-regulation characteristic of a two-output half-bridge converter. In this converter, if the output current of one output is decreased below a certain point, that output itself will get into DCM, and its output voltage will increase, while the the other output voltage will remain relatively stable. In this case, even though the output voltage increase in DCM mode is smaller than that for the flyback converter (in the half-bridge converter, the output voltage only goes up to V_g, when the load current drops to zero), regulating one output will not have much effect on the other output,

because the tracking between the outputs is very poor. Note that for both converters, the variation of the output voltages is relatively small in the continuous conduction mode (CCM); therefore, our main interest will naturally be in the DCM mode of the converter.

In the following chapters, the discussion will be made for the cross regulation characteristic of the most popular multiple output converter types, namely, the flyback converter, the buck forward type converter, and the Ćuk converter. The boost converter, though quite common as a single output converter, is not easily adaptable as a multiple output converter, and therefore is not covered here. In some converters, like the buck forward converter, the cross-regulation characteristic will change when the inductors are coupled. The coupling of the inductors will improve the tracking of the outputs. This is an additional advantage of the coupled-inductor concept. This change of the cross-regulation characteristic will also be discussed in detail. The discussion will focus mainly on the operation of the *ideal* converters, operating in the discontinuous conduction mode. Parasitics of the circuit, such as inductor winding resistance, will not be included, as the effect of these parasitics could be easily found using the state-space averaging method [14].

In the next three chapters, the discussion will concern the following multiple output converters:

1. The cross-regulation characteristic for the flyback converter in continuous and discontinuous conduction mode.
2. The cross-regulation characteristic for the buck type converters in CCM and DCM, with and without coupled-inductors.
3. The cross-regulation characteristic for the Ćuk converter in CCM and DCM, with and without coupled-inductors.

Chapter 13

CROSS-REGULATION FOR MULTIPLE OUTPUT FLYBACK CONVERTERS

The flyback converter (Fig. 13.1a) is one of the basic converter topologies. In the time period when the transistor is on, the inductor stores energy from the input V_g. During the other time period, the transistor is turned off and the inductor releases the stored energy to the load through the diode. The inductor supplies current to the output only during part of the duty cycle, so the output capacitor has to be large to filter out this large current ripple. This characteristic limits the application of the flyback converter to low power applications.

A two-output flyback converter operates essentially the same as the single output version—the three winding magnetic structure stores energy from the input when the transistor is on, and releases the energy to the outputs after the transistor is turned off. Because of the operation of this magnetic structure, it is really a tightly coupled three-winding coupled-inductor, even though it is drawn like a transformer in the circuit.

13.1 FLYBACK CONVERTER IN CONTINUOUS CONDUCTION MODE

The circuit of a two-output flyback converter is shown in Fig. 13.2a. Assuming the turns ratio of the dual winding inductor to be 1 : 1 : 1, the circuit can be drawn as

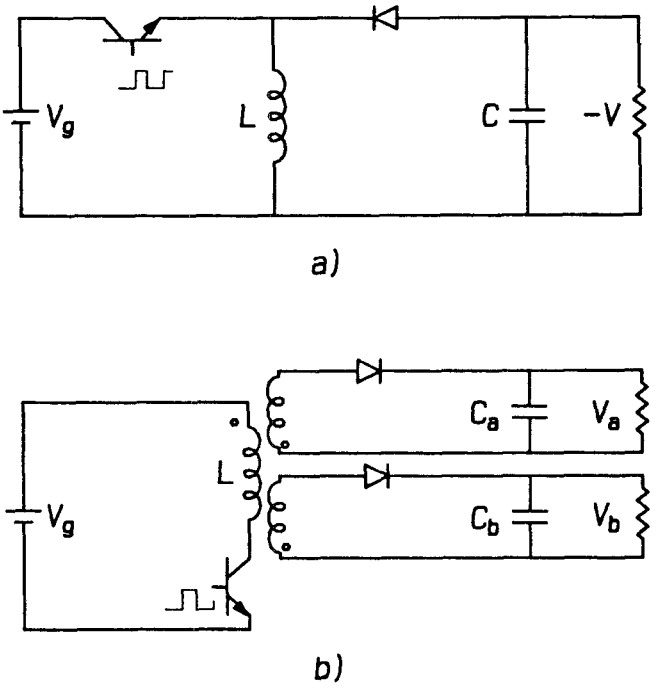

Figure 13.1: a) A single output flyback converter. b) A two output flyback converter.

Fig. 13.2b.

During the period DT_S, the transistor switch is on, and the two diodes are reverse-biased, therefore, the circuit model is as in Fig. 13.2c. During this period, the inductor is connected directly across the input V_g; thus the inductor current ramps up. The two load resistors R_a and R_b are now supported by the two output capacitors. Assuming that $R_aC_a < R_bC_b$, the voltage v_a on capacitor C_a will drop faster than the other capacitor voltage v_b, as shown in Fig. 13.2e. At the end of the period DT_S, v_a is lower than v_b.

During $D'T_S$ (Fig. 13.2d), the transistor switch is off, and the inductor current will ramp down while charging the two output capacitors through the two diodes. Note that at the beginning of $D'T_S$, the voltage on C_a is lower than that on C_b; therefore, D_a will conduct first, and the entire inductor current will be directed to C_a, and the load resistor R_a. C_a will then be charged up by the inductor current, while C_b will continue to

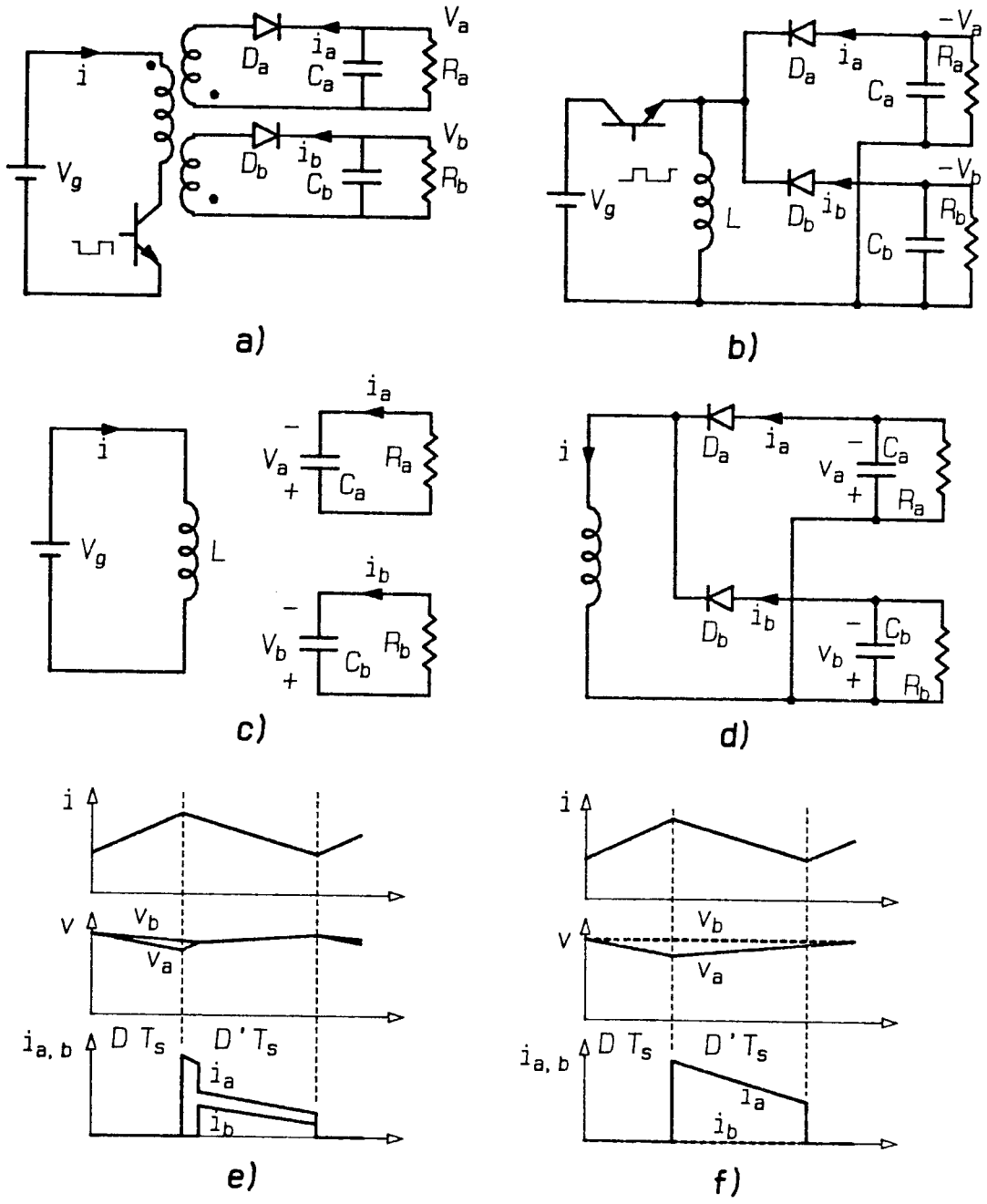

Figure 13.2: a) A two output flyback converter. b) The equivalent circuit for 1 : 1 : 1 *inductor turns ratio. c) The model for the period* DT_s*. d) The model for* $D'T_s$*. e) The current and voltage waveforms. f) The waveforms when the second output is unloaded.*

discharge through the load resistor R_b, as shown in the voltage waveforms in Fig. 13.2e. At the moment the two capacitor voltages become equal, the other diode D_b will start to conduct, dividing the inductor current into both outputs according to the load currents and the capacitor values. From this point on, as long as the inductor current is larger than the sum of both output currents, the two output capacitor voltages will increase together till the end of the switching cycle.

From the capacitor voltage waveforms shown in Fig. 13.2e, one can notice that the average output voltage V_a is lower than V_b, even though the two capacitors are charged to the same voltage at the end of $D'T_S$. It is interesting to notice that, if the second output is unloaded, C_b will not discharge at all, and D_b will not conduct during the whole switching cycle (Fig. 13.2f). Even in this extreme case, the difference between the two average output voltages is only half the peak-to-peak ripple voltage of the loaded output. If the output capacitors are sufficiently large to keep the output voltage ripple down, the difference between the output voltages will be negligible. In the ideal case, with no resistive and switching losses, the voltage conversion ratio of the flyback converter can be found by the volt-second balance on the inductor:

$$V_a = V_b = V_g \frac{D}{D'} \tag{13.1}$$

which is the same as the single output flyback converter.

13.2 FLYBACK CONVERTER IN DISCONTINUOUS CONDUCTION MODE

In the DCM mode, the inductor current falls to zero before the end of the switching cycle; in this third period, labeled as D_3T_S in Fig. 13.3a, both diodes are cut off, and the inductor current remains at zero till the end of the switching cycle. The question now is: Do both diodes turn off at the same time? If not, how does this affect

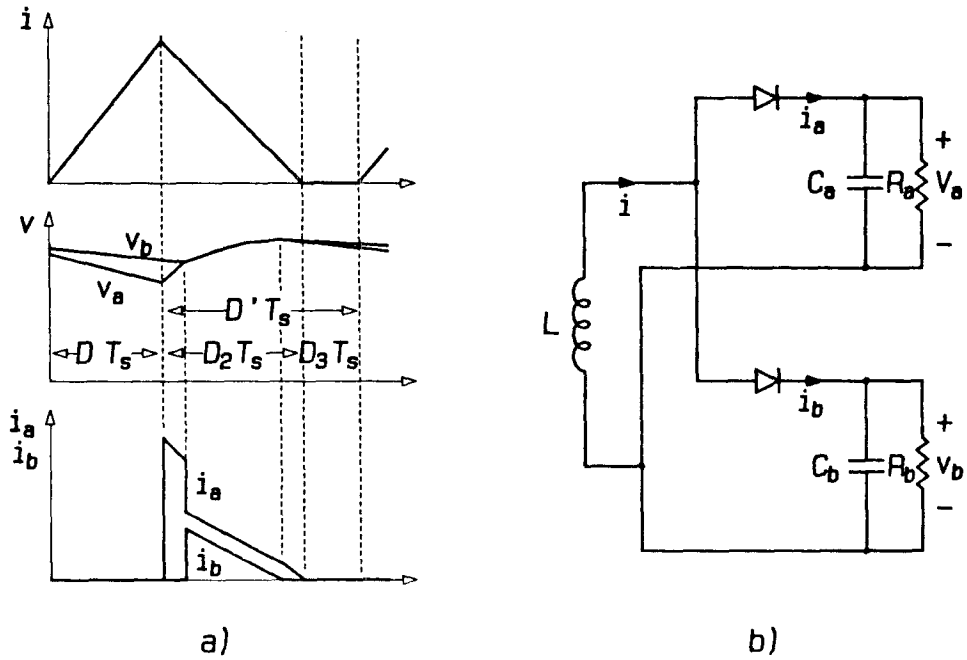

Figure 13.3: a) The voltage and current waveforms in DCM mode. b) The output circuit of the converter when the transistor is off.

the output voltage?

The output circuit of the two output flyback converter is shown in Fig. 13.3b. In the time period D_2T_S, the transistor is off, and the inductor current i_L decreases; so do the two diode currents i_a and i_b, as shown in Fig. 13.2e. If the current in one of the diodes reaches zero before the other one, that diode will turn off, and the inductor current will go only into the other diode. The current in the diode of the first output D_a is:

$$i_a = \frac{v_a}{R_a} + C_a \frac{dv_a}{dt} \tag{13.2}$$

The current in the other diode D_b is:

$$i_b = \frac{v_b}{R_b} + C_b \frac{dv_b}{dt} \tag{13.3}$$

In the period D_2T_S, the inductor current is decreasing; when the inductor current drops below the total load current, the capacitors will start to discharge to support the load

current. In this case, from the assumption $R_aC_a < R_bC_b$, C_b will discharge more slowly than C_a, and v_b will become higher than v_a. Therefore, we would expect D_b to turn off first.

Following our expectation, first assume that i_b falls to zero before i_a. At $t = T^-$, just before the current in D_b falls to zero, both diodes are still conducting, so the two capacitors are still connected together through the diodes; therefore:

$$i_a \rightarrow i_L \qquad i_b \rightarrow 0 \qquad v_a = v_b = v \qquad \frac{dv_a}{dt} = \frac{dv_b}{dt} = \frac{dv}{dt} \tag{13.4}$$

By solving (13.3) for $\frac{dv_b}{dt}$ and substituting into (13.2), we can write:

$$i_a = i_{L\ (t=T^-)} = -\frac{C_a}{C_b}\frac{v}{R_b} + \frac{v}{R_a} = v\,C_a\left(\frac{1}{R_aC_a} - \frac{1}{R_bC_b}\right) \tag{13.5}$$

Note that since $R_aC_a < R_bC_b$, i_a is always greater than zero when D_b turns off; this confirms our earlier expectation that D_b will turn off before D_a.

After D_b is turned off, C_b discharges through R_b, and the inductor current flows through D_a until it falls to zero, when D_a also turns off. The inductor current will then remain at zero until the beginning of the next switching cycle, and each capacitor will discharge through its correspondent load resistance. After both diodes are turned off (D_3T_S in Fig. 13.3a), both capacitor voltages will decrease gradually.

As in the continuous mode, the average output voltages will differ less than half the output ripple voltage of the first output and usually can be ignored. In this case, for an ideal flyback converter, using the volt-second balance on the inductor, and the 100% efficiency property of the converter, the dc voltage conversion ratio for the DCM mode is found to be also identical to the single output flyback converter:

$$V_a = V_b = V_g\frac{D}{\sqrt{K}} \tag{13.6}$$

where

$$K \equiv \frac{2L}{R_a \parallel R_b}f_s$$

Note that in the discontinuous conduction mode, the output voltages are load-dependent. However, to the first order, both output voltages are always equal.

Even in the CCM mode of the converter, if the inductor current falls below the level given in Eq. (13.5), D_b will cut off, and the inductor current will continue to flow through D_a. The only difference is that because the inductor current is always larger than zero, D_a will not turn off before the end of the switching cycle.

It is interesting to notice that, for a flyback converter, even in the continuous conduction mode, unless the two outputs have the same time constant ($R_aC_a = R_bC_b$), one of the diodes always turns on later than the other, and if the inductor current falls below a certain value, one diode will turn off before the other. However, the difference between the two output voltages is always less than half the output voltage ripple.

For a flyback converter with three or more outputs, it can be shown that at the beginning of $D'T_S$, the diodes turn on in the order of the time constants of the corresponding output (the load resistance and the output capacitor), the smaller the time constant, the lower the output voltage will be at the beginning of $D'T_S$, therefore the earlier the diode will turn on. If, before the end of $D'T_S$, the inductor current falls below a certain level, the diodes will turn off one by one in the opposite order, until the last diode turns off when the inductor current reaches zero.

The voltage tracking between the output voltages in a multi-output flyback converter, in both CCM and DCM modes, is always very good. However, the output currents of the converter are always discontinuous. To obtain low voltage ripple on the outputs, one has to use very large output capacitors. Therefore, the flyback converter is usually only used in low power applications.

Chapter 14

CROSS-REGULATION FOR MULTIPLE OUTPUT BUCK TYPE CONVERTERS

14.1 THE FAMILY OF BUCK TYPE CONVERTERS

The basic single output buck converter is shown in Fig. 14.1a. Several methods can be used to combine the transformer into the circuit to isolate the output from the input, also to obtain multiple output voltages. Fig. 14.1b–e shows four of such circuits. Note that, for the forward converter, a special circuit is needed to reset the magnetizing inductance of the transformer, while in the other three converters, the transformer is reset by the push-pull action of the switching transistors. However, for all the converters shown, the basic operation is identical.

For the forward converter with 1:1:1 transformer turns ratio, during the period DT_S the transistor switch is on. The two inductors L_a, L_b are connected through the diodes D_{1a}, D_{1b} directly to the supply voltage V_g. The other two diodes D_{2a}, D_{2b} are turned off by the reverse biasing of V_g. Therefore, the circuit model for this time period can be drawn as Fig. 14.2a. During the period $D'T_S$, the transistor and the two diodes D_{1a}, D_{2a} are off, the two inductor currents will continue to flow through the other two diodes D_{2a} and D_{2b}. At the same time, the transformer magnetizing inductance is reset through the reset winding and the diode D_3. However, this reset circuit is needed only because the transformer is not ideal (has finite magnetizing inductance), and will

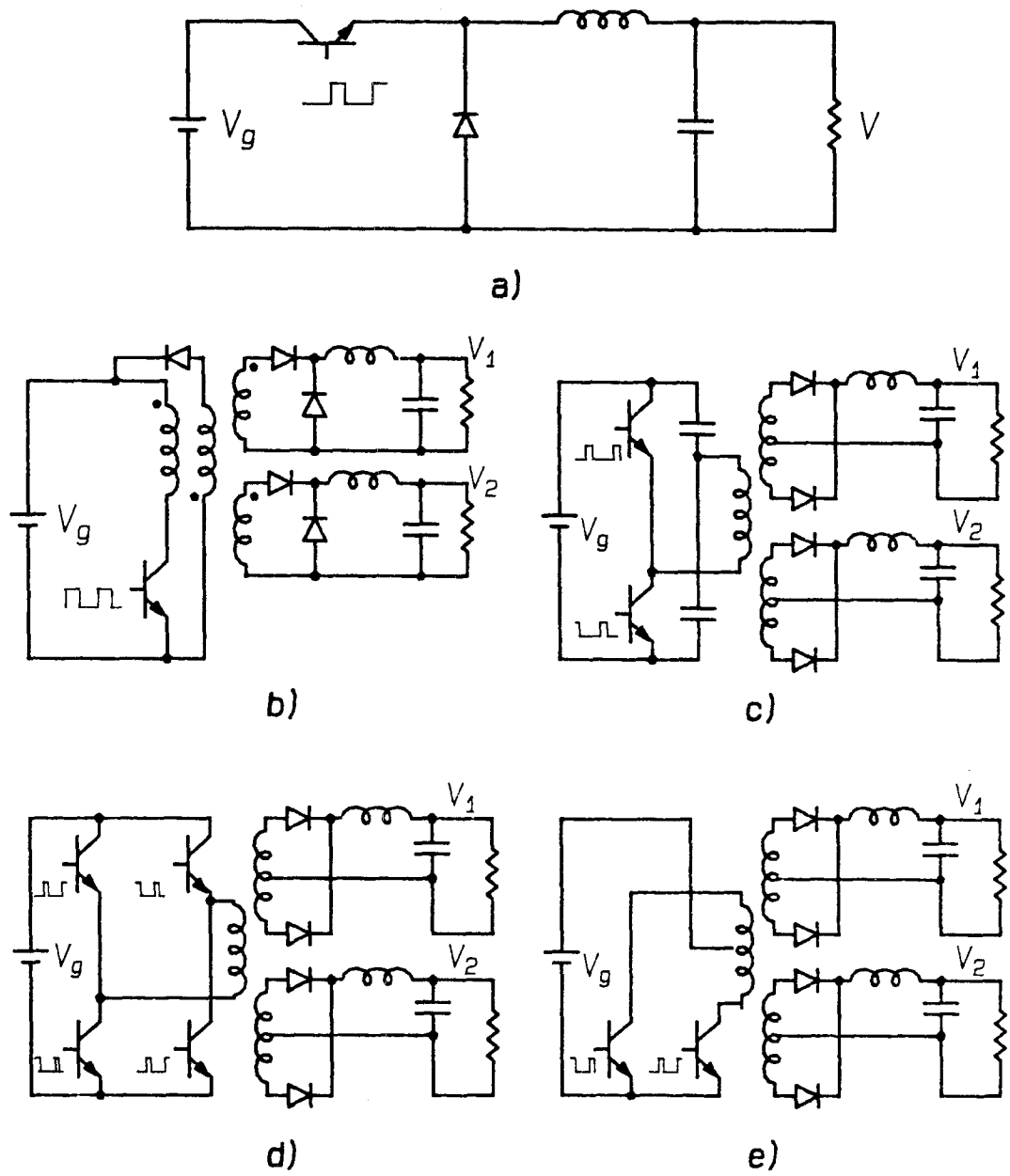

Figure 14.1: a) The basic buck converter. b) Two-output forward converter. c) Two-output half-bridge converter. d) Two-output full-bridge converter. e) Two-output push-pull converter.

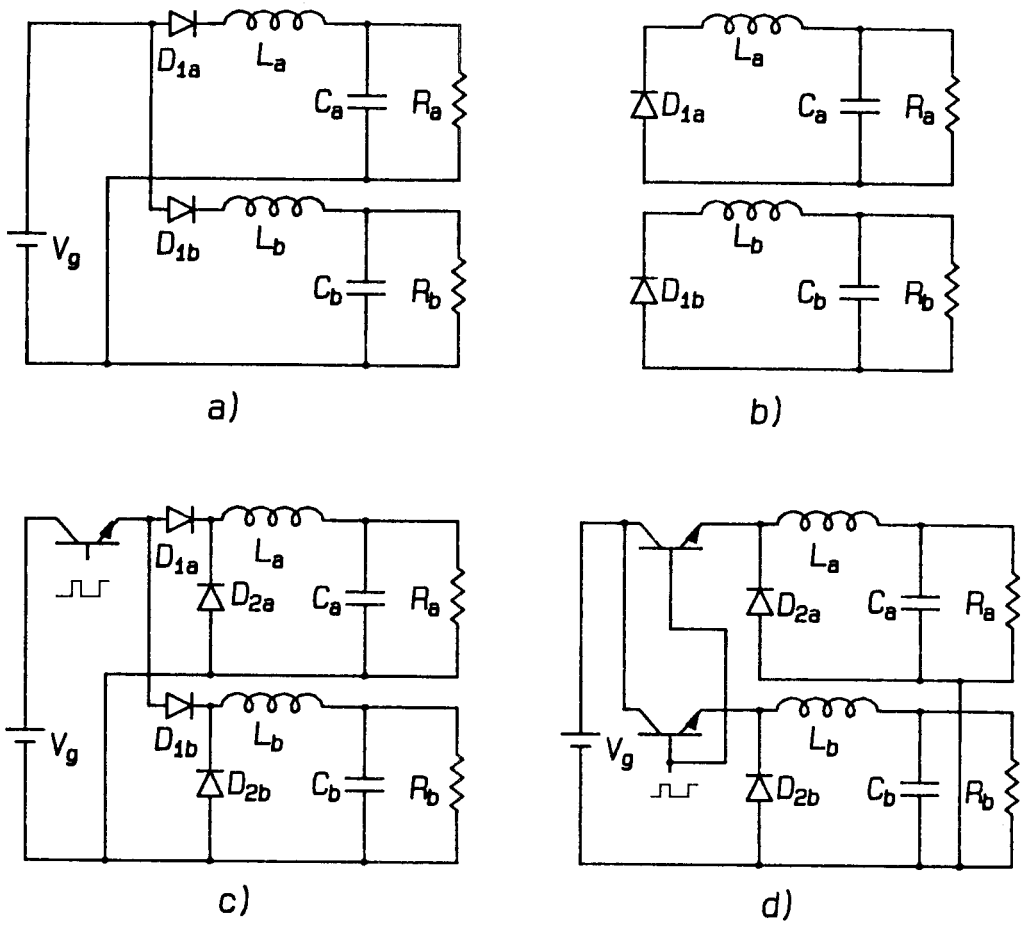

Figure 14.2: a) The circuit model for the time period DT_s for a two-output forward converter, assuming 1:1:1 transformer turns ratio. b) The circuit model for the period $D'T_s$. c,d) The equivalent circuits for the buck type converters.

be neglected in further discussion. The circuit model for this period can be drawn as Fig. 14.2b.

Combining the circuit models for the two time periods, the converter can be drawn as Fig. 14.2c, or as in Fig. 14.2d. As shown in Fig. 14.2d, a two-output forward converter operates just like two *separate* buck converters.

Forward converters with more outputs and other multiple output converters in the buck family can also be drawn as separate buck converters, one converter for each output.

14.2 MULTIPLE OUTPUT BUCK TYPE CONVERTERS WITHOUT COUPLED-INDUCTORS

Since a multiple output buck type converter is equivalent to separate converters driven by the same duty ratio, their operation in CCM nd DCM modes is just the same as separate buck converters, whose voltage transfer ratio is given in (12.1) (12.2) for ideal converters (no inductor winding resistances, no transistor and diode voltage drops, etc.). It should be clear now that each converter will have its own discontinuous conduction mode, which will not be affected by the operating condition of the other converters. So for the multi-output buck type converters, while the tracking of the output voltages is good when all the outputs are in the CCM mode, if one or more outputs goes into DCM mode, there will be *no tracking* at all between those output voltages.

The only real difference between a multiple output buck type converter and separate buck converters is the positioning of the parasitic resistances of the circuit elements in the converter model. In a single output buck type converter, all the parasitics can be lumped together into one resistor at the output or reflected to the input in the model (Fig. 14.3a,b). In a multiple output buck type converter, the parasitic resistances are divided into two parts. One part, which consists of the dc resistance of the transformer primary, the forward voltage drop and "on" resistance of the transistor switch, also the source impedance, is located at the *common input* of the individual converters in the model. The other part, the dc resistance of the transformer secondary, voltage drop of the diodes, and the inductor dc resistance, is at the outputs in the model or can be reflected to the *separated input* of each ideal converter in the model. Only the resistances *after* the separation will affect the cross-regulation, since the resistor at the common input will affect both outputs at the same rate, when there is a change in the load current at either output. Fig. 14.3 shows the circuits for a single output and a

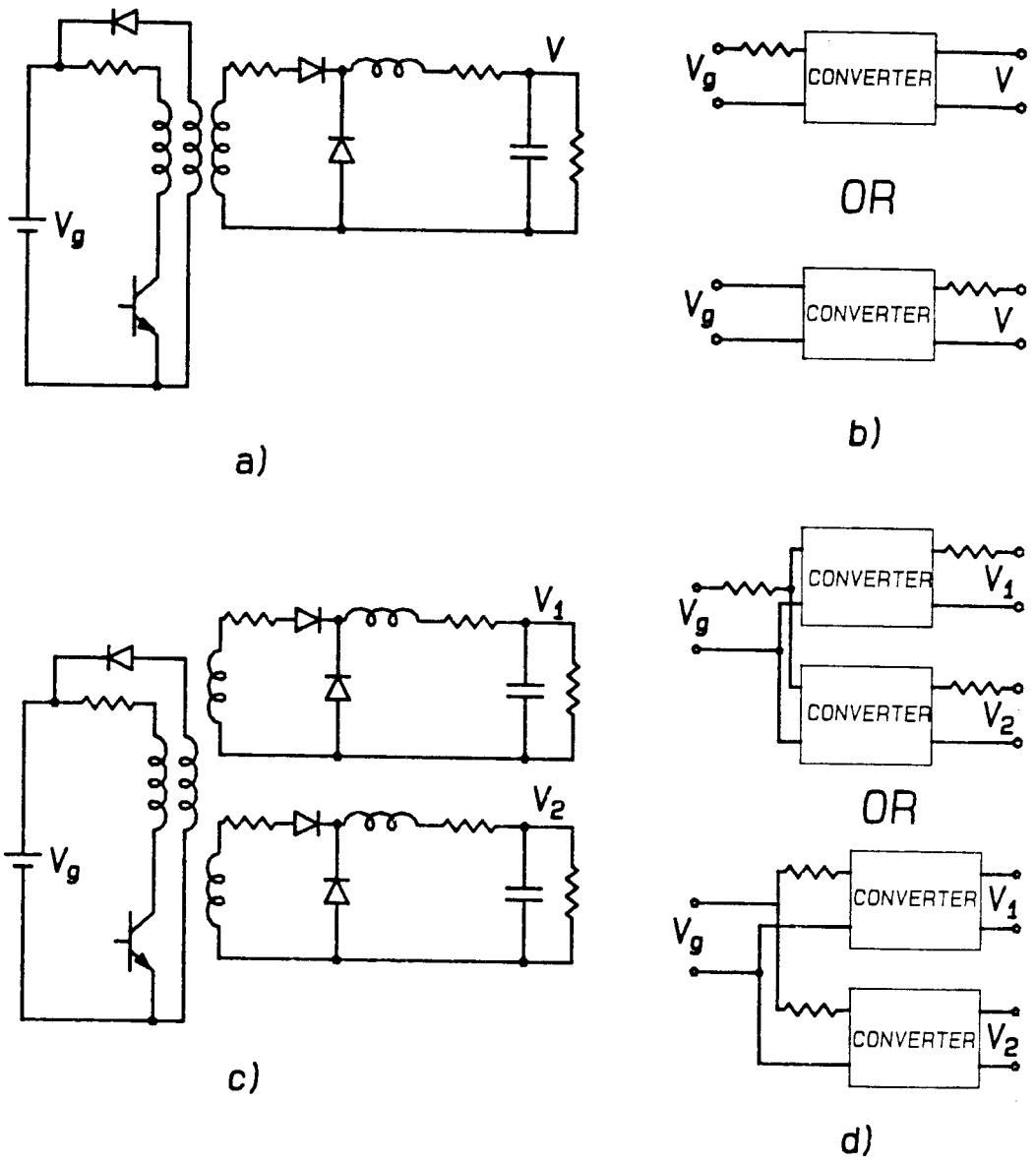

Figure 14.3: a) A single output buck forward converter with parasitics. b) The model for the single output converter. c) A two-output forward converter with parasitics. d) The model for the two-output converter.

three-output forward converter and their equivalent circuits.

14.3 MULTIPLE OUTPUT BUCK TYPE CONVERTERS WITH COUPLED-INDUCTORS

14.3.1 Coupled-Inductors with No Leakage

Figure 14.4a is the equivalent circuit for a two-output buck type converter with an isolation transformer turns ratio 1:1:1. The two inductors in the circuit can be moved to the negative side of the load as shown in Fig. 14.4b. If we tightly couple the two inductors, the circuit can finally be drawn as Fig. 14.4c. In this circuit, if the voltage drops of the diodes are identical, the circuit can be further simplified as Fig. 14.4d. In this circuit, the inductor ripple current is split between the two outputs according to the value of two output capacitors. Since now it is only one converter with two separate outputs, the voltage tracking is very good in both CCM and DCM modes. However, if there is a slight difference in the diode voltage drop, or a small error in the turns ratio of the isolation transformer, there will be a very large ripple current in both outputs. Since there is no leakage in the coupled-inductors, this ripple current is only limited by the ESR of the output capacitors. Despite this drawback, the buck type converter with tightly coupled inductors is still being used to overcome the voltage tracking problem.

14.3.2 Coupled-Inductors With Leakage Inductances

In a buck type converter with coupled-inductors, if the inductors are designed with the appropriate leakage inductance and turns ratio, all the ripple current can be steered into one of the outputs. Figure 14.5a shows the circuit model for two-winding coupled-inductors designed to obtain zero current ripple on the secondary winding. As discussed in Chapter 5, the leakage inductance L_{l_1} and L_{l_2} has to be relatively high to

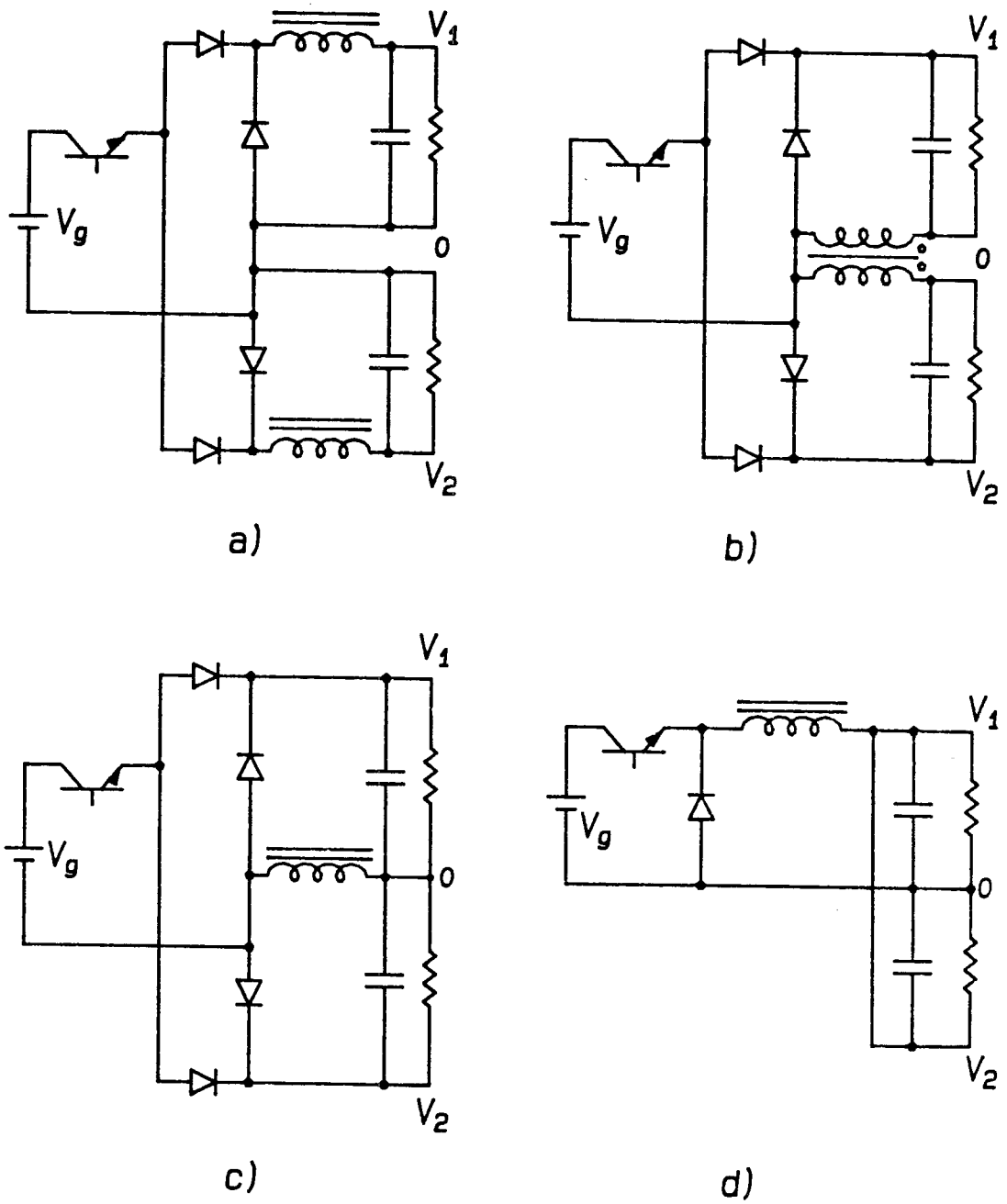

Figure 14.4: a) The equivalent circuit for multiple output buck type converters. b) Redrawing the circuit, moving the inductors to to the negative side of the output, and coupling the inductors. c) The equivalent circuit for tight coupling inductors. d) If the diode drops are identical,the circuit becomes just a single converter with two separate loads.

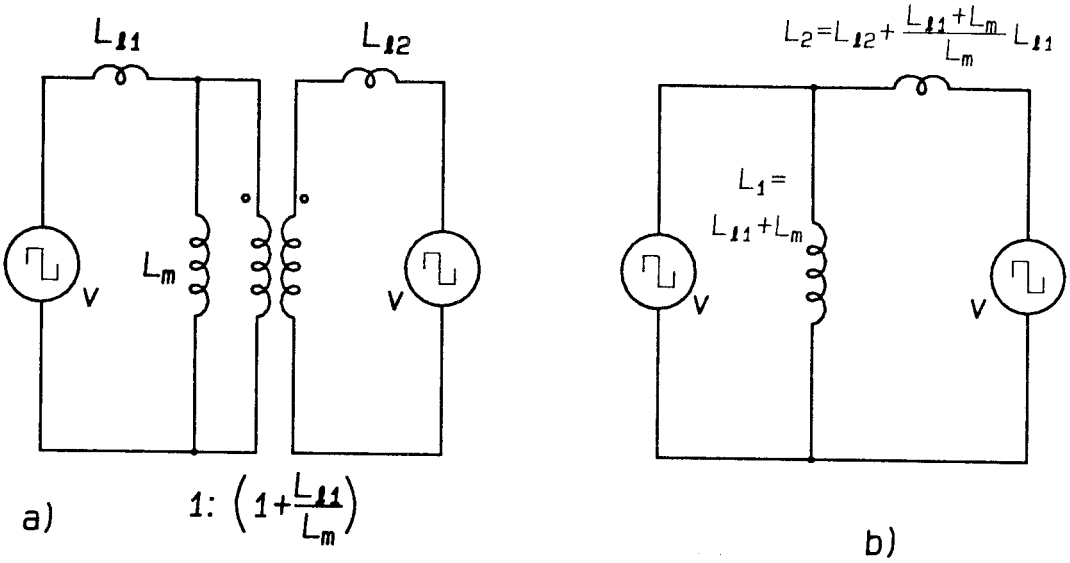

Figure 14.5: a) Coupled-inductors to obtain zero current ripple in the secondary winding. b) Equivalent circuit for the coupled inductor.

obtain low residual ripple and sensitivity. This circuit model can be redrawn as Fig. 14.5b, if one end of the input and output winding is allowed to be connected. If the leakage inductances L_{l_1} and L_{l_2} are high, L_2 in Fig. 14.5b will also be high.

Redrawing the circuit shown in Fig. 14.4b, using the coupled-inductor model shown in Fig. 14.5, one can redraw the circuit as in Fig. 14.6a. Assuming that the load current of the first output V/R_a is sufficiently large so that i_1 will not fall to zero during the entire switching cycle, the converter will be in the CCM mode; the circuit models for the two time periods DT_S and $D'T_S$ can then be drawn as Fig. 14.6b,c. The voltage and current waveforms for both inductors are shown in Fig. 14.6d. Note that since the voltage ripple of the first output (v_a) is very small, and during the entire switching cycle, either D_{1a} or D_{2a} will be conducting, the second output voltage V_b will always be equal to V_a regardless of the second load current. Then the voltage across the inductor L_2 is always zero, resulting in zero current ripple ($i_2 = V/R_b$) in that inductor. Therefore, during $D'T_S$, the current in the diode D_{2b} is the same as the load current, and the diode

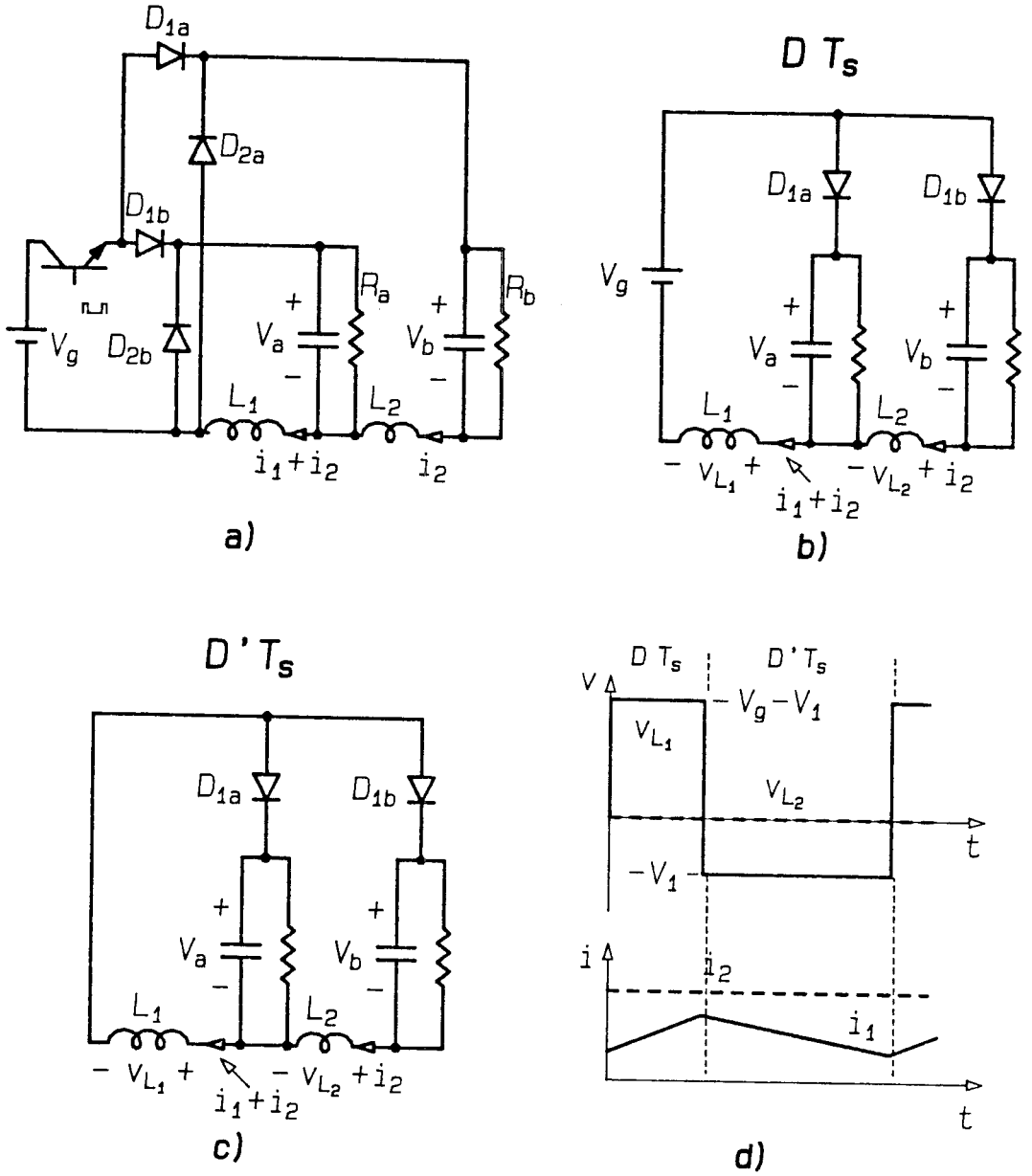

Figure 14.6: a) Circuit model for coupled-inductor buck type converter giving zero current ripple in L_2. b) The model for the time period $D\,T_S$. c) The model for $D'T_S$. d) The voltage and current waveforms for the two inductors.

will never turn off before the end of the switching cycle. Also, since the current in L_1 is the sum of the two output currents $i_1 + i_2$, and i_2 has no ripple, all the inductor ripple will be in the first output current i_1. As long as the peak ripple current in L_1 is less than the average of i_1, i_1 will never fall to zero.

The above discussion shows that, for a two-output coupled-inductor buck converter using the coupled-inductors shown in Fig. 14.5, as long as the current i_1 does not drop to zero, the converter will be in CCM mode. In this case, the second output current i_2 has no ripple, and the output voltages will have very good tracking. Reducing the current of the second output will *not* make that output go into DCM nor affect the tracking between the outputs, as in the converter with uncoupled inductors.

If the load current of the first output in Fig. 14.6 is small so that i_1 reaches zero before the end of the switching cycle, the converter is in the discontinuous conduction mode. The diode D_{2a} will turn off when i_1 falls to zero, and there will be three states in one switching cycle, as shown in Fig. 14.7a-c. The inductor voltage and current waveforms are shown in Fig. 14.7d. Note that the second inductor current no longer has zero current ripple. The volt-second balance on the two inductors and the 100% efficiency for an ideal converter leads to:

$$(V_g - V_a)\,D - V_a D_2 - V_b \frac{L_1}{L_1 + L_2} D_3 = 0 \tag{14.1}$$

$$(V_a - V_b)(D + D_2) - v_2 \frac{L_2}{L_1 + L_2} D_3 = 0 \tag{14.2}$$

$$\frac{D\,(D + D_2)}{2\,f_S} \left(\frac{V_g - V_a}{L_1} - \frac{V_a - V_b}{L_2} \right) V_g = \frac{V_a^2}{R_a} \tag{14.3}$$

where f_S is the switching frequency. Solving these equations gives the two output voltages:

$$V_a = V_g \frac{2\left(\frac{L_2}{L_1} + D\right)}{1 + \frac{L_2}{L_1} + \sqrt{\left(\frac{L_2}{L_1} + 1\right)^2 + \frac{L_2}{L_1}\left(\frac{L_2}{L_1} + D\right)\frac{4K}{D^2}}} \tag{14.4}$$

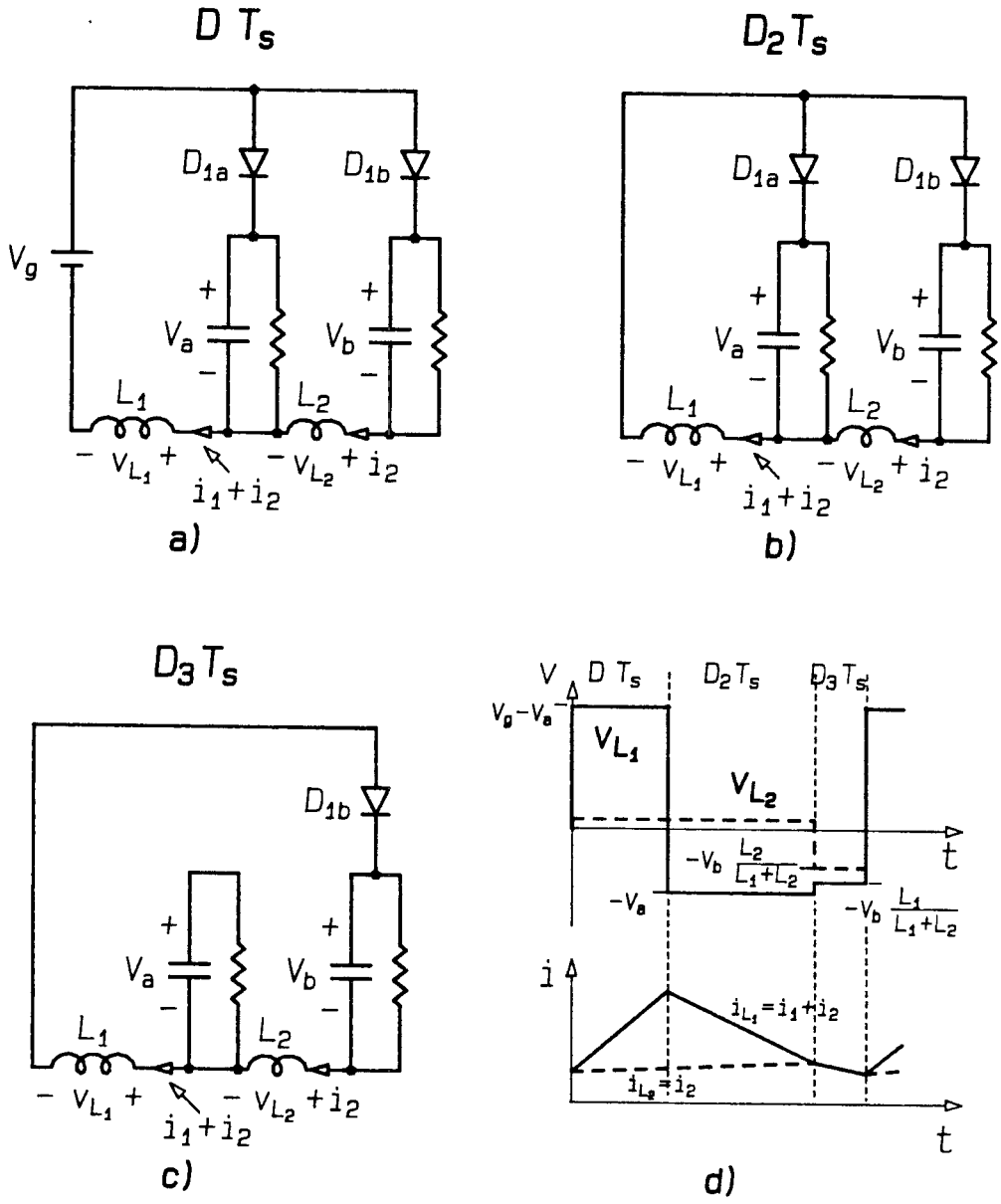

Figure 14.7: Circuit models for coupled-inductor buck type converter with the first output in DCM. a) The model for the time period DT_S. b) The model for D_2T_S. c) The model for D_3T_S. d) The voltage and current waveforms for the two inductors.

$$V_b = V_g D \tag{14.5}$$

where K is given by:

$$K \equiv \frac{2L_1}{R_a} f_S$$

When the parameter K is larger than a critical value of K_{crit}, the converter will be in continuous conduction mode. K_{crit} is found to be:

$$K_{crit} = 1 - D \tag{14.6}$$

For comparison, the output voltage and K_{crit} for a single output buck converter are [15]:

$$V = V_g \frac{2}{1 + \sqrt{1 + \frac{4K}{D^2}}} \tag{14.7}$$

$$K_{crit} = 1 - D \tag{14.8}$$

From these equations one can observe:

1. The value of V_b is the same as when the converter is operating in continuous conduction mode. This comes as no surprise, as the second output is still in CCM. However, the current ripple for this output is no longer zero.

2. The equation for of V_a is very similar to the result for a single output buck converter. V_a depends on the load of that output but does not depend on the load of the other output.

3. When $L_2 \rightarrow 0$, $V_a \rightarrow V_b = DV_g$, which is the same as using the tightly coupled inductors.

4. If the first output is open, then $K = 0$, and the output voltage of the first output will be:

$$V_a = V_g \frac{\frac{L_2}{L_1} + D}{\frac{L_2}{L_1} + 1} \tag{14.9}$$

If the leakage in the coupled-inductors is very high, $(L_2/L_1 \rightarrow \infty)$, the two inductors are essentially uncoupled, thus $V_a \rightarrow V_g$, which is the same result as separate converters.

If the leakage is very low, $V_a \rightarrow V_b$, the tracking becomes very good, just as in the case of tightly coupled inductors.

The basic result is: While increasing the leakage inductance of the coupled-inductors reduces the sensitivity of the zero ripple condition when the converter is in continuous conduction mode, it makes the tracking of the two outputs voltages worse when the converter is in discontinuous conduction mode.

If the output currents of the converters are further reduced, the diode D_{2b} will also turn off before the end of the switching cycle, and there will be four states for the converter, as shown in Fig. 14.8. The output voltages can be found using the same methods. In this case, both output voltages will be load-dependent. As in the last case, the lower the leakage inductance, the better the tracking between the two outputs.

For buck type converters with more than two outputs, the basic results are essentially the same, namely, the higher the leakage inductance the lower the sensitivity of the zero ripple condition, but the worse the output voltage tracking.

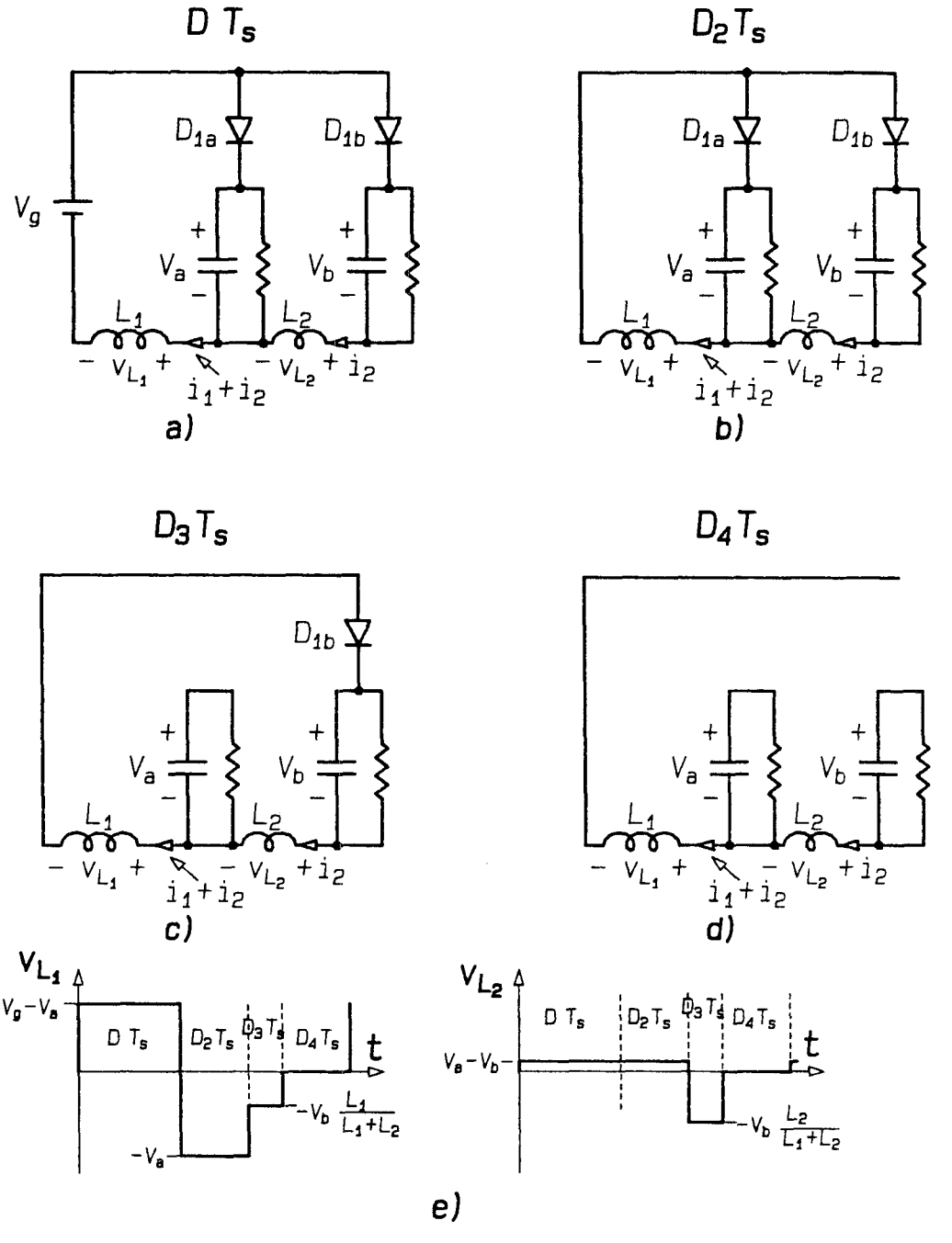

Figure 14.8: Circuit models for coupled-inductor buck type converter with both outputs in DCM. a) The model for the time period DT_S. b) The model for D_2T_S. c) The model for D_3T_S. d) The model for D_4T_S e) The voltage and current waveforms for the two inductors.

Chapter 15

CROSS-REGULATION FOR ĆUK CONVERTERS

15.1 ĆUK CONVERTER WITH SEPARATE INDUCTORS

15.1.1 The Continuous Conduction Mode

The circuit of a two output Ćuk converter is shown in Fig. 15.1a. If the turns ratio of the isolation transformer is 1 : 1 : 1, the circuit can be drawn as Fig. 15.1b.

During the period DT_S, the transistor is on, and the two diodes are reverse-biased; therefore, the circuit model is as Fig. 15.1c. During this period, the inductor on the input side is connected directly across V_g, so the inductor current i ramps up. The two energy transfer capacitors C_a, C_b discharge through the two output inductors into the loads. The two output inductor currents i_a, i_b will also ramp up, assuming that $i_a/C_a > i_b/C_b$, V_{C_a} will drop faster than V_{C_b}, as shown in Fig. 15.1e. At the end of this period, the voltage V_{C_b} on capacitor C_b will be higher than V_{C_1}.

During $D'T_S$, the transistor switch is off, and the input inductor current i will ramp down while charging the two energy transfer capacitors through the two diodes. The currents of each output inductor i_a, i_b also flows through the corresponding diode. Note that at the very beginning of $D'T_S$, the voltage on C_a is less than that on C_b; therefore, D_a will conduct first, the entire input inductor current i *and* the current in the second output inductor i_b will be directed to C_a; the voltage on C_a will increase, while

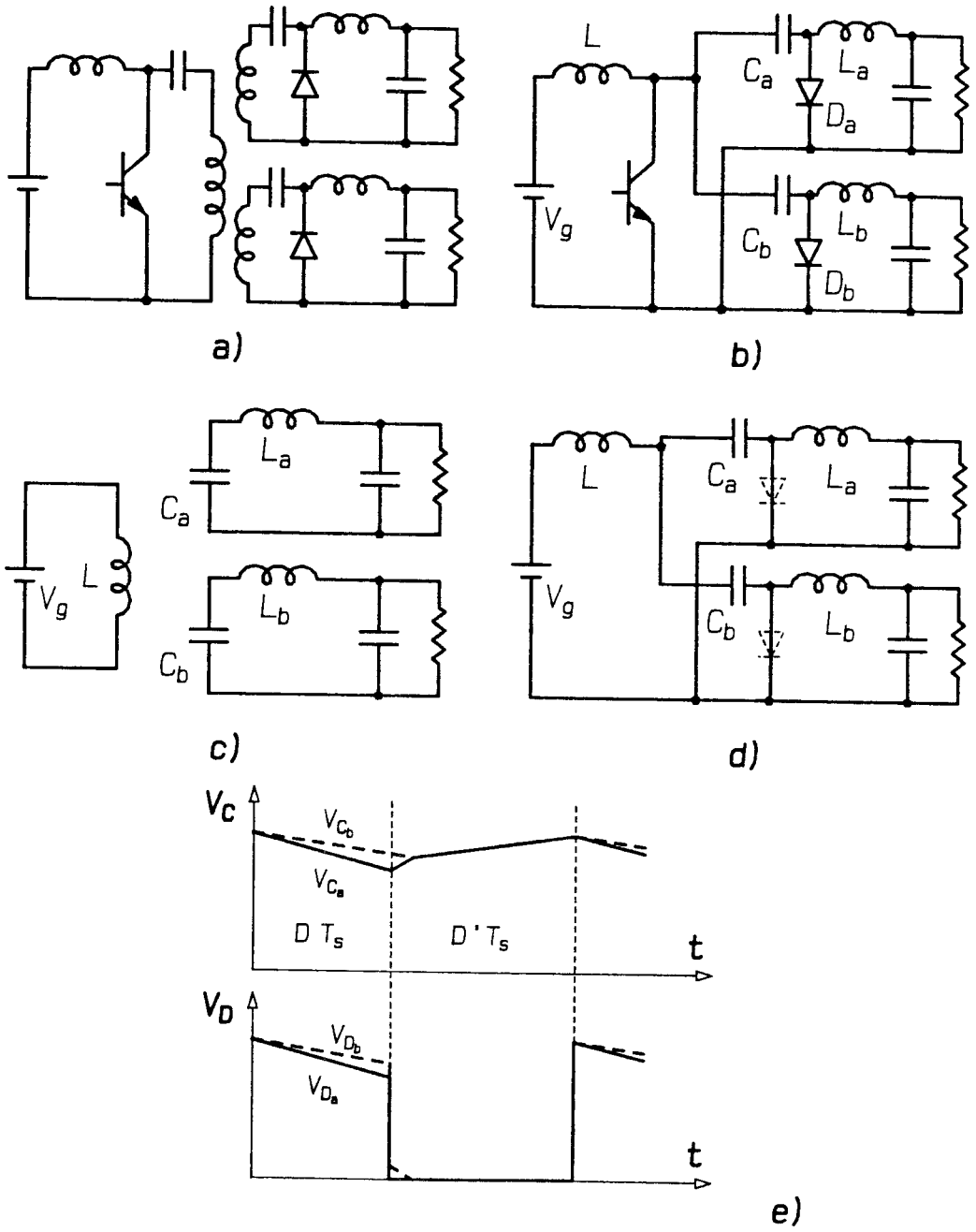

Figure 15.1: a) A two-output Ćuk converter. b) The equivalent circuit assuming 1:1:1 transformer turn ratio. c) The model for DT_S. d) The model for $D'T_S$. e) The waveforms for the two energy transfer capacitors and the diodes.

C_b will continue to discharge by i_b, as shown in the voltage waveforms in Fig. 15.1e. During this short time period, the current of all three inductors will pass through D_a. At the moment the two capacitor voltages become equal, the other diode D_b will start to conduct, dividing the input inductor current according to the values of the energy transfer capacitors. For this part of the switching cycle, each diode conducts the corresponding output inductor current and a portion of the input inductor current. From this point on, as long as both diodes are conducting, the two energy transfer capacitor voltages will increase (or decrease, if the input inductor current falls below zero) together till the end of the switching cycle.

From the voltage waveforms on the two diodes, one can notice that the output voltage (which is the average of the diode voltage) of the first output V_1 is lower than V_2. This difference is just the difference between the two waveforms of the energy transfer capacitors averaged throughout the whole switching cycle [8]. If the energy transfer capacitors are sufficiently large, the difference between the output voltages is negligible. In the ideal case, with no resistive and switching losses, the voltage conversion ratio of the Ćuk converter can be found by the volt-second balance on the inductor:

$$V_a = V_b = V_g \frac{D}{D'} \tag{15.1}$$

which is the same as the single output Ćuk converter.

Note that if the input inductor current i drops below zero before the end of the switching cycle, the converter still does not go into the discontinuous conduction mode. The input inductor just draws its (negative) current by discharging the two energy transfer capacitors. In this case, the current in each diode is the corresponding output inductor current less a portion of the input inductor current, providing that the sum of the two currents is greater than zero.

If the inductor current of one output (say i_2) falls below zero before the end of

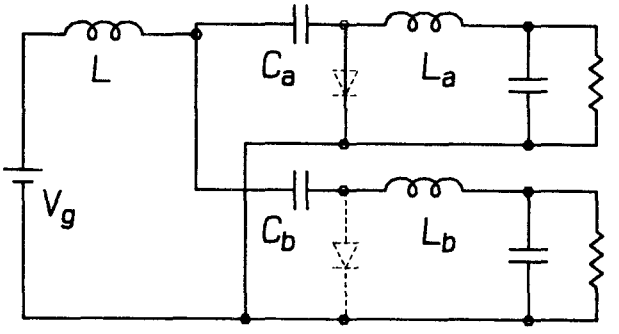

Figure 15.2: The circuit model for the time period $D'T_S$ after one diode turns off.

the switching cycle, the diode for that output (D_b) will still stay on, the diode current is a portion of the input inductor current less the current in that output inductor, providing that the sum is larger than zero.

If the current in one diode, say D_b, falls to zero before the end of the switching cycle, the diode will turn off, and the circuit model will be as shown in Fig. 15.2, 15.3c. In this time period, the sum of all three inductor currents flows through D_a. However, even though D_b is cut off, the large energy transfer capacitors will keep the voltage on D_b very close to the voltage on D_a. Therefore, both output voltages will still be essentially the same as in the continuous conduction mode. As in the continuous conduction mode, increasing the value of the energy transfer capacitor will help the output voltage tracking. The converter will go into discontinuous conduction mode only when the *sum of all three inductor currents* drops to zero, and D_a also cuts off. This compares with the single output Ćuk converter, where the converter goes into DCM when the *sum of both inductor currents* falls to zero [16].

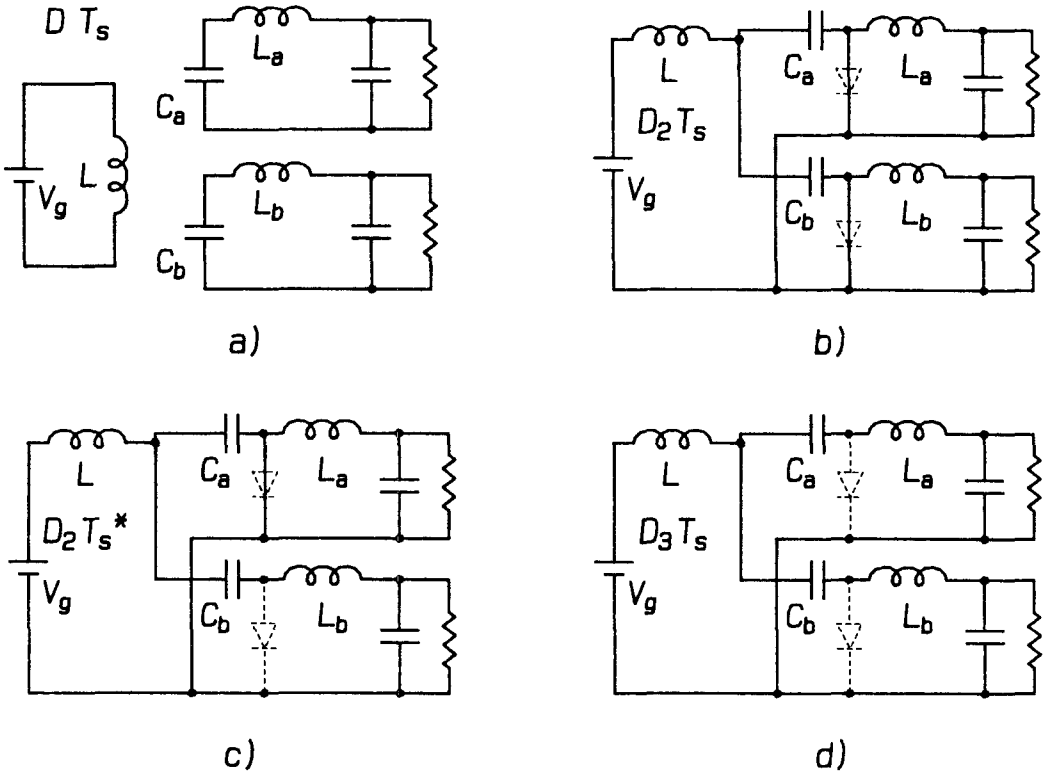

Figure 15.3: a) The model for the time period DT_S. b) The model for D_2T_S. c) The model for D_2T_S, after one diode turned off. d)The model for D_3T_S, when both diodes are off.

15.1.2 The Discontinuous Conduction Mode

If the sum of the three inductors fall to zero before the end of the switching cycle, the converter is in the discontinuous conduction mode. In this third period, labeled as D_3T_S in Fig. 15.3d, both diodes are cut off, and the inductor currents remain at zero till the end of the switching cycle. Note that even though both diodes are cut off, the energy transfer capacitors will keep the voltage waveforms on the diodes essentially identical. Since the output voltage is the average of the diode voltage, the identical diode voltage waveform means very good tracking even in the DCM mode. As in the cases where at

least one diode is conducting, increasing the value of the energy transfer capacitor will improve the output voltage tracking.

For an ideal two output Ćuk converter, using the volt-second balance on the inductor, and the 100% efficiency property of the converter, we also find the dc voltage conversion ratio for the DCM mode to be identical to the single output Ćuk converter[16]:

$$V_a = V_b = V_g \frac{D}{\sqrt{K}} \tag{15.2}$$

where

$$K \equiv \frac{2(L \parallel L_a \parallel L_b)}{R_a \parallel R_b} f_S$$

Note that in the discontinuous conduction mode, the output voltages are load dependent. However, to the first order, both output voltages are equal.

For a Ćuk converter with three or more outputs, it can be shown that at the beginning of DT_S, the diodes will turn on one by one, depending on the voltage on the energy transfer capacitor at that time. The converter will not go into the discontinuous conduction mode unless the sum of *all* of the inductor currents falls to zero. And even in the DCM mode, the tracking of the output voltages is very good.

15.2 ĆUK CONVERTER WITH COUPLED-INDUCTORS

In a Ćuk converter with coupled-inductors, the ripple current is usually steered to the input or one of the outputs. However, the current in each diode is still the corresponding output current plus part of the input inductor current. The operation of the converter is the same as that of the converter with separate inductors. Using the canonical equivalent circuit model for steady state (dc) also shows that the effects of the parasitic resistors are the same for both the separated and the coupled-inductor converters.

Chapter 16

CONCLUSIONS

The coupled-inductor concept was introduced into the field of power electronics a few years ago. It was demonstrated that the concept offers a number of advantages over separate inductors, including reduced size and weight, possible zero ripple current on all but one winding. However, very few designs were actually using the coupled-inductors. This situation is mainly due to the lack of the analysis of the structure, especially combining the zero ripple condition with the dc saturation conditions. For coupled-inductors using the traditional winding technique, the inherent high sensitivity of the zero ripple condition to the air-gap and turns ratio adjustments also prohibited their widespread use. This presentation gives the long-awaited solution for the sensitivity problem—high leakage between the coupled-inductor windings.

The zero ripple phenomenon of coupled-inductors depends only on the leakage of the winding that carries all the ripple current and on the physical turns ratio of the windings. The leakage of the other windings has no effect on this zero ripple condition. To obtain zero ripple and reduce the sensitivity to various errors in the manufacturing process, one has to introduce a *well-controlled* amount of leakage into the coupled-inductor structure.

For multiple output converters with several inductors, combining all the inductors into one single structure gives even more savings. The introduction of the new coupled-inductor structure using standard EE and EI-cores makes the coupled-inductors

practical for this type of converters.

Besides the zero ripple condition, or ac condition, the dc condition, that is preventing the core from saturating under the dc currents in the coupled-inductors, is also very important for the proper operation of the converter.

For the standard EI and EE-cores the inherent leakage of the center leg winding is found to be well behaved and can be easily characterized as a "leakage parameter" l. The introduction of this leakage parameter l in Chapter 8, together with the dc analysis in the same chapter, makes the deriving of the closed form solution for a coupled-inductor design possible. By use of this closed form solution, a straightforward design procedure for the multi-output coupled-inductor structure is given for the first time.

Several models of the magnetic structure were used in this presentation. For solving certain problems, using one model can be much easier than using another. Using the proper methods, one can easily solve many problems which seem to be impossible to tackle.

The cross-regulation problem of a multiple output converter in the continuous conduction mode results from the non-idealities in the circuit. In the discontinuous conduction mode, the cross-regulation is an inherent feature of the circuit topology. For some converter topologies, coupling the inductors can improve the cross-regulation in the discontinuous conduction mode.

During the preparing of this presentation, several designs have been made using these methods, including the 150W converter example in Chapter 11, all with very good results. With the proper modeling and analyzing, the coupled-inductor approach will be used more and more frequently in the future.

REFERENCES

[1] Slobodan Ćuk, "Switching Dc-to-Dc Converter with Zero Input or Output Current Ripple," IEEE Industry Applications Society Annual Meeting, 1977 Record, pp. 1131-1146.

[2] Slobodan Ćuk and R. D. Middlebrook, "Coupled-Inductor and Other Extensions of a New Optimum Topology Switching Dc-to-Dc Converter," IEEE Power Electronics Conference, 1977 Record, pp. 1110-1126.

[3] H. H. Skilling, *Electrical Engineering Circuits,* John Wiley and Sons: New York, 1957, Chapter 12.

[4] M.I.T. Staff, *Magnetic Circuits and Transformers,* John Wiley and Sons: New York, 1943, Chapters 12 and 17.

[5] C. A. Desoer and E. K. Kuh, *Basic Circuit Theory,* McGraw-Hill: 1969.

[6] J. K. Watson, *Applications of Magnetism,* John Wiley and Sons: New York, 1980.

[7] Slobodan Ćuk and William M. Polivka "Analysis of Integrated Magnetics to Eliminate Current Ripple in Switching Converters," Proc. Sixth International PCI'83 Conference.

[8] Shi-Ping Hsu, "Problems in Analysis and Design of Switching Regulators," Ph.D. Thesis, California Institute of Technology, Department of Electrical Engineering, Pasadena, California, Sept., 1979.

[9] William M. Polivka, "Applications of Magnetics to Problems in Switched-Mode Power Conversion," Ph.D. Thesis, California Institute of Technology, Department of Electrical Engineering, Pasadena, California, Feb., 1984.

[10] Abraham A. Dauhajre, "Modelling and Estimation of Leakage Phenomena in Magnetic Circuits," Ph.D. Thesis, California Institute of Technology, Department of Electrical Engineering, Pasadena, California, April, 1986.

[11] Slobodan Ćuk and Zhe Zhang, "Power Electronics Circuits," Proc. China 1985 International Conference on Circuits and Systems, pp. 362-369, 1985.

[12] Colonel Wm. T. Mclyman, *Magnetic Core Selection,* Marcel Dekker Inc.: 1982.

[13] Abraham Dauhajre and R. D. Middlebrook,"Simple PWM-FM Control for an Independently Regulated Dual Output Converter," Proc. Tenth International Solid State Power Conversion (Powercon 10) March 1983, pp. D-3.1-8

[14] W. M. Polivka, P. R. K. Chetty, and R. D. Middlebrook, "State-Space Average Modelling of Converters with Parasitics and Storage-Time Modulation," IEEE Power Electronics Specialists Conference, 1980 Record, pp. 119-143.

[15] Slobodan Ćuk and R. D. Middlebrook, "A General Unified Approach to Modelling Switching Dc-to-Dc Converters in Discontinuous Conduction Mode," IEEE Power Electronics Specialists Conference, 1977 Record, pp. 36-57.

[16] Slobodan Ćuk, "Discontinuous Inductor Current Mode in the Optimum Topology Switching Converter," IEEE Power Electronics Specialists Conference, 1978 Record, pp. 1131-1146.

Appendix A

LEAKAGE PARAMETER CHARACTERIZATION AND MEASUREMENT

A.1 LEAKAGE FLUX, LEAKAGE RELUCTANCE AND LEAKAGE INDUCTANCE

As discussed in Chapter 2, in two winding coupled-inductors shown in Fig. A.1a, part of the flux generated by the primary winding is not coupled through the secondary. This is the *leakage flux* of the primary Φ_{l_1}. The leakage flux is usually in the air surrounding the structure; therefore, it is a distributed quantity. However, in the reluctance model (Fig. A.1b), this leakage flux path can be represented by a single *leakage reluctance* $\mathcal{R}_{l_1}$. In the circuit model (Fig. A.1c) it is modeled as a single *leakage inductance* L_{l_1}. Likewise, the leakage flux path of the secondary is modeled as $\mathcal{R}_{l_2}$ and L_{l_2}.

The flux distribution in the new EI-core coupled-inductor structure is also quite simple, making it possible for the corresponding reluctance and circuit models to have separate leakage reluctances or leakage inductances for each winding (Fig A.2). In a switching converter using coupled-inductors, the value of the leakage in the primary winding (the winding into which the ripple is steered) has an important role in obtaining the zero ripple condition. To simplify the design of the new coupled-inductor structures,

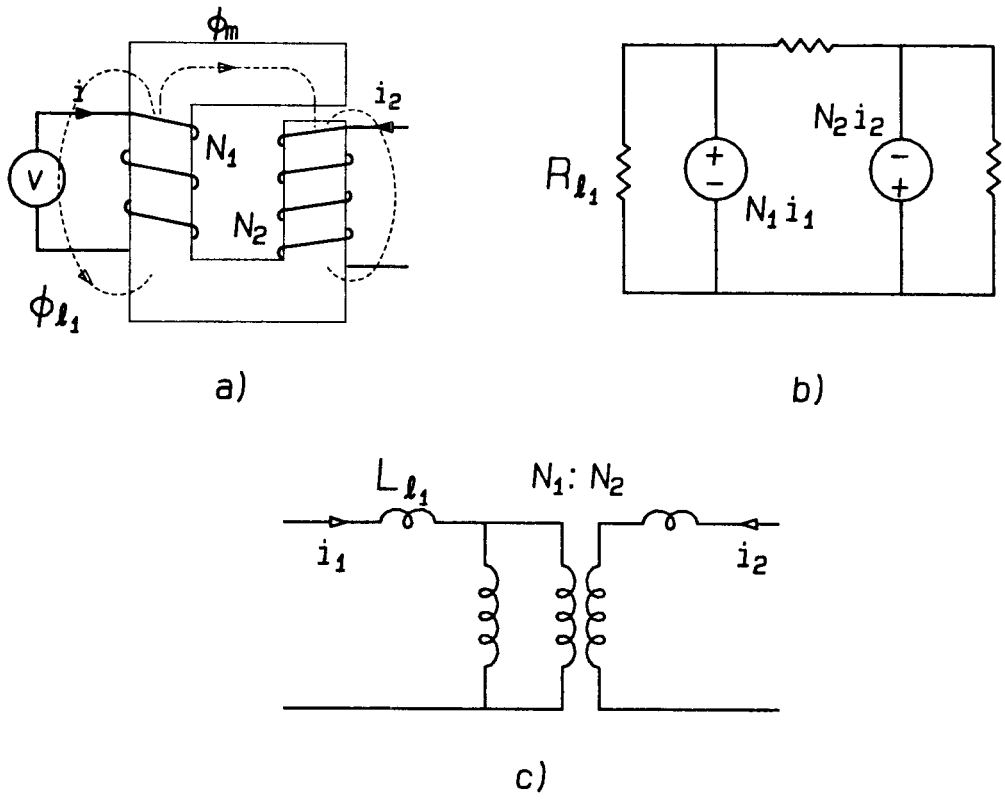

Figure A.1: a) The leakage flux of the primary winding in two-winding coupled-inductors. b) The leakage is represented by a leakage reluctance in the reluctance model. c)In the circuit model the leakage is represented by a leakage inductance.

a new *leakage parameter* is introduced in Chapter 8.

A.2 THE LEAKAGE PARAMETERS

The leakage parameter is introduced with the development of the design procedure of the new EI-core coupled-inductor structure, since the EI and EE-cores used are commercially readily available and are more or less standardized. However, a similar procedure can be used for defining the leakage parameter for other core types, providing that a reasonably accurate reluctance model can be found.

The leakage flux of a magnetic structure is spread out in space as shown

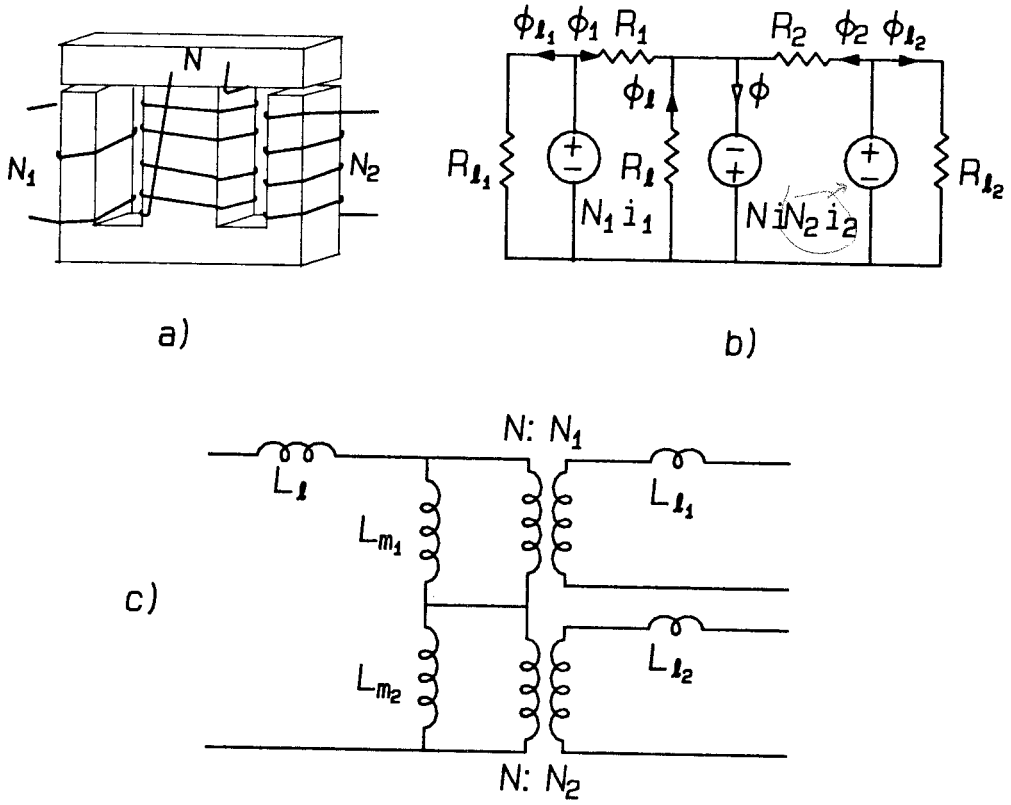

Figure A.2: a) The new EI-core coupled-inductor structure. b) The reluctance model. c)The circuit model.

in Fig A.3a. However, we can assume that all the leakage flux of the center winding is confined by an additional leg with the same cross section (S) as the center leg (Fig A.3b). The required air-gap l in this extra "leakage leg" to make the reluctance of this flux path equal to the reluctance of the leakage flux path in the original structure (Fig A.3a) is called the leakage parameter. A similar definition can be used for defining the leakage parameter l_s for the secondary windings. Although the leakage of the secondary windings has no effect on the zero ripple condition, it is used to estimate the sensitivity of the structure.

Another parameter l_f is used to simulate the effect of the fringing flux of the air-gap (Fig. A.4a). The fringing flux at an air-gap makes the air-gap reluctance smaller

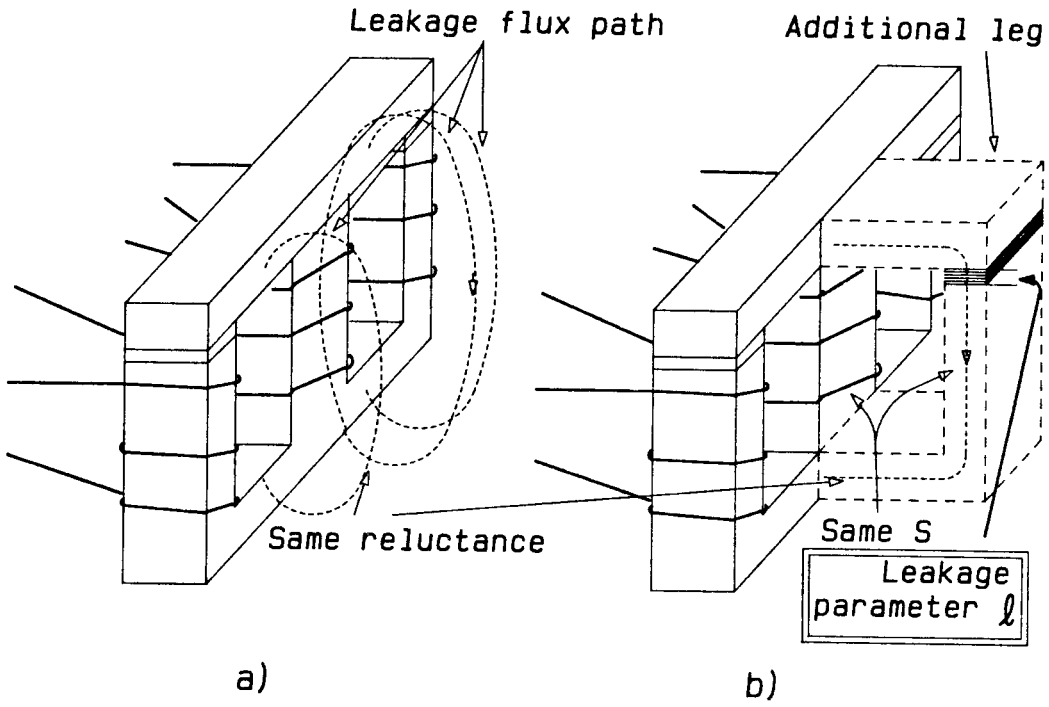

Figure A.3: a) The leakage flux of the center leg is spread out in air. b) Making an additional magnetic branch to simulate the leakage flux path.

than it otherwise should be. Experimental data shows that the effect of this fringing flux is very close to a fixed reluctance in parallel with the calculated reluctance of the air-gap (Fig. A.4b). Therefore an additional magnetic branch with the same cross section as the branch with the air-gap can be used to simulate the fringing flux (Fig. A.4c). The required gap l_f for this branch is the *fringing parameter.*

A.3 THE MEASURING SETUP

The setup for measuring the leakage parameter for a gapped EI-core is shown in Fig. A.5. The air-gap x for both legs is the same. To simplify the calculation, the windings on the three legs should have the same number of turns ($N = N_1 = N_2$). To minimize the error from the positioning of the I-piece, one winding is used on each

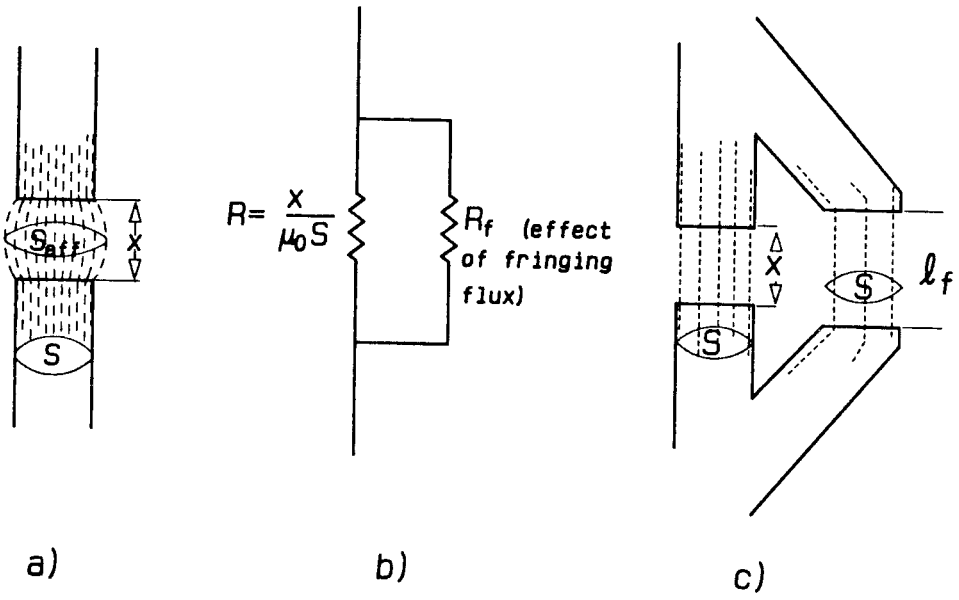

Figure A.4: a) The fringing flux of an air-gap makes the cross section of the core seems to be larger. b) The effect of the fringing flux is the same as a fixed reluctance across the calculated air-gap reluctance. c) This fixed reluctance can be simulated using another fixed gap magnetic branch across the original air-gap.

outer leg, and the two windings are connected in series. Thus, in the voltage ratio measurement, if the I-piece is positioned slightly toward one leg, the voltage on that winding will increase, while the voltage on the other winding will decrease, compensating the voltage change on first leg.

The measurement procedure is as follows:

First, apply a voltage source ($20 \sim 200kHz$) on the input winding. Measure the output voltage on the two outer windings and adjust the position of the I-piece (Fig. A.5a), so that the voltage on the two outer windings are equal. Make sure that the I-piece is in line with the E-piece of the core, and clamp the two pieces together with non-magnetic material.

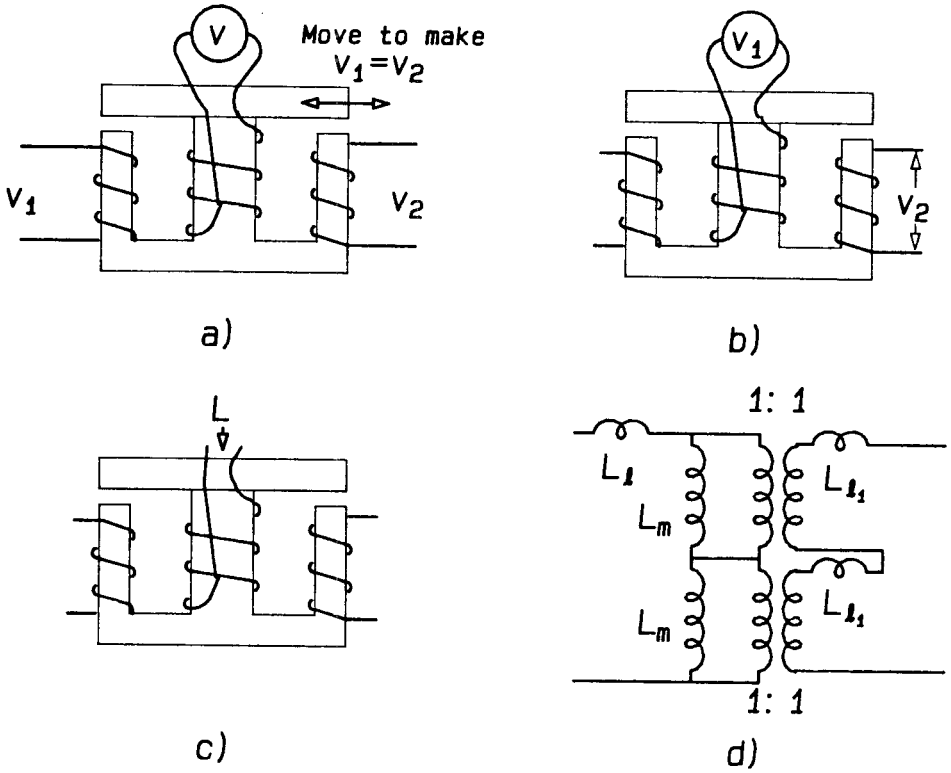

Figure A.5: The measurement setup for the Leakage parameter l. a) Positioning the I-piece. b) Measuring the voltage transfer ratio. c) Measuring the center leg winding inductance.d) The circuit model of the structure.

Secondly, connect the two outer windings in series (in phase), and measure the voltage ratio v_2/v_1 (Fig. A.5b), using the same voltage source at the center winding.

Then, measure the input inductance L (the inductance of the center winding), as shown in Fig. A.5c.

From the circuit model (Fig. A.5d) and the data obtained above, the leakage inductance L_{l_1} is calculated from:

$$\frac{v_2}{v_1} = \frac{L - L_l}{L} \tag{A.1}$$

or

$$L_l = \left(1 - \frac{v_2}{v_1}\right) L \tag{A.2}$$

Then the leakage permeance $\mathcal{P}_l$ is obtained by:

$$\mathcal{P}_l = \frac{L_l}{N^2} \tag{A.3}$$

Finally, the leakage parameter l is calculated as:

$$l = \frac{\mu_0 S}{\mathcal{P}_l} \tag{A.4}$$

where S is the cross section of the center leg of the core.

The secondary leakage does not affect the zero ripple condition. However, it will affect the sensitivity of the structure. To obtain the leakage of the secondary, repeat the measurement procedure shown above, but reverse the primary and secondary windings. The voltage ratio v_1/v_2 (output winding driven) and the output inductance L_{out} can be used for finding the secondary leakage permeance:

$$L_{l_1} = \left(1 - \frac{v_1}{v_2}\right) \frac{L_{out}}{2} \tag{A.5}$$

The factor 1/2 exists because the total output leakage inductance consists of the leakage inductance of the two output windings in series.

The secondary leakage permeance $\mathcal{P}_{l_1}$ is obtained by:

$$\mathcal{P}_{l_1} = \frac{L_{l_1}}{N^2} \tag{A.6}$$

If necessary (it is usually more convenient to use the leakage permeance in the sensitivity calculation), the secondary leakage parameter l_s can be calculated as:

$$l_s = \frac{\mu_0 S}{\mathcal{P}_{l_1}} \tag{A.7}$$

The fringing parameter can be found by first calculating the magnetizing inductance from the air-gaps:

$$L_{m_c} = \frac{N^2 \mu_0 S}{x} \tag{A.8}$$

where x is the air-gap used in the measurement setup. The real magnetizing inductance L_m is:

$$L_m = L - L_l \tag{A.9}$$

The difference is due to the fringing flux around the air-gap. Therefore, the fringing parameter is:

$$l_f = \frac{N^2 \mu_0 S}{L_m - L_{m_c}} \tag{A.10}$$

Example: Measurement of an EI-50 core with two equal gaps

$$N = N_1 = N_2 = 100T, \qquad x = 1.59mm \tag{A.11}$$

The inductance of N is measured to be 4.53 mH and the voltage transfer ratio is -2.91dB (0.715). The primary leakage inductance calculated from (A.2) is 1.29mH, and the primary leakage parameter l calculated from (A.4) is 2.24mm.

A.4 IS THE LEAKAGE PARAMETER A CONSTANT?

To use a single leakage parameter l to characterize the center leg leakage, this parameter has to be relatively insensitive to the winding configuration and the size of the air-gap. Two additional experiments are done to insure this.

A.4.1 Leakage vs. Winding Configuration

Special measurement setups are used to determine the effect of the winding configuration. In the first setup (Fig. A.6a), both EI and EE-cores are used. The primary winding is wound in a single layer on the center leg, but the secondary consists of four windings, one on top of the other, each wound in a single layer, all on the same outer leg and with the same number of turns. Insulating tape is put in between the windings to make the windings take up most of the window area. A voltage is then applied on the

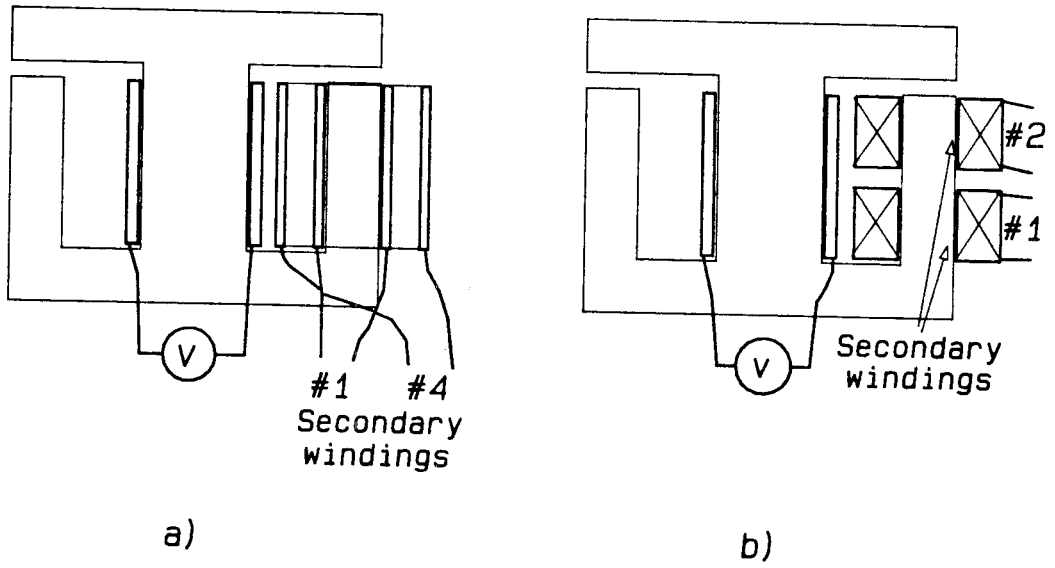

Figure A.6: The measurement setups for determining the effect of the winding configuration.

primary winding, and the voltage on each secondary winding is measured. The difference between the inner most layer and the outer layer is found to be less than 2%, which is insignificant. The same experiment is repeated with a single layer for the outer winding but multiple layers for the center, and the results are similar.

A similar measurement is also done with a single layer on the center, but with two windings with the same number of turns side-by-side on an outer leg (Fig. A.6b). For an EE-core the voltages on the two outer legs are identical, but for an EI-core, the winding toward the gap generates much less (about 20% less) voltage than the other winding, showing that, due to the leakage flux, the flux density in the core is lower toward the gap. Therefore, for coupled-inductors with more than one winding on an outer leg, it is better to utilize an EE-core to simplify the design, and put the two windings side by side to insure high leakage between the windings.

EI-50 Gapped core, 100 turns/winding

GAP (mm)	ℓ (mm)	ℓ_s mm	ℓ_f mm
3.97	2.15	39.0	2.58
2.59	2.21	31.1	2.20
1.59	2.24	25.8	2.03
1.07	2.27	24.2	1.81
0.64	2.31	22.9	2.23

Table A.1: The leakage parameter vs. the gap size for an EI-50 gapped core.

Another experiment is made to determine the effects of the air-gap size to the leakage parameter. The same experiment as in Section A.3 is repeated for different air-gap sizes, and the leakage parameter is calculated for each gap. The results for an EI-50 gapped core are shown in Table A.1. It shows that for a wide range of gap size (about 1 : 7) the critical leakage parameter l changes only about $\pm 5\%$. The results for EI and EE cores using spacers are slightly worse, as the leakage parameter changes about $\pm 10\%$ for the same 1 : 7 air-gap change. However, using the average as the leakage parameter for several designs shows that the coupled-inductors needs only a slight adjustment (one or two turns) in the secondary windings to obtain minimum ripple after being connected in the converter circuit. The nonessential secondary leakage parameter and the fringing parameter vary more with the air-gap change, but they will not change the coupled-inductor design.

A.5 THE MEASUREMENT AND CALCULATION FOR DIFFERENT EI AND EE-CORES

The same measurement as in Section A.3 is repeated for different EI-cores, with ground air-gaps and spacer gaps, and also for EE-cores with spacer gaps. For each core, the measurement is done for different gap sizes in a wide range of 1:7. The primary and secondary leakage parameters, also the fringing parameter are calculated from each measurement. For each core size the results for different gap sizes are averaged to form the leakage parameters and the fringing parameter for that core. The final results are shown in Table A.2.

A.6 LEAKAGE PARAMETER SPECIFICATION

The data presented in Table A.2 show that the leakage parameter does not change much over a rather wide range of core sizes. As seen in Fig. A.7, the leakage parameter for the smallest EE-10/11 core is $l = 1.09mm$, and it changes only to $l = 4.41mm$ for the largest EE-60 core for which measurements were made. The gross size differences between the two cores visible in Fig A.7 directly translate into a wide power range in which they can be implemented: from as small as a few watts to over a kilowatt. Although respective changes of the leakage parameter over the wide range of core size changes were not too much, since the leakage parameter plays the central role in the design procedure outlined in Chapters 7, 8 and 9, it is very important that this parameter is very accurately specified. Motivated by different application requirements, the magnetics manufacturers are constantly increasing the pool of the available core sizes, offering even cores with the same core cross section but with a different aspect ratio (length to build-up) of the window cross section. Different core geometries would then lead to different leakage parameter values. It is therefore suggested that the magnetic manufacturers include in

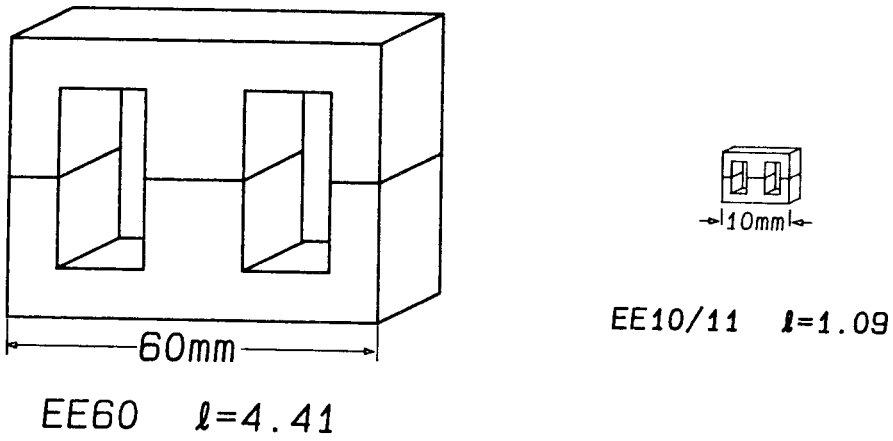

Figure A.7: The leakage parameter of an EE-60 core and the leakage parameter of a EE-10/11 core are fairly close.

their data sheets, both for existing cores as well as for future new cores, another important data: the value of the leakage parameter for that particular core.

	CORE SIZE	ℓ (mm)	ℓ_s (mm)	ℓ_f (mm)
GAPPED EI CORES	EI-60	2.14	28	2.1
	EI-50	2.23	25	1.9
	EI-40	1.60	16	1.1
	EI-30	1.77	18	1.5
SPACER EI CORES	EI-60	4.45	7.4	4.9
	EI-50	4.60	7.6	4.8
	EI-40	3.63	5.1	2.3
	EI-30	3.60	5.8	2.3
	EI-22	2.40	2.7	1.8
	EI-16	1.63	1.9	1.0
	EI-12	1.05	1.5	1.0
SPACER EE CORES	EE-60	4.41	8.6	∞
	EE-50	4.60	9.0	∞
	EE-40	4.15	7.3	∞
	EE-30	3.49	7.2	∞
	EE-16	1.33	2.8	∞
	EE-13	1.30	2.4	∞
	EE-10/11	1.09	2.5	∞

Table A.2: The leakage parameters for different EI and EE-cores.